NTNU

Norwegian University of
Science and Technology

Sensorless Control of Synchronous Machines Used in Adjustable Speed Hydro

Magnus Bolstad

Master of Energy and Environmental Engineering
Submission date: June 2018
Supervisor: Roy Nilsen, IEL

Norwegian University of Science and Technology
Department of Electric Power Engineering

Problem Description

For some high power application, as for instance in Adjustable Speed Hydro (ASH), synchronous machines are used for power generation. In the specialisation project carried out in the fall semester 2017, flux models and sensorless control methods for such a synchronous generator with damper windings was developed to be able to operate such machines without speed- and position- sensors. The performance of the control system depends on the accuracy of the parameters of the flux models. In this master-project, these flux models and control methods shall be analysed in details. The main focus shall be:

- Sensorless control at low speed operation
- Parameter sensitivity of the flux models

If time available, combinations of flux models to improve the behavior of the model in the complete speed-torque plane should be analyzed. In this Master project the tool to be used for simulation shall be Simulink with the Power System Library.

Preface

This is a master thesis submitted to the Department of Electric Power Engineering at the Norwegian university of science and technology, as a final evaluation for the master's degree within energy and environmental engineering. It has been performed the spring semester 2018. Working with this complex problem has not only given me better insight in the field of electric drives, but it has also given me valuable experience within research, independent problem solving and interpretation of results.

I would like to thank my supervisor Roy Nilsen for valuable guidance and support both during the specialisation project the fall semester 2017, and during the work with the master thesis this final semester. His experience within the field has been a great resource, and I am grateful for his willingness to share his knowledge with his students. I would also like to thank master student Emil Mørkved, which has written about the same topic for a six phase induction machine, for many good discussions throughout the last year. Finally I would like to thank my family for supporting me throughout my studies, and my friends for making my time as a student in Trondheim a good time.

Trondheim, June 11, 2018

Magnus Bolstad

Abstract

For some high power applications, as for instance in adjustable speed hydro, ASH, synchronous machines are used for power generation. In this master's thesis, flux models and sensorless control methods for a synchronous generator with damper windings, developed in the specialisation project autumn 2017, has been carefully analysed. A drive is classified as sensorless when no sensors are used for measuring the position or speed, but the position and speed are rather estimated based on the measured voltage and current supplied to the electric machine. Higher reliability, higher robustness, and a reduced size and cost are motivating factors for running electric machines sensorless. The main focus has been on sensorless control at low speed operation, and on parameter sensitivity of the flux models.

Steady state analysis of the current model and the voltage model, which are used to estimate the stator flux linkage, were performed by analytic expressions in Matlab, while the dynamic analysis and the analysis of the sensorless operation were performed by simulations in Simulink. Estimated stator flux linkage and estimated rotor position was used as input to the control system. It was illustrated that the voltage model is sensitive to the estimated stator resistance during low speed operation, and that the sensitivity increases with the generated torque. During steady state operation, only the magnitude of the estimated stator flux linkage was affected by the erroneously estimated resistance, while the angle of the estimated stator flux linkage was unaffected due to the unity power factor control. During dynamics, an erroneous estimation of the stator resistance made the flux linkage estimate drift, resulting in oscillating errors in both the estimated stator flux linkage amplitude and in the estimated stator flux linkage angle. The concept of stator flux linkage drifting, the consequences of it and methods to compensate for it, have been thoroughly explained and illustrated. It has been illustrated how the voltage model is less sensitive to the stator resistance at higher frequencies, and that the speed at the instant when the drifting occurs determines how much the flux linkage will drift. Once the flux linkage has drifted, the offset established is not reduced by increasing the speed, and hence there is a need for drift compensating techniques. Sensorless control without drift compensation did not yield satisfying control, and instability occurred frequently. Changes in torque reference, changes in stator resistance and driving through zero speed are typical scenarios that trigger drifting. It was found that the current model is more sensitive to the q axis inductance while generating a high torque, while the sensitivity to the d axis inductance was highest at lower torques. Steady state analysis revealed that the current model is not completely independent of the speed, as field weakening affects the sensitivity of the model.

When using drift compensation, the machine was able to operate sensorless at low speeds, and to drive through zero speed. The generated torque followed its reference less accurately at low speeds, especially when driving slowly through zero speed while generating a high torque. Providing a torque at standstill for a longer time was not successfully achieved. Finally, attempts were made to improve the sensorless control by combining the flux models in different ways, to obtain a less parameter sensitive closed loop observer. It was concluded that the closed loop observer eliminates the need for an external drift correction method. By further modifications, better flux estimates were obtained for low speeds, both during the first step in torque reference and through zero speed, assuming that the inductances are known with high accuracy.

Sammendrag

Synkronmaskiner brukes typisk for kraftkrevende prosesser, slik som elektrisk kraftproduksjon ved variabelt turtall, ASH. I denne masteroppgaven vil fluksmodellene og metodene for sensorløs kontroll av en synkrongenerator med dempeviklinger, utviklet i prosjektoppgaven høstsemesteret 2017, analyseres nøye. En motordrift betegnes som sensorløs når verken hastighetssensor eller posisjonssensor benyttes. Hastigheten og posisjonen estimeres basert på målt strøm og spenning tilført stator. Fordeler med sensorløs drift er høyere pålitelighet, mer robust konstruksjon, redusert størrelse og mindre kostnader. Hovedfokus har vært på analyse av sensorløs kontroll ved lave hastigheter, og på parametersensitivitetsanalyse av fluks modellene.

Stasjonær analyse ble utført med analytiske uttrykk i Matlab, mens dynamisk analyse og analyse av den sensorløse kontrollen ble utført ved simuleringer i Simulink. Estimert statorfluksforslyngning og estimert rotor posisjon benyttes som input til kontrollsystemet. Det har blitt illustrert at spenningsmodellen er sensitiv for feil i estimert stator motstand ved lave hastigheter, og at denne følsomheten øker for høyere generert moment. Ved stasjonære forhold ble kun amplituden på den estimerte statorfluksforslyngningen påvirket av en feilestimert stator motstand, mens den valgte kontrollstrategien med strøm og spenning i fase eller i motfase sørget for at estimert fluksforslyngningsvinkel ble estimert riktig, uavhengig av den estimerte statormotstanden. Ved dynamikk førte en feilestimert statormotstand til at den estimerte fluksforslyngningen fikk en forskyvning, såkalt drifting. Dette førte til en oscillerende feil i både vinkel og amplitude på den estimerte statorfluksforslyngningen. Drifting av stator fluksforslyngningen, konsekvensen av den, og metoder for å kompensere for den blir nøye forklart og illustrert i denne oppgaven. Det blir illustrert hvordan spenningsmodellen er mindre sensitiv for feil i estimert statormotstand ved høyere hastigheter, og at hastigheten i det øyeblikket driftingen forekommer er avgjørende for hvor mye fluksforslyngningen drifter. Når driftingen først har forekommet, vil offseten som er etablert ikke reduseres eller fjernes ved å øke hastigheten, og det er derfor nødvendig med driftkompensasjon. Sensorløs kontroll uten slik driftkompensasjon resulterte i lite tilfredsstillende styring, og styringen ble ofte ustabil. Endring i momentreferansen, endring i estimert stator motstand og kjøring gjennom null hastighet er typiske scenarier hvor drifting ble observert. Det blir vist at strømmodellen er mer følsom for feil i estimert induktans langs q aksen ved generering av høyt moment, mens følsomheten for feilestimert induktans langs d aksen er høyest ved generering av lave moment. Den stasjonære analysen avdekket også at strømmodellen ikke er totalt uavhengig av hastigheten, ettersom følsomheten for estimerte parametere endret seg ved feltsvekking.

Ved bruk av driftkompensasjon klarte maskinen å operere sensorløst ved lave turtall og gjennom null hastighet. Generert moment fulgte referansen sin dårligere ved lave turtall, spesielt ved kombinasjonen av en sakte nullgjennomgang, og et høyt generert moment. Stillestående momentgenerering, hvor en last blir holdt, var dermed ikke mulig å gjennomføre sensorløst. Det ble forsøkt å forbedre den sensorløse styringen, og å gjøre den mindre følsom for feilestimerte parametere, ved å kombinere de to fluksmodellene på ulike måter til en lukket sløyfe modell. Det konkluderes med at lukket sløyfe modellen fjerner behovet for en ekstern driftkompensasjonsmetode, og at den ved videre modifiseringer kan resultere i bedre fluksestimat ved lave hastigheter, både ved første sprang i momentreferanse og ved gjennomgang av null hastighet, når induktansene antas kjente.

Contents

List of Figures

List of Tables

All figures and illustrations in this thesis are made by the author of this thesis. Simulation results and plots are produced in Simulink and Matlab.

List of Symbols

δ	pole wheel angle	[rad]
ϵ	angle of the stator current vector	[rad]
ω	angular speed	[rad/s]
ω_0	undamped resonance frequency	[rad/s]
ω_n	nominal electrical speed	[rad/s]
ϕ	angle between current and voltage	[rad]
Ψ	flux linkage	[Wb-t]
ψ	flux linkage	[pu]
σ	leakage coefficient	[-]
τ	torque	[pu]
θ	rotor position	[rad or °]
ξ	angle of the stator flux linkage	[rad]
ζ	relative damping/damping ratio	[-]
h_0	open loop transfer function	[-]
h_r	transfer function of regulator	[-]
k	gain	[-]
L	inductance	[H]
u_{con}	control signal PWM	[-]
x	reactance	[pu]
x_{md}	magnetising reactance along d-axis	[pu]
x_{mq}	magnetising reactance along q-axis	[pu]
e	difference between filtered and unfiltered stator flux linkage squared	[pu^2]
I	current	[A]
i	current	[pu]
J	moment of inertia	[kgm^2]
j	$\sqrt{-1}$	[-]

m	closed loop transfer function	[-]
n	rotor speed	[pu]
R	resistance	[Ω]
r	resistance	[pu]
T	time constant	[s]
U	voltage	[V]
u	voltage	[pu]

Subscripts

D	direct axis damper winding quantity
Q	quadrature axis damper winding quantity
d	direct axis stator winding quantity
q	quadrature axis stator winding quantity
f	field winding quantity
a,b,c	stator quantities for phase a,b and c respectively
s	stator
ref	reference value
DTC	direct torque control
est	estimated value

Special Symbols and Notation

$\hat{x}$	Estimated value of the parameter x
$\underline{x}$	Vector/phasor
$\vec{x}$	Space vector
$\angle x$	Angle of x
x	modulus of x

Abbreviations

ASH - adjustable speed hydro
emf - electromotive force
pu - per unit
DTC - direct torque control
DFLC - direct flux linkage control
ITC - indirect torque control
LPF - low-pass filter
MAF - moving average filter
PI - proportional integral

PLL - phase locked loop
PWM - pulse width modulation
CM - current model
VM - voltage model
deg - degrees
est - estimated value

1 Introduction

1.1 Background

In the attempt of reducing harmful pollution related to power generation, there has been an increasing interest in using renewable energy sources such as wind and sun for the recent years. Pumped hydro power as an flexible and easily controllable energy source then plays an important role to ensure reliability, and to stabilise the grid and support other uncontrollable sources. During periods with a surplus of energy from uncontrolled sources, such as wind and sun, the generator can be run as a motor, and pump the water to a higher energy level. This is a classic way of energy storage. Synchronous machines are usually used for industrial applications, such as hydro power plants, due to their high efficiency, high overload capacity and good performance in field weakening area [20]. A conventional synchronous machine in a power plant can only run at one rotational speed, given by the frequency in the grid and the number of pole pairs. By using an adjustable speed hydro machine, ASH, which can operate at adjustable speeds both as a motor and as a generator, the power generation can be optimised further. The ASH machine is able to run at the speed that is optimal for the turbine with respect to the current flow rate and head in the plant. This increases the efficiency during both pumping and power generation. It is also capable to follow the load better than a conventional single speed machine, yielding less fluctuations in the grid frequency [26]. This requires a properly tuned control system, providing accurate speed and torque control.

For the last decades sensorless drives have gained large popularity, and it is the norm of the industry these days [27, p 24]. Despite the terminology, a drive classified as a sensorless drive is not operated completely without sensors, but it has no sensors measuring the position or the speed of the rotor. The position and the speed of the machine is obtained by measuring the voltage and current only. There are several reasons for why it is desired to eliminate the speed and position sensors, traditionally optical or electromagnetic resolvers measuring the position, or tachogenerators measuring the speed [27, p 25]. Some common gains are that the robustness and the reliability of the machine is increased, and that the required maintenance is reduced. Even when a position sensor is installed, it may be desirable to be able to operate sensorless. The machine can then continue to operate in the case of a failure in the sensor. This is especially desirable for larger machines, such as synchronous machines at hydro power plants, where the costs and consequences of a shut down are large. For smaller machines, gains such as reduced cost, lower mass and less wires are more desirable. If the goal of the sensorless operation is to reduce the cost, the equipment necessary to perform the position and speed estimation, such as processors and high quality current and voltage measurement devices, of course have to be cheaper than the sensor which they replace. Several techniques have been developed to achieve sensorless operation, but driving through zero speed is still a well known problem as many of the techniques rely on the induced back emf in some way or another [9]. Methods that are robust enough to perform well through zero speed usually have drawbacks such as cost and parameter dependency [6]. This master‘s thesis will present results from parameter sensitivity analysis of the two most common models used to estimate the stator flux linkage in the machine, the voltage model and the current model. It will also present a method for estimating the rotor position, based on the estimated stator flux linkage. The behaviour of the machine and problems encountered during sensorless

operation and when driving through zero speed will be investigated and documented. Methods to avoid these problems will also be suggested. Finally the current model and voltage model will be combined to obtain a more robust and less parameter sensitive closed loop observer, to improve the sensorless operation through zero speed.

1.2 Structure of the Thesis

Initially some fundamental theory about electric drives used in this thesis is presented. The most important findings from the specialisation project, which this master's thesis is a continuation of, is also presented [4]. In the specialisation project, the equations and the structure of the control system used in this thesis was developed and implemented in Simulink. The current model and the voltage model, which are the two flux estimators used in this work, are then presented. The text is then divided into the following main parts: Steady state analysis and dynamic analysis of the flux estimators, analysis of the sensorless control, and a section about how the two models can be combined to improve the sensorless operation at low speeds. Theory necessary to understand and analyse the results, together with the results, analysis and discussions of the results are presented along the way, in the relevant sections. Towards the end, a final discussion will be presented. In this section it will be discussed what the most important results are, what could have been done differently to make the analysis even more complete, and which possible sources of error that are present. Finally, a conclusion is presented with recommendations for further work.

2 Theory

In this section, fundamental theory about the synchronous machine, and main findings from the specialisation project of Magnus Bolstad will be presented [4]. This includes principles and equations that are required to describe the theory in this master thesis. Derivations performed in the specialisation project is summarised in the appendix of this master's thesis, but it is referred to the specialisation project thesis for a more detailed explanation [4].

2.1 The Synchronous Machine

The electric machine investigated in this work is a three phase, salient pole synchronous machine. The stator windings are supplied by sinusoidal voltages, symmetrically displaced by 120 °. The machine is magnetised by a field winding on the rotor, separately excited by a DC source through slip rings. The machine is illustrated in figure 2.1, where the dq coordinate system is attached to the rotor. The dq coordinate system is attached to the rotor, with the d axis aligned along the same axis as the peak of the flux from the field winding. Short circuited damper windings are mounted in the rotor along both the direct axis and along the quadrature axis to prevent non synchronised operation. The parameters of the machine investigated is summarised in table 4 in appendix A. The reactances are given for rated operation. The $\alpha\beta$ coordinate system is a static reference frame, with the α axis aligned along the phase a axis, and with the β axis aligned 90 ° ahead of the α axis. While discussing control methods, a third coordinate system is introduced, the rotating AB coordinate system, where the the A axis is aligned along the stator flux linkage, and the B axis 90 ° ahead.

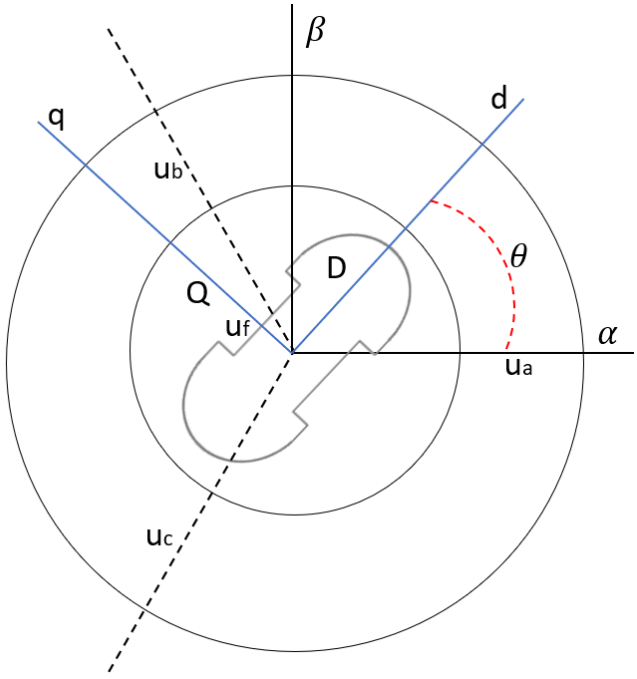

Figure 2.1: dq-modelling of the synchronous motor with damper windings

2.2 Voltage Equations

Any electrical motor with stator windings and rotor windings can be represented by the voltage equations 2.1 and 2.2:

$$U_s = R_s I_s + \frac{d\Psi_s}{dt} \tag{2.1}$$

$$U_r = R_r I_r + \frac{d\Psi_r}{dt} \tag{2.2}$$

The first term is the voltage drop in the winding, while the second term is the induced back emf. The voltage equations for each of the six windings is then expressed as:

$$U_{sa} = R_s I_{sa} + \frac{d\Psi_{sa}}{dt} \qquad U_f = R_f I_f + \frac{d\Psi_f}{dt}$$

$$U_{sb} = R_s I_{sb} + \frac{d\Psi_{sb}}{dt} \qquad U_D = R_D I_D + \frac{d\Psi_D}{dt}$$

$$U_{sc} = R_s I_{sc} + \frac{d\Psi_{sc}}{dt} \qquad U_Q = R_Q I_Q + \frac{d\Psi_Q}{dt}$$

The flux linkages are given by $\Psi = LI$. As the reactances, and thus also the flux linkages are position dependent, the Park transformation is applied to transform the flux linkages, currents and voltages into a synchronously rotating dq reference frame. This eliminates the periodic changes in flux linkages due to saliency and rotation, and hence the voltage equations become independent of time [17, p 434-438]. The transformation to the dq coordinate system is also convenient as the magnetic field and the torque of the machine is then easier to regulate by vector control. In this work, the synchronously rotating dq reference frame is aligned along the rotor of the machine. By assuming a healthy 3-phase system, where the zero current can be neglected, the transformation is performed by multiplying all phasor quantities by the transformation matrix $\mathbf{T}$:

$$\mathbf{T} = \begin{bmatrix} cos(\theta) & cos(\theta - 120^{\circ}) & cos(\theta - 240^{\circ}) \\ -sin(\theta) & -sin(\theta - 120^{\circ}) & -sin(\theta - 240^{\circ}) \end{bmatrix} \tag{2.3}$$

The dq currents are then expressed by:

$$\mathbf{i_{dq}} = \mathbf{T}\mathbf{i_{abc}} \tag{2.4}$$

Expressing the voltage equations in the dq reference frame, as explained by Ned Mohan in the textbook "Advanced Electric Drives", and by dividing all equations by the base values, the per unit voltage equations are obtained [18, p 35-38,153-154]:

$$u_d = r_s i_d + \frac{1}{\omega_n}\frac{d}{dt}\psi_d - n\psi_q \tag{2.5}$$

$$u_q = r_s i_q + \frac{1}{\omega_n}\frac{d}{dt}\psi_q + n\psi_d \tag{2.6}$$

$$u_f = r_f i_f + \frac{1}{\omega_n}\frac{d}{dt}\psi_f \tag{2.7}$$

$$0 = r_D i_D + \frac{1}{\omega_n}\frac{d}{dt}\psi_D \tag{2.8}$$

$$0 = r_Q i_Q + \frac{1}{\omega_n}\frac{d}{dt}\psi_Q \tag{2.9}$$

The flux linkages in the equations are expressed as:

$$\psi_d = x_d i_d + x_{md}(i_D + i_f) \tag{2.10}$$

$$\psi_q = x_q i_q + x_{mq} i_Q \tag{2.11}$$

$$\psi_f = x_f i_f + x_{md}(i_D + i_d) \tag{2.12}$$

$$\psi_D = x_D i_D + x_{md}(i_d + i_f) \tag{2.13}$$

$$\psi_Q = x_Q i_Q + x_{mq} i_q \tag{2.14}$$

2.3 Alternative pu Model

The equations above contains currents in the damper windings, which are not measurable quantities. In the master thesis of Oddmund Grøvan [8], an alternative pu model of the voltages and fluxes was developed, resulting in the same equations as in [28]. The equations were modified further in the specialisation project by Magnus Bolstad, such that the voltage equations contained derivative terms of one current only [4]. New constants were also introduced to simplify the equations. The motivation for these manipulations was to obtain equations that could be used to tune the flux and current controllers by known techniques such as modulus optimum and symmetrical optimum [22, p 102-103]. In this section a summary will be given, while the full derivation from the specialisation project is repeated in appendix C [4]. The following constants are defined:

$$\sigma_{dD} = 1 - \frac{1}{(1+\sigma_d)(1+\sigma_D)} \tag{2.15}$$

$$\sigma_{Df} = 1 - \frac{1}{(1+\sigma_f)(1+\sigma_D)} \tag{2.16}$$

$$\sigma_{qQ} = 1 - \frac{1}{(1+\sigma_q)(1+\sigma_Q)} \tag{2.17}$$

$$r_d^{`} = r_s + \frac{r_D}{(1+\sigma_D)^2} \tag{2.18}$$

$$r_q^{`} = r_s + \frac{r_Q}{(1+\sigma_Q)^2} \tag{2.19}$$

$$r_f^{`} = r_f + \frac{r_D}{(1+\sigma_D)^2} \tag{2.20}$$

$$r_d^{\text{“}} = r_s + (1 - k_{fD})\frac{r_D}{(1+\sigma_D)^2} \tag{2.21}$$

$$r_f^{\text{“}} = r_f + (1 - k_{dD})\frac{r_D}{(1+\sigma_D)^2} \tag{2.22}$$

$$k_{fD} = \frac{\sigma_D}{\sigma_f\left(1 + \sigma_D + \frac{\sigma_D}{\sigma_f}\right)} \tag{2.23}$$

$$k_{dD} = \frac{\sigma_D}{\sigma_d\left(1 + \sigma_D + \frac{\sigma_D}{\sigma_d}\right)} \tag{2.24}$$

$$\sigma_d^{\text{“}} = \sigma_{dD} - k_{fD}\frac{\sigma_D}{(1+\sigma_d)(1+\sigma_D)} \tag{2.25}$$

$$\sigma_f^{\text{“}} = \sigma_{Df} - k_{dD}\frac{\sigma_D}{(1+\sigma_D)(1+\sigma_f)} \tag{2.26}$$

$$\psi_{Rd} = \frac{\psi_D}{1+\sigma_D} \tag{2.27}$$

$$\psi_{Rq} = \frac{\psi_Q}{1+\sigma_Q} \tag{2.28}$$

$$r_{Rd} = \frac{r_D}{(1+\sigma_D)^2} \tag{2.29}$$

$$r_{Rq} = \frac{r_Q}{(1+\sigma_Q)^2} \tag{2.30}$$

$$x_{Md} = \frac{x_{md}}{1+\sigma_D} \tag{2.31}$$

$$x_{Mq} = \frac{x_{mq}}{1+\sigma_Q} \tag{2.32}$$

It is seen that the time constants T_D and T_Q can be written as

$$T_D = \frac{x_{Md}}{\omega_n r_{Rd}} \tag{2.33}$$

$$T_Q = \frac{x_{Mq}}{\omega_n r_{Rq}} \tag{2.34}$$

The final expressions obtained is presented in 2.35 to 2.42 below:

$$u_d = r_d^{\text{“}} i_d + \frac{\sigma_d^{\text{“}} x_d}{\omega_n}\frac{di_d}{dt} - (1-k_{fD})\frac{r_{Rd}}{x_{Md}}\psi_{Rd} + (1-k_{fD})r_{Rd}i_f + k_{fD}(u_f - r_f i_f) - n\psi_q \tag{2.35}$$

$$u_q = r_q^{\text{‘}} i_q + \frac{\sigma_{qQ} x_q}{\omega_n}\frac{di_q}{dt} - \frac{r_{Rq}}{x_{Mq}}\psi_{Rq} + n\psi_d \tag{2.36}$$

$$u_f = r_f^{\text{“}} i_f + \frac{\sigma_f^{\text{“}} x_f}{\omega_n}\frac{di_f}{dt} - (1-k_{dD})\frac{r_{Rd}}{x_{Md}}\psi_{Rd} + (1-k_{dD})r_{Rd}i_d + k_{dD}(u_d - r_s i_d + n\psi_q) \tag{2.37}$$

$$\frac{d\psi_{Rd}}{dt} = -\frac{\psi_{Rd}}{T_D} + \frac{x_{Md}}{T_D}(i_d + i_f) \tag{2.38}$$

$$\frac{d\psi_{Rq}}{dt} = \frac{-\psi_{Rq}}{T_Q} + \frac{x_{Mq}}{T_Q} i_q \tag{2.39}$$

$$\psi_d = x_d \sigma_{dD} i_d + \psi_{Rd} + x_{Md}\sigma_D i_f \tag{2.40}$$

$$\psi_q = \sigma_{qQ} x_q i_q + \psi_{Rq} \tag{2.41}$$

$$\psi_f = \sigma_{Df} x_f i_f + \psi_{Rd} + x_{Md}\sigma_D i_d \tag{2.42}$$

These expressions contain measurable stator currents only, as the currents in the damper windings are eliminated. It is also evident that the voltages and currents are related by a first order transfer function, which were used for tuning the current and flux controllers, and some decoupling terms that were used as feed forward to the output of the controllers. These expressions are presented in appendix C. The decoupling terms are necessary to counteract disturbances on the controllers, caused by fluxes set up in other windings. The expressions obtained are estimated based on equation 2.38 to 2.41, and they yielded satisfying controller parameters that are also used in this thesis.

2.4 Torque Control

The torque control of the motor is performed with the goal of achieving maximum torque per ampere, like in the specialisation project [4]. This is obtained by controlling the power factor to unity. This is possible for the separately synchronous machine as the magnetisation, and all reactive power, is supplied through the field winding. By minimising the required amount of current, losses in supplying lines and cables are reduced, but the main advantage of this technique is that the converters have to handle a lower amount of current. It is then possible to use converters rated for lower power to realise the control system, which is beneficial from an economical point of view. This technique was especially advantageous in the past, when the prices of power electronic converters were higher.

It has been shown by Bühler that the angle of the stator voltage with respect to the q axis, the pole wheel angle δ, is calculated by equation 2.43 during steady state [5, p 18]. In this derivation, which is repeated in appendix D, the stator resistances are neglected.

$$\delta = \frac{\tau_e x_q}{\psi_s^2} \tag{2.43}$$

From equation 2.1, it is observed that if the resistance is neglected, the voltage vector is 90° ahead of the stator flux linkage. Hence, to obtain a power factor of either one or minus one, the current vector is placed 90° in front of, or behind of the stator flux linkage. The possible operations during steady state is illustrated in figure 2.2, which is the phasor diagram of equation 2.5 and 2.6. Positive direction of rotation is counter clockwise when the speed is positive speeds, while it is clockwise when the speed is negative. Figure 2.2a and 2.2d illustrate motor operation, while figure 2.2b and 2.2c illustrate generator operation. As the stator voltage space vector is 90° in front of the stator flux linkage vector, δ also corresponds to the angle of the stator flux linkage with respect to the d axis.

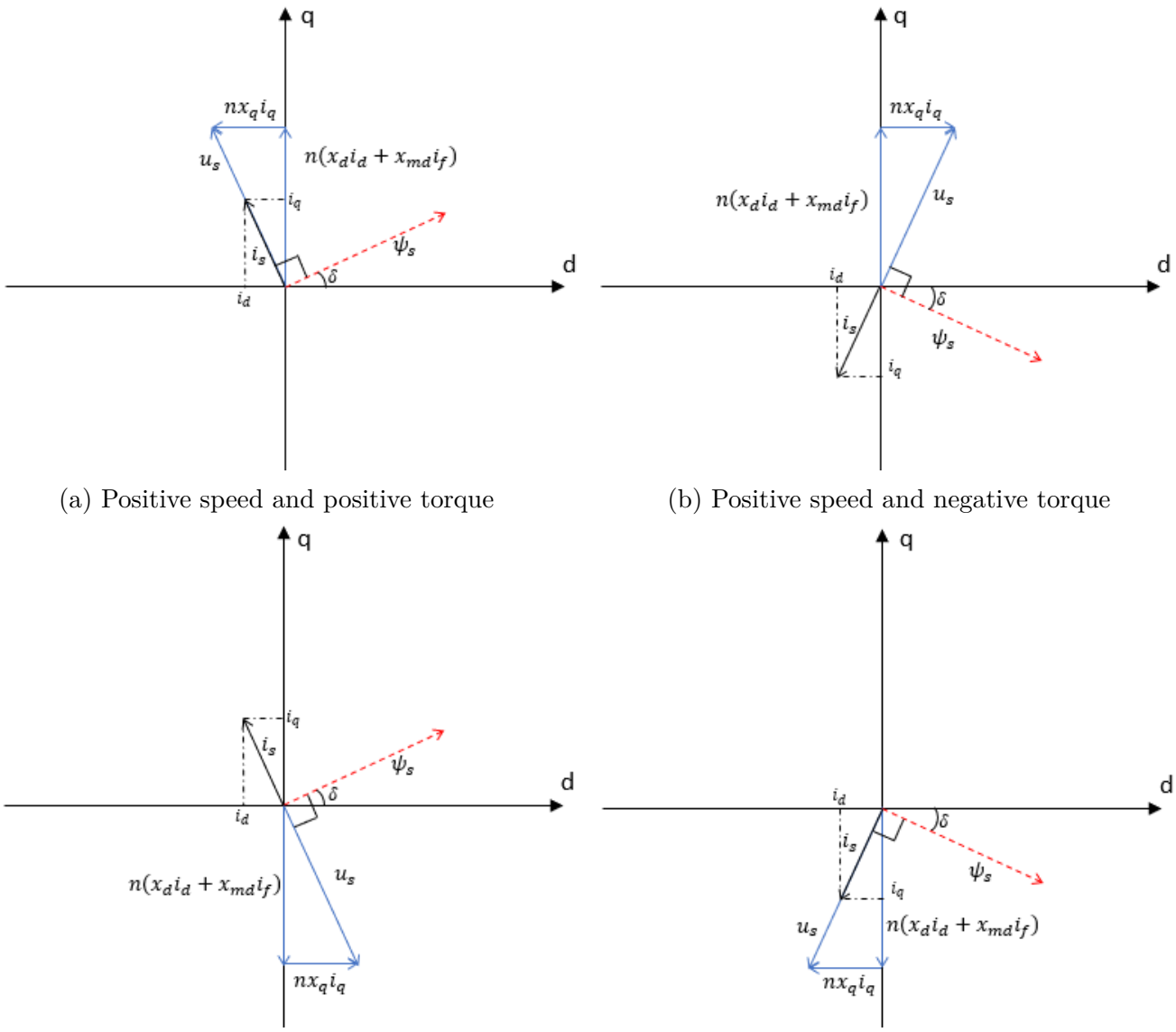

(a) Positive speed and positive torque

(b) Positive speed and negative torque

(c) Negative speed and positive torque

(d) Negative speed and negative torque

Figure 2.2: Phasor diagram during steady state

As seen from the phasor diagram in figure 2.2, it is not possible to obtain the current vector in phase with the voltage vector when the applied torque and the speed have opposite signs. Hence it is chosen to align the current 180 ° apart from the voltage vector instead during generator operation. Unity power factor with negative sign is then achieved.

The electromechanical torque generated in pu is given by equation 2.44, where the AB coordinate system is an arbitrary coordinate system [18, p 145].

$$\tau_{em} = \left[\psi^k_{sA} i^k_{sB} - \psi^k_{sB} i^k_{sA}\right] \tag{2.44}$$

The superscript indicates which coordinate system the quantity is referred to. By aligning the A-axis along the stator flux linkage vector, the following expressions are valid:

$$k = \psi_s \tag{2.45}$$
$$\psi_{sB}^k = 0 \tag{2.46}$$
$$\psi_{sA}^k = \psi_s \tag{2.47}$$
$$i_{sA} = 0 \tag{2.48}$$
$$i_{sB} = i_s \tag{2.49}$$

equation 2.44 is then reduced to

$$\tau_{em} = \psi_s i_s \tag{2.50}$$

The stator current amplitude is hence calculated by equation

$$i_s = \frac{\tau_{ref}}{\psi_s} \tag{2.51}$$

From equation 2.51 it is evident that if the stator flux linkage amplitude is estimated higher than the actual stator flux linkage, the stator current amplitude will reduce, resulting in a too low generated torque. Expressing the torque equation, 2.44, in the dq reference frame, equation 2.52 is obtained:

$$\tau = (x_d - x_q) i_d i_q + x_{md} i_f i_q \tag{2.52}$$

Figure 2.2 reveals that the d-axis current is negative for all operating areas. As the q-axis current is positive for positive torques and negative for negative torques, and as $x_d > x_q$, it is evident from equation 2.52 that the saliency of the machine will give a torque contribution in the opposite direction of the torque reference. It is hence concluded that the unity power factor control applied to the machine does not fully utilise the saliency of the machine, and it may hence not be the most efficient control philosophy if maximum torque is desired.

2.5 Simulation Model and Control System

To analyse the sensorless control and the dynamics of the machine, the machine is modelled and simulated in Simulink by MATLAB, using the ode23tb solver. The maximum time step is 100 μs, and the reset method is robust. The mechanical load is modelled by equation 2.53, which is the typical characteristic of a pump. The constant k is determined such that the machine supplies nominal power at nominal speed.

$$\tau_{load} = k\omega_{mech}^2 \tag{2.53}$$

The advantage of running simulations, compared to performing real life experiments in the laboratory is that the real stator flux linkage is available while simulating. The flux models can then easily be analysed for different scenarios by comparing the estimated flux linkage with the real one. This also makes it easier to find the sources of error when sensorless control lack accuracy, or when it fails. The drawback of simulations compared to real life experiments is that no model perfectly describes the reality, and that they are time consuming to run. This limits the number of scenarios investigated considering combinations of erroneously estimated parameters, modifications of estimators, and operations.

The control structure was set up and tuned in the specialisation project, based on a model where the machine equations, the converters, the PWM and some controllers were already implemented and prepared by supervisor Roy Nilsen [4]. A brief summary of the structure will here be presented. An overview of the model is presented in figure 2.3. The stator voltage is supplied by a three phase inverter, while the field voltage is supplied by a DC-DC full bridge converter. Both of the converters are PWM controlled, with a switching frequency of 3 kHz. The duty ratio is determined by the control structure in the "SM Motor Control" block. A third harmonic signal is injected to the control signal of the stator current inverter to increase the linear range by 15 % [22, p 85]. In the specialisation project it was found that the blanking time in the inverter had to be reduced from 1 μs to 0.1 μs, to reduce ripple in the d-axis current that caused simulation problems. This blanking time may be too short to be used in a real set up, due to the risk of short circuiting an inverter leg [4]. Sampling is performed at each top and each bottom of the PWM signal, yielding a sampling frequency of $\frac{T_{tri}}{2}$, where T_{tri} is the period of the triangular wave in the PWM. In this work this yields a sampling frequency of 6 kHz. This is known as synchronised sampling, or asymmetrical regular sampled PWM. Synchronised sampling is chosen because the ripple is zero at these instants at the triangular wave, due to the zero crossing of the converter [23].

Simplified block diagrams of the simulation model and the control system are presented in figure 2.4 and figure 2.5 respectively. The outer layer of control system implemented in Simulink is also presented in the end of the appendix, on page 146. The control systems act as follows: A torque reference signal is supplied to the model. The stator current reference is calculated based on the torque reference and the estimated stator flux linkage, as explained in section 2.4. As the reference of the stator current is calculated in the dq- coordinate system, while the measured stator current is relative to the stationary reference frame, the estimated rotor position is necessary to perform a dq transformation. The desired d- and q axis currents are then realised by PI current controllers, with moving average filtered measurements as feedback. The duty ratio to the inverter is then determined. The duty ratio to the full bridge converter, supplying the field voltage, is determined by a PI field current controller. The reference signal to the field current controller, limited to 3 pu to avoid burning out the winding, is obtained from a flux controller. The flux controller is a PI controller, with the estimated stator flux linkage magnitude as feedback, aiming for a stator flux linkage of 1 pu in the normal operating region. The stator flux linkage of 1 pu is chosen to reduce the current required to generate a given torque, as seen from equation 2.51. This reduces the losses and the required inverter rating. A stator flux linkage above 1 pu should be avoided due to possible saturation or overmodualtion in the inverter. Hence, if the back emf exceeds $1 - r_s$ pu, the stator flux linkage reference is reduced as the inverse of the rotating speed. This is known as field weakening.

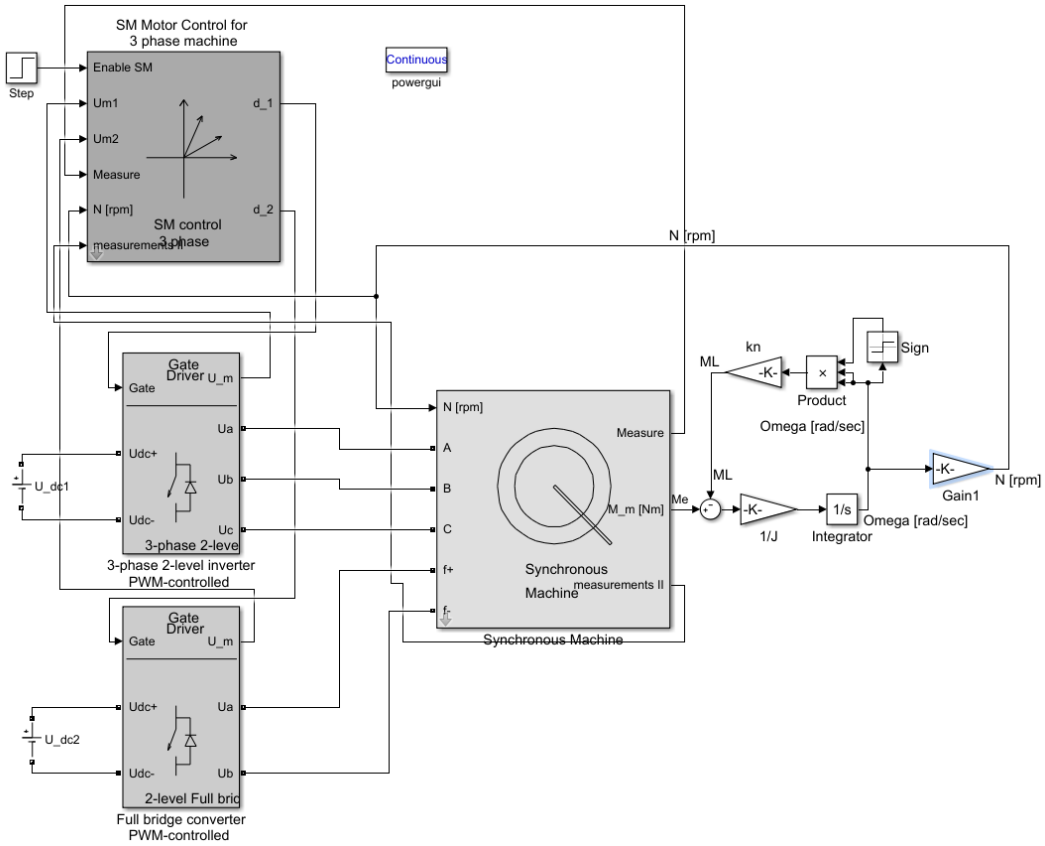

Figure 2.3: An overview of the simulation model

These controllers are analysed in detail, and properly tuned in the project thesis of Bolstad [4]. The same values are used in this work, and they are thus summarised in table 6 in appendix B. The expressions obtained for tuning of the controllers are also repeated in appendix E. As the stator currents are controlled based on the torque reference, the drive is current controlled. This way of controlling the machine is known as indirect torque control, ITC, by Kaukonen in his doctoral thesis [13]. An advantage with this method is that all currents will become smooth and controllable, while a drawback with the method is that knowledge about the rotor position is necessary to transform the quantities between the stationary and the rotating reference frame. Hence, most of the sensorless drives in the literature are controlled by direct torque control, DTC, or by direct flux linkage control, DFLC, where knowledge about the rotor position is not required. In DTC the flux is controlled directly, and hence DTC achieves a more accurate and rapid flux control than ITC. The obtained controller parameters yielded satisfying control, as illustrated by the step responses in figure 2.6, where a step of 1 pu is applied. Accurate knowledge of all machine parameters and rotor position is assumed in figure 2.6.

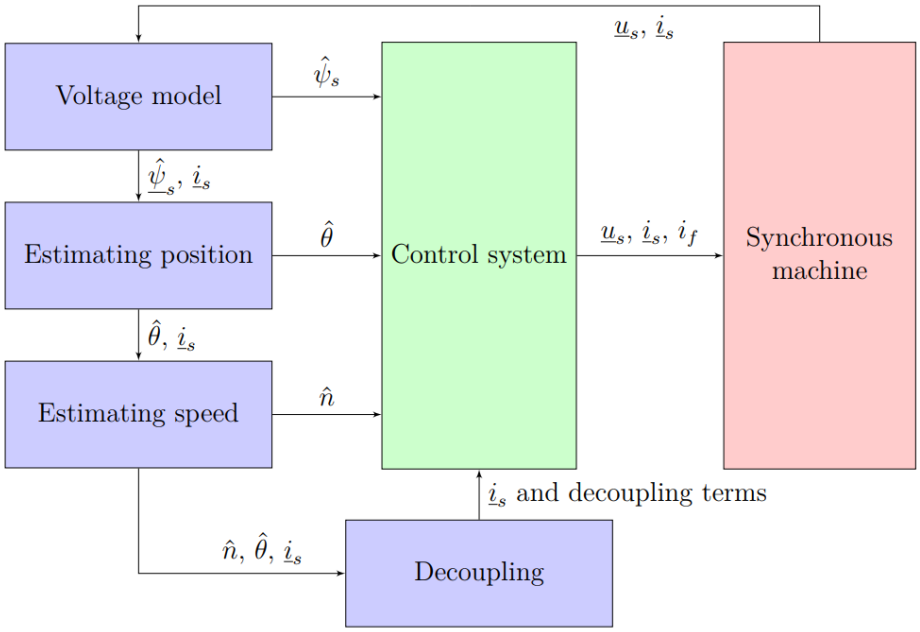

Figure 2.4: Simplified overview of the simulation model

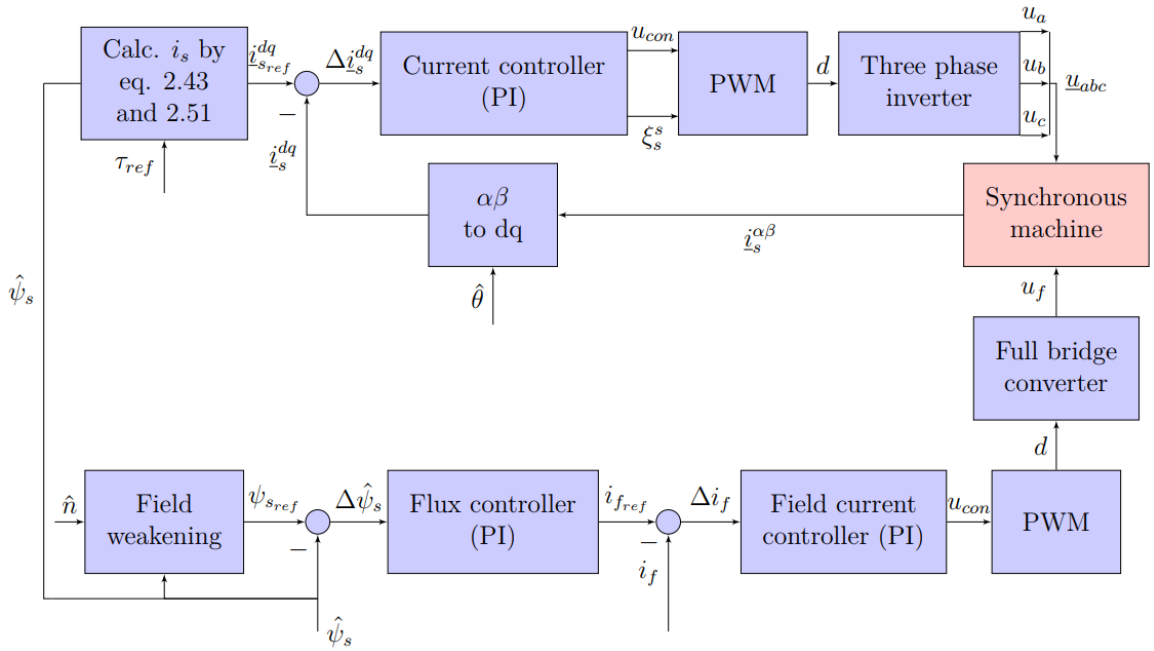

Figure 2.5: Simplified overview of the control system

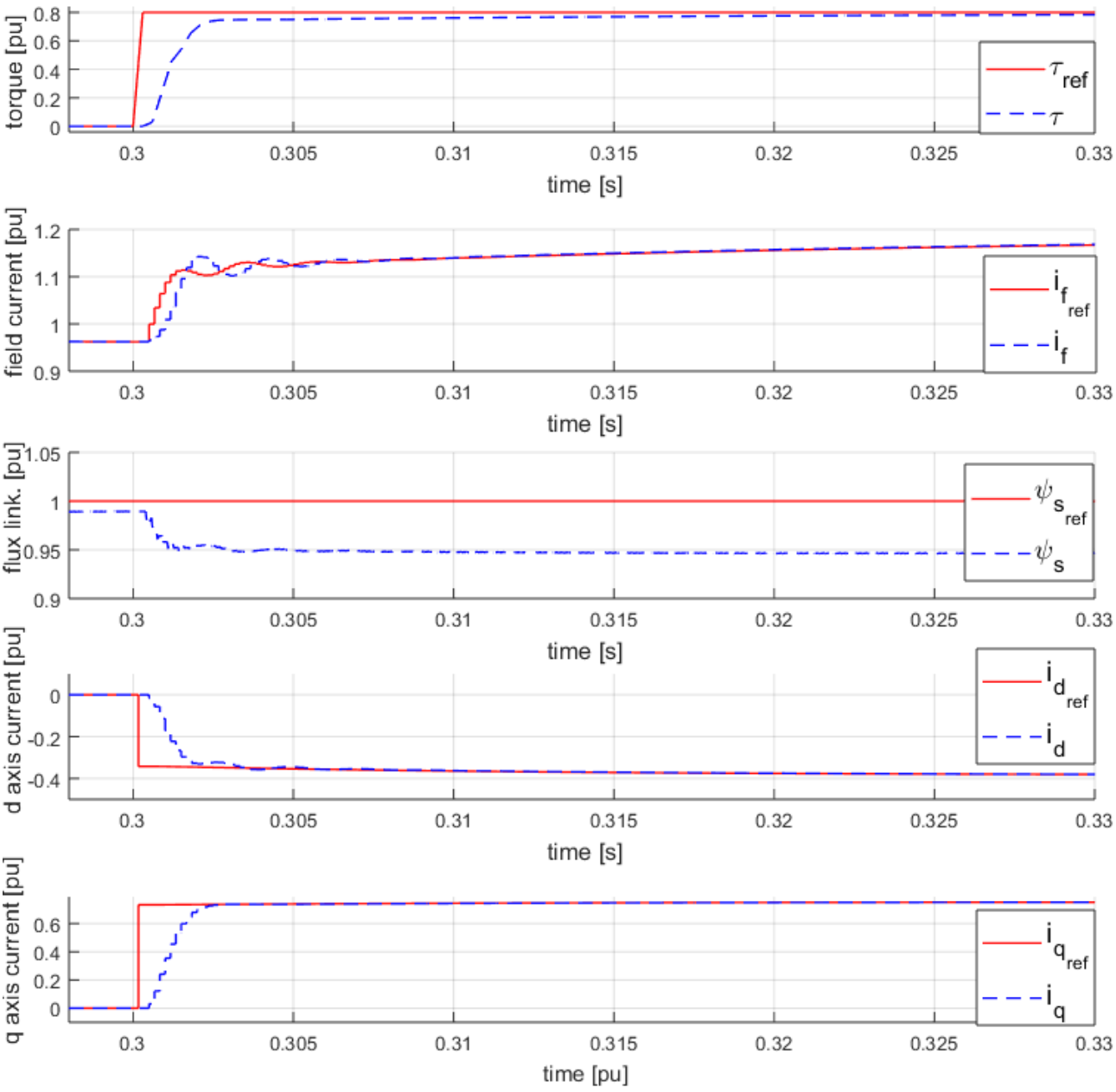

Figure 2.6: Responses after step in torque reference

From figure 2.6, it is evident that a small error remains between the stator flux linkage and its reference. This error is removed entirely after approximately 1 s, as illustrated in figure E.1 in appendix E, where some of the same results as in figure 2.6 is presented, but now for a longer time range.

3 Stator Flux Linkage Estimation

The estimation of the rotor position and speed is based on an estimated stator flux linkage. There are several ways of obtaining an estimate of the stator flux linkage, with the current model and the voltage model as the most common methods. The methods for estimating the flux linkage are also known as observers or state estimators, as they estimate a state of the model. In this section the current model and the voltage model will be explained in detail. It will become evident how the two models are sensitive to different parameters and states of the machine. This is summarised in table 1, where "x" indicates dependency.

Table 1: Dependency table

Parameter	Symbol	Influence on	
		Voltage model	Current model
stator resistance	r_s	x	
damper winding D resistance	r_D		x
damper winding Q resistance	r_Q		x
field winding resistance	r_f		
d-axis reactance	x_d		x
q-axis reactance	x_q		x
field winding reactance	x_f		
damper winding D reactance	x_D		x
damper winding Q reactance	x_Q		x
stator leakage reactance	x_{s_σ}		x
stator voltage	u_s	x	
stator current	i_s	x	x
field current	i_f		x
rotor position	θ		x
rotor speed	n	x	

3.1 Current Model

The current model utilises knowledge of the currents of the motor to estimate the stator flux linkage. Using equation 2.40 and 2.41, the stator flux linkage is obtained as:

$$\underline{\psi_s} = \psi_d + j\psi_q$$

From equation 2.40 and 2.41 it is evident that the accuracy of the current model depends on the accuracy of the estimated inductances in the machine. The damper winding flux linkages are estimated from equation 2.38 and 2.39, and depend thus on the the resistances in the damper windings during transients. As the calculations are performed in the dq-reference frame, the rotor position is required as input to the model. The current model is sometimes considered as sensitive to speed, based on the assumption that the error in speed measurement is proportional to the

speed [19]. This makes the current model more accurate in the lower speed region. If it is assumed that the sensor measures the speed perfectly, which will be the case when using speed or position sensor in this work, the sensitivity of the current model will be independent of the speed in the normal operating area. It will however be illustrated later, in section 4, that the current model is affected by field weakening. Field weakening is enabled as the speed exceeds 1 pu, and hence the current model depends indirectly on the speed.

The current model requires good knowledge of the inductances and their saturation characteristics, as these parameters have large influence on equation 2.38- 2.42. From equation 2.38- 2.42 it is also obvious that if the flux linkages through the damper windings are constant, which is the case during steady state, the damper winding resistances will not affect the stator flux linkage estimate. This is illustrated in the simulation results presented in figure 3.1, where a constant torque reference of 0.3 pu is applied after the initialisation period. A simulation was run with correctly estimated rotor resistances, and another one where both the stator resistance and the damper winding resistances were estimated 50 % below the actual value. All other parameters were assumed correctly estimated, and the rotor position was measured. From figure 3.1 it is evident that the estimated flux follows the measured value perfectly throughout the whole simulation when all parameters are correctly estimated, while an error of up to 0.3 pu occurs during the transient when the damper winding resistances are underestimated. When the rotor flux linkages ψ_D and ψ_Q stabilises, steady state operation occurs, and the stator flux linkage is estimated perfectly for both scenarios. The inductances are not very sensitive to temperature [19], and hence the current

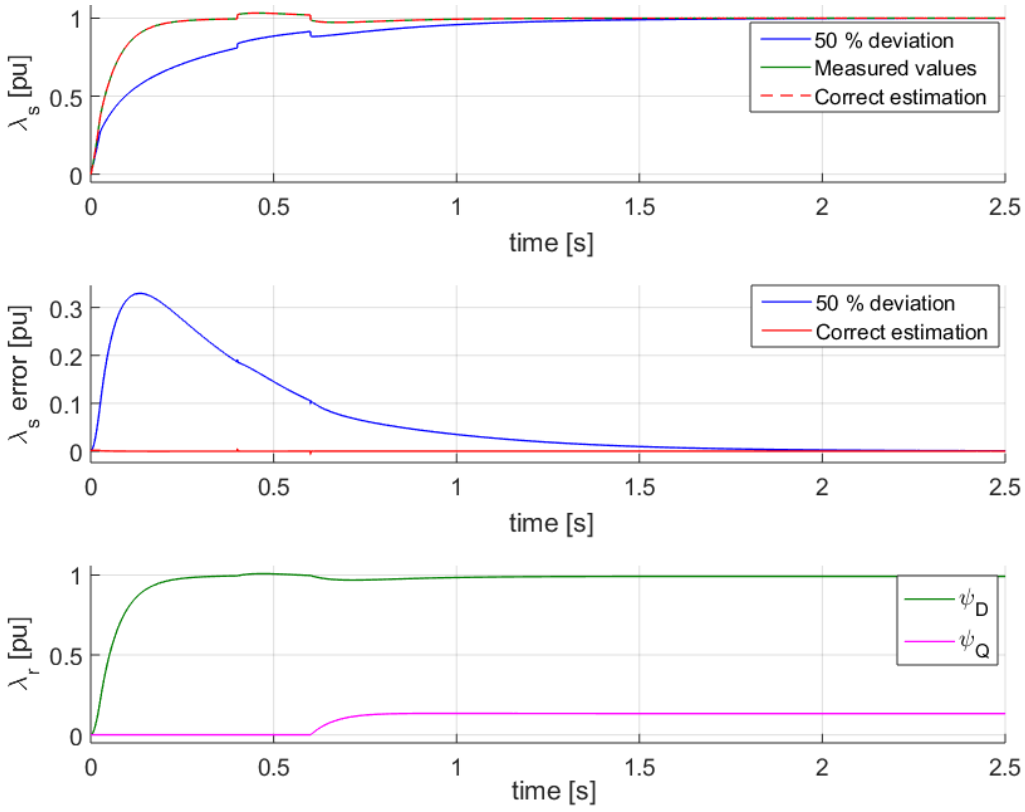

Figure 3.1: Stator flux estimation with erroneous estimated rotor resistances

model is considered as independent of the temperature during steady state.

3.2 Voltage Model

The voltage model is based on utilising both the measured stator voltage and the measured stator current to obtain an estimate of the stator flux linkage. The stator flux linkage is found by solving equation 2.1 for the stator flux linkage, as expressed in equation 3.1. The integration is performed in the stationary reference frame. This model is independent of the inductances, but it depends heavily on the stator resistance. As no rotor position is required as input, this model is heavily used when running sensorless. The model is also easy to use, as the only parameters required are the stator resistance, and the measured voltages and currents. On the other hand, the integrated back emf is low for low rotational speeds, and hence the flux linkage estimation may be less accurate during operation around zero speed. This is a well known problem that will be investigated in this thesis.

$$\underline{\psi}_s = \int_0^t (\underline{u}_s - r_s \underline{i}_s) dt \tag{3.1}$$

Since the rotor position is not required to use the voltage model, this method will be used in this thesis when the rotor is moving. The current model will be used during magnetisation and initialisation of the machine, where the rotor is at stand still, and the position is known. When a torque reference is applied to the machine, the voltage model is activated, and the estimated flux linkage obtained from the current model during initialisation is used as initial value.

When all parameters in equation 3.1 are known with high accuracy, the stator flux linkage is estimated with high accuracy. However, if there are inaccurate voltage or current measurements, or if the estimated stator resistance deviates from the actual resistance in the machine, the amplitude of the stator flux linkage will be erroneously estimated. An inaccurate estimate of the stator flux linkage will further cause an erroneous input to the control system, resulting in an error in the generated torque in the machine. Another parameter affecting the voltage model is the speed of the rotor. How sensitive the current model and the voltage model are to different parameters in different operating scenarios is investigated in this work.

3.3 Position and Speed Estimation

As the drive is current controlled, the rotor position is required. The rotor position can be estimated by measuring the phase and the amplitude of the induced ripple in the stator current, due to the ripple in field winding current, as explained by Alaküla [1]. In this work however, the rotor position relative to the stator phase a axis, θ, will be estimated based on the estimated stator flux linkage. The estimation of the rotor position is based on the expression developed in the specialisation project of Magnus Bolstad [4]. When the stator flux linkage, the stator current, and their angles with respect to the stator phase a-axis is known, the position of the rotor can be found by trigonometry. Equation 3.2 was developed in the project thesis based on the properties illustrated in figure 3.2. The full derivation of the expression is repeated in appendix G. The expression was discretised by the trapezoidal rule, also known as the Tustin method, and implemented in Simulink [2, p 477-484].

$$sin(\xi_s^s - \theta) = \frac{\left[\sigma_{qQ}x_q + \frac{x_{Mq}}{1+T_Q s}\right]}{\psi_s} i_s sin(\epsilon_s^s - \theta) \tag{3.2}$$

In the specialisation project, equation 3.2, which is an implicit equation, was manipulated further to an explicit equation bu using trigonometric identities [4].

$$\begin{aligned} tan(\theta) &= \frac{sin(\theta)}{cos(\theta)} \\ &= \frac{sin(\xi_s^s) - \frac{\left[\sigma_{qQ}x_q + \frac{x_{Mq}}{1+T_Q s}\right]}{\psi_s} i_s sin(\epsilon_s^s)}{cos(\xi_s^s) - \frac{\left[\sigma_{qQ}x_q + \frac{x_{Mq}}{1+T_Q s}\right]}{\psi_s} i_s cos(\epsilon_s^s)} \end{aligned} \tag{3.3}$$

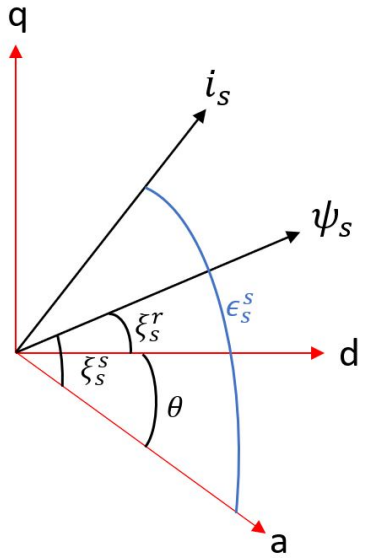

Figure 3.2: Estimated and measured quantities related to the different coordinate systems

It turned out that equation 3.3, which was used for estimating the rotor position during the specialisation project yielded good results during steady state, but it lack accuracy during dynamics. The reason for this, and why the explicit equation is not valid, was found during the work with this master's thesis. This is thoroughly described in appendix G.2.

As equation 3.2 is an implicit equation, it is solved by an approximation. The rotor position from the last sample is used as input to the right hand side of the equation, making it possible to solve for θ on the left hand side. To compensate for this delay in the input position, the product of the sampling time and the estimated speed of the last time step, which is approximately equal to the angular distance travelled by the rotor since the last sample, is added to the input. This algorithm is illustrated as a block diagram i figure G.2 in appendix G. Another possible realisation, which was not chosen, is to solve the equation by iteration in MATLAB for each time step. When the rotor position is known, the speed is easily obtained by using the definition of differentiation:

$$\omega[k] \approx \frac{\theta[k] - \theta[k-1]}{T_{samp}} \tag{3.4}$$

To find the position, knowledge about the initial position is necessary. Methods for estimating the initial rotor position of separately excited machines has been developed and patented, e.g the method of by Blaschke and Dreiseitl, utilising a voltage step in the rotor winding and measuring the induced voltages in the stator windings [3]. In this thesis, freedom is given to rotate the rotor before starting from stand still, and hence it is possible to rotate the rotor to a known initial position, $\theta = 0$, before starting the sensorless operation. The initial position along the a-axis is achieved by applying a constant voltage vector along the a-axis during a short initialising period. This results in a period with a constant a-axis DC current, and a negative DC current of half the magnitude in the b-axis and the c-axis. This is implemented in the control structure by making the d-axis current reference equal to a constant value, while setting the rotor position input to the current controller equal to zero. The initialisation of the rotor is performed for 0.2 s only, to reduce the simulation time. In a real set up, this period should probably be longer, especially for larger machines. The rotor will move in an unpredictable direction during initialisation, which may be critical and not acceptable in some applications. The current model is used for estimating the stator flux linkage during this initialisation, as the speed is low. When the rotor has moved to its initial position, and the machine is properly magnetised, the torque reference is applied to the control systems.

In figure 3.3, the accuracy of equation 3.2 and 3.4, and how sensitive the expressions are to the torque reference applied is evaluated. The actual measured flux linkage is used as input to the model, and the model runs with sensors to avoid errors related to the flux linkage estimation. These analysis are performed because the estimated rotor position is used as input to the simulation model during sensorless operation, and it will hence influence all other position dependent results.

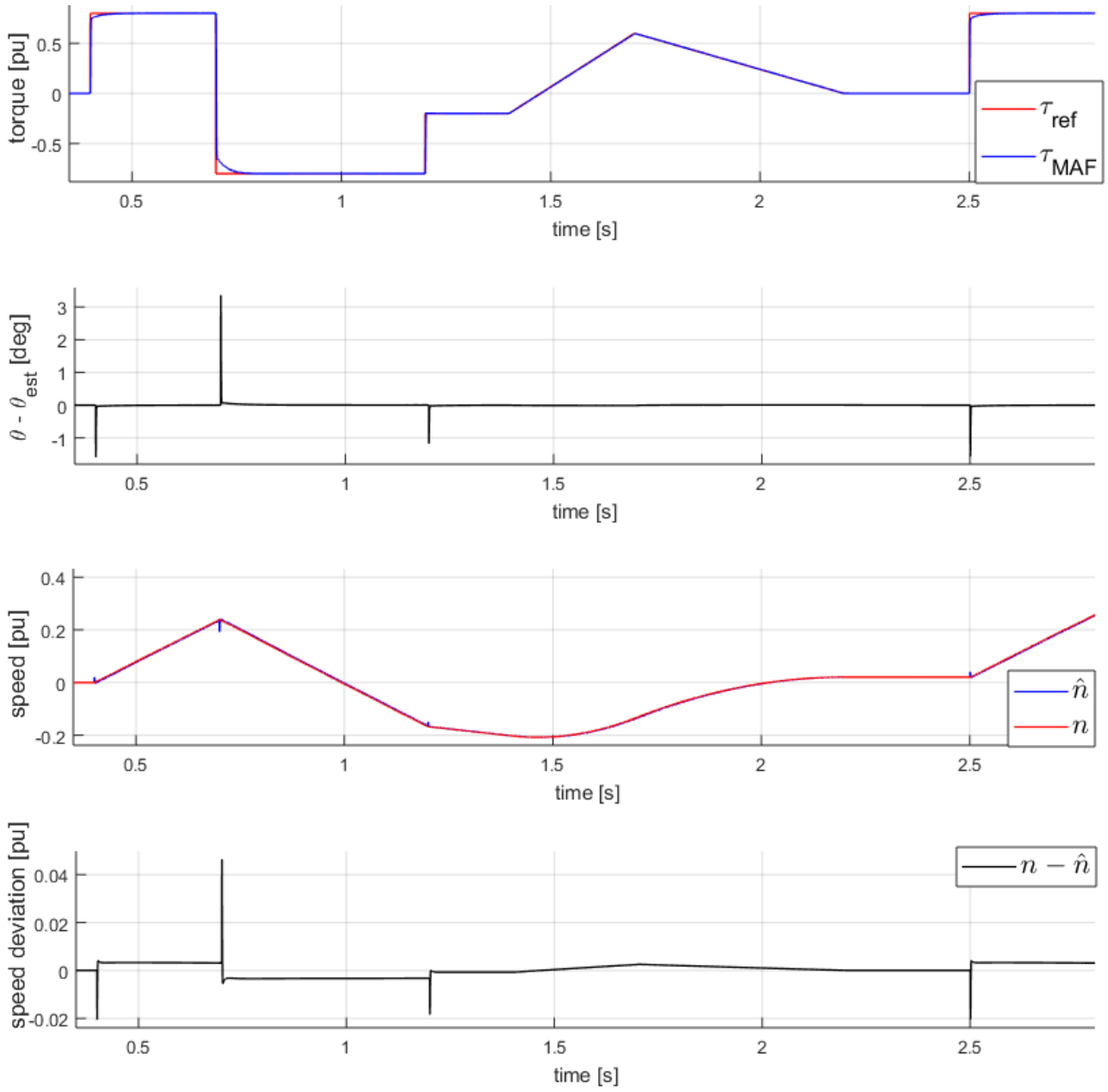

Figure 3.3: Evaluation of the rotor position estimation

From figure 3.3 it is confirmed that except from the spikes during steps in torque reference, the estimation of rotor position is accurate through the whole simulation. The dependence on the torque reference applied is negligible. The spikes has a short duration of 2.5-3 μs, and are due to similar spikes in the estimation of the q-axis current, $i_q = i_s sin(\epsilon_s^s - \theta)$. Delays in the system, or physical limitations such as the inertia of the machine, may be reasons for these short but significant errors. The speed is also estimated accurately, and even at the instants of steps in torque reference, the deviation from the actual speed is less than 0.05 pu. The spikes could be removed by using a slower filter at the output of the estimated position or speed, or by applying a more advanced technique to find an estimate of the speed, such as phase-locked loop. Care must

be taken if a slower filter is used, as it will cause a lag for all frequencies, which is not desired. All over, the estimation is considered as satisfying, and it is concluded that these expressions yield results accurate enough to control the machine sensorless.

3.4 Parameter Deviations

In this section the parameters affecting the sensorless operation, and the way deviations and errors in the estimated values occur is discussed. Inaccurate estimations of these parameters will influence both the tuning of the controllers, as the controller parameters are determined based on transfer functions of the system, and the flux linkage estimation, as discussed in section 3. This work will focus on the latter influence.

3.4.1 Resistances

The estimated stator resistance, r_s, is a very important parameter for estimating the stator flux linkage by the voltage model, as this value directly influences the integral in equation 3.1. An erroneously estimated value of this resistance will hence give erroneous flux linkage estimation. The rotor resistances in the damper windings, r_D and r_Q will affect the stator flux linkage estimated by the current model during transients, while during steady state operation they have no influence on this estimate.

The actual resistance in an electric machine is highly dependent on the temperature. The temperature in the windings increase with the loading of the machine, and hence it will vary during operation. If this is not accounted for during operation, erroneous flux linkage estimation will occur. The temperature dependence of the resistance is assumed to be linear, as given by equation 3.5:

$$R_T = R_{T_0}(1 + \alpha(T - T_0))))) \tag{3.5}$$

Where T is the temperature, T_0 is the reference temperature, R_{T_0} is the resistance at the reference temperature, and R_T is the actual resistance at the current temperature. How much the resistance changes with temperature is given by the material dependent coefficient α, which is $0.0038\,\frac{1}{K}$ for copper [24]. Figure F.1 in appendix F illustrates graphically how a resistance of 1 pu increases with temperature. The frequency dependent skin effect will also influence the resistances is some degree, but this effect is often assumed to be negligible compared to the influence by the temperature variations. As the temperature will vary during operation both in the stator and in the rotor, some correlation between the stator resistance, the damper winding resistances and the field winding resistance is expected. In high power applications, such as electric ship propulsion, temperature sensors are usually required on several locations in the motor. The estimated resistances are then updated during operation by expressions such as equation 3.5. However, as the temperature sensors may break down, or contain offsets, a sensorless control method that is less sensitive to the estimated resistances will increase the reliability of the drive.

3.4.2 Inductances

The stator reactances, x_d and x_q appears directly in equation 2.40 to 2.42, and indirectly in equation 2.38 and 2.39, and they hence influence the estimated flux linkage heavily when the current model is used. Erroneous estimated inductances, which affect the reactances, will hence give an erroneous estimated stator flux linkage. Variation of inductances during operation, due to saturation, is usually taken into consideration by updating the inductance values, based on operation point [13]. The saturation characteristic of electric machines can be found by performing off-line tests, also known as identification run. Hence, if the inductances are correctly estimated, and the saturation characteristic is known, they should not cause any problems during steady state operation. The inductances are assumed to be independent of temperature, as these variations usually can be neglected [19].

The reactances along the d- or q axis are expressed by

$$x_d = x_{md}(1 + \sigma_d) \tag{3.6}$$
$$x_q = x_{mq}(1 + \sigma_q) \tag{3.7}$$
$$x_D = x_{md}(1 + \sigma_D) \tag{3.8}$$
$$x_Q = x_{mq}(1 + \sigma_Q) \tag{3.9}$$

Hence, when the effect of erroneous estimated x_d, x_q, x_D and x_Q are investigated, it comprises an error in either the magnetising inductance or the leakage inductance. In [13], it is stated that the leakage inductances are less saturation dependent than the magnetising inductance for a synchronous machine, and that they hence can be assumed to be constant. This is however contradicted in the in the PhD thesis of Tom Fagernes Nestli, arguing that this assumption only is valid if non leakage flux flows through the stator yoke, or through any of the teeth [19]. If some leakage flux flow through the teeth, this inductance will saturate as the iron in the teeth saturate.

3.4.3 Current and Voltage Measurement

Error in the stator voltage may typically occur because the voltage is not measured directly on the terminals, but rather calculated based on the measured DC link voltage and on the control signal of the inverter. Nonlinear switching losses, or erroneous estimation of the blanking time compensation may cause erroneous estimates of the stator voltage. Another source of error is that the digital sampling assumes a constant value of the voltage and current between each sampling interval. Also the current measurement may be erroneous due to DC offsets, discretisation errors and nonlinearities in the sensor [9], [19].

4 Steady State Sensitivity Analysis

In this section, the sensitivity of the voltage model and the current model with respect to estimated parameters, speed and torque is investigated. All errors, such as errors in estimated stator flux linkage, in speed, in rotor position and in generated torque are defined as the difference between the actual value in the machine and the estimated value, as described mathematically by equation 4.1 and 4.2. This convention must be kept in mind while interpreting the results in the rest of this thesis, as it affects the signs of the errors.

$$\text{error} = \text{actual value} - \text{estimated value} \tag{4.1}$$

$$\Delta X = X - \hat{X} \tag{4.2}$$

The conclusions made are heavily based on 3D plots made in Matlab. The procedure is clearly stated in the text, but the Matlab code used to generate the 3D plots are still attached in appendix P for convenience.

4.1 Voltage Model

In this subsection, it will be investigated how an error in stator resistance influence the voltage model during steady state, and how sensitive this model is to the torque reference and the speed of the machine. It is assumed that that the applied control philosophy, with unity power factor and unity flux linkage in the normal operating region is achieved. In regions where the speed is above 1 pu, the stator flux linkage is reduced to $\frac{1}{n}$. While using the voltage model, the stator current and the stator voltage are measured. Assuming that the control system provides the desired stator flux linkage, the actual torque in the machine is then also equal to the reference value.

By transforming equation 3.1 into the frequency domain, equation 4.3 is obtained:

$$jn\underline{\psi_s} = \underline{v_s} - r_s\underline{i_s} \tag{4.3}$$

Where n is the speed in pu. The stator current and the stator voltage are measurable quantities, assumed to be correctly measured, and hence they are the same both in the real machine and in the estimated model. The stator flux linkage is then estimated by equation 4.4

$$\underline{\hat{\psi}_s} = \frac{\underline{v_s} - \hat{r}_s\underline{i_s}}{jn} \tag{4.4}$$

From equation 4.4, the following conclusions are made: As a result of the unity power factor control strategy, with the voltage in phase with or 180 ° apart from the current, an erroneous resistance will cause an error in the estimated stator flux linkage amplitude only, while the angle of the estimated stator flux linkage is unaffected by the estimated stator resistance. Hence, the error in stator flux linkage angle becomes zero for all steady state scenarios. Whether the stator flux linkage magnitude is estimated too long or too short depends on whether the stator resistance is estimated too high or too low, and whether the machine is in motor operation or generator operation.

To illustrate the concept, a phasor diagram for a scenario is presented in figure 4.1, where $i_s = 0.8\,\text{pu}$, $n = 0.5\,\text{pu}$, $\psi_s = 1$ and $\hat{r}_s = 0.8 r_s$. The stator resistance in this example is multiplied by a factor of five compared to the value in the actual machine, to make it easier to see the influence of the stator resistance. The speed is positive for all scenarios, and hence figure 4.1a and 4.1b, where the torque is positive, illustrate motor operation. Figure 4.1c and 4.1d, where the torque is negative, illustrate generator operation. During motor operation, the voltage and the current are in phase. An underestimated stator resistance in equation 4.4 then results in a too high estimated stator flux linkage magnitude. During generator operation, the voltage and the current are displaced by 180 °, and thus an underestimated stator resistance results in a too low estimated stator flux linkage magnitude. If the stator resistance is overestimated, the the stator flux linkage would be estimated too low during motor operation and too high during generator operation. In the scenario illustrated in figure 4.1, the estimated flux linkage is 7.7 % larger than the real one during motor operation, yielding a negative flux linkage amplitude error. During generator operation, the stator flux linkage is estimated 7.7 % lower than the actual stator flux linkage, yielding a positive flux linkage amplitude error. As the expression used to calculate the rotor position, expression 3.2, contains the stator flux linkage, the erroneously estimated flux linkage will also result in a displaced dq- coordinate system.

Furthermore it is evident from equation 4.4 that the estimated stator resistance has a greater impact on the estimated stator flux linkage when the stator current is high, as these two properties are multiplied. An incorrect estimate of the stator resistance will also be amplified during low speed operation, as the speed occurs in the denominator of equation 4.4. It is hence expected that an incorrect estimate of the stator resistance is most severe in the scenarios where the machine generates a high torque at low rotational speed. How the deviation between actual and estimated flux linkage amplitude, torque and rotor position change as function of speed and torque is illustrated in figure 4.2 to figure 4.4. The error is defined as the actual value minus the estimated value. In the steady state sensitivity analysis, the speed is varied from -2 pu to +2 pu, while the torque reference is varied form -1 pu to +1 pu. The increment is 0.05 pu for both of the properties. The error is set to zero in the regions where the machine is not able to operate due to flux weakening, and due to the upper limit of 1 pu for the stator current.

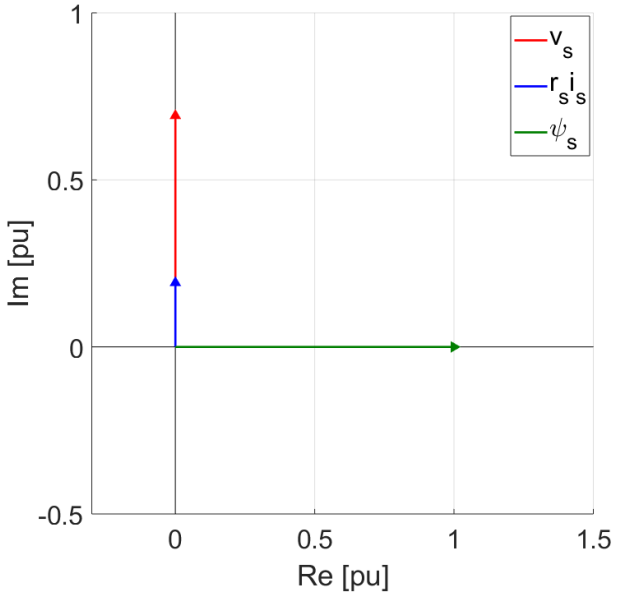

(a) Actual values

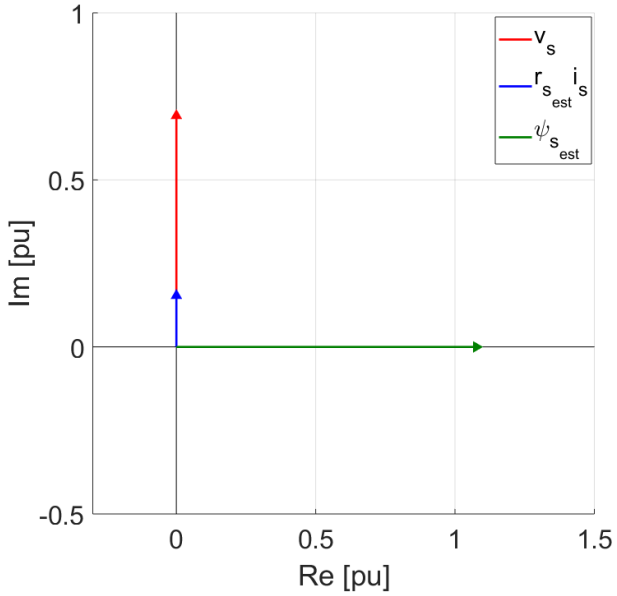

(b) Estimated values, $\hat{r}_s = 0.8r_s$

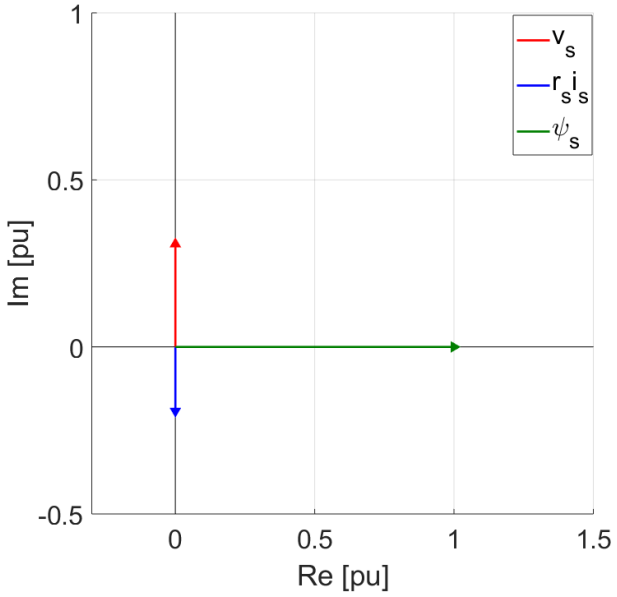

(c) Actual values

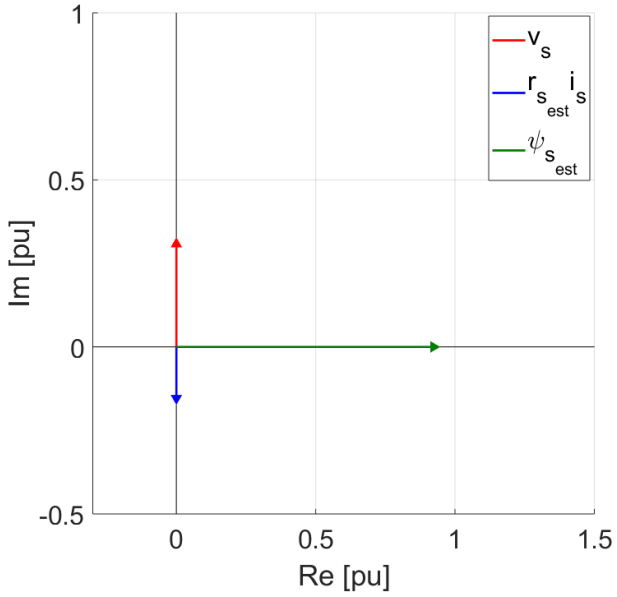

(d) Estimated values, $\hat{r}_s = 0.8r_s$

Figure 4.1: Phasor diagram for voltage model during steady state

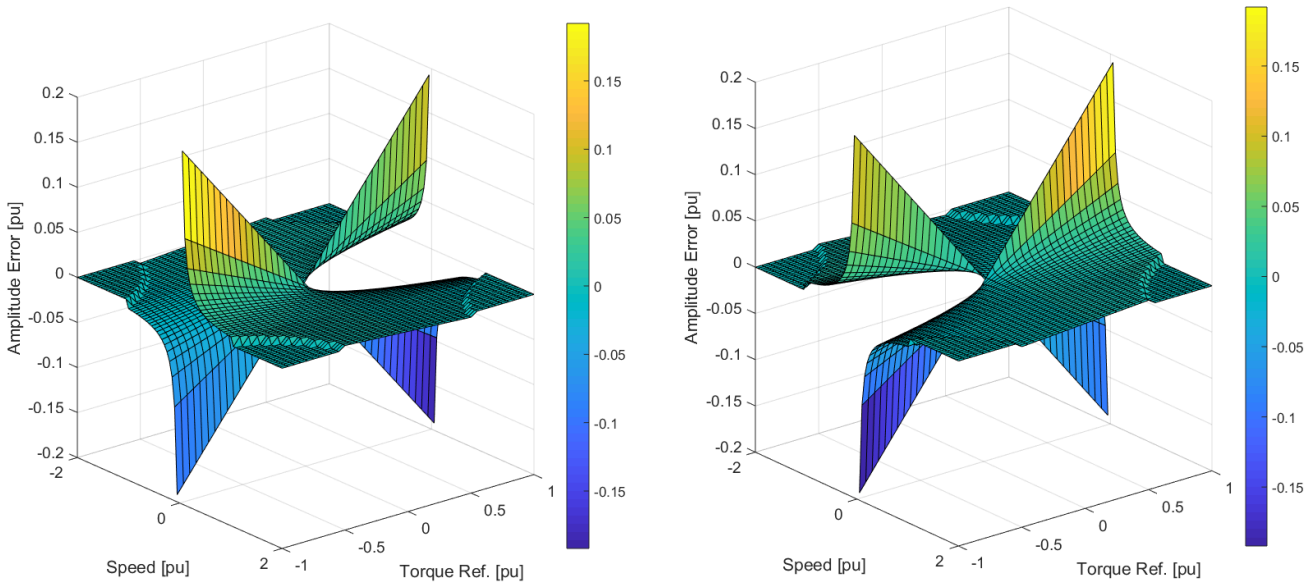

(a) $\hat{r}_s = 0.8r_s$ (b) $\hat{r}_s = 1.2r_s$

Figure 4.2: Error in estimated stator flux linkage amplitude for 20 % deviation in estimated stator resistance

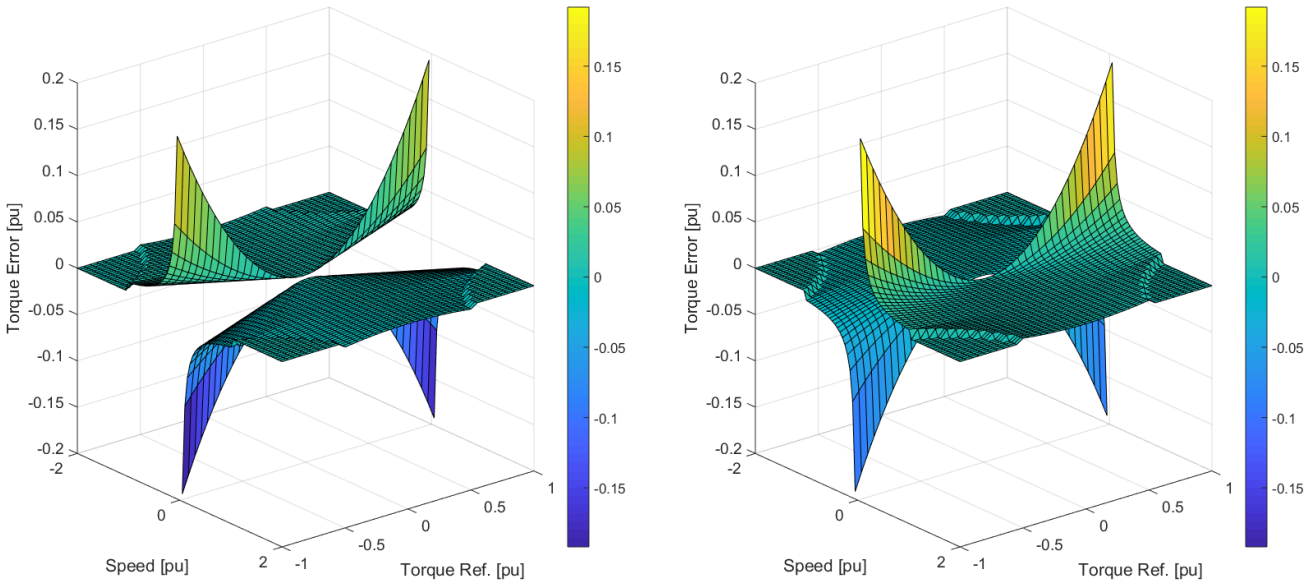

(a) $\hat{r}_s = 0.8r_s$ (b) $\hat{r}_s = 1.2r_s$

Figure 4.3: Error in estimated torque for 20 % deviation in estimated stator resistance

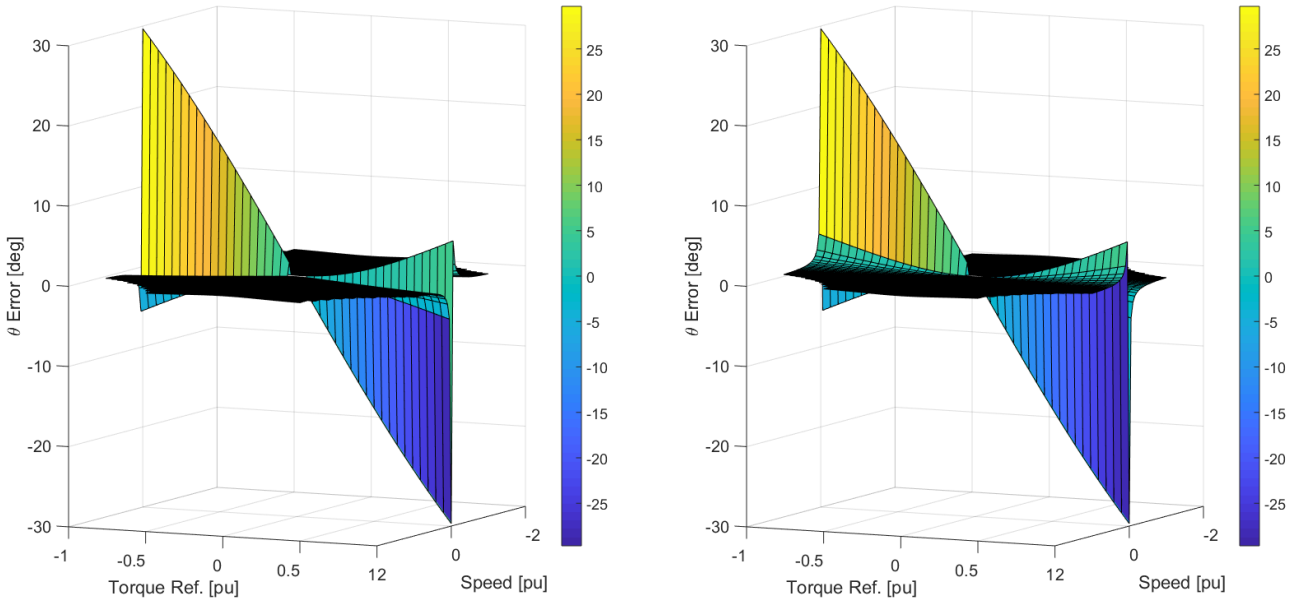

(a) $\hat{r}_s = 0.8 r_s$ (b) $\hat{r}_s = 1.2 r_s$

Figure 4.4: θ error for 20 % deviation in estimated stator resistance

The first observation made from figure 4.2 to figure 4.4 is how all the three errors, in estimated stator flux linkage magnitude, in estimated flux linkage angle, and in estimated rotor position, increase as the speed approaches zero. This is in accordance with the sensitivity plots presented in [19], where it is stated that the largest estimation errors generally occur at low stator frequencies. As expected, all the properties also change in opposite directions for the two scenarios where the estimated stator resistance is either 20 % higher or 20 % lower than the actual stator resistance.

From figure 4.1 it is evident that when the estimated resistance is underestimated, the error in estimated stator flux linkage amplitude increases to a positive value during generator operation, and to a negative value during motor operation for low speeds. The error also increases with the magnitude of the torque reference applied, as a higher stator current is required to generate a higher torque. Both of these observations are expected from the previous discussion. It is also observed that for higher speeds, such as 0.7 pu, the flux linkage estimate is more or less independent of the torque reference in the investigated scenario. The peak value of the amplitude error is ± 0.192 pu both when the resistance is underestimated, and when it is overestimated by 20 %. With smaller increments in speed, this value would increase significantly as the speed approaches zero. The maximum deviations in figure 4.2 occurs when the speed is ± 0.05 pu and the torque is ± 1 pu. These points are at the highest torque references and the lowest speeds investigated. This scenario is illustrated in the phasor diagrams in figure 4.5a and 4.5b.

From figure 4.5a and 4.5b it is obvious that for low speeds, the induced back emf becomes low. The $r_s \underline{i}_s$ vector is then larger relative to the stator voltage, than what is the case for higher speeds, as illustrated for $n = 0.8\,\text{pu}$ in figure 4.5c and 4.5d. In equation 4.4, the term containing the erroneous resistance will get more impact relative to the voltage in the nominator for low speeds. At the same time the low speed in the denominator will amplify the expression. This explains why the amplitude error increases drastically when the speed approaches zero. In figure 4.5a and figure 4.5b, the estimated stator flux linkage is estimated significantly too high, while in figure 4.5c and figure 4.5d there is a much smaller difference between the actual and the estimated stator flux linkage. A stator resistance of 0.048 pu estimated 20 % too low corresponds to a deviation of only 0.0096 pu between the actual and the estimated resistance. Still, this small error cause an error of 0.19 pu in the estimated flux linkage amplitude at the worst case operation points investigated, and the error will grow further for lower speeds. Figure 4.2a is repeated in appendix H, with another angle of view and with data cursors included.

For higher speeds the voltage model is not only less sensitive to errors in the estimated resistance, but also to possible errors in the measured voltage. Since the voltage applied then is higher, due to a higher back emf, any error such as offsets in the estimated stator voltage becomes smaller relative to the integrated stator voltage in equation 4.4.

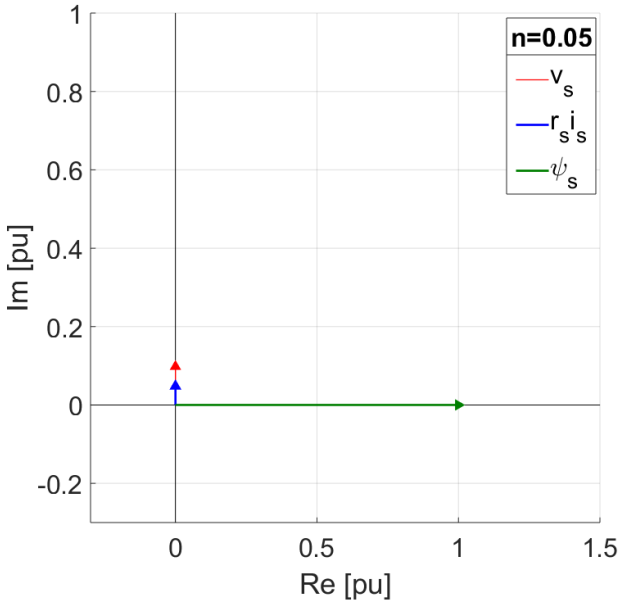

(a) Actual values, low speed

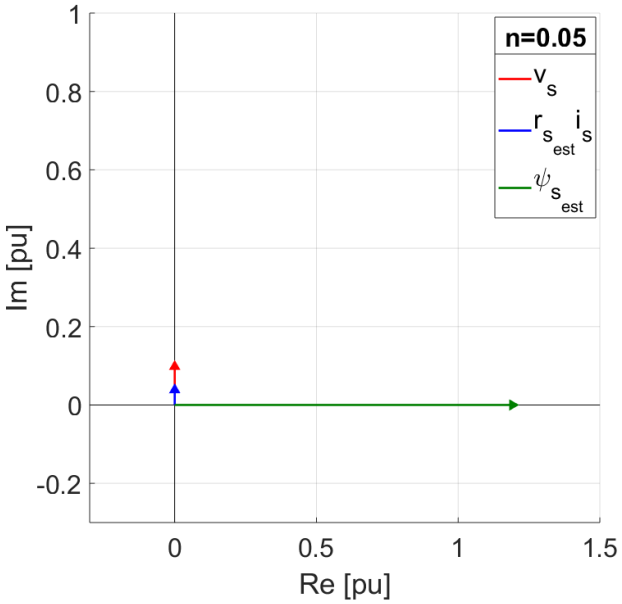

(b) Estimated values, $\hat{r}_s = 0.8r_s$, low speed

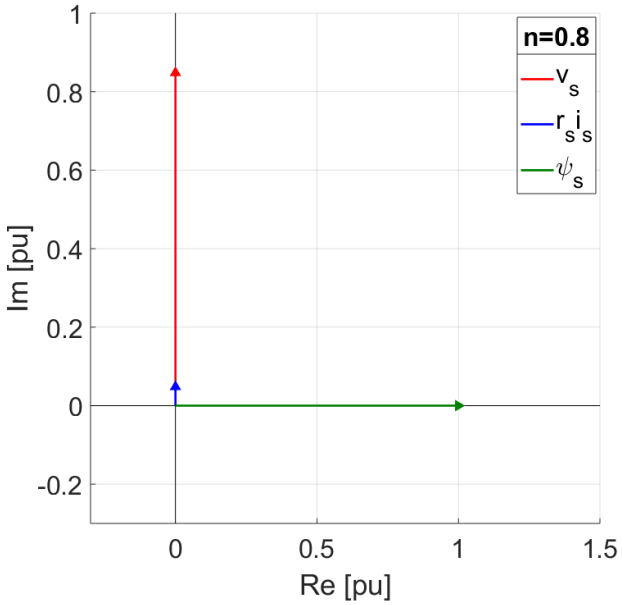

(c) Actual values, high speed

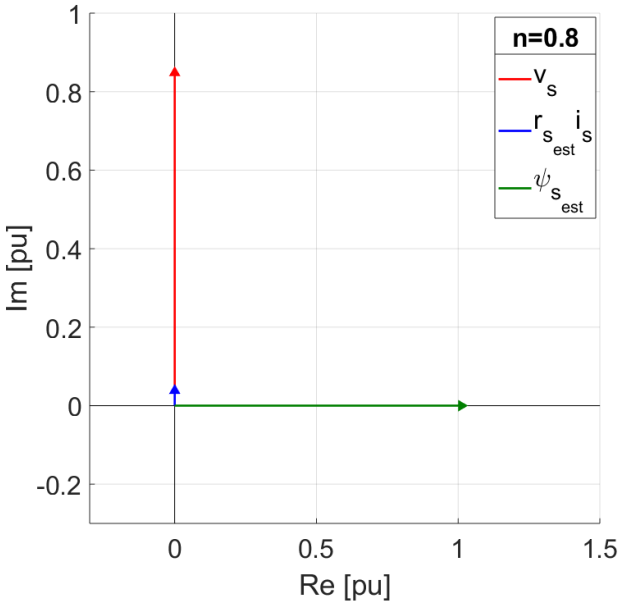

(d) Estimated values, $\hat{r}_s = 0.8r_s$, high speed

Figure 4.5: Voltage model for low and high speed

How the error in estimated stator flux linkage increases when the speed approaches zero is also illustrated, with a increment of 0.0001 pu in the speed, in figure 4.6. The stator resistance is underestimated by 20 %. Figure 4.6 verifies that the error in flux linkage amplitude increases towards infinity as the speed approaches zero.

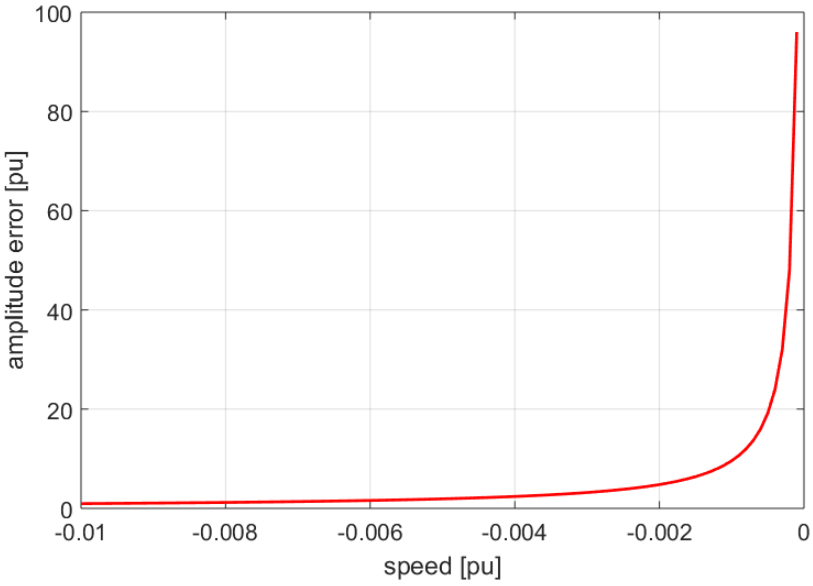

Figure 4.6: Error in estimated stator flux linkage amplitude around zero speed, $\tau_{ref} = 1\,\text{pu}$

The error in generated electromechanical torque also gets a high positive or negative value as the speed becomes low, as seen from figure 4.3. As for the amplitude error, the peak values are $\pm 0.192\,\text{pu}$ both when the stator resistance is estimated too high and when it is estimated too low. It should be kept in mind that when the error in estimated generated torque is positive, the actual torque in the machine is higher than the estimated one. During dynamic analysis in Simulink, that is performed later, both the flux linkage magnitude and the estimated rotor position will influence the generated torque, as these values affect the control system. In this steady state analysis, the voltage model is expressed in the stator oriented reference frame, and hence the error in estimated torque is independent of the rotor position. The generated torque will then depend on the stator flux linkage amplitude and the stator currents only. This relation is evident from figure 4.2 and figure 4.3, as the error in estimated amplitude and the error in estimated torque change in the same direction for positive torque, and in opposite directions for negative torques. The reason why the error in the estimated stator flux linkage amplitude and the error in estimated torque change in opposite directions for negative torques is that the sign of the torques are included in the expressions. A large negative real torque and a less negative estimated torque results in a negative error, even though the magnitude of the real torque is larger than the magnitude of the estimated one. The correlation between the error in stator flux linkage amplitude and the error in estimated torque is illustrated for positive torque references by a scatter plot in figure 4.7. The estimated resistance is 1.2 times the actual resistance in the two scenarios investigated. By using the polynomial curve fitting command in Matlab, based on least square method, it is evident that that the error in estimated stator flux linkage amplitude and the error in estimated torque are related by a second order polynomial. This is because the stator flux linkage amplitude is linearly dependent on the stator current, the torque depends on the stator current squared, as the estimated flux is multiplied by the stator current, and both the properties are linearly dependent on the error in estimated stator resistance. The coefficient of the second order polynomial changes with the speed of the machine. For the operation in figure 4.7a, the coefficient is 5.2, while for the operation in

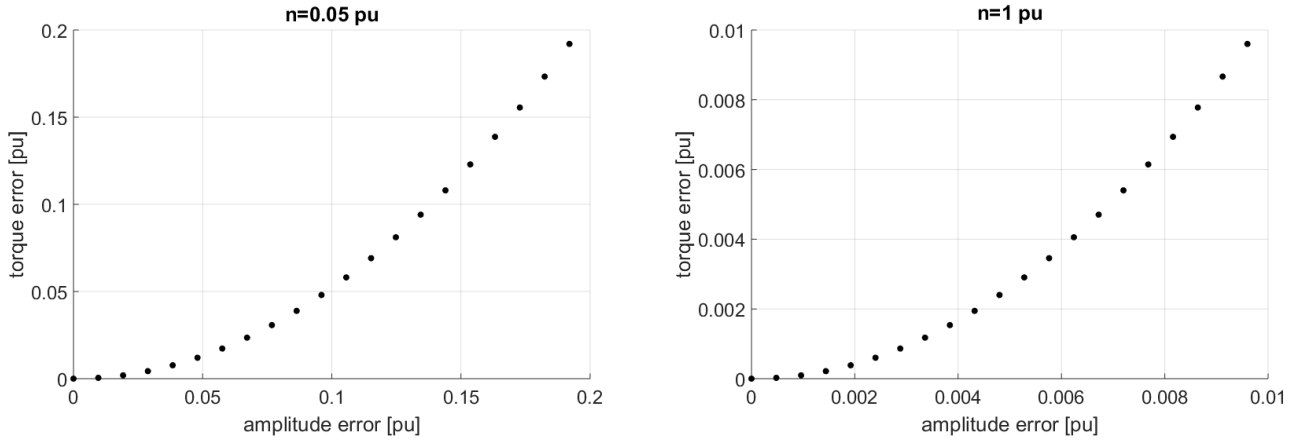

(a) n=0.05 pu, $\Delta\tau \approx 5.2(\Delta\psi_s)^2$ (b) n=1 pu, $\Delta\tau \approx 104.2(\Delta\psi_s)^2$

Figure 4.7: Correlation between error in estimated flux linkage amplitude and estimated torque for positive torque references. $\hat{r}_s = 1.2r_s$

figure 4.7b, the coefficient is 104.2. The results illustrate a positive correlation. When the error in estimated amplitude is positive, the estimated flux linkage amplitude is lower than the actual flux linkage amplitude in the machine, and hence the generated torque is also estimated too low, as the current is assumed independent of the estimated flux. The peak values of the amplitude error and the torque error are similar for the lowest and the highest torque reference, where the stator current is 0 pu and 1 pu respectively. This is because the $i_s = i_s^2$ at these operating points. In the analysis of the sensorless operation, conducted later in section 6, the current controller will control the stator current such that the estimated torque is equal to the reference torque. If the stator flux linkage is estimated too low, this will result in too high current from equation 2.51, generating a too high torque. Even if this dynamic from the controller is not included in this steady state analysis, it is evident that it gives the same relation between the error in estimated flux linkage amplitude and the error in estimated torque.

In figure 4.3, the error in estimated torque is plotted for a stator resistance that is estimated 20 % above and 20 % below the actual value. How the error in torque depends on the deviation between the estimated and the actual resistance is illustrated in figure 4.8. The maximum torque errors is represented in a 2D plot, as a function of speed and error in estimated resistance, in the speed-torque error plane. From figure 4.3 it is known that these maximum values occur at a torque reference of ± 1 pu. From figure 4.8, it is evident that the torque estimation will become accurate for high speeds, 1.5 pu-2 pu, even when the stator resistance is overestimated by 100 %. The error will also get high around zero speed, even for small deviations between the real and the estimated stator resistance. This is avoided only if the stator resistance is estimated correctly. For the speed range between zero speed to approximately 1 pu, the torque error will depend heavily on the accuracy of the estimated resistance. This is illustrated in figure 4.8b, where the torque error is plotted as a function of how much the stator resistance is overestimated at $n = 0.15$ pu. The line drawn from the first to the last point illustrates how the torque error depends linearly on the stator resistance estimation during steady state.

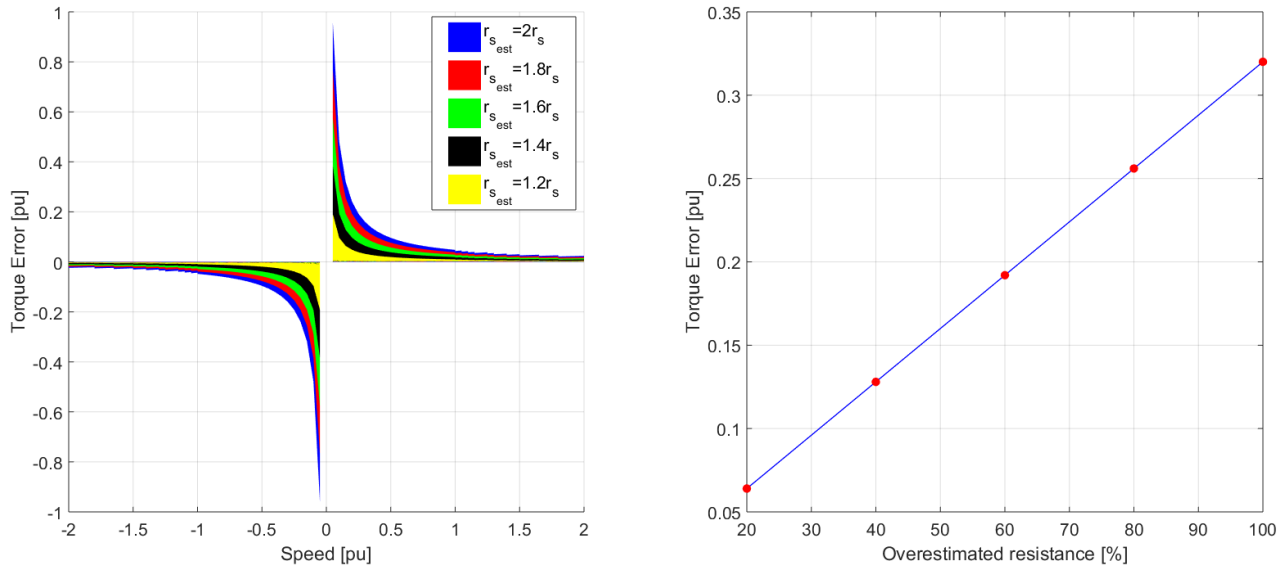

(a) Torque Error in the speed-Torque error plane

(b) Maximum values for $(n, \tau_{ref}) = (0.15, -1)$

Figure 4.8: How the error in estimated torque depends on stator resistance

The error in estimated rotor position is presented in figure 4.4. The same results, but with the error at zero rotor speed excluded is presented in figure 4.9. This makes it easier to analyse the shape of the figure in detail. It is evident that also this error increases for low speeds, and for high torques. During steady state operation, the instant when the stator flux linkage is aligned with the stator phase a axis is investigated. Expression 3.3, which is now valid because this is a steady state consideration, is then reduced to equation 4.5.

$$tan(\theta) = \pm\left[\frac{-\sigma_{qQ}x_q + x_{Mq}}{\hat{\psi}_s} i_s\right] \tag{4.5}$$

The accuracy of the rotor position estimation will hence depend on the accuracy of the estimated stator flux linkage and on the stator current. This explains why the estimation is less accurate for low speeds and for high torque references, as the stator flux linkage estimate has been illustrated to be poor at these operating points, and the large current amplifies the error even more in equation 4.5. It is also evident how the estimation of rotor position fails at zero speed, as the stator flux linkage cannot be estimated by the voltage model at zero speed. From figure 4.9, it is found that when the stator resistance is estimated too low, the peaks in error are 5.5 °, positive for positive torque and negative for negative torque, and they occur during generator operation. During motor operation the error peaks are at 4.2 °, positive for negative torque, and negative for positive torque. When the resistance is estimated too high, the surface plot of the error looks quite similar, but with another orientation. The highest peaks then occur during motor operation.

The results presented in this section states that even for steady state operation, the voltage model is inaccurate for low speed when the stator resistance is not estimated correctly. Even a 20 % deviation in a small resistance, such as 0.048 pu, will result in an error of 0.19 pu in the estimated flux linkage amplitude, when the speed is 0.05 pu and the torque reference is 1 pu. This

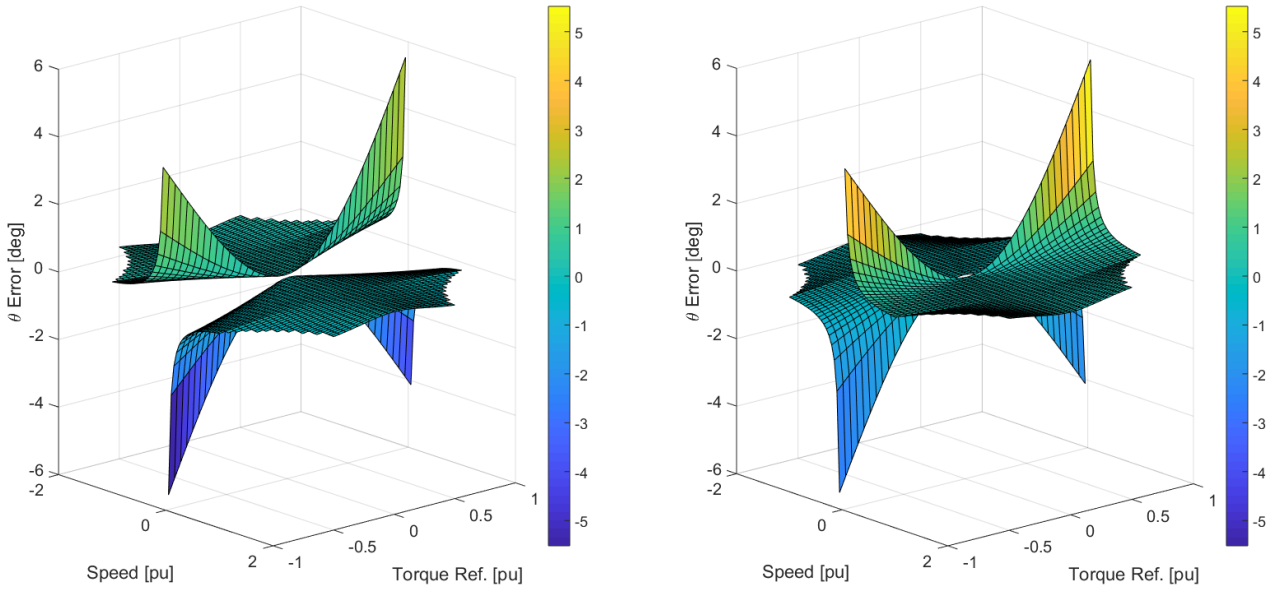

(a) $\hat{r}_s = 0.8r_s$ (b) $\hat{r}_s = 1.2r_s$

Figure 4.9: Deviation in estimated rotor position, zero speed excluded

will cause en error of 0.19 pu between the real and the estimated torque, which will influence the torque control of the machine. It is concluded that the voltage model is very sensitive to erroneous estimated stator resistances for low speed, and that the accuracy of the model also depends heavily on the torque reference applied. From this it is obvious that operations with high loading and with low speed, which is typical for lifts, may be challenging for a machine running sensorless, utilising the voltage model only. For higher speeds, as the induced back emf increases, the model is more robust, and the model is not very sensitive to errors in the estimated resistance or in the estimated voltage. Furthermore, as the only immeasurable quantity in the voltage model is the stator resistance, which is not saturation dependent, it is concluded that the model is well suited for higher speeds.

4.2 Current Model

A similar steady state sensitivity analysis as performed for the voltage model is also performed for the current model. As the model estimates the stator flux linkage in the dq reference frame, it is heavily dependent on the accuracy of the estimated rotor position used as input. To avoid this source of error, and to analyse the sensitivity of the model to the estimated parameters only, this analysis assumes that the rotor position is measured with high accuracy. The stator voltage, the stator current and the field winding current are also assumed to be known with high accuracy, as they are measured quantities. From equation 2.38 to 2.41, it is evident that the stator flux linkage estimation depends on the rotor resistances r_D and r_Q during transients only. Hence only the inductances and the measured currents will influence the flux linkage estimation during steady state, as expressed by equation 4.6 and 4.7.

$$\psi_d = x_d \sigma_{dD} i_d + x_{Md}(i_d + i_f) + x_{Md}\sigma_D i_f \tag{4.6}$$

$$\psi_q = \sigma_{qQ} x_q i_q + x_{Mq} i_q \tag{4.7}$$

From equation 2.10 and 2.11, it is known that equation 4.6 and 4.7 can be expressed, in a more traditional way, by equation 4.8 and 4.9 during steady state. These expressions will be used in this analysis to reduce the amount of parameters in the model.

$$\psi_d = x_d i_d + x_{md} i_f \tag{4.8}$$

$$\psi_q = x_q i_q \tag{4.9}$$

First, the stator current i_s is determined by equation 2.51, and the angle between the d-axis and the stator flux linkage is found by 2.43. The estimated stator flux linkage is then found by decomposing the stator flux linkage reference into its d- and q components, $\hat{\psi}_d$ and $\hat{\psi}_q$. A stator flux linkage of 1 pu is used as a reference value in the normal operating range, while the reference is reduced by the inverse of the speed for speed above ± 1 pu to obtain field weakening. The estimated stator flux linkage and torque are then assumed to be equal to their reference values, which are not necessarily the same as the actual flux linkage and torque in the real machine. To obtain 1 pu stator flux linkage, the field current is given by equation 4.10 [5, p 18].

$$i_f = \frac{\psi_s^2 + \hat{x}_d \hat{x}_q i_s^2}{\hat{x}_{md}\sqrt{\psi_s^2 + \hat{x}_q^2 i_s^2}} \tag{4.10}$$

The dq currents supplied are then found by solving equation 4.8 and 4.9 for i_d and i_q respectively, using the estimated reactances and the estimated stator flux linkage. If these current components are now inserted back into equation 4.8 and 4.9 with the actual inductances, the actual stator flux linkage in the machine is found. From equation 4.8 and 4.9, it is evident that the estimation is independent of the rotor speed. However, it will later in this section be shown that the rotor speed still influence the result in some degree, as field weakening is applied for speeds above 1 pu. Since the position and currents are known, it is also evident from equation 4.8 and 4.9 that the deviation between the real and the estimated stator flux linkage in the motor depends on the accuracy of the estimated inductances and the currents supplied only. The difference between the actual and the estimated torque is given by

$$\Delta\tau = i_q \Delta\psi_d - i_d \Delta\psi_q \tag{4.11}$$

The errors are, as in the voltage model, defined as actual values in the machine minus the estimated values. This time the reference torque is equal to the estimated torque, while in the voltage model it was equal to the actual torque produced. By assuming erroneously estimated x_d and x_q, while keeping the leakage inductances constant, the effect of a varying the magnetising inductances x_{md} and x_{mq} is investigated.

4.2.1 Sensitivity to x_d

A deviation of 20 % in the inductance along the d-axis is now investigated. The results presented in figure 4.10 and 4.11 confirm that the amplitude error and torque error are independent of the speed within the normal operating range, where the speed is within ± 1 pu. Furthermore, it is evident that the error in both torque and flux linkage amplitude are quite symmetrical for the cases when the inductance is overestimated and underestimated by 20 %. The amplitude error has a high degree of symmetry about the torque-speed plane, while torque error has a high degree of symmetry about the speed-Torque error plane. Please be aware of that the coordinate system is rotated from figure 4.11a to figure 4.11b. When the d-axis inductance is underestimated by 20 %, the maximum error in estimated stator flux linkage amplitude is 0.29 pu, while the maximum error in estimated torque is ± 0.23 pu. When the inductance is overestimated by 20 %, the maximum error in estimated stator flux linkage is -0.18 pu, and the maximum error in estimated torque is ± 0.147 pu.

It is observed that the amplitude error is less sensitive to an incorrectly estimated x_d for higher torques. This is in contrast to the voltage model, where an incorrect estimation of the resistance is more severe for higher torques. Why the sensitivity decreases with the torque reference applied is explained by a scenario illustrated in figure 4.12a, where $\hat{x}_d = 0.8 x_d$, the speed is 0.5 pu and the torque is increased from 0.3 pu to 0.8 pu. For a given torque reference, a certain current along the q-axis is required. The flux controller is assumed to ensure that the stator flux linkage has the magnitude of 1 pu, as discussed in section 2.5. This is indicated by the dashed circle. The d-axis current has to be negative to obtain unity power factor. To increase the torque, the q-axis current is increased, making also ψ_q larger. As seen from figure 4.12a, this is at the cost of ψ_d to avoid exceeding a flux linkage magnitude of 1 pu. The smaller stator flux linkage along the d-axis makes the error between the actual and the estimated ψ_d smaller, and since ψ_q is independent of x_d, ψ_q is still correctly estimated. Hence the error between actual and estimated stator flux linkage ,$\Delta\psi_s$, becomes smaller.

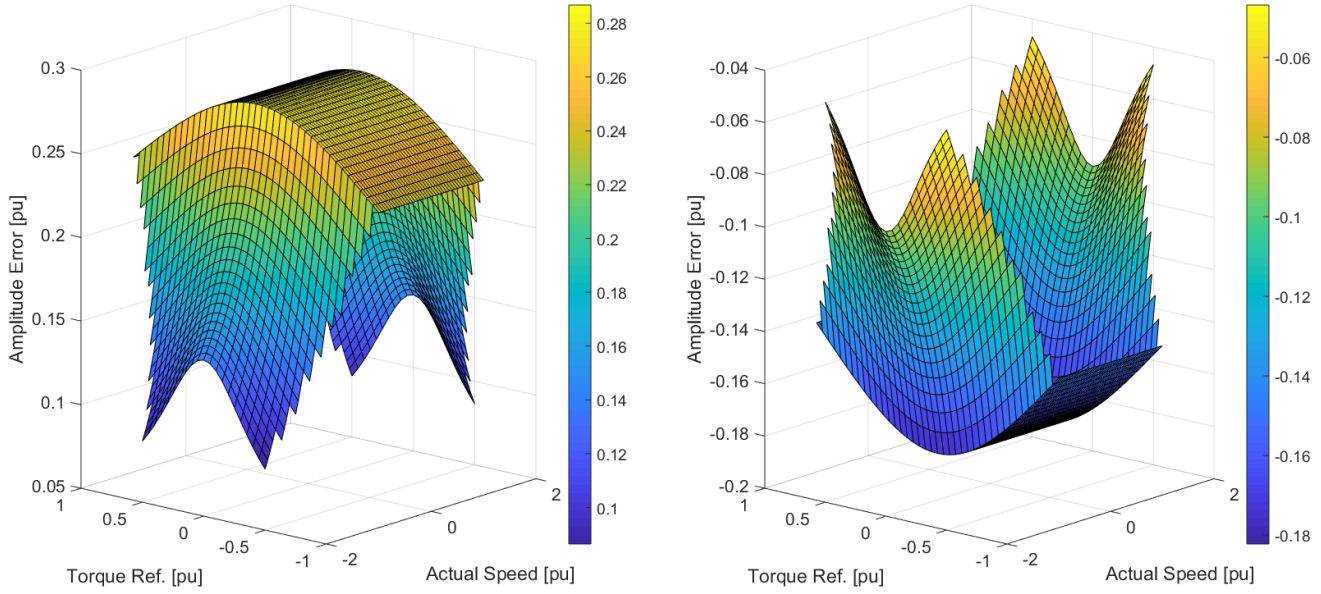

(a) $\hat{x}_d = 0.8x_d$ (b) $\hat{x}_d = 1.2x_d$

Figure 4.10: Error in estimated stator flux linkage amplitude for 20 % error in $\hat{x}_d$

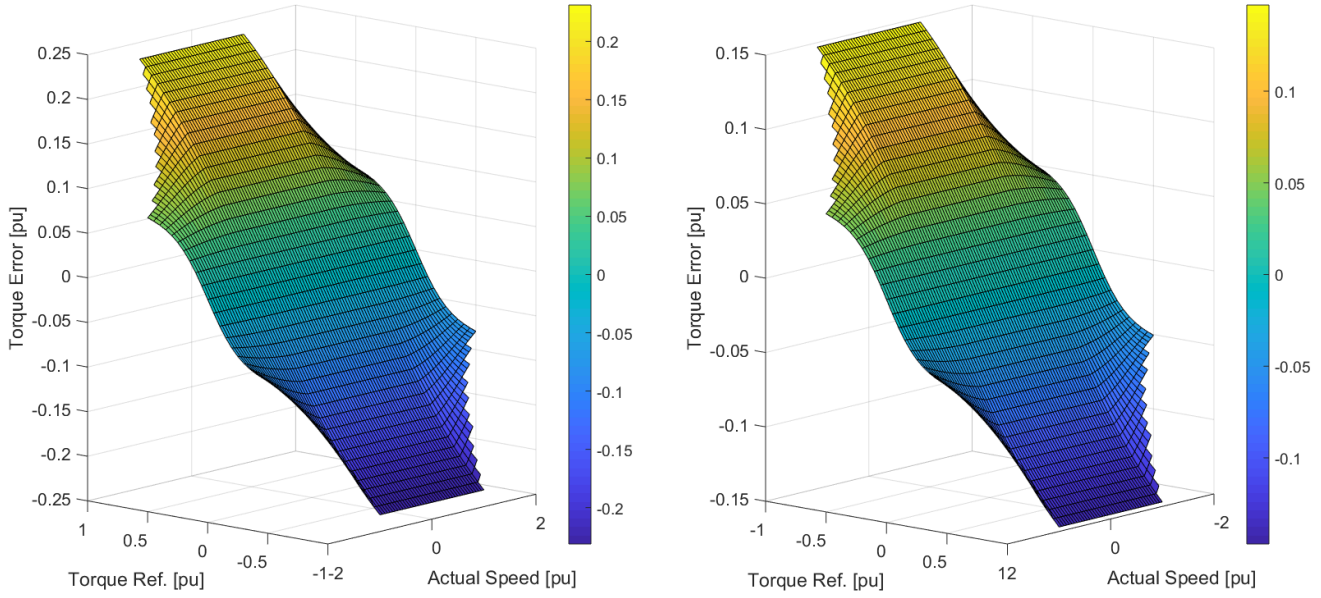

(a) $\hat{x}_d = 0.8x_d$ (b) $\hat{x}_d = 1.2x_d$

Figure 4.11: Error in estimated torque for 20 % deviation in estimated stator reactance along the d-axis

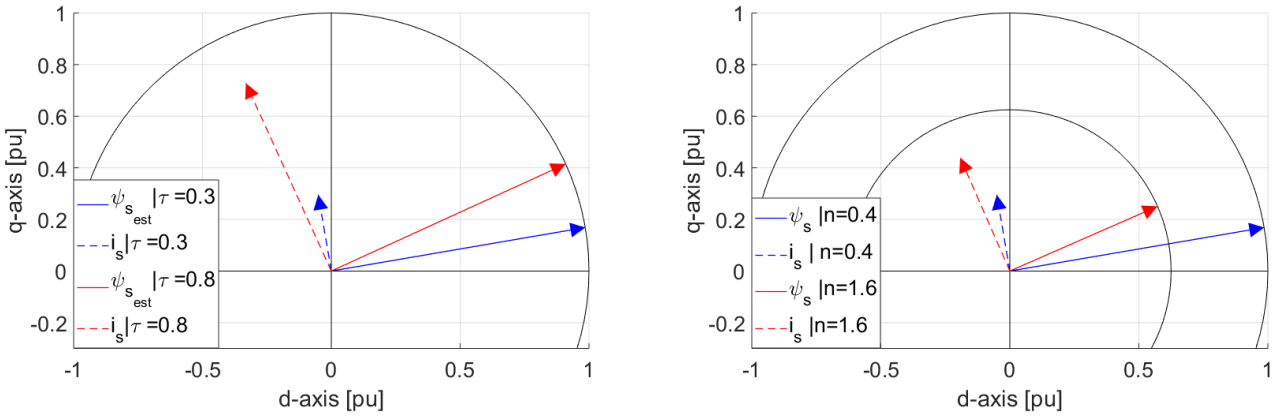

(a) Increasing the torque while the speed is constant

(b) Increasing the speed into field weakening area, while the torque is constant

Figure 4.12: Phasor diagram for two scenarios, $\hat{x}_d = 0.8x_d$

Another important result from figure 4.10 is that the amplitude error decreases drastically towards zero in the field weakening region, when the torque is kept constant and the speed exceeds ± 1 pu. This is illustrated by an example in figure 4.12b, where the torque is 0.3 pu for both cases, while the speed is 0.4 pu in the first case and 1.6 pu in the second case. As the speed exceeds 1 pu, field weakening is applied. The maximum stator flux linkage is reduced as the inverse of the speed, as indicated by the inner dashed circle. To obtain the same torque with less flux, which is possible as long as the stator current do not exceed 1 pu, the q-axis current must increase. By reasoning in the same way as for the scenario in figure 4.12a, it is evident that ψ_d is reduced, and that the error in stator flux linkage amplitude becomes smaller. These considerations are valid both when x_d is underestimated and when it is overestimated. The error is reduced both for an increasing torque reference, and for an increasing speed in the field weakening region when the d axis inductance is erroneously estimated. The error is reduced from a positive value towards zero when the inductance is underestimated and from a negative value towards zero when the inductance is overestimated.

The error in estimated torque when x_d is incorrectly estimated is presented in figure 4.11. As long as x_q is correctly estimated, equation 4.11 reduces to equation 4.12.

$$\Delta\tau = i_q \Delta\psi_d \tag{4.12}$$
$$= i_q[i_d \Delta x_d + i_f \Delta x_{md}] \tag{4.13}$$
$$= i_q \Delta x_{md}(i_d + i_f) \tag{4.14}$$

As $\Delta\psi_d$ correlates quite good with $\Delta\psi_s$, which is evident by comparing figure 4.10a and 4.13, the plot of the error in estimated torque will look quite similar to the product of the stator flux linkage amplitude error in figure 4.10 and the q-axis current in figure 4.14b. From figure 4.14b and 4.15a it is evident that the q-axis current changes significantly more than $\Delta\psi_d$ along the torque reference axis, and the current will hence have a larger influence on the shape of the torque. A

cross section of the error in the estimated torque is plotted in figure 4.15b, where it is revealed that the derivative of the error is reduced for higher torques. This is due to the reduced error in ψ_d at higher torque references, but also because the q-axis current flattens slightly for higher torques.

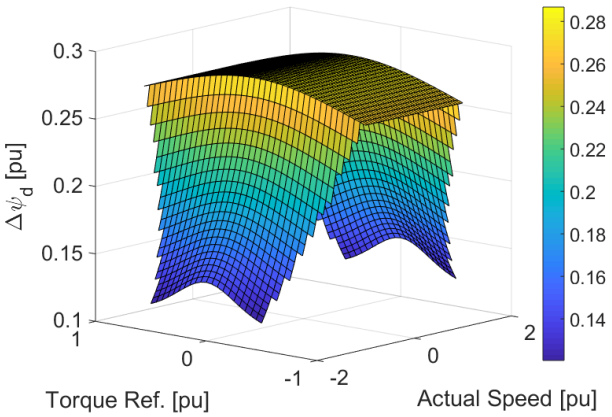

(a) Amplitude error in ψ_d

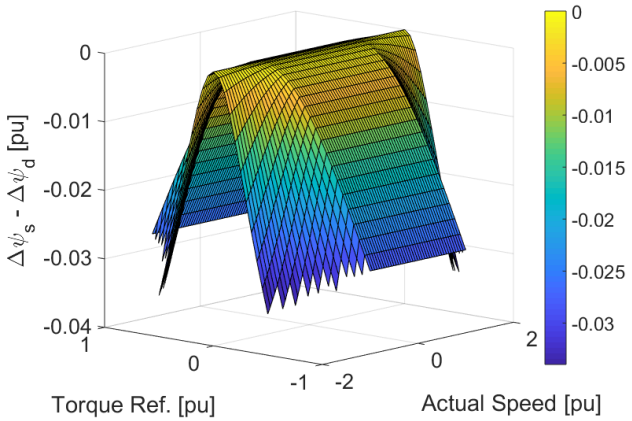

(b) Difference between amplitude error in ψ_s and in ψ_d

Figure 4.13: Relation between $\Delta\psi_s$ and $\Delta\psi_d$ for $\hat{x}_d = 0.8x_d$

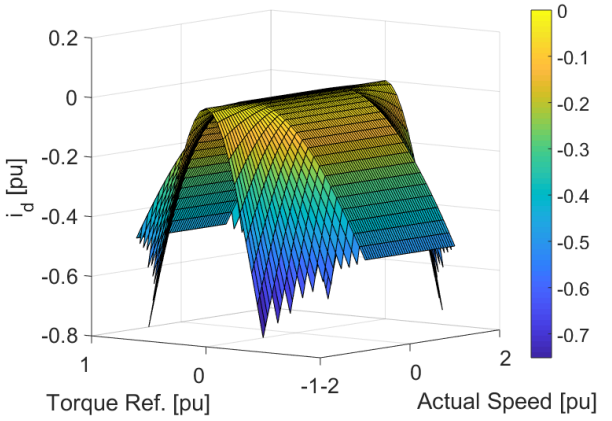

(a) d-axis current for $\hat{x}_d = 0.8x_d$

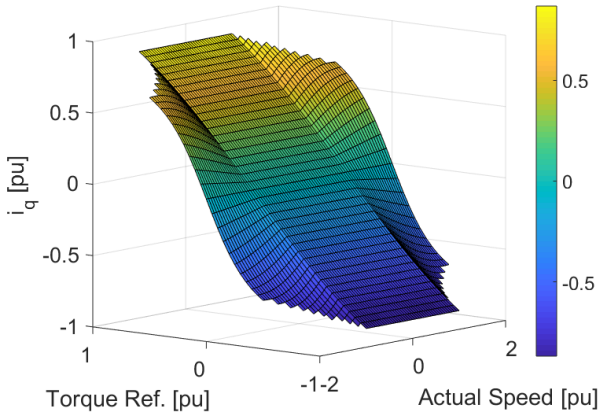

(b) q-axis current for $\hat{x}_d = 0.8x_d$

Figure 4.14: The d- and q-axis currents when $\hat{x}_d = 0.8x_d$

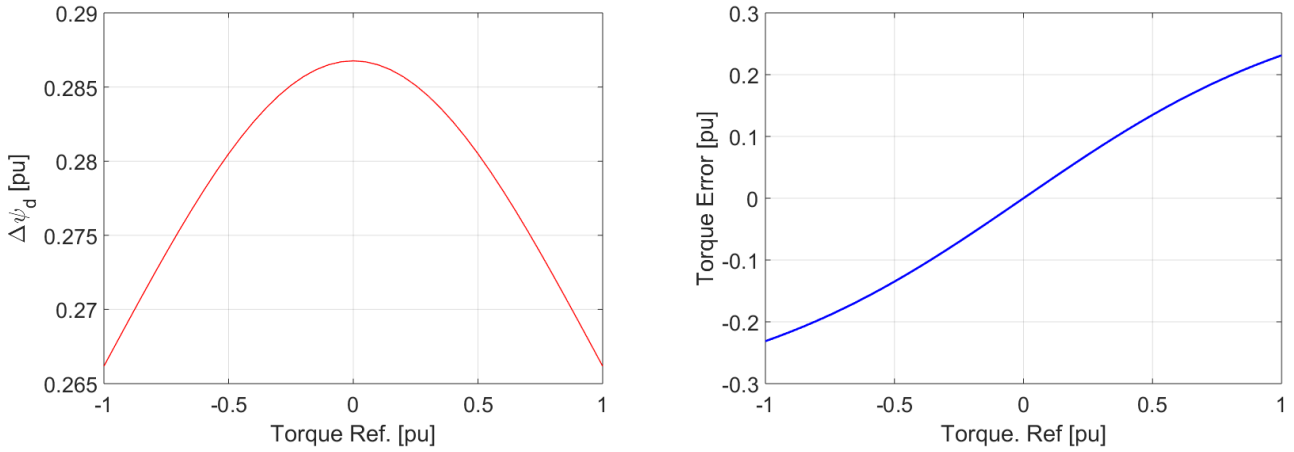

(a) Error in estimated ψ_d for $n = 0.5\,\text{pu}$ (b) Torque error for $n = 0.5\,\text{pu}$

Figure 4.15: Error in estimated d-axis stator flux linkage and the error in estimated torque, $\hat{x}_d = 0.8x_d$

4.2.2 Sensitivity to x_q

A similar analysis as was performed for the d-axis inductance, x_d, is now performed for the q-axis inductance, x_q.

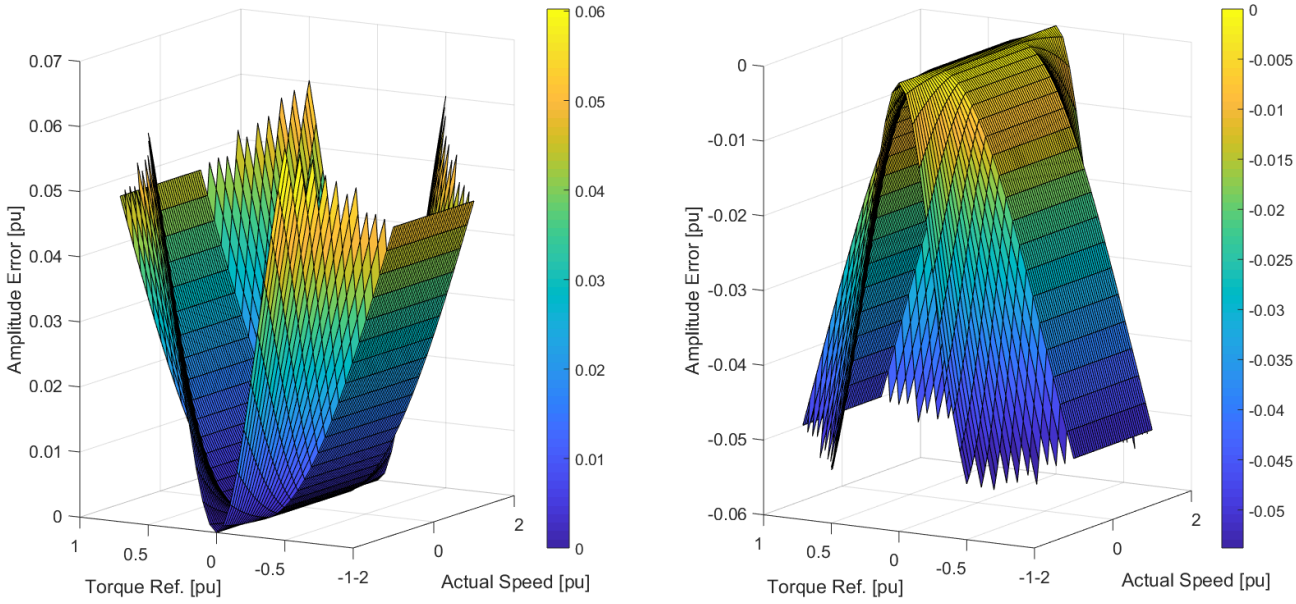

(a) $\hat{x}_q = 0.8x_q$ (b) $\hat{x}_q = 1.2x_q$

Figure 4.16: Error in estimated stator flux linkage amplitude for 20 % error in estimated stator inductance along the q-axis

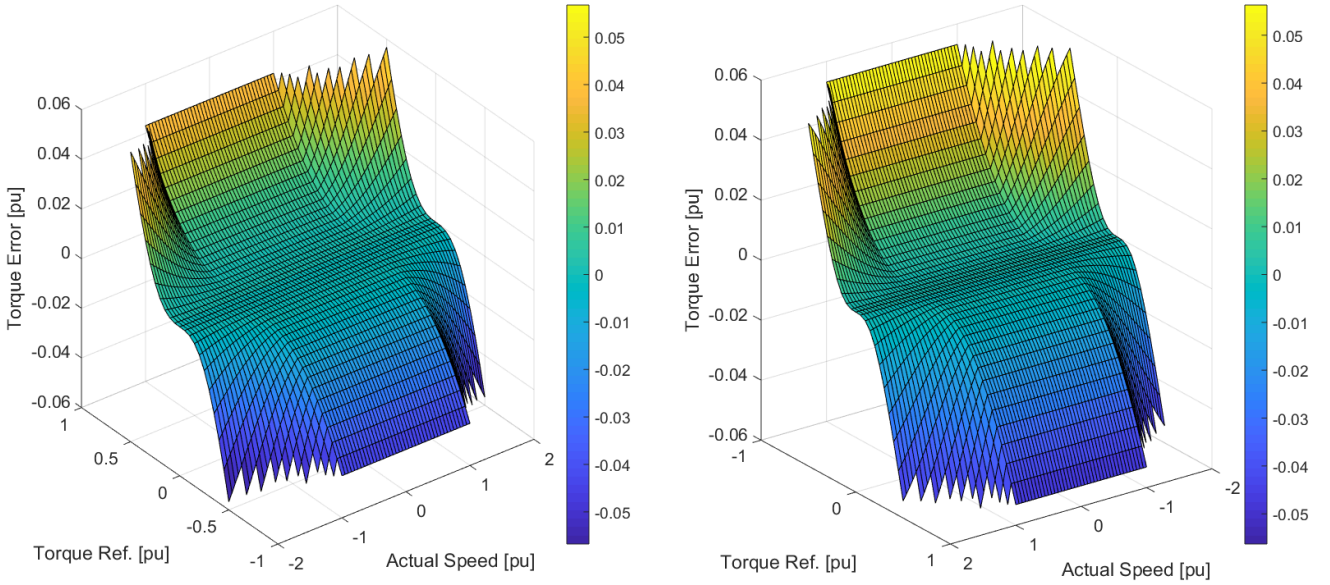

(a) $\hat{x}_q = 0.8x_q$ (b) $\hat{x}_q = 1.2x_q$

Figure 4.17: Error in estimated torque for 20 % error in estimated stator inductance along the q-axis

As for the analysis of the d-axis inductance, there is a high degree of symmetry in the case of underestimated and overestimated q-axis inductance. It is observed that the errors in estimated stator flux linkage amplitude and torque are significantly smaller than for the scenario where x_d is erroneously estimated. This is because the d-axis inductance is more than twice as large as the q-axis inductance, and hence an inaccurate estimation of x_q is less severe than an inaccurate estimation of x_d for the estimated stator flux linkage. Maximum amplitude error is found to be 0.060 pu, while the torque error is found to be ± 0.057 pu, both occurring when $\hat{x}_q = 0.8x_q$. However, the maximum errors in the case of an overestimated inductance are not very different. The maximum error in estimated stator flux linkage amplitude is then -0.054 pu, while the maximum error in estimated torque is ± 0.057 pu, which is the same as when the inductance is underestimated. The coordinate system is rotated from figure 4.17a to figure 4.17b.

Both the error in estimated stator flux linkage amplitude and the error in estimated torque are heavily dependent on the torque reference of the machine, with the highest errors occurring at the highest torque references. This is opposite to the results in section 4.2.1, where x_d is inaccurately estimated. As discussed in section 4.2.1, a larger torque magnitude requires a larger q-axis current. This increases the q-axis stator flux linkage, and hence $\Delta\psi_q$ increases. Since $\Delta\psi_d$ is zero for this scenario, the amplitude error $\Delta\psi_s$ increases with the torque reference. When the torque reference is zero, both i_q and ψ_q are zero, and hence there is no error in the estimated flux linkage amplitude or in the estimated torque. In the field weakening region, the errors in the estimated stator flux linkage amplitude and the estimated torque also increase. This is because the q-axis current is increased also in this situation, as was illustrated for an inaccurate estimation of x_d in figure 4.12b.

When x_q is erroneously estimated, while x_d is estimated correctly, equation 4.11 is reduced to equation 4.15.

$$\Delta\tau = -i_d \Delta\psi_q \tag{4.15}$$
$$= -i_d i_q (x_q - \hat{x}_q) \tag{4.16}$$

The d-axis current, plotted in figure 4.18a, is negative for all operation points due to the unity power factor control strategy, and i_q will vary with the torque reference as in figure 4.18b. Hence, the following conclusions are made from equation 4.16: When the estimated q axis inductance is smaller than the real q axis inductance, positive error in the estimated torque occurs for positive q axis currents, and negative error in the estimated torque occurs for negative q axis currents. When the estimated inductance is overestimated, a positive q-axis current yields a negative error in the estimated torque, while a negative q-axis current yields a positive error in the estimated torque. These relations are illustrated in figure 4.17.

The correlation between the error in estimated stator flux linkage and the error in estimated torque is summarised for positive torque references in figure 4.19, where the inductances are underestimated by 20 %. The results are valid in the normal operating area, where field weakening is not applied. The error in estimated torque increases in magnitude with the torque reference, since the q-axis current magnitude increases heavily. The error in estimated stator flux linkage amplitude either increases or decreases with the torque reference, depending on which inductance that is erroneously estimated, as discussed previously in this section. This causes a negative correlation when x_d is underestimated, figure 4.19a, and a positive correlation when x_q is underestimated, figure 4.19b.

It is also possible that x_d and x_q are both overestimated, that they are both underestimated, or a combination where one of them is underestimated while the other one is overestimated. The peak values for the different scenarios are summarised in table 2.

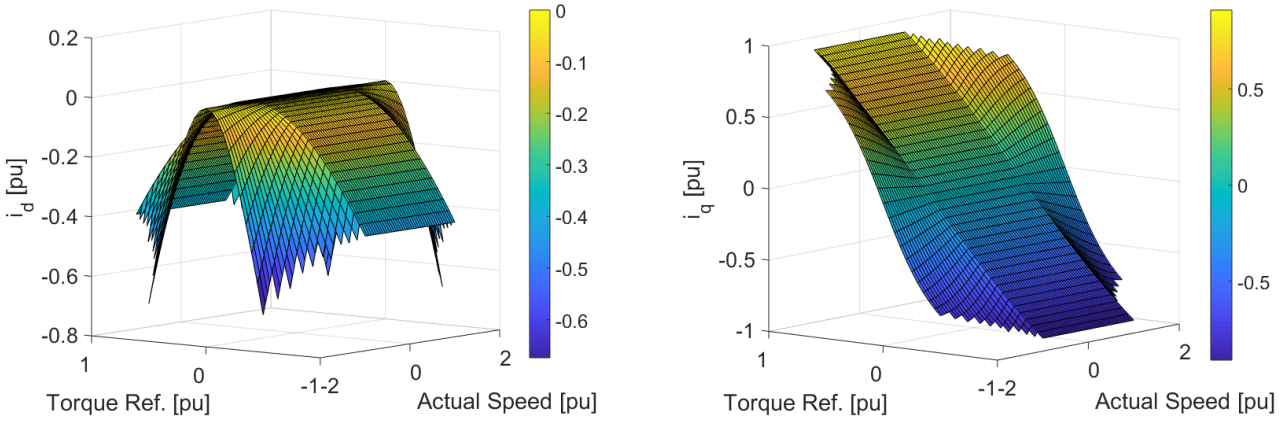

(a) d-axis current for $\hat{x}_q = 0.8x_q$

(b) q-axis current for $\hat{x}_q = 0.8x_q$

Figure 4.18: The d- and q-axis currents when $\hat{x}_q = 0.8x_d$

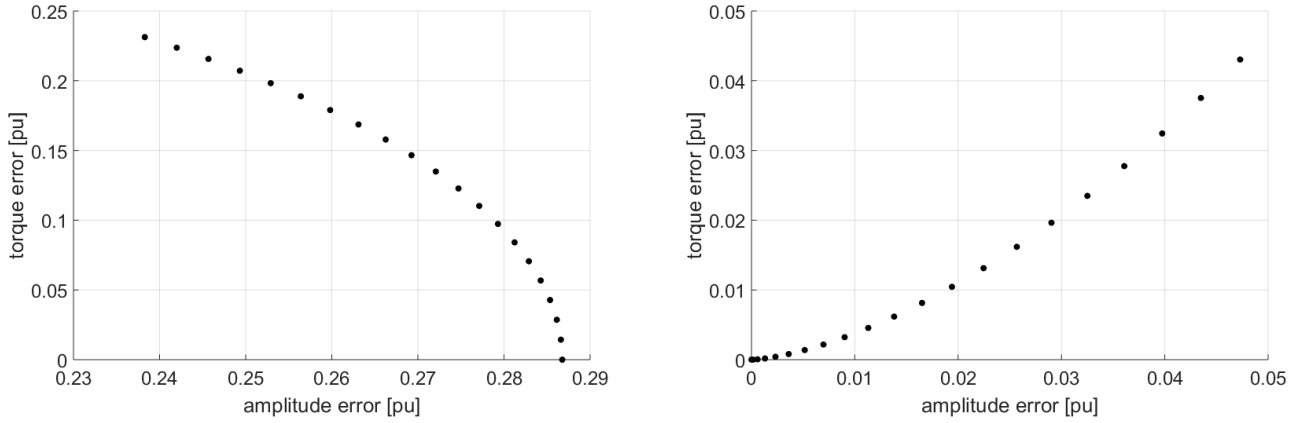

(a) $\hat{x}_d = 0.8x_d$ (b) $\hat{x}_q = 0.8x_q$

Figure 4.19: Correlation between error in estimated stator flux linkage amplitude and estimated torque for positive torque references, $\hat{x} = 0.8x$

Table 2: Maximum errors in the current model

$\frac{\hat{x}_d}{x_d}$	$\frac{\hat{x}_q}{x_q}$	$\hat{\psi}_s$ error [pu]	$\hat{\tau}$ error [pu]
1	1	0	0
0.8	1	0.29	$\pm$0.23
1.2	1	-0.18	$\pm$0.15
1	0.8	0.060	$\pm$0.057
1	1.2	-0.054	$\pm$0.057
0.8	0.8	0.29	$\pm$0.29
1.2	1.2	-0.19	$\pm$0.19
0.8	1.2	0.29	$\pm$0.16
1.2	0.8	-0.18	$\pm$0.12

From table 2 it is evident that the best estimations occur when the d-axis reactance is accurately estimated. It is also evident that the error in the estimated amplitude correlates more with the estimated d-axis reactance than what the error in estimated torque does.

From the results of the steady state analysis in this section, it is evident that the voltage model is very sensitive to the accuracy of the estimated stator resistance for lower speeds, even during steady state operation. A 20 % deviation in a stator resistance of 0.048 pu, that is a deviation as small as 0.0096 pu, may cause a large error of 0.19 pu in the estimated stator flux linkage magnitude, and in the estimated electromechanical torque. The impact of the stator resistance for a given speed increases as the torque reference of the machine increases. This is especially evident at speeds close to zero. The voltage model is more robust for higher speeds. When using the current model, the accuracy of the stator flux linkage estimation and the torque estimation depend on the stator current supplied, and on the estimated inductances in the machine during steady state. It was revealed that an erroneously estimated d axis inductance has less influence on the current model for high torque references and in the field weakening region, while an erroneously

estimated q axis inductance has more influence on the model at these operating points. It was also evident that a bad estimation of the d axis inductance is more severe than a bad estimation of the q axis inductance, for the purpose of flux linkage estimation, as the d axis inductance has a higher value than the q axis inductance. It was found that the voltage model is suitable for high speeds. As the current model do not depend on the speed in the normal operating area, and as the inductances are less likely to be saturated for low speeds, it is concluded that it is desirable to use a combined model that trusts the current model more for lower speeds, and the voltage model more for higher speeds.

5 Dynamic Analysis

Deviation between the estimated and the actual stator resistances is a likely scenario as the motor resistances depend heavily on temperature, which vary during operation of the motor. In a real life situation, it is also likely that the current and voltage measurement is somewhat inaccurate, as discussed in section 3.4. This will result in drifting. Drifting occurs because there is no negative feedback in equation 3.1, and it is a problem that has to be taken care of if the flux linkage estimate is to be used for control of the machine. In this section, the concept of drifting will be explained and illustrated, and it will be investigated how drifting affects the flux linkage estimation and the control of the machine. The actual stator flux linkage, as well as the measured rotor position, will be used as input to the control system throughout section 5, as it is initially desired to investigate the behaviour of the voltage model during dynamics only. This is realistic scenario occurring when accurate information about the position and the reactances are available, as the current model then estimates the stator flux linkage perfectly. It corresponds to that the voltage model runs in parallel with the rest of the system.

5.1 The Concept of Flux Linkage Drifting

Drifting is a known problem related to flux linkage estimation by the voltage model, and it is most easily explained by the following example. If the machine is initially excited by a DC voltage vector, the applied voltage is equal to the resistance times the current. The stator flux linkage estimated from equation 3.1 is then a constant vector aligned along the current vector. If the estimated stator resistance is estimated too small, the estimated stator flux linkage will increase with time due to the integration of the constant positive current times the error in estimated resistance. This is evident from equation 5.2. The stator flux linkage vector is thus estimated too long.

$$\underline{\hat{\psi}_s} = \int_0^t (\underline{u_s} - \hat{r}_s \underline{i_s}) dt \tag{5.1}$$

$$= \int_0^t (\underline{u_s} - r_s \underline{i_s}) dt + \int_0^t (\underline{i_s} \Delta r_s) dt \tag{5.2}$$

$$\Delta\psi_s = \psi_s - \hat{\psi}_s \tag{5.3}$$

$$= -\int_0^t (\underline{i_s} \Delta r_s) dt \tag{5.4}$$

Consider that the estimated stator resistance is then updated to the actual value, and that a torque reference is simultaneously applied to the machine. Correcting the stator resistance from an erroneous value to the correct value will stop the estimated stator flux linkage from increasing, but the flux linkage phasor is still estimated too long. The stator current becomes an AC current instead of a DC current, as the torque reference is applied, and both the real and the estimated stator flux linkages will start rotating. The trajectories of the tips of the stator flux linkage phasors will make two circles, with the same shape and size since the integral in equation 5.1 is now correct, but with different initial starting points for the tip of the estimated flux vector when the step in torque is applied. This makes the origin of the estimated circle displaced with respect to

the actual circle. It seems like the origin of the estimated stator flux linkage vector trajectory has drifted away from the origin of the actual stator flux linkage vector, illustrated by space vectors in figure 5.1a, and hence the name drifting. In this scenario, the erroneous estimation of the stator flux linkage when the torque is applied causes an initial offset to the integral in equation 5.1. The integral is correct after the estimated stator resistance is adjusted to $\hat{r}_s = r_s$, but the offset remains, moving the origin of the circle. This scenario was simulated in Simulink with $\hat{r}_s = 0.8 r_s$ during the DC magnetisation. The simulation result is presented in figure 5.1b and figure 5.2, where a torque reference of 0.8 pu is applied after 0.6 s of DC magnetisation.

The error in estimated flux linkage magnitude and flux linkage angle as a function of time are presented in figure 5.2. After the step in torque reference is applied in figure 5.2, the estimated stator flux linkage starts oscillating at the rotational frequency of the rotor, while the actual flux linkage amplitude remains constant, resulting in an oscillating amplitude error. When the simulation model performs the transformation from Cartesian coordinates in the $\alpha\beta$ domain, as in figure 5.1, into polar coordinates, the transformation is solely based on the coordinates of the end of the flux linkage vector. The starting point of the vector is assumed to be constant. From figure 5.1 it is then obvious that if the real and the estimated flux linkage vectors have the same origin, the estimated vector must have a longer magnitude than the actual vector during some parts of the period, and a shorter magnitude during other parts of the period, to move along the trajectories indicated. This explains the oscillating error in estimated flux linkage amplitude.

The erroneously estimated stator flux linkage magnitude was expected from the steady state analysis. The deviation between the angle of the actual and the estimated stator flux linkage however, $\Delta\xi_s^s$, do not correspond with the steady state analysis, where it was postulated that this error would become zero due to the unity power factor control strategy. This is because during steady state, there is no drifting, but only a change in the length of the estimated stator flux linkage. When the flux linkage vector drifts away from the origin during dynamics, as in figure 5.1, a deviation between the actual and the estimated angle is unavoidable. Consider the following example: Both the actual and the estimated flux linkage vector in figure 5.1 are initially aligned along the α axis. When the torque reference is applied, they both start rotating with the same angular velocity, but they will no longer be aligned. Consider for instance when they have both travelled $\frac{\pi}{2}$ rad from the α axis, and they point along the β axis, the two vectors are obviously not in phase. Like the error in estimated amplitude, the error in estimated angle also oscillates at the rotational frequency of the rotor.

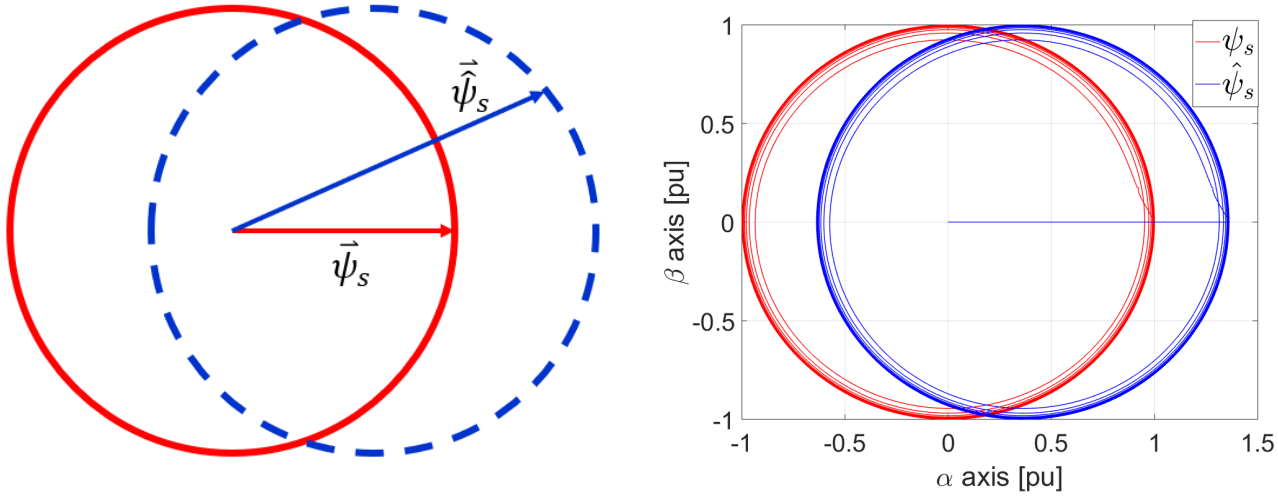

(a) Illustration of stator flux linkage drifting (b) Simulation result

Figure 5.1: $\hat{r}_s = 0.8 r_s$ during DC magnetisation, and $\hat{r}_s = r_s$ when the torque is applied

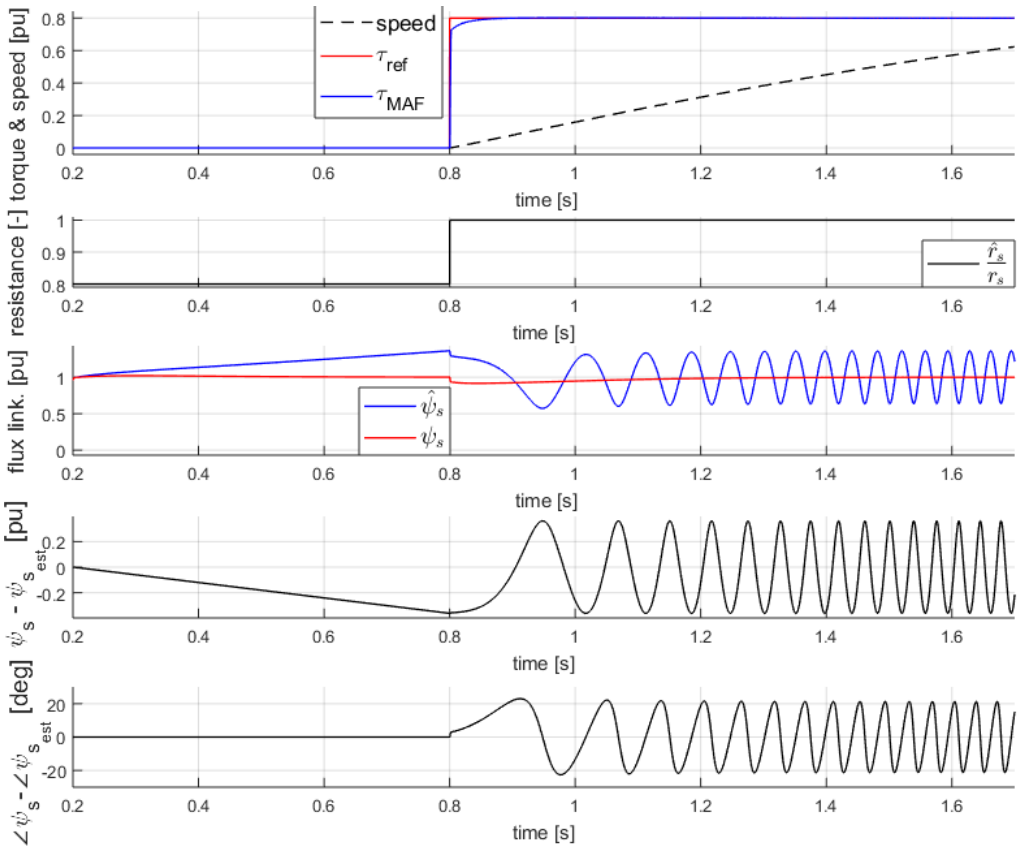

Figure 5.2: Time series of the scenario in figure 5.1b

From equation 5.1 and 5.2, the following reasoning is performed: DC offsets in voltages and currents, as discussed in section 3.4.3, will give a constant erroneous contribution to the integral. This will cause an accumulation of error in the flux linkage estimation, and the flux linkage will drift further away from its original position for each sampling. This is illustrated in figure 5.11a in section 5.2, where a drift compensation method is explained. An offset of 0.05 pu is added to phase a in the stator. It is evident how the estimated flux linkage drifts away without bounds when no drift compensation is applied. As the supplied voltage is sinusoidal, the stator current in the voltage integral is periodical and symmetrical around zero during steady state operation. The estimated stator resistance is multiplied by this current, and hence an erroneously estimated resistance will not move the origin of the flux linkage trajectory during steady state. When the torque reference is changed, transients will occur in the stator currents, and an incorrect estimate of the stator resistance will make the origin drift. It is concluded that the error in the estimated flux linkage amplitude due to an inaccurately estimated resistance occurs during both steady state and during dynamics, while drifting due to an inaccurately estimated stator resistance will occur during dynamic situations only. DC offsets in voltage and current measurement will cause drifting during both steady state operation and during dynamic operation.

Drifting due to an erroneously estimated stator resistance is also illustrated in the simulation results in figure 5.3, where the stator resistance is initially correctly estimated. No initial DC magnetisation is performed in this case. The simulation is run with speed sensors, and the moment of inertia of the machine is reduced to accelerate the machine faster. While the motor is producing a constant torque of 0.3 pu, and the rotor has obtained a constant speed of 0.61 pu, the estimated resistance is reduced by 50 %. This simulates the situation where the actual stator resistance is higher than the estimated one, which may typically occur due to heating of the resistance. Even if the error in estimated stator resistance is more likely to increase gradually in a real situation, and not this much, this scenario is useful for illustrating the drifting. From figure 5.3, it is evident how the voltage model estimates the stator flux linkage perfectly when the stator resistance is correctly estimated, but as the estimated resistance is changed, the error in estimated amplitude and estimated angle of the stator flux linkage start oscillating. A major difference between this scenario and the previous one in figure 5.2, is that the resistance is now erroneously estimated while an AC voltage is supplied.

From the results in figure 5.3, it is interpreted that the rotating estimated stator flux linkage drifts due to the dynamics caused by the change in stator resistance. This is evident from the oscillations in the estimated flux linkage amplitude error and in the estimated flux linkage angle error. It is also known that the magnitude of the flux linkage phasor will change as the estimated resistance changes. It is important to note that a new steady state is obtained, and that no drifting occurs in this new steady state. The flux vector keeps rotating along a new circular trajectory, with a new size and a new origin. This is due to the sinusoidal voltages. The new flux linkage trajectory has a larger radius, as the stator resistance is underestimated and the machine operates as a motor. When the estimated stator resistance is updated to the correct value after some time, it is evident that the error in estimated stator flux linkage angle and magnitude still oscillate. This is a very important observation. The amplitudes of the oscillations are now even larger, due to the dynamics caused by the second change in resistance. The actual and the real flux linkage trajectories now have the same size and shape, but the estimated trajectory still has a displaced

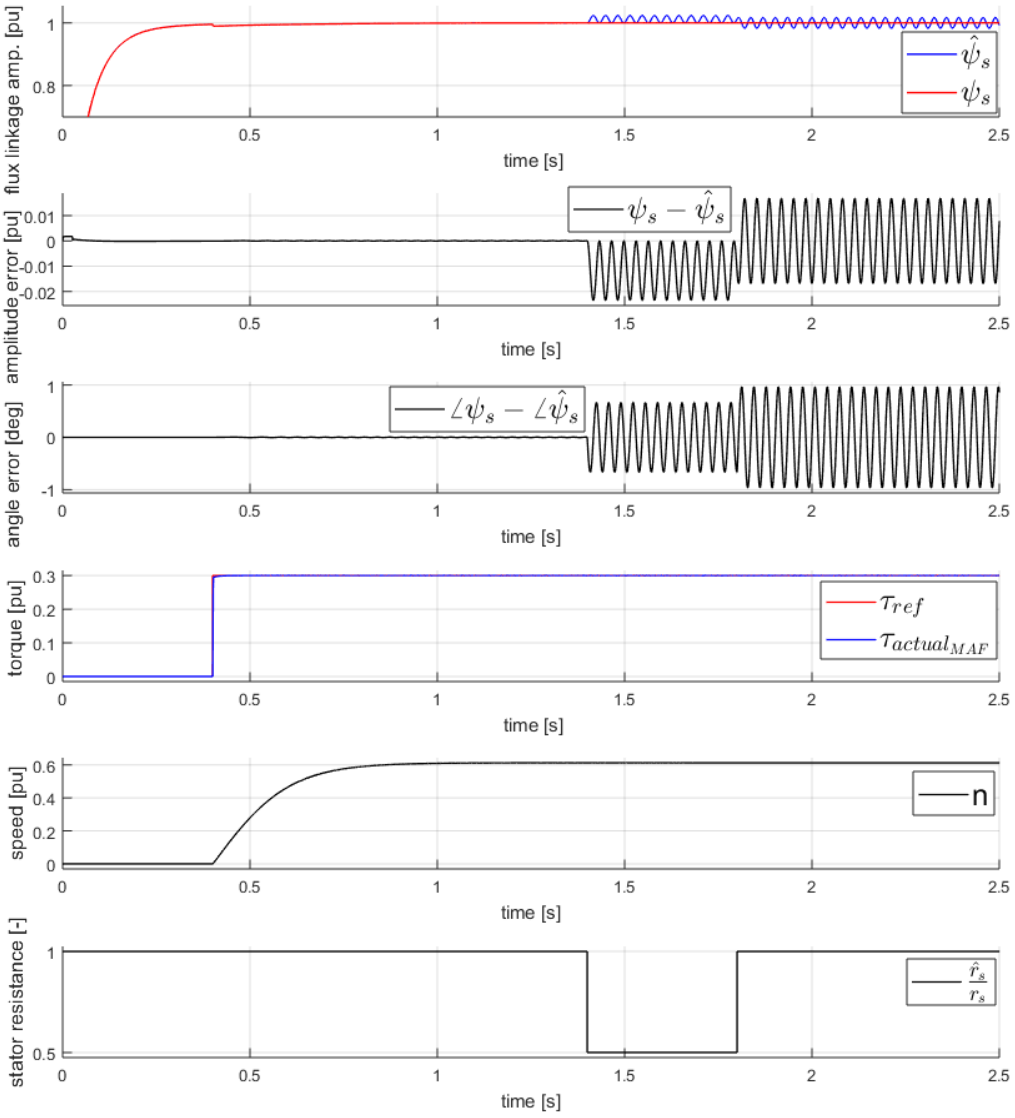

Figure 5.3: Drifting due to a sudden change in the estimated stator resistance

origin. This causes the oscillating errors. It is concluded that the offset established is not removed by updating the estimated resistance to the correct value.

From the steady state analysis, it was concluded that the voltage model is more reliable, and less sensitive to the accuracy of the estimated stator resistance for higher speeds. It is also known that the stator flux linkage integral in equation 3.1 is more exposed to drifting during low speed operations [13]. These statements are supported by the results presented in figure 5.4, where the estimated stator resistance is changed from the actual stator resistance to half of the actual stator resistance after 1 s at three different speeds. The same torque reference is applied in all three scenarios, to obtain the same stator current, but the moment of inertia of the rotor is changed. It is evident from the figure that the higher the rotor speed is when the resistance is changed, the smaller the error in both magnitude and angle of the estimated stator flux linkage become. This

is in accordance with equation 5.5, as the frequency occurs in the denominator after integrating the sinusoidal current.

$$\begin{aligned}\Delta\psi_s &= -\int \Delta r \underline{i}_s dt = -\Delta r i_{peak} \int e^{j\omega t} \\ &= \frac{\Delta r}{\omega} i_{peak} e^{j\omega t}\end{aligned} \tag{5.5}$$

Equation 5.5 states that the error in estimated flux linkage decreases linearly with the frequency of the supplied current, which is supported by the results in figure 5.4. It is concluded that how much the stator flux linkage drifts, is highly dependent on the speed of the motor in the instant when the dynamic, and hence also the drifting, occur.

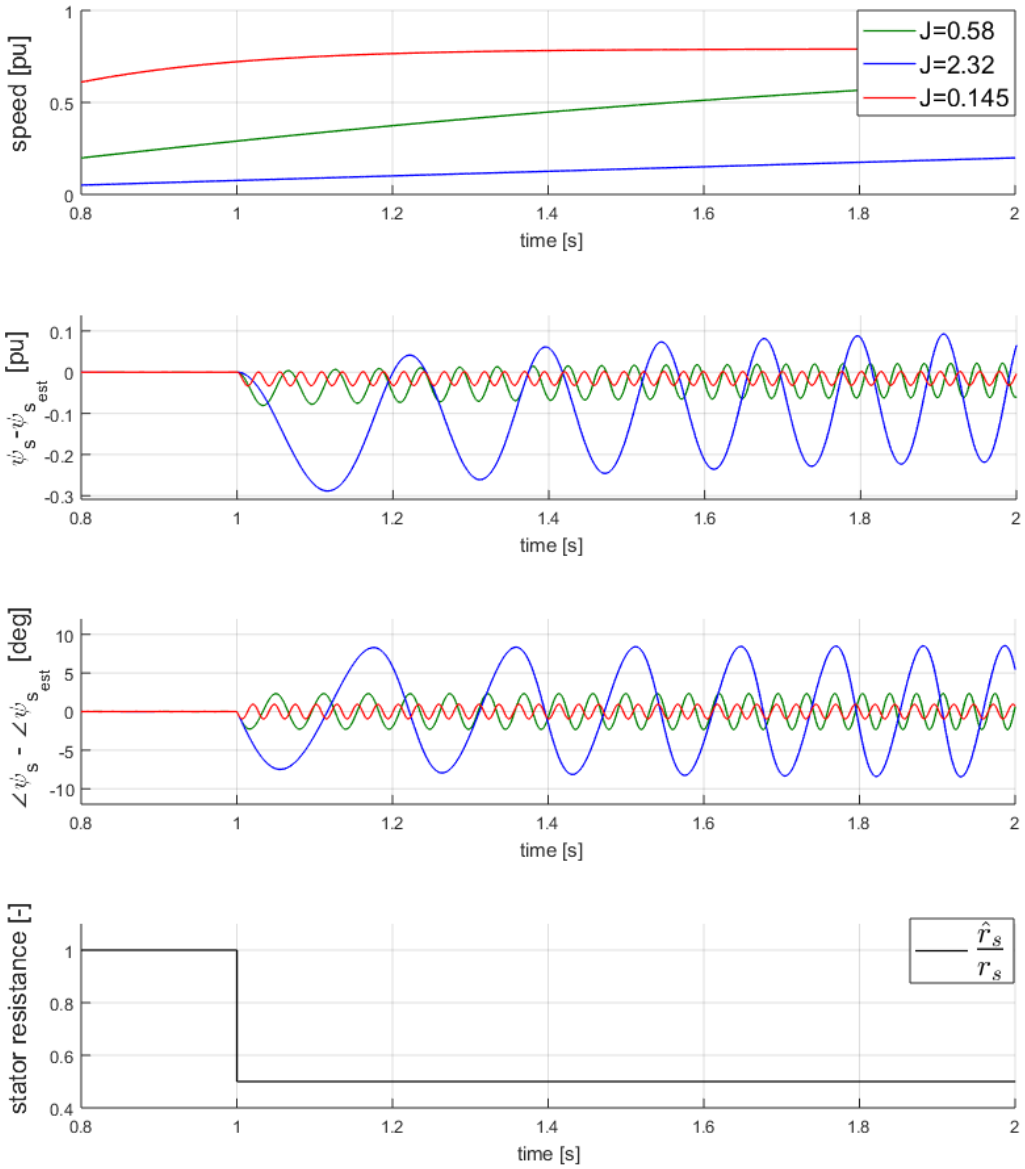

Figure 5.4: Changing $\hat{r}_s$ at three different speeds

As previously mentioned, no drifting will occur during steady state, if the estimated stator resistance is the only parameter in the voltage model that deviates from the actual parameters in the machine. From figure 5.4 it is interpreted that the flux linkage vectors move along constant trajectories after the resistance is changed, even if the speed increases. Increasing the speed when a new steady state is obtained apparently does not remove the offset, and hence the error in both estimated flux linkage magnitude and in the estimated angle remain. This is not evident from equation 5.5. This observation is even more evident in figure 5.5, where the estimated stator resistance is half of the actual stator resistance for the whole time range. It is evident that the error in both estimated stator flux linkage amplitude, and in estimated stator flux linkage angle, oscillate with constant amplitudes through the whole spectre of speeds. It is summarised that the offset in the drifted stator flux linkage is not removed by correcting the parameters, nor by increasing

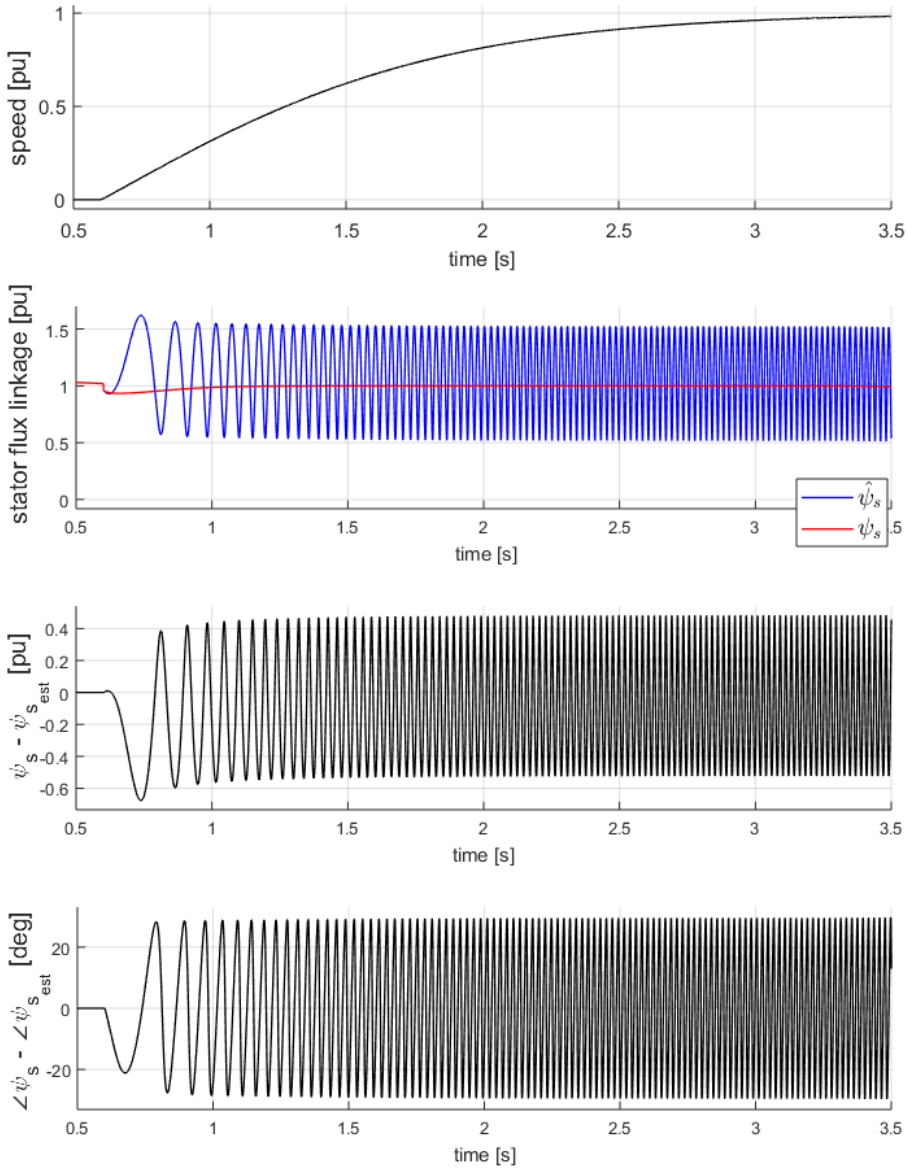

Figure 5.5: Constantly erroneous estimated stator resistance while the speed increases, $\hat{r}_s = 0.5r_s$

the speed. These are important observations that were not revealed by the steady state analysis. The erroneously estimated stator resistance gives an offset to the integral. By increasing the speed or by correcting the stator resistance, future contributions to the integral in equation 3.1 become correct, and hence the trajectory of the estimated flux linkage gets the correct size and shape. The trajectory is however still displaced, as the offset is still in the integration. The history of the integration process is hence of importance. The offset could be removed by using a high pass filter, filtering away the DC component, but in this thesis another correction method is applied. This method is explained in section 5.2.

The oscillations in flux linkage magnitude will give a bad torque control during sensorless operation, as the stator current is determined by the estimated stator flux linkage, as in equation 2.43 and equation 2.51. Both the oscillating magnitude, and the error in estimated flux linkage angle will give bad estimates of the rotor position. This is illustrated in figure J.1 in appendix J. Hence a way of compensating for the drifting is necessary.

5.1.1 Behaviour of the Voltage Model When Driving Through Zero Speed Without Correction

To analyse the voltage model during dynamic low speed operations, and how the flux linkage estimation depends on the estimated stator resistance, simulations were run with three different estimates of the stator resistance. It is reminded that the measured position and the actual flux linkage from the machine model is used to control the machine. In figure 5.6, the motor is accelerated before it slowly drives through zero speed as a ramp.

From figure 5.6 it is evident that the stator flux linkage is estimated perfectly in the whole speed range when the stator resistance is equal to the actual resistance. A stator resistance estimated 20 % above or 20 % below the actual resistance gives an oscillating error both in the estimated stator flux linkage amplitude, and in the angle of the estimated stator flux linkage, as described previously. The obtained flux linkage estimates reveal a a high degree of symmetry between the scenarios where the stator resistance is overestimated and where it is underestimated, as expected from the steady state analysis. The most important observation is how the oscillating error between the estimated and the actual stator flux linkage amplitude and the oscillating error between the estimated and the actual stator flux linkage angle both increase after the rotor has passed through zero speed, and how the new and larger errors remain as the speed increases in negative direction. This reveals that the estimated flux linkage drifts as the motor crosses zero speed. During the zero crossing, the supplied frequency is very low. One might consider it as a short time interval with a DC voltage supplied. The erroneously estimated stator resistance will have a small influence on the generated electromechanical torque even if the actual flux linkage is used as input to the control system, as the PI controllers were tuned based on the stator resistance in the specialisation project. However, this influence was found to be negligible in this scenario, and hence the generated torque and the speed of one of the three scenarios only is included in figure 5.6.

In this section it was stated and argued by simulation results that the drifting due to deviation between the estimated and the actual resistance occurs during dynamics only, because the resis-

tance in equation 5.1 is multiplied by a quantity that is symmetrical around zero during steady state operation. However, if an offset occurs in the voltage measurement, as discussed in section 3.4.3, this offset will be integrated for each sampling, and the error will accumulate. Hence, this will cause a constantly drifting flux linkage vector. This is illustrated in figure 5.11a in section 5.2, with and without correction, where an offset of 0.05 pu is added to phase a. The estimated flux linkage then drifts away without any correction, and the flux linkage estimate can not be used for sensorless control. As expected, the estimate of the stator flux linkage becomes less accurate when the speed is reduced, as long as $\hat{r}_s \neq r_s$, and the estimated flux linkage drifts when the machine drives through zero speed. The speed of the machine in the instant when the drifting occurs is of vital importance for how much the flux linkage will drift. If drifting occurs, neither updating the stator resistance to a correct value, nor increasing the speed removes the offset. It is concluded that a correction method is necessary to obtain accurate control in the low speed operating region.

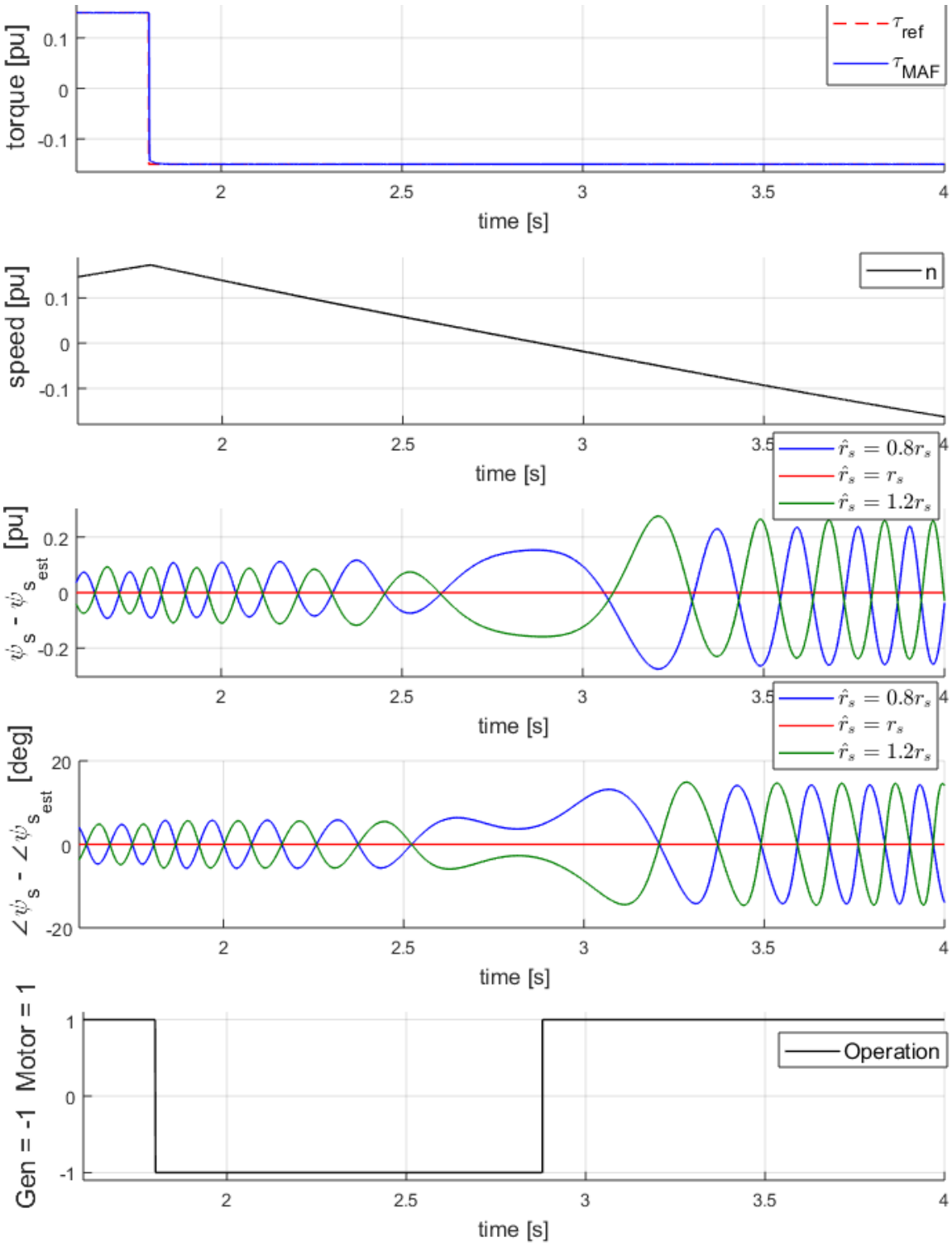

Figure 5.6: Driving through zero with the voltage model, no correction

5.2 Flux Linkage Drifting Correction

To correct for the drifting, the "correction method based on the square of the stator flux linkage amplitude", suggested by Niemelä is initially used [21]. According to Niemelä, the method works above 0.5 Hz, when 50 Hz is the nominal frequency. This method was implemented and explained in the specialisation project of Bendik Fossen [7]. For convenience, the explanation is repeated here. This master thesis will also illustrate and analyse the performance of the correction method on the investigated machine, by presenting simulation results. Furthermore, it will be discussed how the different parameters should be tuned, as the behaviour of the investigated separately excited synchronous machine is somewhat different from that of the permanent magnet machine studied by Bendik Fossen. Improving the correction term k_T was also mentioned as recommended further work by Fossen [7].

The method is based on that if the square of the stator flux linkage magnitude is subtracted from the square of the same signal lowpass filtered, an error signal, e, that has its peaks at the same instants as the stator flux linkage estimate squared is obtained. The error signal and the estimated stator flux linkage squared are oppositely directed, as seen from the simulation results in figure 5.7, meaning that the error signal, e, is oppositely directed to the eccentricity of the stator flux linkage estimate. The error signal from equation 5.6, which also correlates with the error in the estimated stator flux linkage magnitude, thus indicates how much the stator flux linkage should be corrected to counteract displacement of the flux vector trajectory. The error obtained from 5.6 is multiplied by a correction constant, $k_{\psi_{corr}}$, and by the estimated stator flux linkage to obtain a correction vector aligned along the estimated stator flux linkage. The estimated stator flux linkage after correction is now expressed as in equation 5.7.

$$e = \hat{\psi}^2_{s_{LPF}} - \hat{\psi}^2_s \tag{5.6}$$

$$\underline{\hat{\psi}_s}[k+1] = (1 + k_{\psi_{corr}} e)\underline{\hat{\psi}_s}[k] \tag{5.7}$$

In figure 5.7, the results from a simulation without correction enabled, where the estimated stator resistance is half of the actual stator resistance in the synchronous machine is presented. It is evident that a positive error in the estimated stator flux linkage amplitude, which indicates that the actual stator flux linkage vector has a larger magnitude than the estimated stator flux linkage vector, occurs approximately simultaneously as the correction signal is positive. Hence, a positive correction signal is added to the estimated flux linkage, correcting the estimate towards the actual value. When the flux linkage amplitude is estimated too long, the error is negative, and a negative correction signal is added to the estimate.

To improve the step response of the lowpass filter, a zero point was implemented in the lowpass filter by Bendik Fossen [7]. The derivative term is included such that the filtered value will follow the unfiltered value better during fast changes in stator flux linkage, such as during step changes in torque. The lowpass filter expressed in equation 5.8 is discretised in equation 5.10.

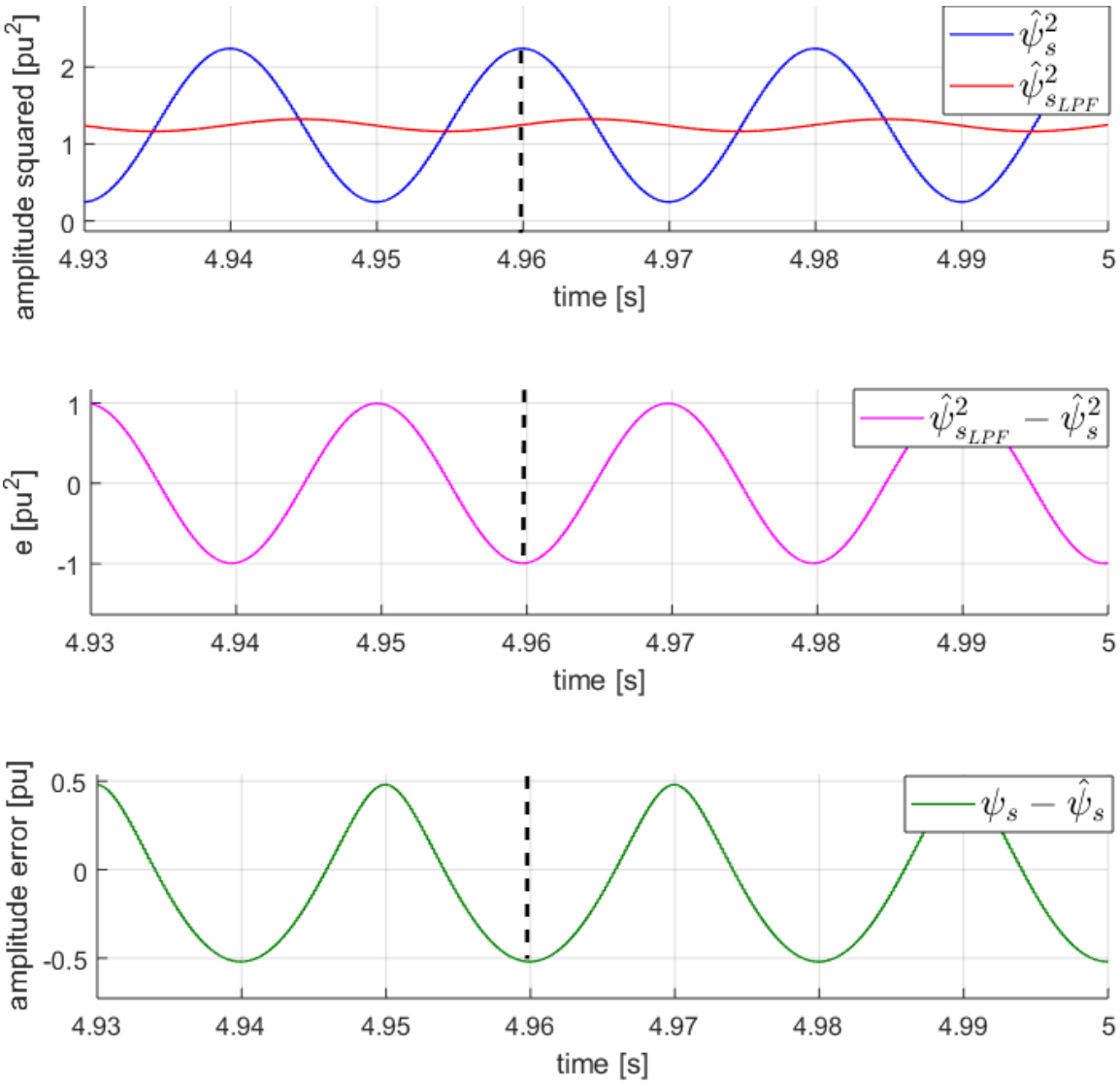

Figure 5.7: The drift correction method illustrated

$$LPF = \frac{1 + sT_2}{1 + sT_{filter}} \tag{5.8}$$

$$k_T = \frac{T_2}{T_{filter}} \tag{5.9}$$

$$y[k+1] = y[k] + \frac{T_{sample}}{T_{filter}}(u[k] - y[k]) + k_T(u[k] - u[k-1]) \tag{5.10}$$

As the speed of the rotor varies during operation, so does the speed of the rotating stator flux linkage. Hence, the filter time constant, T_{filter}, in the low pass filter is made adaptive. The filter time constant is made dependent on the speed by equation 5.11, with a maximum value of 1.75 to avoid a too high filter time constant at very low speed speeds.

$$T_{filter} = min\Big(1.75, \frac{2}{nf_n}\Big) \tag{5.11}$$

"Drifting is a relatively slow phenomenon" [21]. During rapid changes in torque, such as step changes, the stator flux linkage will change rapidly due to rapid changes in the stator current. This will cause an error between the lowpass filtered flux linkage and the unfiltered flux linkage. As this is no drifting, no correction is required, and an undesired correction has to be avoided in these cases. This is achieved by implementing an adaptive k_T, as explained in the doctoral thesis of Julius Luukko [15], [16]. A signal proportional to the torque reference, in this case the torque generating current component orthogonal to the stator flux linkage, i_B, is subtracted from the same signal filtered through a lowpass filter. The value obtained is multiplied by a constant k_{T_0} to get k_T, as expressed in equation 5.12. Hence when there is no change i torque, $k_T = 0$, and the derivative term in equation 5.10 is not activated. During steps in the torque reference, k_T gets high, and the filtered estimate of the stator flux linkage squared is forced towards the unfiltered value. This is performed to minimise the error signal, e, in the next time step. At the same time, $k_{\psi_{corr}}$ is set to zero, as seen from equation 5.13, to avoid correction during the current time step.

$$k_T = min(1, k_{T_0}[i_B - i_{B_{filtered}}]) \tag{5.12}$$

$$k_{\psi_{corr}} = (1 - k_T k_2) k_{\psi_{corr_0}} \tag{5.13}$$

$k_T k_2 \leq 1$, and k_2 and $k_{\psi_{corr_0}}$ are adjustable gains. K_T is limited to 1, to avoid amplification at low frequencies. I this work, it will be investigated how sensitive the flux estimation is to changes in the constants k_{T_0} and k_2. The value of $k_{\psi_{corr_0}} = 0.0075$, used by Bendik Fossen seems to be wisely chosen, as both an increase and decrease in the value gives less satisfying results. The correction algorithm is implemented in a subsystem in Simulink which will be referred to as the correction block, the correction algorithm or the correction method based on the square of the stator flux linkage amplitude throughout this thesis. Minor changes are made on the implemented model made by Bendik Fossen, provided by supervisor Roy Nilsen [7]. The sensorless operation with the correction block both enabled and disabled will be investigated.

How the correction block compensates for the drifting is illustrated in figure 5.8, with the corresponding time series presented in figure 5.9. A torque reference of 0.8 pu is applied after 0.4 s. The stator resistance is estimated 20 % too low, during the whole simulation. Initially, the correction method based on the square of the stator flux linkage amplitude is not enabled, and it is evident how the flux linkage drifts away from the origin. As expected, the tip of the estimated stator flux linkage moves along a constant circle with a larger diameter, and with a displaced origin, when a new steady state is obtained. This is observed by the blue circle in figure 5.8, and by the oscillating error signals, with constant amplitude, in figure 5.9. After 1s, the correction algorithm is enabled, and the flux linkage is corrected back to its original position. The two trajectories now get the same origin, which removes the error in estimated flux linkage angle entirely, and makes the deviation between actual and estimated magnitude constant. This is evident from the green circle in figure 5.8. The magnitude is still estimated too long, as the estimated stator resistance makes the integral in equation 5.2 erroneous. If the stator resistance was estimated too high, the magnitude would be estimated too short, as Δr_s then would be negative in equation 5.2, and as the machine operates as a motor. The same results as in the steady state analysis are then obtained. How much, and in which direction the flux linkage drifts without the correction depends on whether the estimated resistance is estimated too high or too low, and on how much the estimated value deviates from the actual value. This is illustrated in figure I.1 in appendix

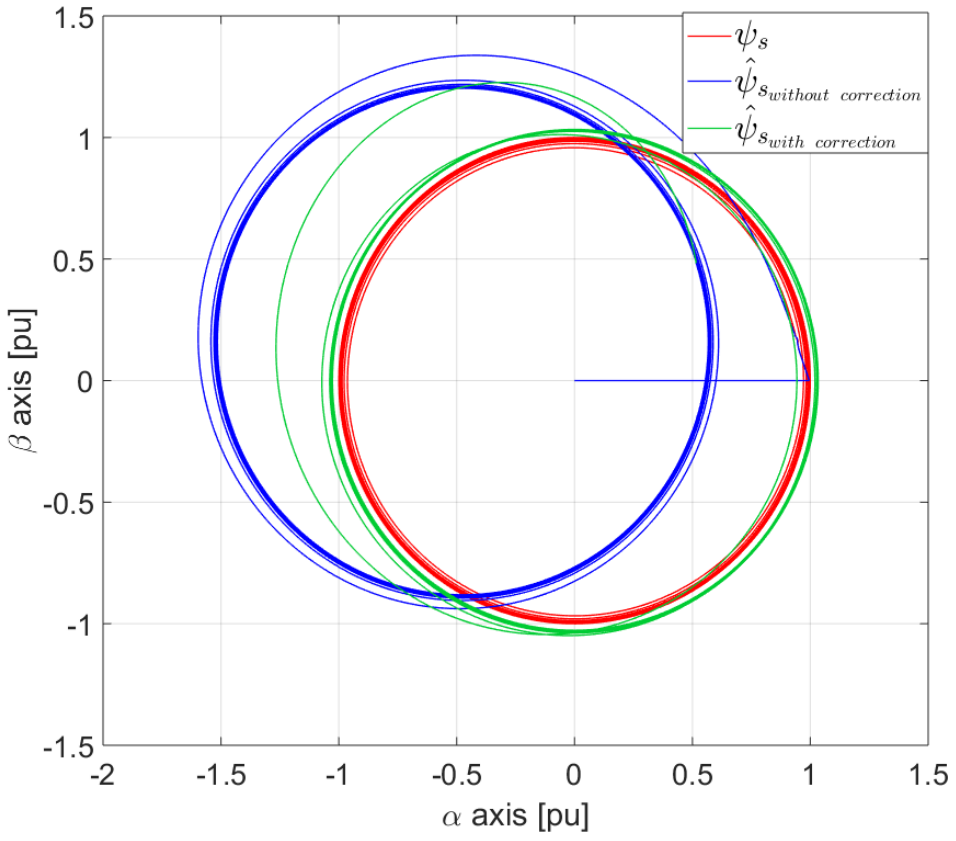

Figure 5.8: Stator flux linkage trajectory during drifting, $\hat{r}_s = 0.5 r_s$

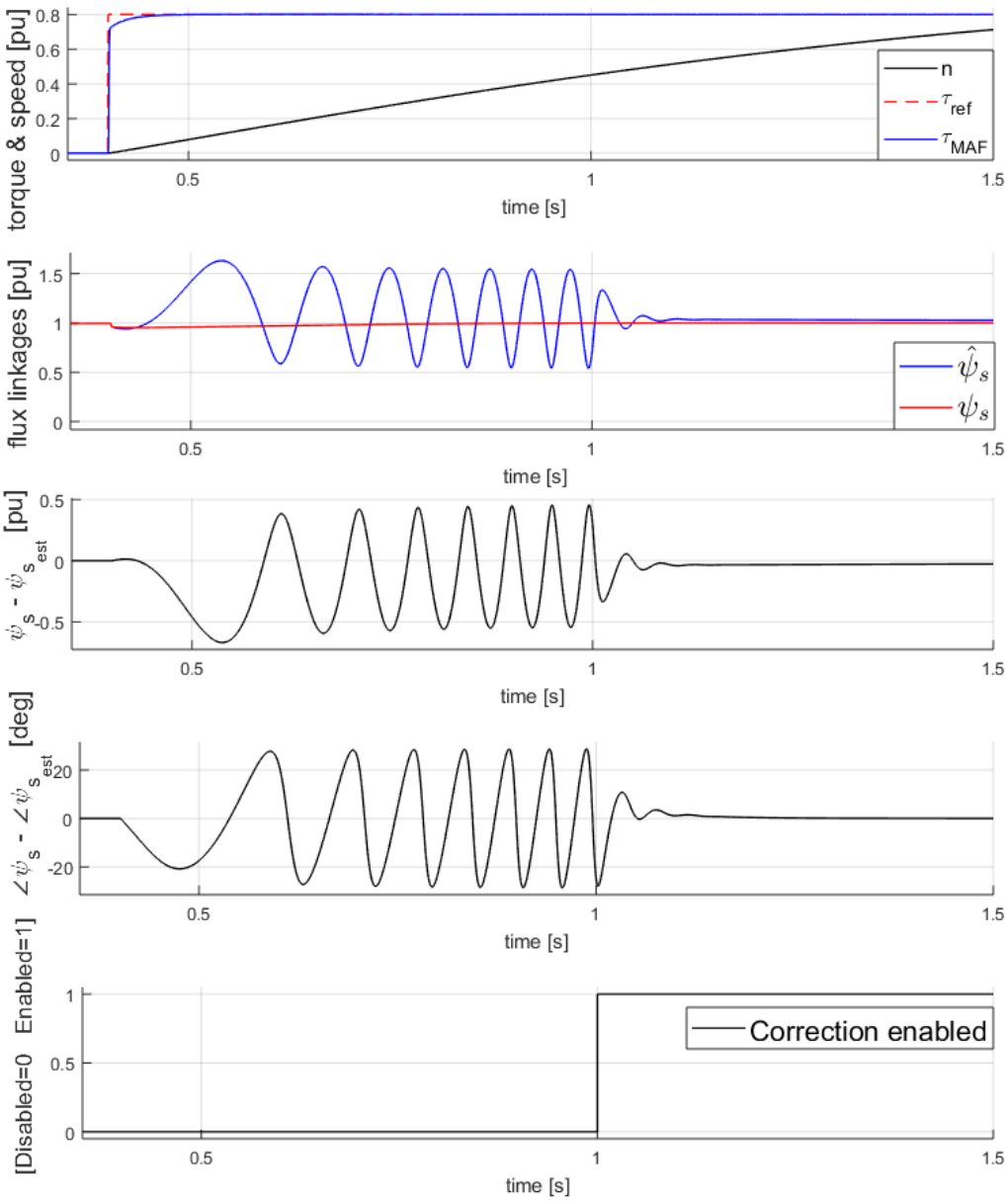

Figure 5.9: Time plot of figure 5.8

I, where the stator resistance is erroneously estimated of different degree during a step in torque reference. It was also illustrated in section 5.1 that the drifting is highly dependent on the speed in the moment when drifting occurs. The speed during drifting is approximately equal for all the scenarios in figure I.1, as the same torque reference is applied. Whether the machine operates as motor or generator will also influence the direction of the drifting.

The same conclusions are made from the time series analysis in figure 5.10, where the same scenario as in figure 5.3 is investigated, but this time the stator flux linkage correction is enabled. It is evident from the figure that the oscillations in estimated stator flux linkage amplitude error is damped out due to the correction algorithm, while a constant error in the estimated magnitude

remains as long as the stator resistance is incorrectly estimated. The error in estimated stator flux linkage angle is removed entirely. This indicates that the estimated stator flux linkage and the actual stator flux linkage now have the same starting point. The drifting has been compensated for, and the purpose of the correction algorithm is obtained. If the estimated resistance is also updated to be equal to the actual stator resistance while the correction algorithm is enabled, as after 1.8 s in figure 5.10, the constant error in estimated flux linkage magnitude is removed entirely. The stator flux linkage is then estimated perfectly. This can be obtained by on-line parameter estimation. It is concluded that the correction based on the square of the flux linkage amplitudes removes the offset completely, but additional actions must be performed to compensate for the deviation between actual and estimated stator flux linkage magnitude during steady state.

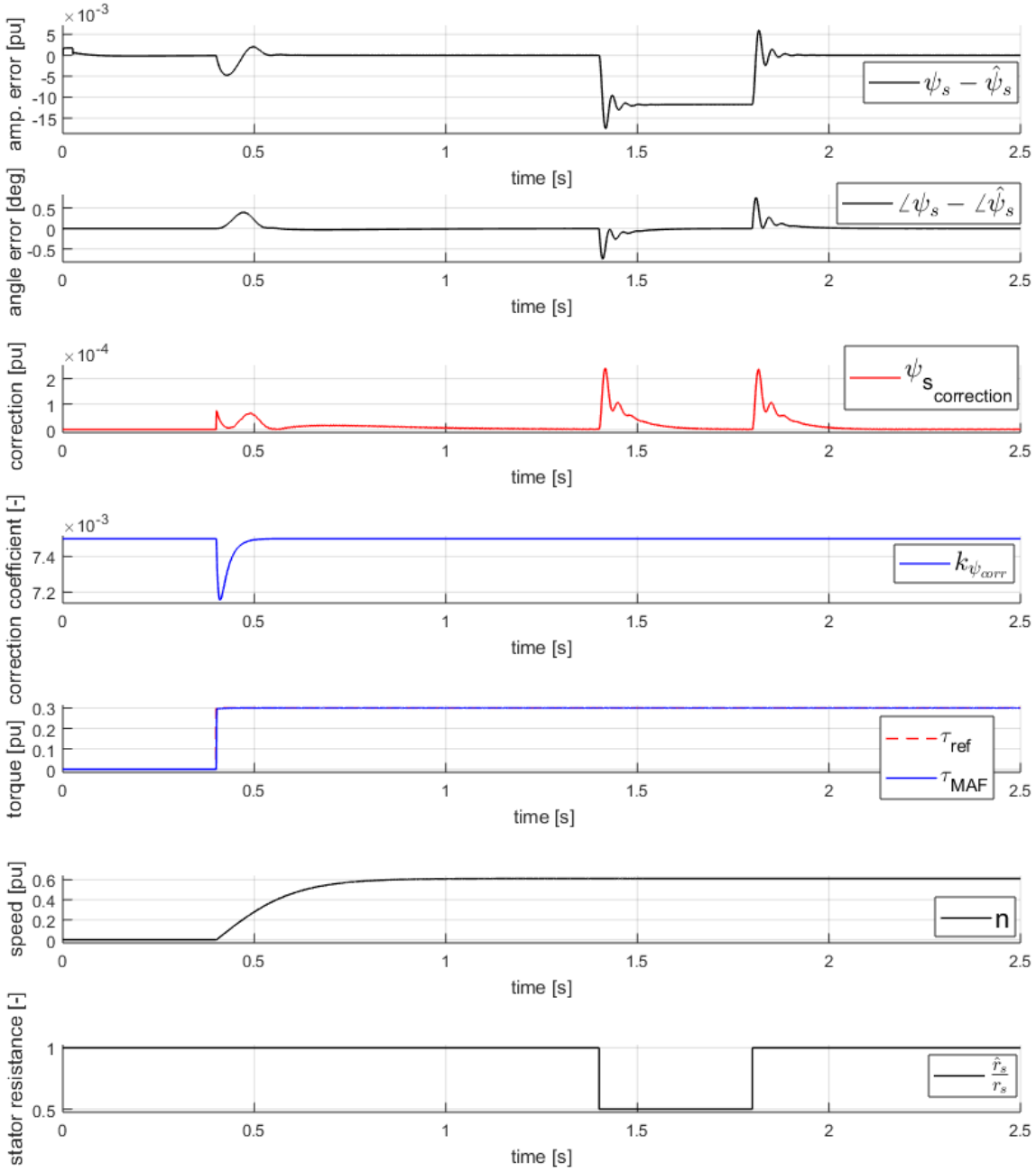

Figure 5.10: Drifting due to a sudden change in the estimated stator resistance

By comparing figure 5.3 and 5.10, it is also evident that the behaviour is better without the correction as long as the stator resistances are correctly estimated. Without the correction, the stator flux linkage is estimated correctly throughout the whole simulation when the stator resistance is estimated correctly. Hence, any contribution from the correction algorithm will act as a disturbance on the flux linkage estimate, which was also concluded in [7]. From figure 5.10 it is observed that the correction coefficient, $k_{\psi_{corr}}$, is reduced during the torque step, but not entirely to zero as intended. A correction signal, $\psi_{s_{correction}}$, is hence generated from the correction algo-

rithm, disturbing the stator flux linkage estimate. Error occur between the real and the estimated flux linkage amplitude, and between the real and the estimated flux linkage angle, when the step in torque reference is applied. This indicates that the gains k_T and k_2 in the correction algorithm are not optimally tuned. This will be analysed more thoroughly in section 6.2.2

In figure 5.11 it is illustrated how the estimated stator flux linkage drifts when there is an offset in the voltage measurement. An offset of 0.05 pu is added to the measured voltage in the stator phase a. Position sensor and actual stator flux linkage is used in the control of the machine. In figure 5.11a, no compensation is applied, and hence the flux linkage drifts away from the origin without bounds, as discussed in section 5.1. The drifting is in the same direction as the offset, that is along the phase a axis in this case, which is aligned along the α axis. In figure 5.11b, the correction method based on the square of the stator flux linkage amplitude is applied. It is evident that the flux linkage do not become origin centred, as in the previous scenarios, but the drift compensation stops the flux linkage from drifting without bounds. A new steady state is obtained, with a displaced origin. It is hence concluded that the correction method based on the square of the stator flux linkage amplitude is improving the flux linkage estimate during measurement offsets, but that it works better for compensating drifting due to erroneously estimated stator resistances.

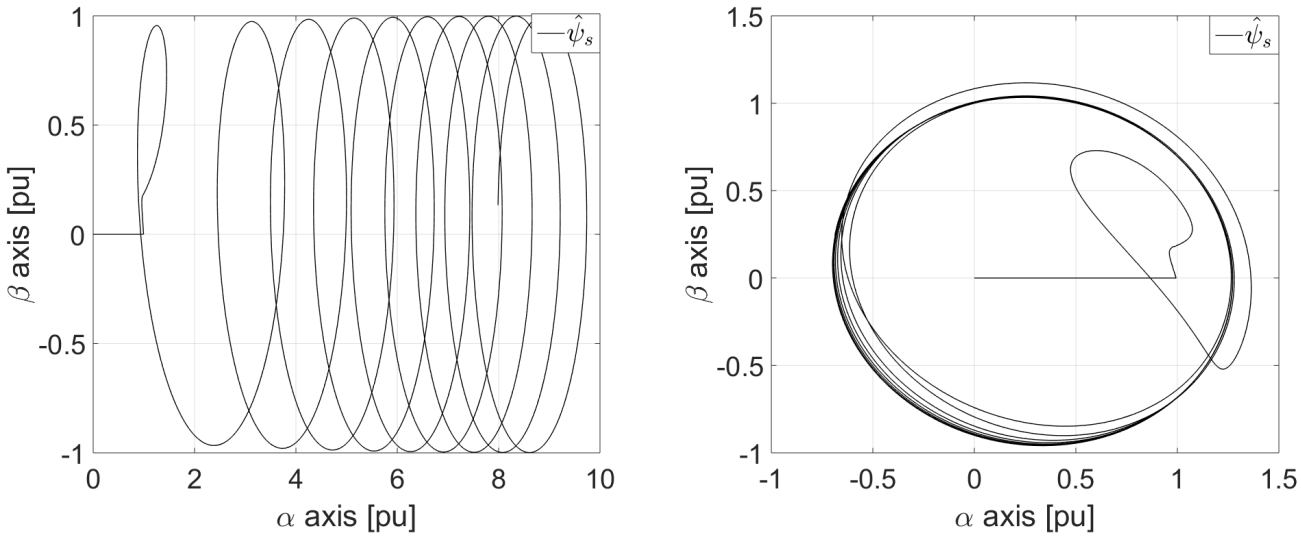

(a) Without compensation

(b) With compensation

Figure 5.11: Drifting due to 20 V (0.05 pu) DC offset in phase a

6 Sensorless Operation

So far it has been investigated how the voltage model is affected by parameters in the model during steady state, and during dynamics dynamics, when the control system has used the actual flux linkage and the measured position as input. Now, sensorless operation will be investigated. The estimated rotor position and the estimated stator flux linkage will now be used as input to the control system. Both of these properties will influence the generated torque. The orientation of the stator current is calculated in the dq coordinate system, and both the angle and the magnitude of the stator current is calculated based on the magnitude of the stator flux linkage, as seen from equation 2.43 and 2.51. As the control system is based on the estimated input, as flux linkage and rotor position, there will be dynamics between the actual and the real stator flux linkage. This dynamic has not been included in the analysis performed so far.

6.1 Without Correction

The attempt of running sensorless without correction is presented in figure 6.1, where the estimated resistance is estimated 20 % too low and 20 % too high through the whole simulation. The results are repeated in larger scale in figure J.2 and figure J.3 in appendix J. No initialisation of rotor position is performed. As expected, the oscillatory flux linkage will result in an oscillatory generated torque. What is more surprising is the asymmetry between the two scenarios when the stator resistance is underestimated and when it is overestimated. It is revealed that when the resistance is underestimated by 20 %, the error in estimated flux linkage magnitude and flux linkage angle, and the difference between the reference torque and the actual torque oscillate with amplitudes that increase with time during motor operation, as the flux linkage estimate and the stator current influence each other. During generator operation, the errors oscillate with a more or less constant amplitude. This may indicate that the amplitudes of the oscillating error signals increase with the speed. When the stator resistance is estimated too high, the errors decay with time during motor operation, while they remain constant during generator operation. The control fails in the first scenario, as the estimated angle exceeds 180 °. In figure 6.1 this happens some time after the machine has driven through zero speed, as the machine then starts operating as motor in the negative rotational direction, after operating as generator for some time, and the errors continue to increase. In the scenario with an overestimated resistance however, the control of the machine remains stable after crossing zero speed, despite massive oscillations in the flux estimate, generated torque and speed. In both cases the control of the machine is far from satisfying. If the machine is used for pumped hydroelectric storage, the oscillating generated torque and speed will cause wear and tear, and potentially damage the pump and other constructions, due to the movement of massive amounts of water. The same observations were made when the torque reference was in the opposite directions during both motor and generator operation. This indicates that when running sensorless without correction, it is more severe if the stator resistance is estimated too low, than if it is estimated too high. Hence, for the purpose of sensorless control, the stator resistance should be overestimated during motor operation, if the machine for some reason has to run sensorless without any correction. It should be noted that overestimating the resistances is not recommended from an energy point of view, as the actual current flowing in the windings is larger than the estimated current. This may in the worst case burn out the windings.

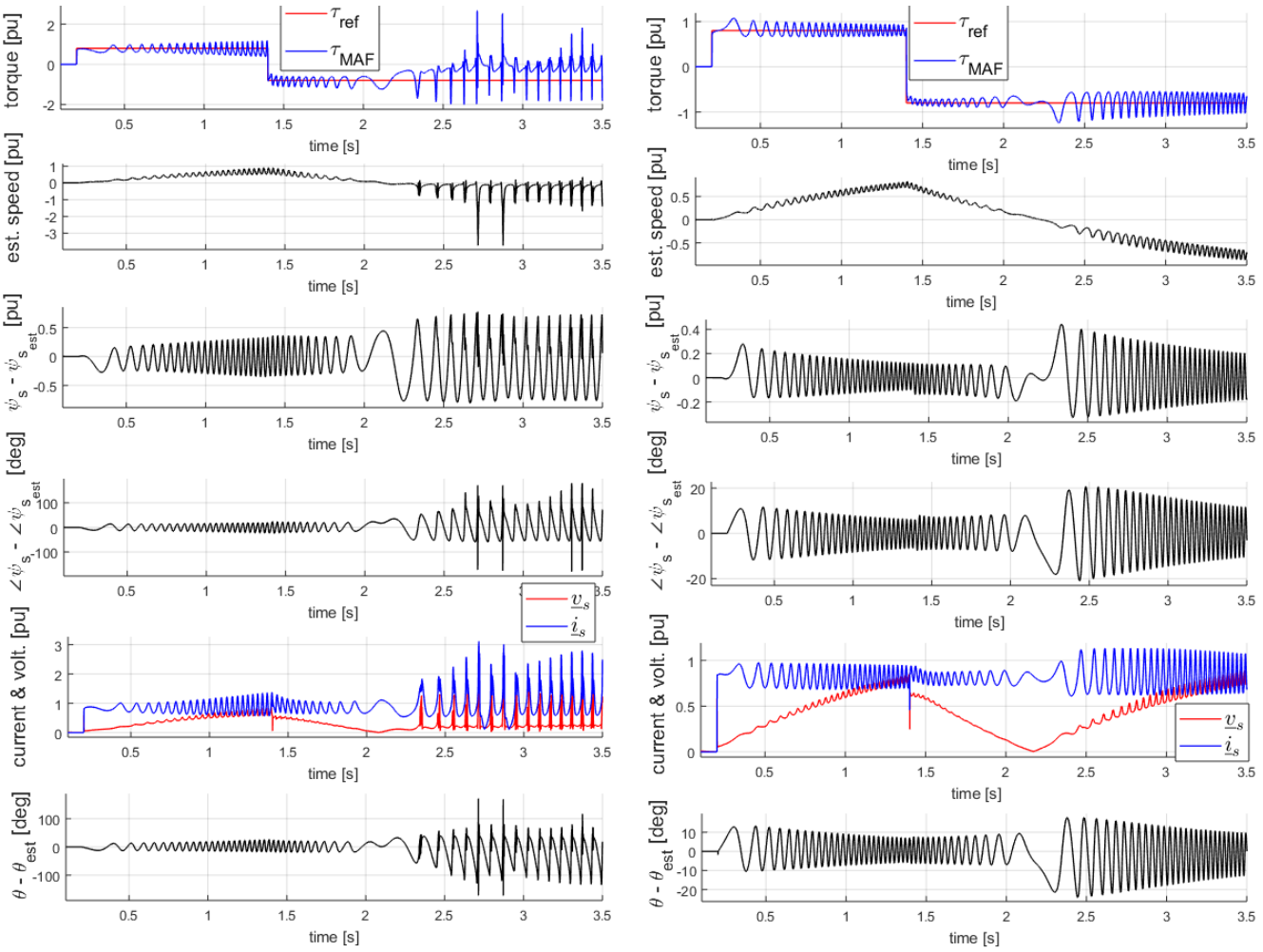

(a) $\hat{r}_s = 0.8r_s$ (b) $\hat{r}_s = 1.2r_s$

Figure 6.1: Sensorless operation without correction

6.2 With Correction

A quite similar torque reference as in figure 6.1 is applied once again to the machine, but this time the correction algorithm is enabled. The only difference in torque reference is that DC magnetisation is now performed for 0.2 s after the magnetisation by the field winding. The results for the three scenarios where the stator resistance is estimated correctly, 20 % too low and 20 % too high is presented in figure 6.2. Several observations are made from the figure. It is observed that the largest deviation between actual and estimated stator flux linkage occur while the speed is low; during the first step in torque reference, and when the machine drives through zero speed. At the first step in torque, error occurs for all the simulated scenarios, even when the stator resistance is correctly estimated, indicating bad performance of the correction algorithm at start up. This is more thoroughly discussed in section 6.2.1. While driving through zero speed, the deviation between actual and estimated stator flux linkage is more evident in the scenarios where $\hat{r}_s \neq r_s$, but there is still a very small deviation when the resistance is correctly estimated. This error is

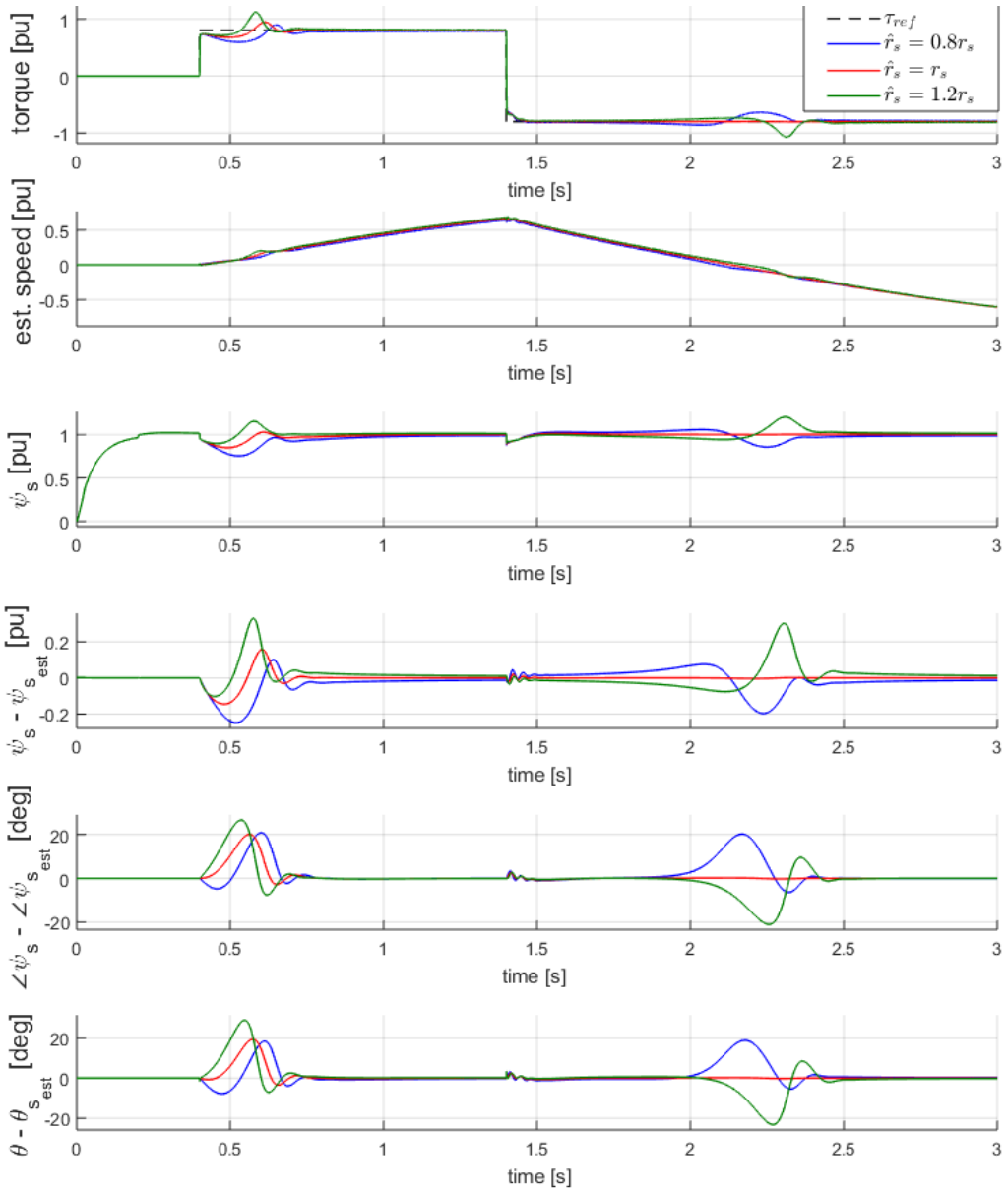

Figure 6.2: Sensorless operation with correction

however very small, 0.003 pu error in estimated flux linkage amplitude, and 0.2 ° in estimated flux linkage angle, and hence it is approximated equal to zero. It is also evident from the figure that not only the estimated, but also the actual stator flux linkage in the machine is exposed to drifting, as the actual stator flux linkage amplitude is different in the three scenarios. This is because the control, which determines the actual stator flux linkage, is based on the flux linkage estimate.

To clearly demonstrate how much the flux estimation and the control of the machine depends on the estimated resistance, simulations were run where the stator resistance is estimated correctly, where it is estimated 20 % too low, and where it is estimated 50 % too low. The two latter scenarios will occur at 91 °C and 288 °C, if the stator resistance is correctly estimated at 25 °C and

then treated as a constant value through the whole operation. The $\hat{r}_s = 0.5r_s$ scenario is hence not very likely. Like in the steady state analysis, the accuracy of the estimates decrease as the deviation between the actual and the estimated stator resistance increases. This emphasises the importance of an accurate estimate of the stator resistance to obtain accurate control. However, it is also evident that even though the generated torque is only half of the reference when the machine drives through zero speed, for $\hat{r}_s = 0.5r_s$, the speed of the machine is not very affected due to the moment of inertia of the machine and the relatively short time interval in the region of very low speed.

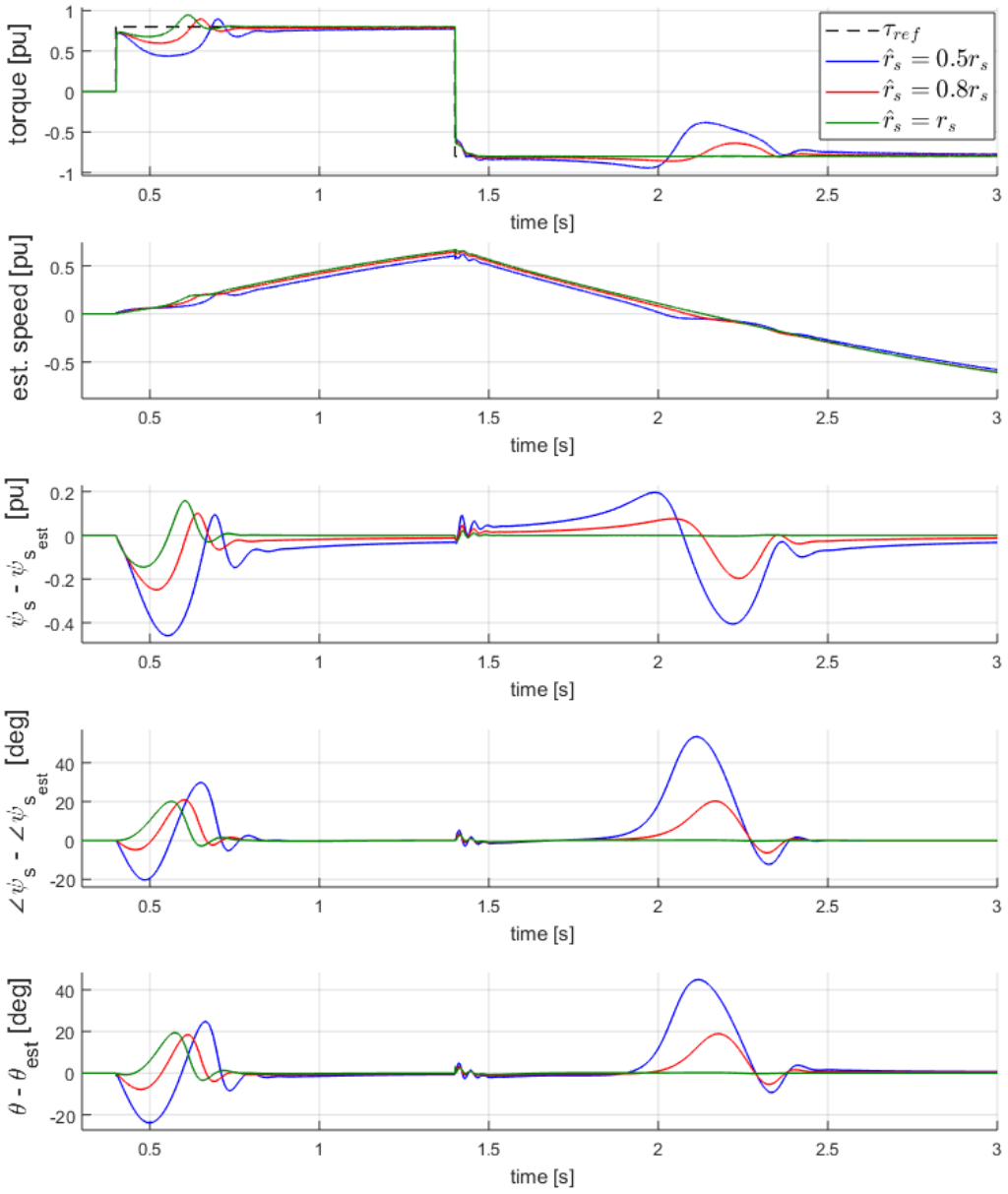

Figure 6.3: Sensorless operation with correction, $\hat{r}_s = 0.5r_s$,$\hat{r}_s = 0.8r_s$ and $\hat{r}_s = r_s$

6.2.1 Analysis of the Correction Method

In this subsection, the behaviour of the drift correction method will be analysed in detail. A simulation was first run with the same parameters as Bendik Fossen implemented in his specialisation project [7], $k_{T_0} = k_2 = 1$, presented in figure 6.4. When the parameters are estimated correctly, and there are no errors in the current and voltage measurements, there is no need for correction. The flux linkage is estimated correctly, and all contributions from the correction block will then act as a disturbance, which was also concluded by Fossen [7].

The first observation made is that the stator flux linkage estimate is disturbed at each step in torque. As explained in section 5.2, this will cause a difference between the filtered and the unfiltered flux linkage squared. To avoid unintended correction from equation 5.7, $k_{\psi_{corr}}$ must be set to zero. This does not happen in figure 6.4, indicating that the correction algorithm has room for improvements. The gains k_{T_0} and k_2 are parameters that can be tuned to improve the performance, such that the correction requested from the LPF is suppressed. This is investigated further in section 6.2.2.

From figure 6.4 it is also observed that the error in both flux linkage amplitude and in flux linkage angle is significantly larger for the first step in torque reference than for the other steps, even if the other steps are larger. This can be explained by that the speed is zero during the first step, while the speed is higher during the other steps. The adaptive filter is apparently better for higher frequencies. The maximum filter time constant of 1.75 s can be adjusted to obtain a more optimal lowpass filter for low speed operation, but the method will still fail at zero speed, as it is impossible to filter something with zero frequency. If the initialisation of rotor position is also performed by DC magnetisation, as described previously, this will make matters worse. A positive d-axis current is then applied, and from equation 2.40, this causes the flux linkage magnitude to increase. The flux controller will try to compensate by decreasing the field current, but this dynamic is not fast enough. When the torque reference is applied, the stator d axis current will become negative, affecting the flux linkage as seen from equation 2.40. This causes a large and fast change in the flux linkage that the low pass filter in the correction block will recognise. Hence, the error in estimated amplitude and in estimated angle during start up depend on how large the d axis current is during initialisation of rotor position. The angle error in figure 6.4 is above 19 °, which is a relatively high value. The amplitude error is 0.15 pu.

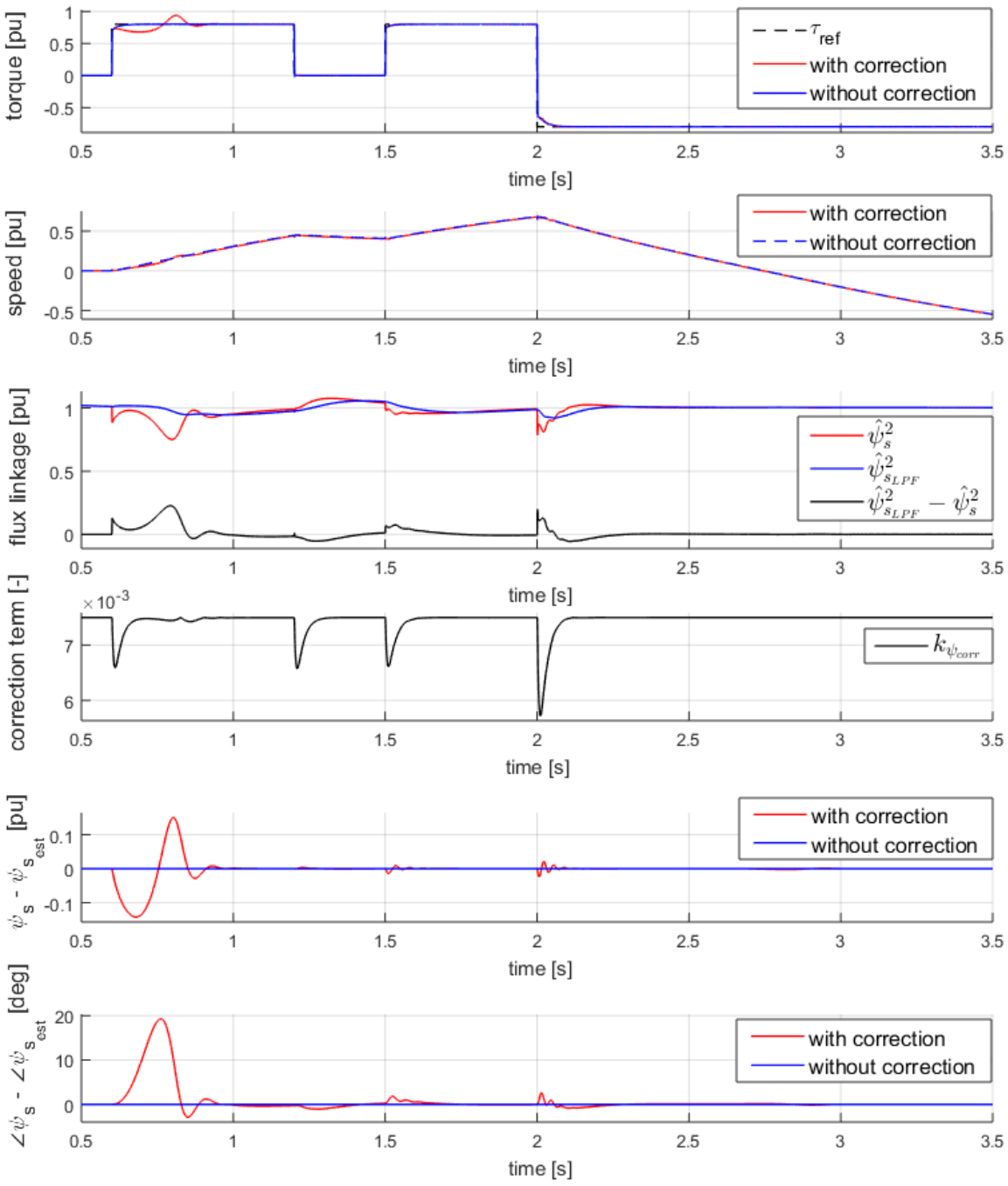

Figure 6.4: Sensorless operation with correct parameter estimation

6.2.2 Tuning of the Correction Parameters

To investigate the tuning of the correction block, the correction constant k_{T_0} is increased by a factor of 10 and by a factor of 50, as presented in figure 6.5. The stator resistance is estimated correctly. It is evident that both amplitude error and error in angle is decreased by increasing the constant k_{T_0}, as seen from figure 6.5. This will cause k_T to reach the value of 1 for a larger amount of time, disabling the correction block. However, as the torque generating current which is used as input to equation 5.12 contains ripple, and varies somewhat even at constant torque reference due to small variations in the stator flux linkage, k_{T_0} must not be too large. This would result in disabling the correction block for all torque references, also when correction is desired. This

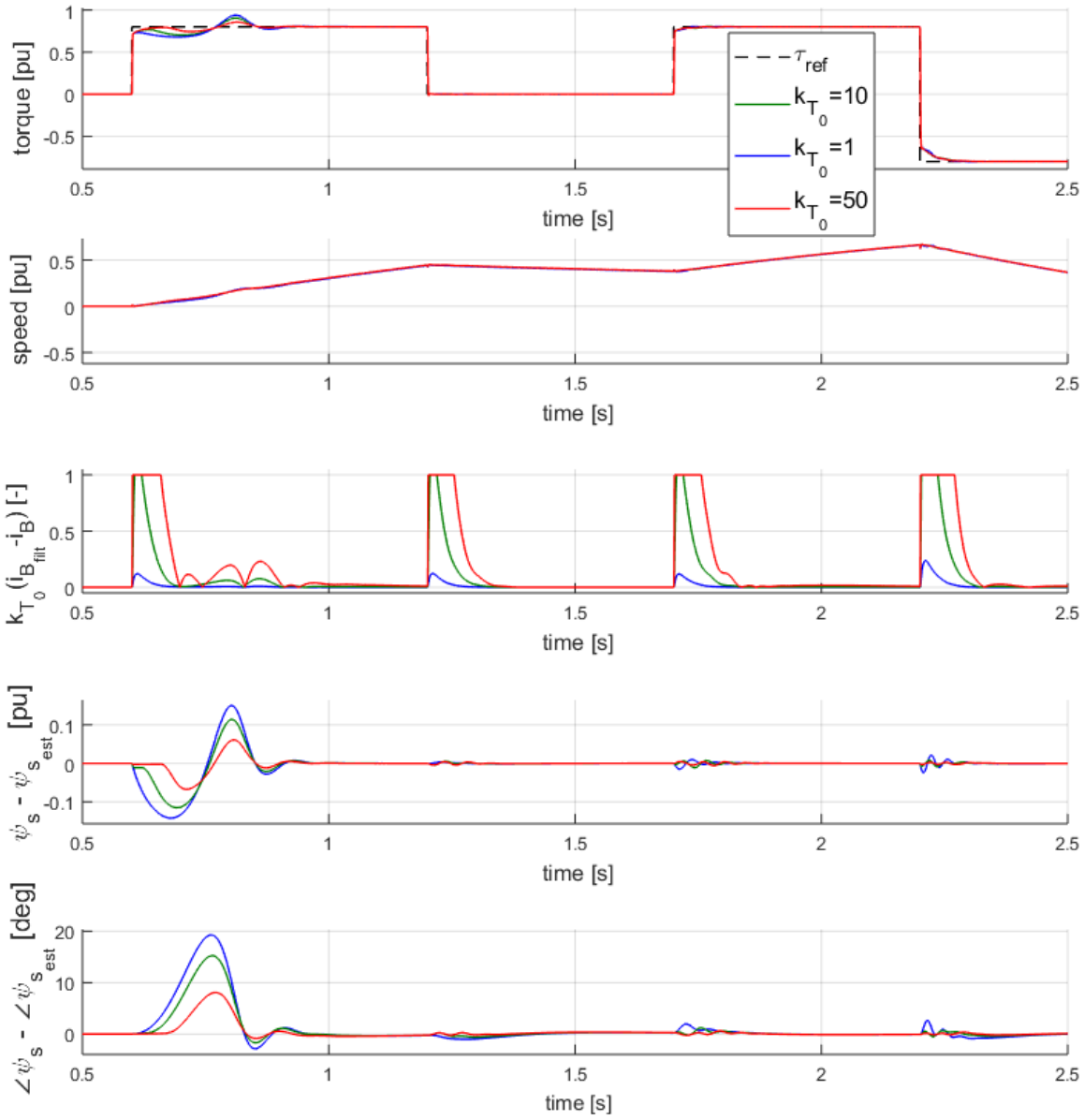

Figure 6.5: The effect of increasing k_{T_0}, sensorless operation

tendency is observed for $k_{T_0} = 50$ between 0.7 s and 0.9 s, where $k_{T_0}(i_{B_{filtered}} - i_B) \neq 0$ even if there is no changes in the torque reference. The lowpass filtering of i_B should be performed carefully, as a too slow filter will result in that the correction block reacts to the significant flux change during step in torque, before the k_T constant counteracts the undesired correction. Modifying this filter is out of scope of this thesis, but it is mentioned as a possible way of improving the flux estimation during the first step in torque reference.

The effect of increasing the constant k_2 has also been investigated. Like k_{T_0}, k_2 has the purpose of avoiding undesired drift correction during changes in torque, but it will not influence the derivative term in the LPF. The correction term $k_{\psi_{corr}}$ is however disabled for smaller changes in torque generating currents by increasing k_2, than by increasing k_{T_0}, as the signal multiplied by k_{T_0} is limited to one before it is multiplied by k_2. The results are presented in figure K.1 in appendix K. The results are not very different from when k_{T_0} is increased, and the same conclusion is made. Both k_{T_0} and k_2 should be as high as possible to avoid correction during torque steps when the stator resistance is correctly estimated, since no correction is necessary. If the stator resistance is erroneously estimated, a too high value will disable the correction also when correction is required, due to ripple and other small variations in the torque generating current. Hence, the correction parameters should be determined based on the accuracy of the estimated parameters in the flux models. Optimal values will vary from machine to machine, and from operation to operation. It is suggested to find these experimentally in the lab for the relevant machine and application.

6.2.3 Very Low Speed Operation

So far, it has been illustrated how both the voltage model and the correction method based on the square of the stator flux linkage amplitude fail at low frequencies, but the speed of the machine has not been significantly influenced due to the fast zero crossing. Hence, the performance of the machine while operating at very low frequencies, below 0.1 pu, for longer time periods will now be investigated. In figure 6.6, a torque reference of 0.05 pu is applied after initialising the machine. The stator resistance is underestimated by 20 %. Some oscillations are evident in both the error in the estimated flux linkage magnitude, and in the error in estimated flux linkage angle. This is expected as the correction algorithm fails at such low frequencies. However, the machine is still able to operate in in this region without loosing stability, and from the torque characteristic it is evident that the sensorless operation would satisfy some drives with lower requirements to accuracy in generated torque. The successful operation is due to the light loading of the machine. In the steady state analysis it was illustrated how the voltage model is more sensitive to the estimated stator resistance at higher torque references, due to the high current supplied. In the scenario in figure 6.6, the load of the machine has a pump characteristic, given by equation 2.53, and hence the loading is very low for such low speeds.

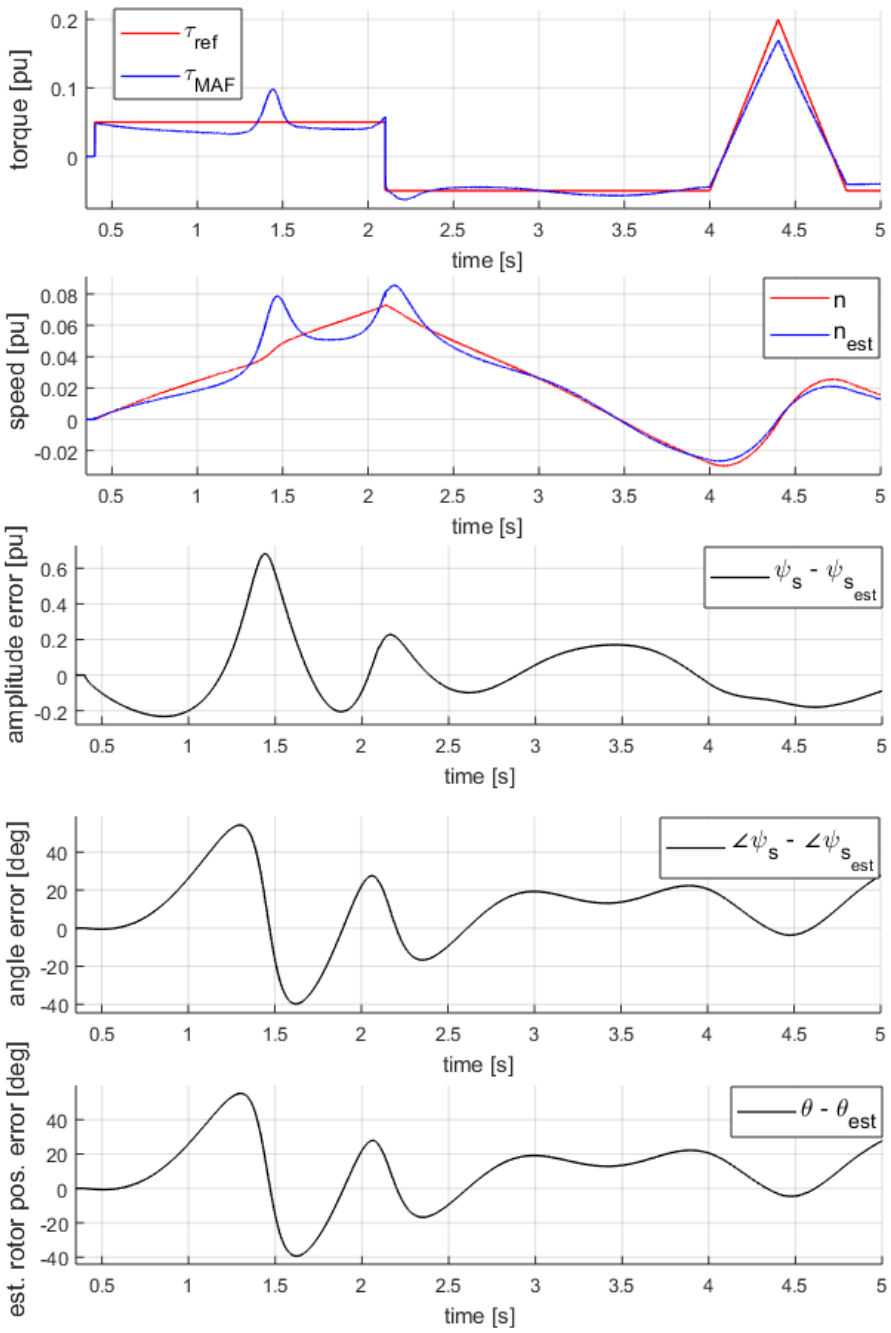

Figure 6.6: Sensorless operation at very low speed, $\hat{r}_s = 0.8 r_s$

6.2.4 Driving Through Zero Speed

The steady state analysis illustrated that the voltage model is most challenged for low speed operation. Even a small deviation between the actual and the estimated stator resistance causes a significant error in the estimated stator flux linkage. From dynamic analysis it was found that the estimated stator flux linkage drifts while the machine drives through zero speed. It will now be investigated in detail how the machine performs while driving sensorless through zero speed. In

figure 6.7 the machine is accelerated to 0.5 pu before a negative torque reference is applied. The operation as the speed crosses zero speed is investigated when the stator resistance is correctly estimated, when it is overestimated by 20 % and when it is underestimated by 20 % through the whole simulation.

As expected, small deviations between the actual and the estimated flux linkage occur after the step in torque, as discussed previously, but the main observation from figure 6.7 is what happens as the speed is reduced. The machine drives through zero speed somewhere between 1.6 s and 1.8 s, depending on the estimated resistance. It is evident that the error in both estimated amplitude and in estimated angle increase when the speed is around 0.25 pu, and that they peak some time after

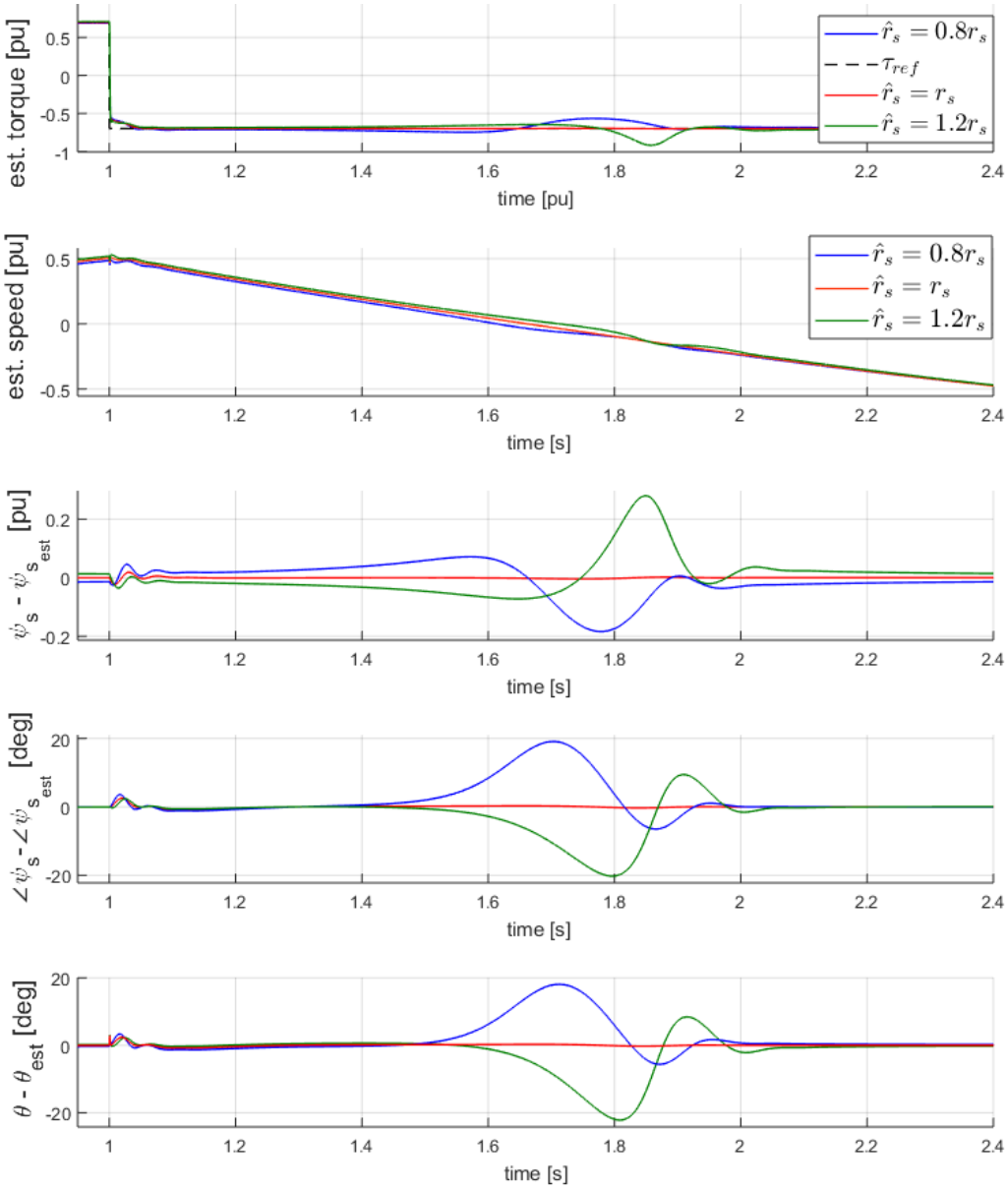

Figure 6.7: Sensorless operation through zero speed, with correction

the machine has crossed zero speed. This is both because the flux linkage estimates drift when the speed approaches zero, if $\hat{r}_s \neq r_s$, and due to that the correction method fails at low frequencies. As the speed increases in negative direction, the drift is again compensated for, yielding zero error in the estimated stator flux linkage amplitude.

It is also evident that the error in estimated rotor position has a peak value of $\pm 20\,^\circ$, which is much higher than the $5\,^\circ$ depicted by the steady state analysis. This is due to the significant error in estimated stator flux linkage angle, $\Delta\xi_s^s$, which will contribute heavily to the error in estimated rotor position, as seen from equation 3.2. This error was not revealed by the steady state analysis. Despite the erroneous estimate of the stator resistance, the torque follows its reference quite good, and the machine drives smoothly through zero speed. The duration with a significant deviation between actual and estimated stator flux linkage is not long enough to disturb the control significantly.

If the machine drives fast enough through zero speed, the erroneous torque control will not influence the speed significantly, due to the moment of inertia of the machine. The longer the machine operates at low speeds, the more severe is an erroneously estimated stator flux linkage and an erroneously generated electromagnetic torque. As the estimated flux linkage drifts when driving through zero speed, from figure 5.6, it seems reasonable that the slower the machine drives through zero speed, the more the estimated flux linkage will drift. Hence, it is expected that it is more challenging for the machine to drive slowly through zero speed. This is confirmed by the results presented in figure 6.8. The machine is controlled sensorless thorough zero speed while $\hat{r}_s = 0.8 r_s$. The torque reference applied is the same in all three scenarios, but in the moment of inertia is different in each scenario, to obtain different accelerations. In one scenario the moment of inertia is doubled, in one it is halved, and in the last one it is multiplied by four compared to the original value. As expected, the slower the machine drives through zero speed, the larger the deviation between actual and estimated stator flux linkage gets. This affects the estimated rotor position and the generated torque.

The load applied so far has the characteristics of a pump, and hence the load has been zero while the machine has driven through zero speed. If a torque is generated, the machine will then drive quickly through the critical low speed region. From the steady state analysis it is evident that the sensitivity of the voltage model, with respect to the stator resistance, increases for higher torque references and at lower speeds. To analyse the scenario where the machine drives slowly through zero speed, and at the same time generates a high torque, a constant load is applied. The observations from the steady state analysis are supported by the simulation results presented in figure 6.9, where two scenarios, both with $\hat{r}_s = 0.8 r_s$, are investigated. The machine drives through zero speed in the same amount of time in the two scenarios, but with a heavier loading in one of the scenarios than in the other. This is achieved by a constant load, applied after 0.9 s, that is greater than the generated torque. The difference between the generated torque and the load is similar for both of the scenarios to obtain the same angular acceleration. As expected, the flux estimates are less accurate when the generated torque is high, 0.4 pu, than when it is low 0.2 pu, with the maximum error in estimated flux linkage amplitude and in estimated flux linkage angle occurring around the instant when the speed crosses zero. The error in estimated rotor position has peak values of $13\,^\circ$ and $36\,^\circ$ at light loading and heavy loading respectively, which is

a significant difference. It was attempted to run a third scenario, with a loading of 0.8 pu and a generated torque of 0.6 pu while crossing zero speed. This caused the error in estimated rotor angle to exceed 180 °, the control fails, and the dq currents are no longer constant during the constant torque reference. This is illustrated in figure L.1 in appendix L.

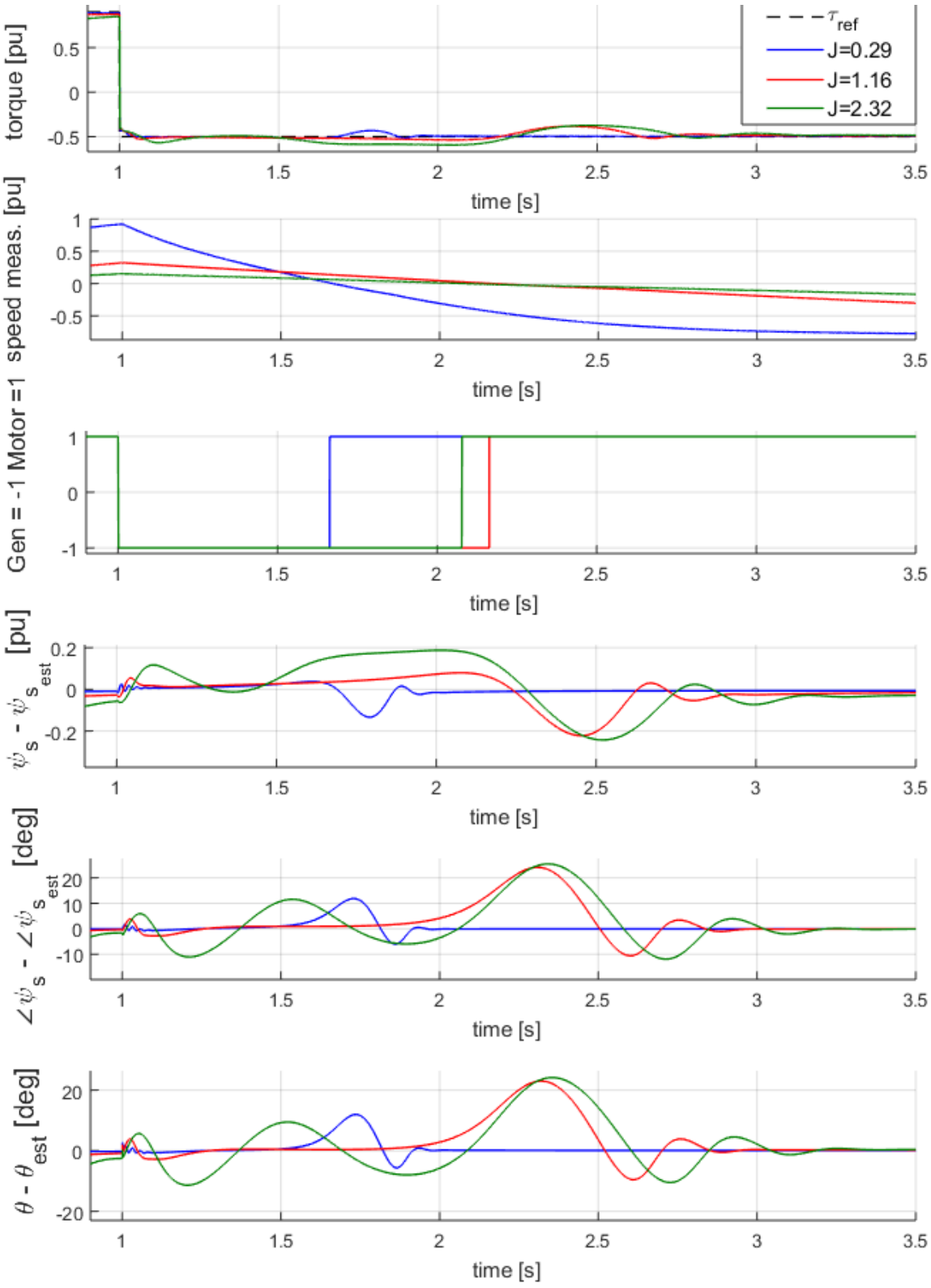

Figure 6.8: Driving through zero speed with three different slopes, $\hat{r}_s = 0.8r_s$

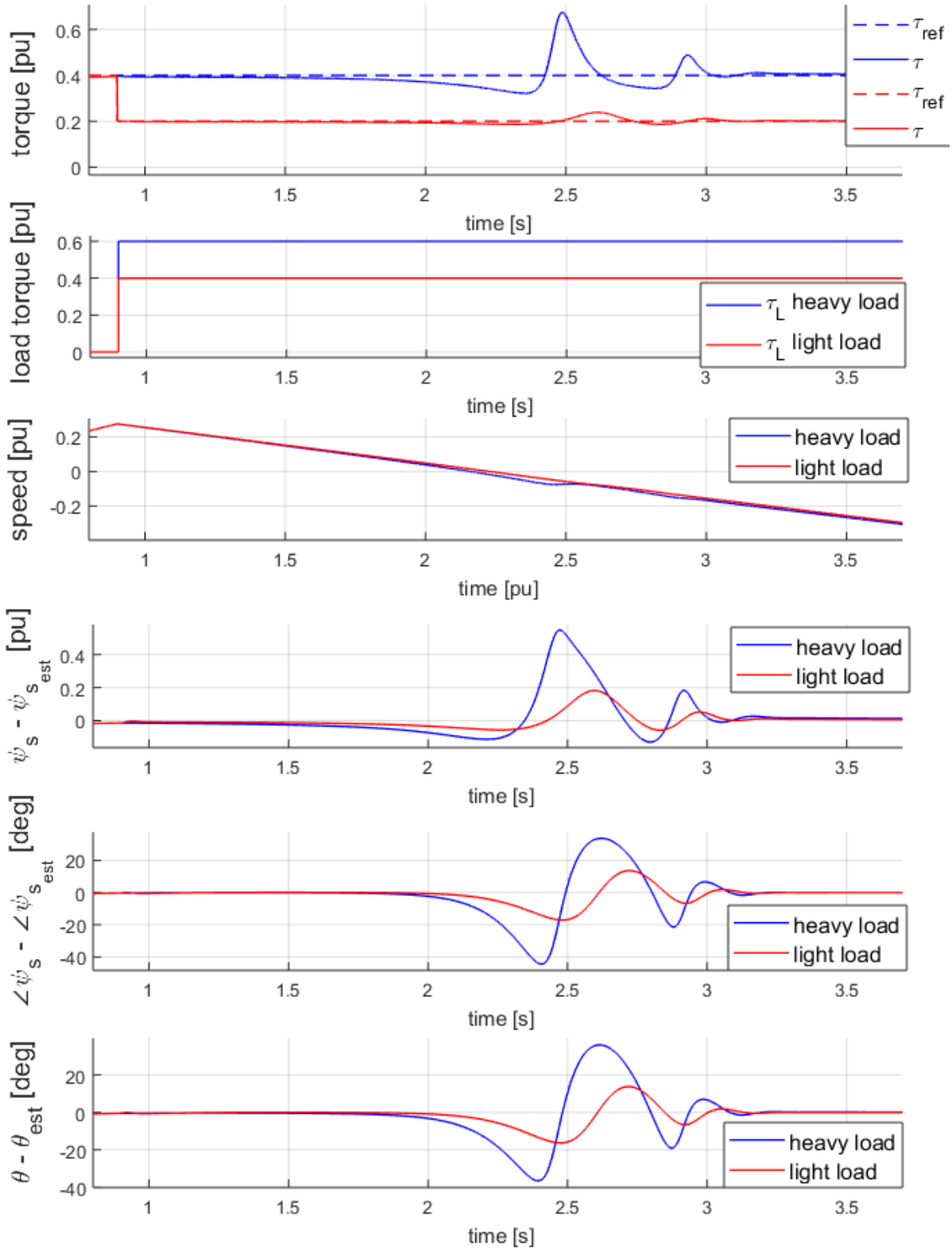

Figure 6.9: Driving through zero speed with a constant light generated torque and load (red) and with a constant heavy generated torque and load (blue)

6.2.5 Standstill Operation

The results presented in figure 6.8 and figure 6.9 indicate that the most challenging operation for the machine is while generating a torque, and holding a load, at standstill. This is required for applications such as lifts for use in buildings or cranes. As there is no generated back emf at standstill, this will result in a very small stator voltage, equal to the voltage drop across the stator resistance, while the stator current is high. Hence, the stator flux estimate by the voltage model will become extremely sensitive to the estimated stator resistance, as concluded from the steady state analysis. This worst case scenario was simulated by applying a constant load of the same value as the torque reference, $\tau_{ref} = \tau_{load} = 0.8\,\text{pu}$, while the rotor is at standstill. The results with and without correction is presented in figure 6.10, where $\hat{r}_s = 0.8 r_s$.

From the results in figure 6.10 it is evident that the error in estimated stator flux linkage, and hence also the error in estimated rotor position increase with time, and eventually exceeds 180 °. Due to the erroneously estimated rotor position, the current controller will act in a coordinate system that is not properly oriented, and currents are set up in wrong directions. This results in a speed of 2 pu with correction, and 4 pu without correction, when the machine was intended to stand still. Hence it is concluded that the machine is not able to hold a load at standstill during sensorless operation, as long as $\hat{r}_s \neq r_s$. If the stator resistance is estimated correctly, and all measurements are perfectly accurate, simulations indicate successful operation. Such a scenario is however not very realistic in real life, due to the temperature dependence of the resistance, measurement noise and other inaccuracies. Even when temperature sensors are installed, and the characteristics of both the stator resistance and the inductances are known with high accuracy, some small deviations are likely to occur during the operation. The correction method will also disturb the operation somewhat, as discussed previously. It should be noted that the results in figure 6.10 are unphysical, as the torque generated is far above what is permitted by the current limitations. That the machine fails while operating sensorless at standstill is expected, as it is well known in the academic community that methods that are solely based on the back emf will fail for longer periods at zero speeds [11].

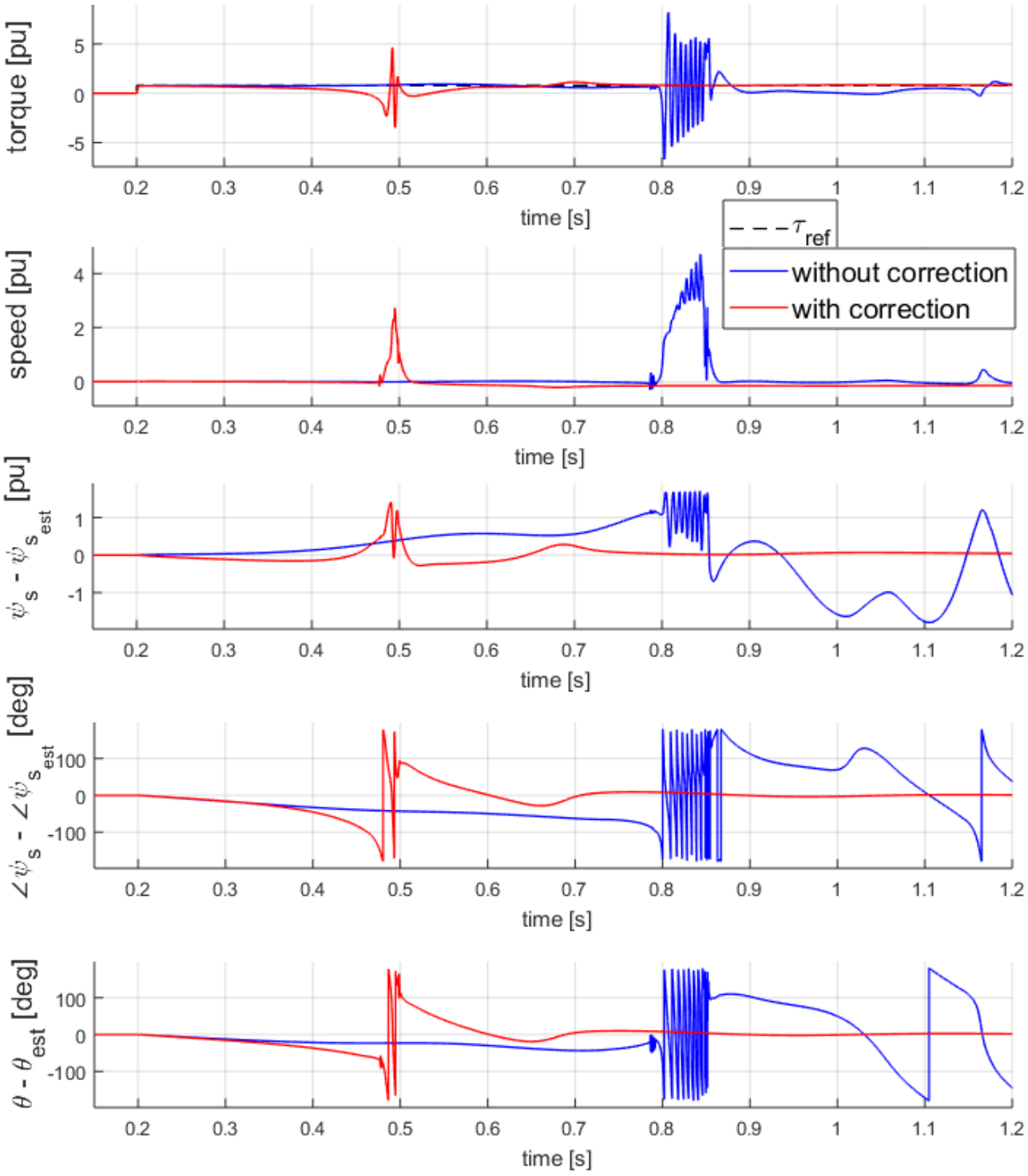

Figure 6.10: Sensorless operation at standstill, $\hat{r}_s = 0.8r_s$

6.3 Sensitivity of Inductances and Rotor Resistances

So far, most of the analysis have involved the sensitivity of the voltage model with respect to the stator resistance. The voltage model do not require any rotor information, and it is hence used as the main model during sensorless operation. The importance of estimating the resistance accurately is evident by now, and since the stator resistance is a parameter that often change during operation, the estimated stator resistance is likely to deviate from the actual value.

During magnetisation of the machine, the stator flux linkage estimate from the current model is used to initialise the voltage model. In this section, it will be analysed how the current model is influenced by erroneously estimated inductances and damper winding resistances during dynamic operation. It will also be investigated what happens if the voltage model is incorrectly initialised. The current model during dynamics is expressed by Laplace transforming equation 2.38 and 2.39, and inserting them into equation 2.40 and equation 2.41 respectively. This yields equation 6.1 and 6.2

$$\psi_d = x_d \sigma_{dD} i_d + \frac{x_{Md}}{1 + T_D s}(i_d + i_f) + x_{Md}\sigma_D i_f \tag{6.1}$$

$$\psi_q = \sigma_{qQ} x_q i_q + \frac{x_{Mq}}{1 + T_Q s} i_q \tag{6.2}$$

By assuming constant leakage coefficients, the estimated parameters which will influence equation 6.1 and 6.2 are the magnetising inductances x_{md} and x_{mq}, and the rotor resistances r_D and r_Q. The effect of a changing the magnetising inductance will here be obtained by adjusting x_d and x_q in the simulation model.

6.3.1 Erroneous Estimated Inductance

In figure 6.11, the behaviour of the machine when the q axis inductance, x_q, is overestimated and underestimated by 20 % is presented. Measured rotor position is used as input to the model, and all other parameters are assumed correctly estimated to reduce the sources of error. The output of the current model is used as input to the control system. As predicted by the equations, the stator flux linkage is estimated perfectly during the magnetisation and initialisation period, as the flux linkage then is along the d axis only. When the step in torque reference is applied, there is a high degree of symmetry for the two scenarios where the inductance is overestimated and underestimated. An underestimated x_q results in an estimated flux linkage amplitude that is too low, causing a positive error. When the q axis inductance is overestimated, the error becomes negative. The steady state behaviour is similar during both motor and generator operation, when the magnitude of the applied torque is the same in the two scenarios, and by longer simulations it was also revealed that no changes occur in the flux linkage when the rotor drives through zero speed. These are the same observation as were made in the steady state analysis. Dynamic operation occur during steps in the torque reference. From equation 6.2, it is evident that an underestimated q axis, which results in an underestimated x_{Mq}, reduces the numerator in the transient term. Hence, the estimate will be less sensitive to the changes in the q axis current during dynamics. When the negative step in torque reference is applied after 1 s, and the q axis current becomes negative, the actual stator flux linkage will decrease faster than the estimated one, resulting in a negative error

for a short time interval. As the current in the damper windings decay, steady state operation is again achieved. When the q axis inductance is overestimated, the flux model will be too sensitive to changes in the q axis current. The estimated flux amplitude then changes more rapidly in the negative direction than the actual flux linkage during the step in torque after 1 s, resulting in a short period with a positive error.

As expected, the q axis current is higher when the flux linkage is estimated too low, compared to when the flux linkage is estimated too high. This is a result of equation 2.51 implemented in the control system. If the flux linkage magnitude is estimated too low, it results in a too high generated torque, while if the estimated flux linkage magnitude is too high, the generated torque will become too low. The deviation between the torque reference and the generated torque is small for both scenarios. It is concluded that the stator flux linkage estimate provided by the current model is accurate enough to be used in the control of the machine, even with a 20 % error in the estimated q axis inductance, when the position or speed is measured. A similar simulation, but with the d axis underestimated and overestimated by 20 %, and all other parameters assumed correctly estimated is given in figure M.1 in appendix M. This result is not analysed in detail, but it is evident that the machine looses control when the d axis is overestimated, and that the d axis current is oscillating with a high frequency both for an underestimated and for an overestimated d axis inductance. The high frequent oscillation in the d axis current is related to the high frequency oscillations in the stator flux linkage, which is not included in the figure. Also the field current oscillates with a high frequency in these cases. One might say that the d axis inductance has a greater influence on the flux than the q axis inductance.

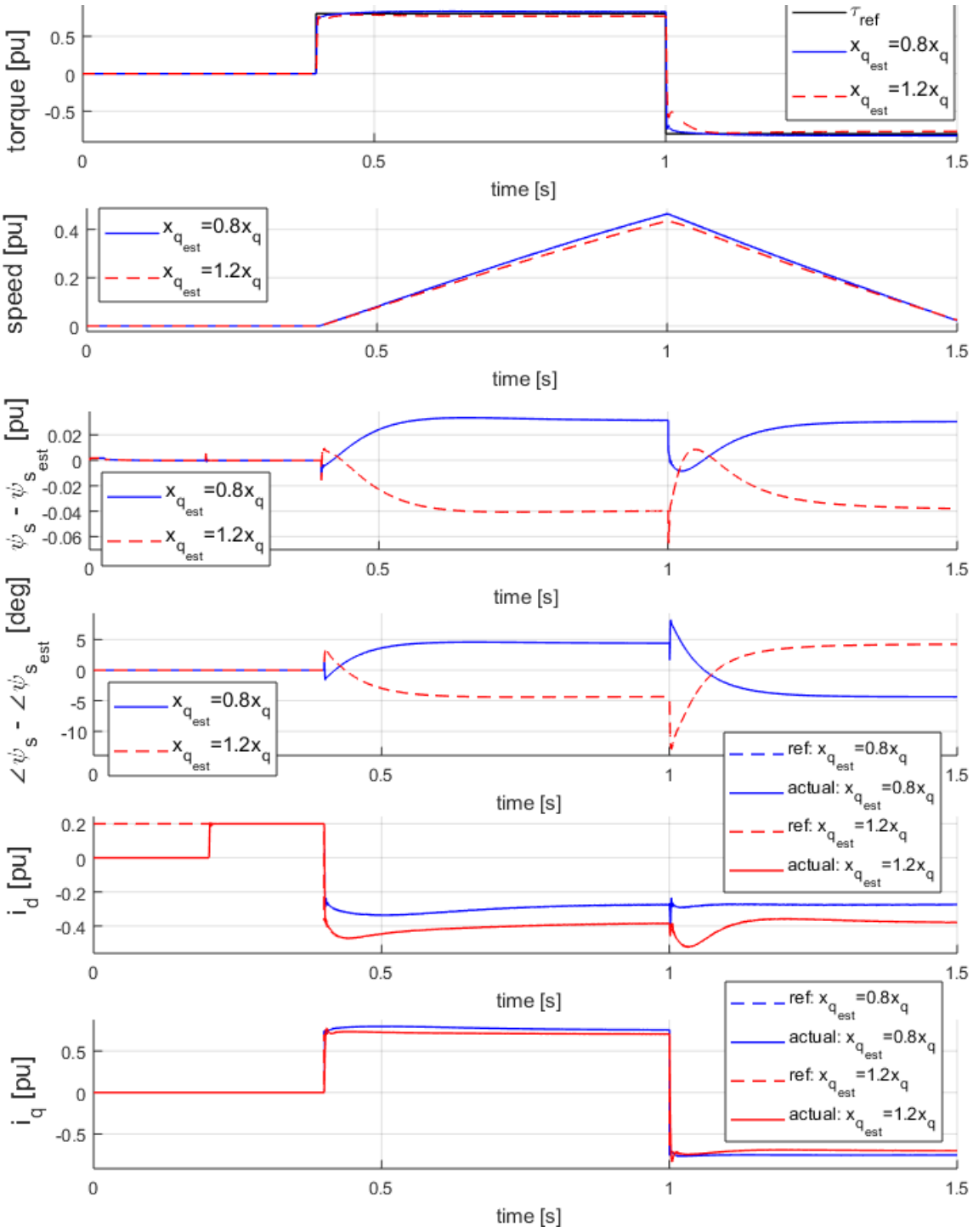

Figure 6.11: Stator flux linkage estimation by the current model when the q axis inductance is underestimated and overestimated by 20 %

6.3.2 Erroneous Initialisation of the Voltage Model

During both the magnetisation of the machine by the field winding, and during the DC magnetisation performed to move the rotor to its initial position, the stator flux linkage has a d axis

component only. This flux linkage is estimated by the current model. Assuming constant leakage coefficients, the d axis inductance, the damper winding inductance and the resistance in the d axis damper winding are the only parameters of importance for the accuracy of the flux linkage estimation during this period. As the current model is sensitive to the damper winding resistances during transients only, which was also illustrated in section 3.1, r_D will not influence the initial value of the voltage model if the magnetising and initialisation period is long enough for the stator flux linkage to obtain a steady state value.

In the specialisation project of Bendik Fossen, the actual stator flux linkage in the machine was used as input to initialise the voltage model. It was revealed by simulations that without initial values to the voltage model, oscillations in the estimated stator flux linkage amplitude and in the estimated stator flux linkage angle occurred, even when all machine parameters were correctly estimated [7]. Incorrect initialisation of the voltage model is here analysed by simulating a scenario where both damper winding resistances are underestimated by 20 %, while all other parameters are assumed correctly estimated. The result is presented in figure 6.12. Magnetisation and initialisation of the rotor position is performed for 0.4 s, before the voltage model starts integrating at the step in torque reference at t=0.4 s. The underestimated damper winding resistance along the d axis, r_D, increases the time constants in equation 6.1. This reduces the estimated flux linkage along the d axis during dynamics, resulting in a positive amplitude error. The error in estimated stator flux linkage amplitude decreases as the damper winding current, i_D, decays. As the initialisation period is not long enough to obtain steady state, an error of 0.05 pu in the estimated flux linkage amplitude occurs during the step in torque reference. The initial error in the estimated amplitude corresponds to an offset in the voltage model. As all parameters in the voltage model are estimated accurately, the estimated flux linkage follows a circle shaped trajectory with the correct radius, but with a displaced origin proportional to the initial offset. The results obtained are quite equal to the results obtained by Bendik Fossen for the PM machine used in his project thesis, yielding the same conclusion: Oscillations occur in both flux linkage amplitude error and in flux linkage angle error without correction. The correction algorithm corrects the flux linkage estimate, but it takes some time before the offset is removed entirely. It is concluded that erroneous initialisation of the voltage model, just like drifting due to incorrectly estimated stator resistance, gives offset to the estimated flux linkage that must be compensated for.

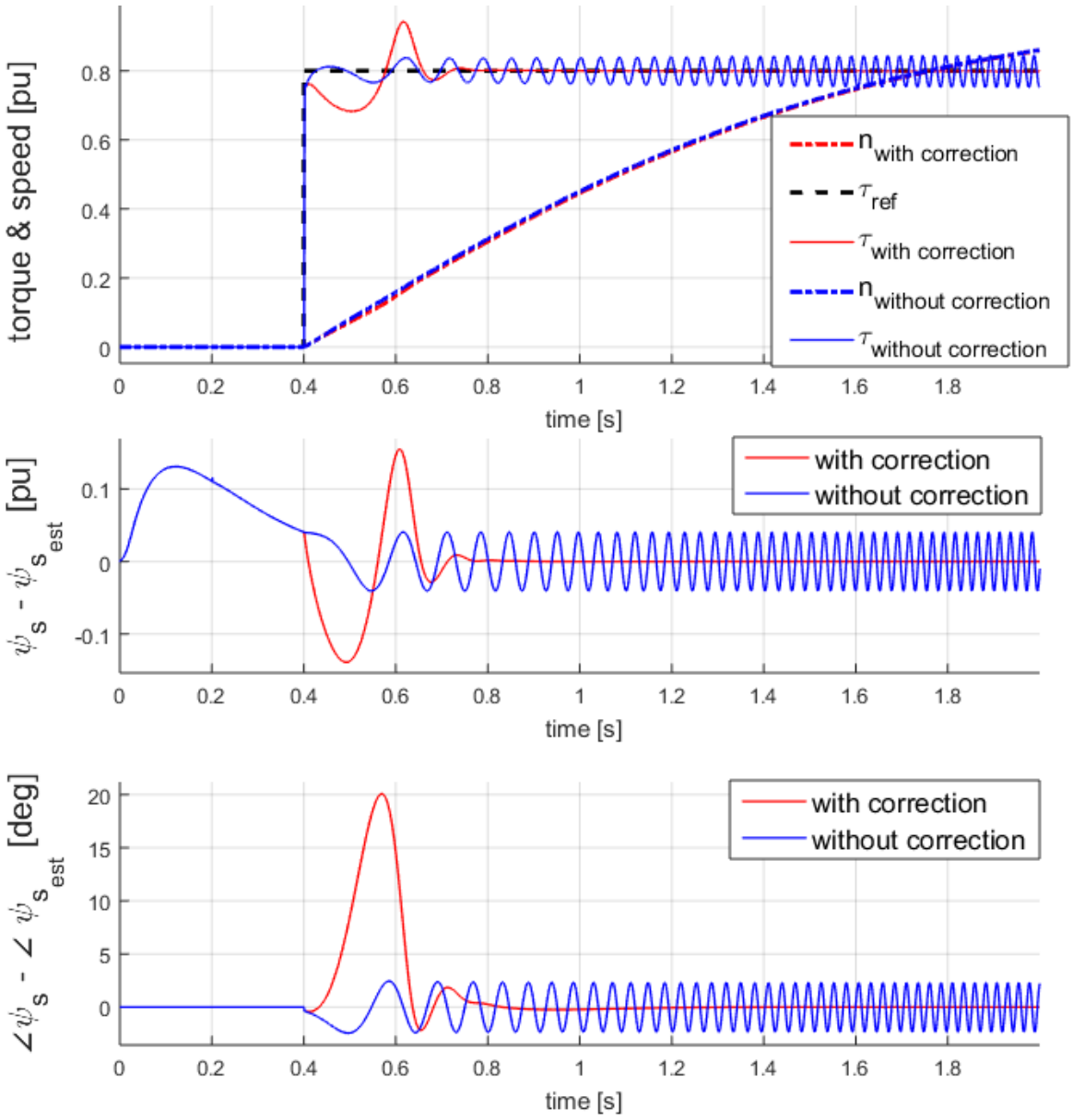

Figure 6.12: Sensorless operation with erroneous initialisation of the voltage model

7 Improving the Flux Linkage Estimation

In the attempt of improving the operation at low speeds, a combination of the voltage model and the current model is utilised. The goal is to obtain an estimator that is less sensitive to the estimated machine parameters such as stator resistance, rotor resistance, stator current and stator voltage. In this section, different combinations of the voltage model and the current model is discussed and analysed. Unless otherwise stated, both damper winding resistances and the stator resistance are underestimated by 20 % in the simulation results presented, and the stator flux linkage estimated by the voltage model is used as input to the control system.

7.1 Combining the Voltage Model and the Current Model

Separately, the current model and the voltage model estimate the stator flux linkage based on the measured inputs to the models only, and they are hence open-loop observers [12]. By utilising also the outputs from the models, it is believed that better estimations will be obtained. As a first attempt this is realised by using the difference between the estimated stator flux linkage from the voltage model, and the estimate from the current model as a feedback to the voltage model. The rotor position estimated by the voltage model is used as input to the current model. The difference between the models is added to the integral in the voltage model, as a compensation, and hence it acts as a stabilising feedback term. This corresponds to a closed loop observer. This way of correcting the voltage model is previously used, e.g in DTC for induction machines by Lascu, Boldea and Blaabjerg [14]. The closed loop observer for the separately excited synchronous machine investigated is illustrated as a block diagram in figure 7.1. This implementation will be referred to as the "correction by feedback method", or simply "the closed loop observer" in this thesis. The motivation is that the current model will act as a filter, as the dq currents are filtered by the time constants of the damper windings. Furthermore the current model is not exposed to drifting, and when the inductances are assumed correctly estimated, the estimated rotor position is the only source of error in the current model during steady state. In figure 7.2, the stator flux linkage estimate from the current model alone, with the estimated rotor position calculated from the voltage model used as input, is compared with the flux linkage estimate from the voltage model alone. Both the damper winding resistances and the stator resistance are underestimated by 20 %, no drift correction is enabled and all other parameters are assumed correctly estimated. It is revealed that the current model estimates the flux linkage amplitude significantly better than the voltage model, while the flux linkage angles estimated by the two models are quite similar. The flux linkage angle estimated by the current model is slightly worse than the flux linkage angle estimated by the voltage model. This makes sense, as the flux linkage angle from the current model is heavily based on the estimated position from the voltage model.

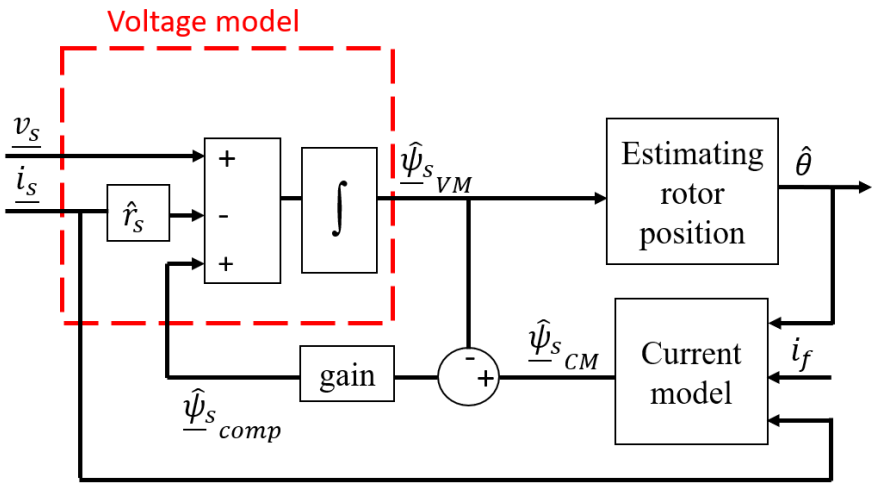

Figure 7.1: Combining the voltage model and the current model

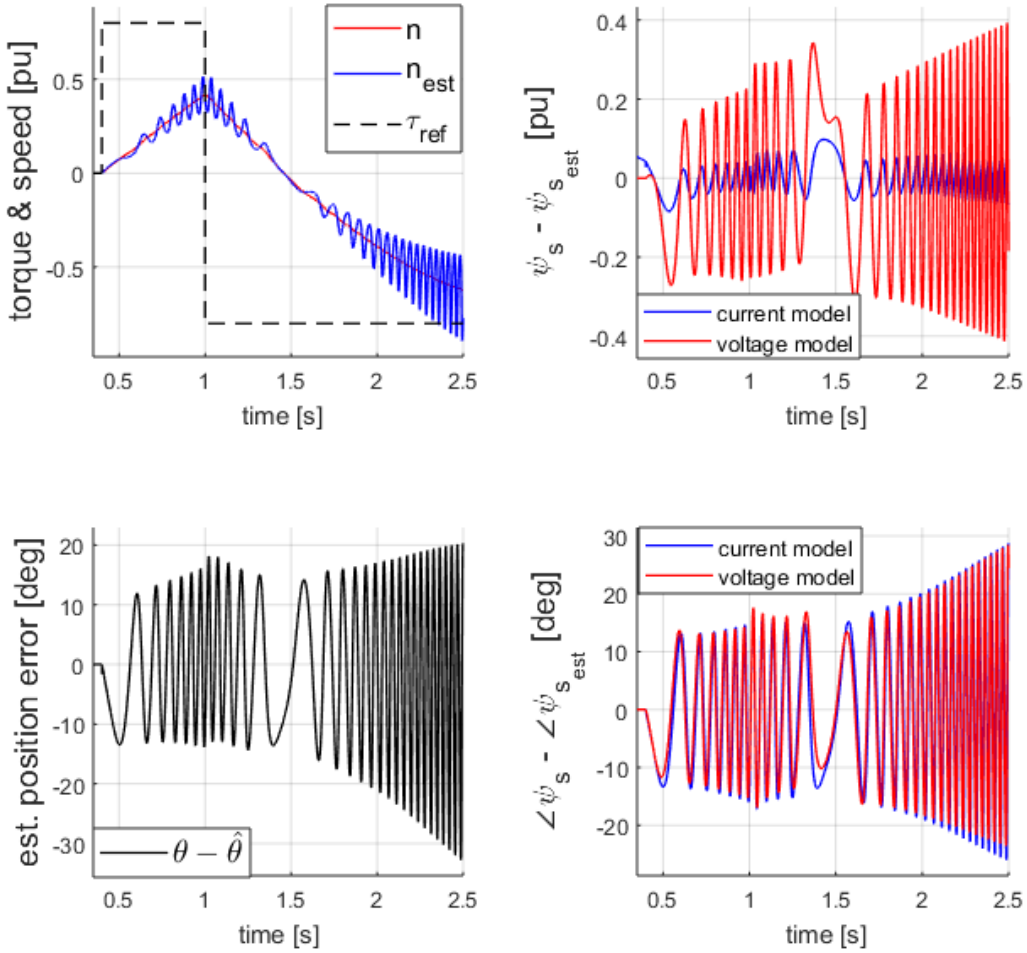

Figure 7.2: Flux linkage estimates by VM and CM without correction, $\hat{r} = 0.8r$

When disabling the correction method based on the square of the stator flux linkage amplitude, the difference between the voltage model and the current model as feedback to the voltage model, with unity feedback gain, yields the results presented in figure 7.3 when running sensorless. The flux estimate from the compensated voltage model is used as input to the control system. From the results in section 6.1, it was evident that sensorless operation was not possible without correction. From figure 7.3, where both the damper winding resistances and the stator resistance are underestimated by 20 %, it is observed that the feedback from the current model has a stabilising effect on the flux linkage estimate. After some oscillations in the estimated stator flux linkage immediately after start up, the flux linkage estimate becomes smooth, and the generated torque follows its reference with a small steady state error of approximately 0.01 pu. The rotor position is also then estimated with high accuracy. When the speed reduces and approaches zero, the error in estimated stator flux linkage angle, and hence also the error in estimated rotor position, increases towards 180 °. The control system fails in generating a torque equal to the reference, resulting in an torque error of above 1 pu after approximately 2.2 s. A high positive torque is generated, even if the torque reference is negative, as the control system acts in a disoriented dq coordinate system. Furthermore, the speed is estimated to decrease during this peak in torque error, while the real speed actually increases. The consequence of this is discussed in the final discussion in section 8. The same results as in figure 7.3, but with the stator flux linkage estimate from the current model, and the stator flux linkage estimated without any correction or feedback included, are presented in figure N.1 in appendix N. The torque reference is slightly different in figure N.1, but this is not of importance. In figure N.1, the stator resistance is the only erroneously estimated parameter. A major improvement in the estimated flux linkage and in the generated torque is observed for high speeds when using the closed loop observer, compared to when no correction or feedback is used.

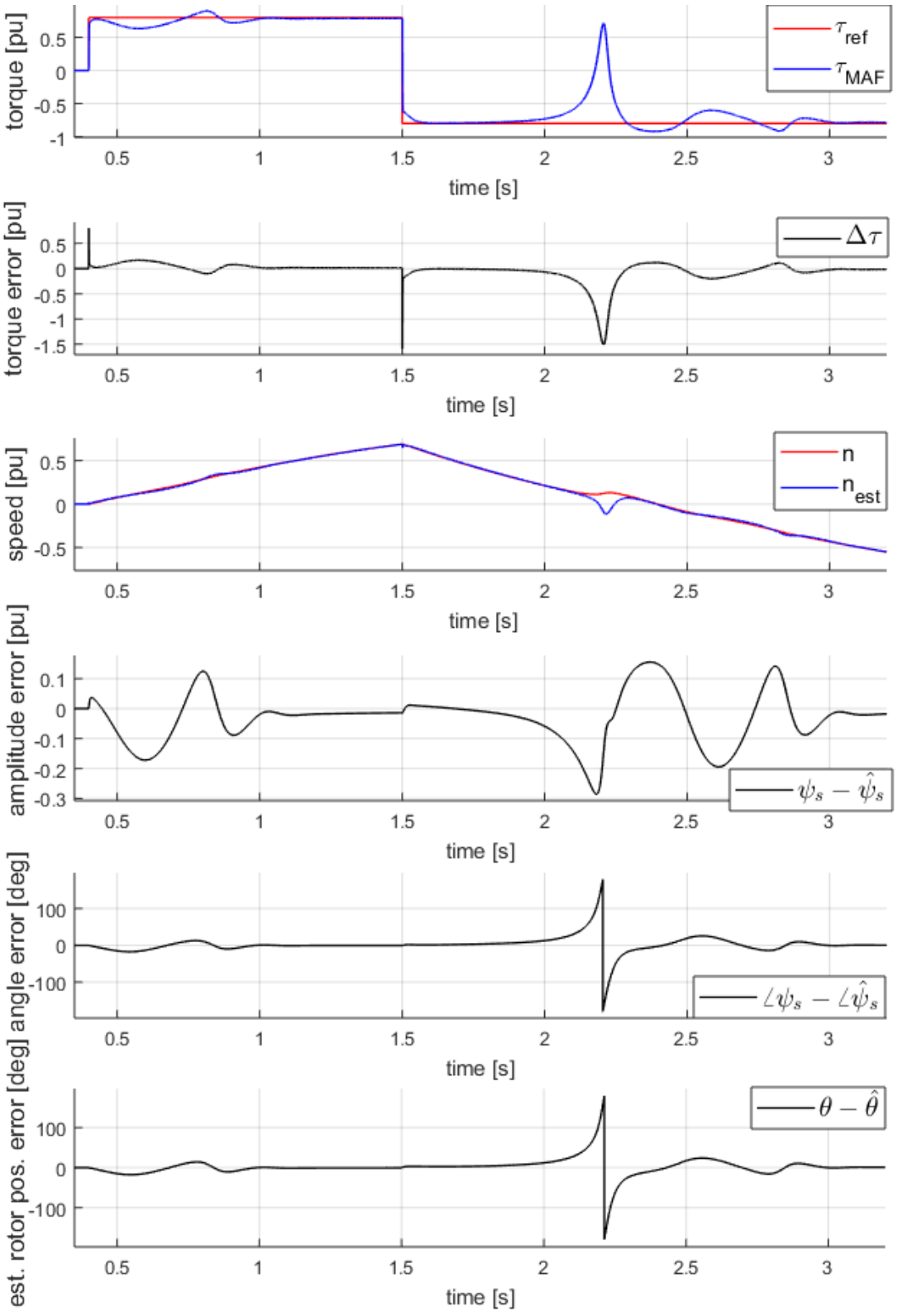

Figure 7.3: Sensorless operation with feedback to the voltage model, $\hat{r} = 0.8r$

In the results presented in figure 7.2 and figure 7.3, both the stator resistance and the rotor resistances are assumed to be underestimated by 20 %. All resistances in the model will change in some degree due to temperature during operation, but in real life the stator resistance will be more exposed to variations in temperature than the resistances in the damper windings, as there is a larger amount of current flowing in the stator winding than in the damper windings. It is evident that the correction works at high speeds, even for a 20 % deviation between estimated and actual damper winding resistances, but the accuracy of the estimated damper winding resistances will still influence how good the feedback correction method works. In figure 7.2 and figure 7.3, the inductances are assumed to be correctly estimated. The q axis inductance will influence the estimated rotor position input to the current model, and both the d and q axis inductances will influence the current model directly. Thus the feedback performance is also dependent on the knowledge about the inductances. At this stage, it is found that the correction method works as an alternative to the correction method based on the square of the stator flux linkage amplitude for higher speeds, but it is not satisfying at low speed operation without further modifications.

To improve the performance, and to operate successfully through zero speed, the feedback signal is modified further. In previous research, a PI controller has been used in the feedback loop, intended to remove the DC offset, drifting and initial condition errors [25]. Another option investigated in the literature is to multiply the feedback by an expression depending on the speed of the machine. The feedback expression makes the voltage model dominate above a determined crossover frequency, while the current model dominate at frequencies below this limit [29]. In this work, by running several simulations with different gains in the feedback, and by attempting to use a PI controller with different parameters in the feedback, it was found that the machine drives successfully through zero speed if the feedback is reduced. It was observed that the feedback caused the instability while driving through zero speed, and this was the motivation for reducing the gain. The unity gain in the feedback loop is now replaced by a gain of 0.1. This seems to be some sort of optimal value for the investigated scenario, as decreasing the feedback further reduces the effect of the compensation term too much. In figure 7.4, the behaviour of the machine with this alternative feedback is compared with the behaviour when the correction method based on the square of the stator flux linkage amplitude is enabled. The response when both methods are enabled simultaneously is also presented. The simulations were performed with 20 % underestimated resistances in both damper windings and in stator windings. As previously discussed, the resistances do not influence the initial value of the voltage model if the magnetisation and initialisation period is long enough, but to save simulation time the actual stator flux linkage in the machine is now used as input to the voltage model during magnetisation and initialisation. In this way problems related to erroneously initialisation of the voltage model is avoided. The results reveal that the closed loop observer estimates the stator flux linkage better than the voltage model with correction at the first step in torque reference, while the correction method based on the square of the flux linkage amplitude performs slightly better while the motor drives through zero speed. By using the closed loop observer instead of the correction method based on the square of flux linkage amplitude, the peak value of the amplitude error is reduced from -0.25 pu to -0.21 pu, while the error in estimated flux linkage angle is reduced from 21 ° to -13 ° during the first step in torque. While driving through zero speed, the peak in amplitude error is increased from -0.2 pu to -0.28 pu, while the peak of the angle error is reduced from 20 ° to 17 °. By investigating the generated torque, it is observed that there are minor differences between the two methods. The combination of the two models yields

a response that seems to be a slightly better than the response obtained by the correction based on the square of the flux linkage amplitude. The torque control is slightly better during the first step in torque reference with the closed loop observer included, than with the correction method based on the square of the stator flux linage amplitude only, while sensorless control through zero speed is similar for the combination of the models, and by using the correction method based on the square of the flux linkage amplitude alone, which are both better than the closed loop observer alone. However, the all over performance is not significantly improved.

To find an optimal gain, and possible time constants if a PI controller is used, further investigations must be made. This is more practically to perform in the lab, as simulations are more time consuming. By the values applied in this work so far, the closed loop observer without further modifications do not improve the low speed flux estimates significantly, but it has been proven to be an alternative to the correction method based on the square of the stator flux linkage amplitude when the stator resistance and the damper winding resistances are underestimated by 20 %, and the inductances are known with high accuracy. The need for external drift compensation is eliminated, as the feedback in the closed loop observer corrects for the drifting. The gain of 0.1 in the compensating feedback will be used in the closed loop observer throughout the rest of this thesis.

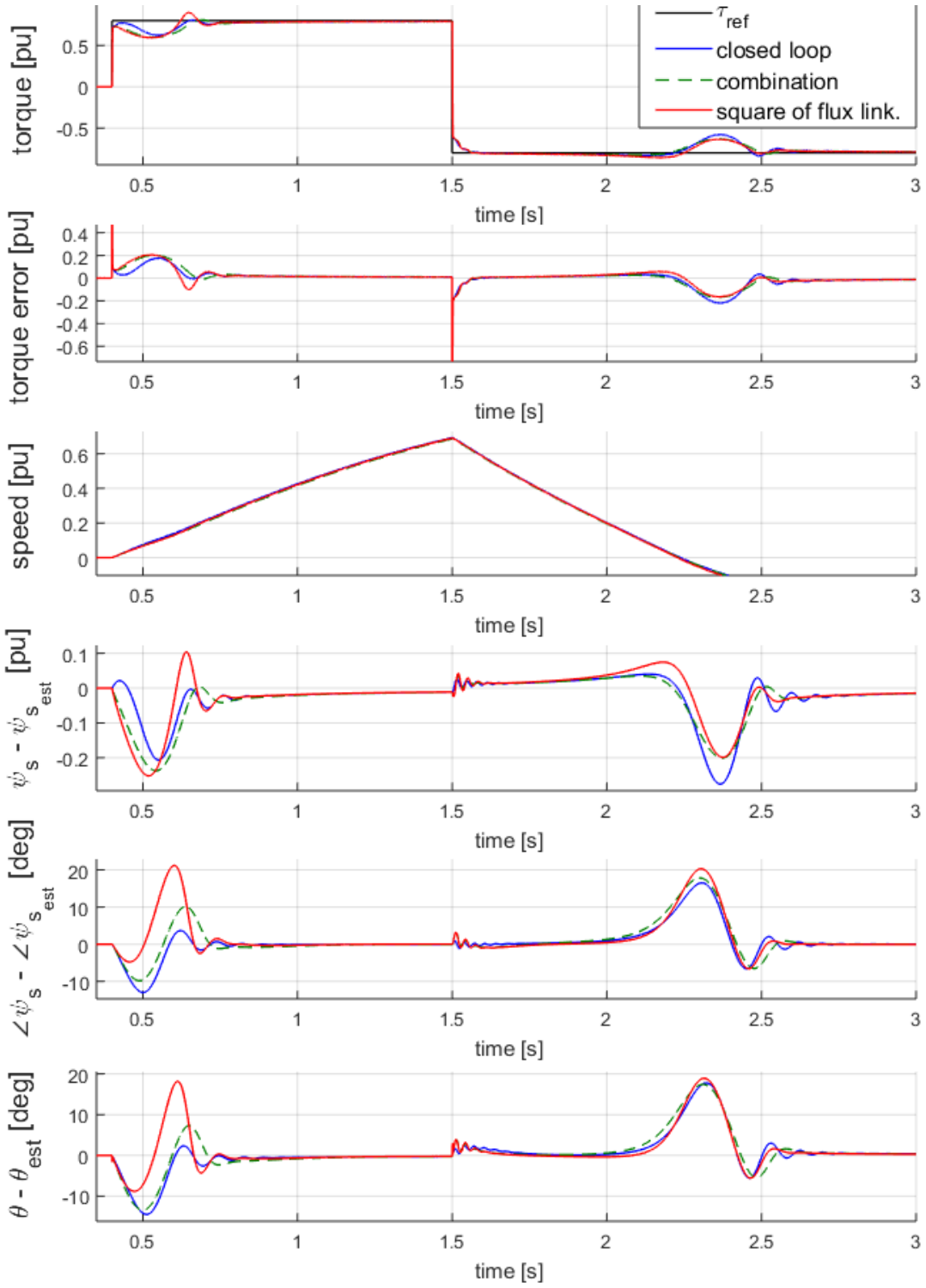

Figure 7.4: Comparing the correction methods: Difference between VM and CM as feedback with gain of 0.1, the method based on the square of the stator flux linkage amplitude, and a combination of them

7.2 Phase Locked Loop

To improve the closed loop observer based on the difference between the estimated stator flux linkage from the current model and the one from the voltage model, the estimated rotor position which is used as input to the current model is filtered by a phase locked loop, PLL. The motivation is that the PLL will act as a lowpass filter, giving a smoother and more accurate rotor position estimate while driving though zero speed. This may be beneficial if the estimated rotor position oscillates around the actual position. The estimated rotor position from the voltage model is the input to the PLL. The error between the input and the filtered output is the input to a PI controller, with the estimated rotor frequency as output. This value is scaled from Hz to radians before it is integrated, yielding the filtered estimated rotor position. A block diagram is presented in figure 7.5. $\hat{\theta}_{PLL}$ in figure 7.5 is used as input to the current model, while the unfiltered $\hat{\theta}_{VM}$ is used as rotor position input to the control system. The open loop transfer function of the PLL is given by equation 7.1, yielding the closed loop transfer function in equation 7.3.

$$h_{0_{PLL}} = \frac{k_p(1+T_i s)}{T_i s}\frac{\omega_n}{s} \tag{7.1}$$

$$m_{PLL} = \frac{h_{0_{PLL}}}{1+h_{0_{PLL}}} \tag{7.2}$$

$$= \frac{1+T_i s}{1+T_i s+\frac{T_i}{\omega_n k_p}s^2} \tag{7.3}$$

$$h = \frac{1+Ts}{1+2\zeta\frac{s}{\omega_0}+(\frac{s}{\omega_0})^2} \tag{7.4}$$

As the input to the PLL has the shape of a ramp, and the open loop transfer function contains two integrators, no steady state error occurs. By comparing equation 7.3 with the general transfer function of a second order system with two conjugated poles, a zero point in the left half plane and unity gain, equation 7.4, the parameters of the PLL is obtained as a function of the desired relative damping, ζ, and the desired undamped resonance frequency, ω_0 [2, p 149]:

$$k_p = 2\zeta\frac{\omega_0}{\omega_n} \tag{7.5}$$

$$T_i = \frac{2\zeta}{\omega_0} \tag{7.6}$$

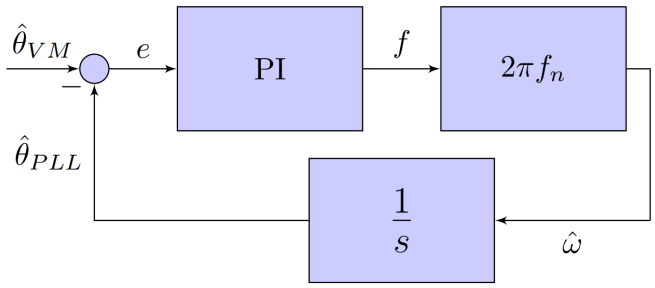

Figure 7.5: The PLL presented as a block diagram

By inserting equation 7.5 and 7.6 into equation 7.3, the closed loop transfer function of the PLL is obtained as function of ω_0 and ζ, as in equation 7.7.

$$m = \frac{1 + 2\zeta\frac{s}{\omega_0}}{1 + 2\zeta\frac{s}{\omega_0} + (\frac{s}{\omega_0})^2} \tag{7.7}$$

The scaled step response of the PLL can be plotted by choosing $\omega_0 = 1$, as this property will not influence the overshoot, but only scale how fast the response will be. The scaled step response of the PLL for different damping ratios is presented in figure O.1 in appendix O. By choosing a relative damping, such as $\zeta = 0.8$, the PLL can be tuned by adjusting the resonance frequency. The difference between the current model and the voltage model is used as feedback, with the gain of 0.1, as this value was found satisfying previously in section 7.1. Simulations with resonance frequencies between 30 rad/s and 100 rad/s are presented in figure O.2 in appendix O. As before, both the damper winding resistances and stator winding resistance are underestimated by 20 %, while the inductances are assumed correctly estimated. It is evident from figure O.2 that an undamped resonance frequency of 50 rad/s gives the best response, considering both the estimate during step in torque, and while crossing zero speed.

In figure 7.6, the flux linkage estimation and the sensorless operation with a closed loop observer with feedback gain of 0.1, with and without filtering the estimated rotor position input to the current model by a PLL, is presented. Relative damping of 0.8 and resonance frequency of 50 rad/s is used. Figure 7.6 reveals that the PLL improves the estimated stator flux linkage significantly throughout the whole simulation. This yields better estimates of the rotor position, and the generated torque follows its reference with high accuracy both during start up and through zero speed. The error in generated torque during the first step in torque reference is reduced from 0.18 pu to 0.03 pu, while the error when the machine drives through zero speed is reduced from -0.22 pu to 0.12 pu. The flux estimates from the current model in the same scenario as in figure 7.6 is given in figure O.3 in appendix O. The more accurate rotor estimate input gives smaller errors in the estimated stator flux linkage amplitude from the current model. The stator flux linkage angle estimated by the current model is improved for most of the operation by using the PLL, but after crossing zero speed the estimate actually becomes worse with the PLL than without it. However, as the sensorless control is based on the stator flux linkage estimate and rotor position from the voltage model, which are both improved, the PLL improves the sensorless operation in this scenario.

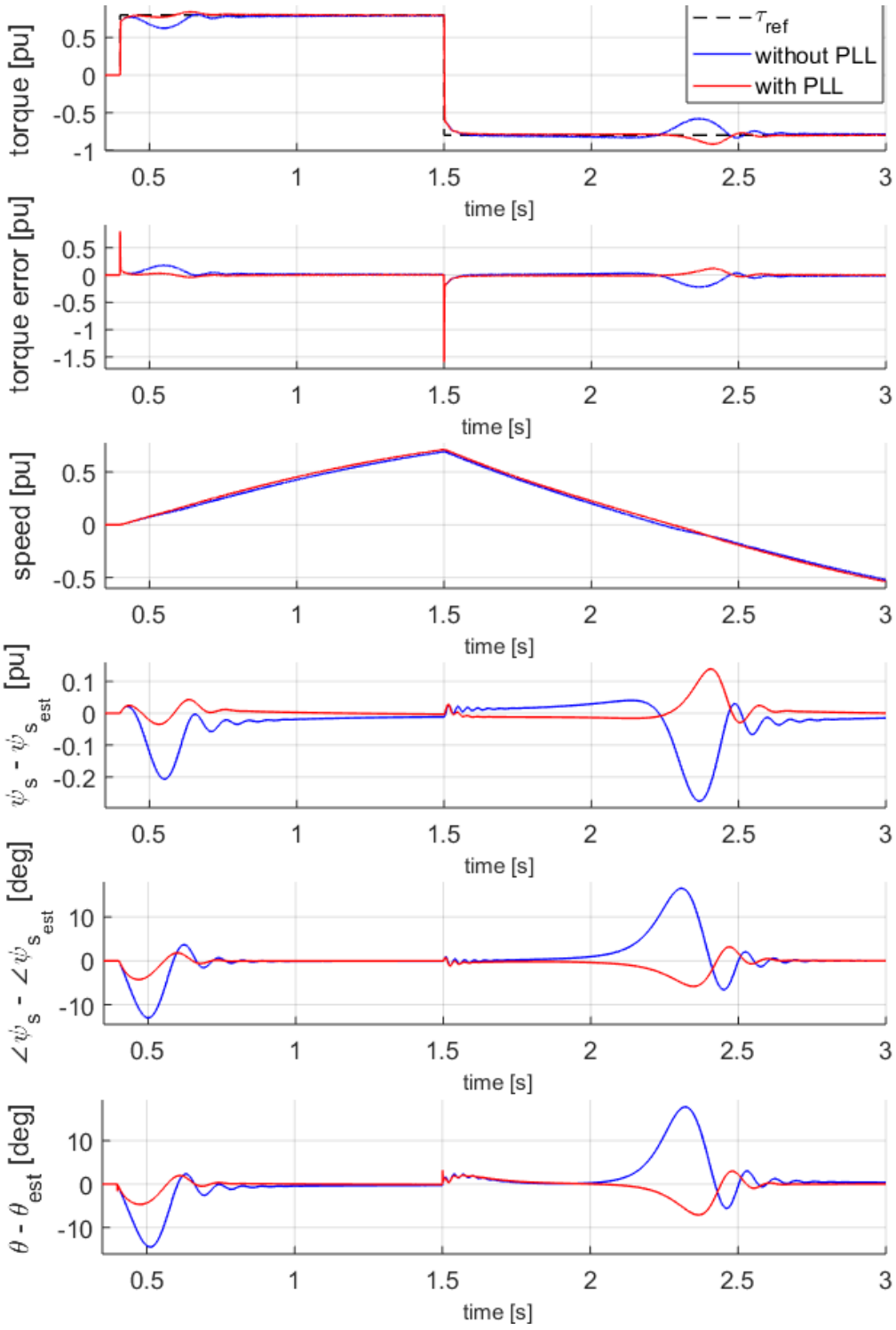

Figure 7.6: Sensorless operation with feedback correction, with and without PLL

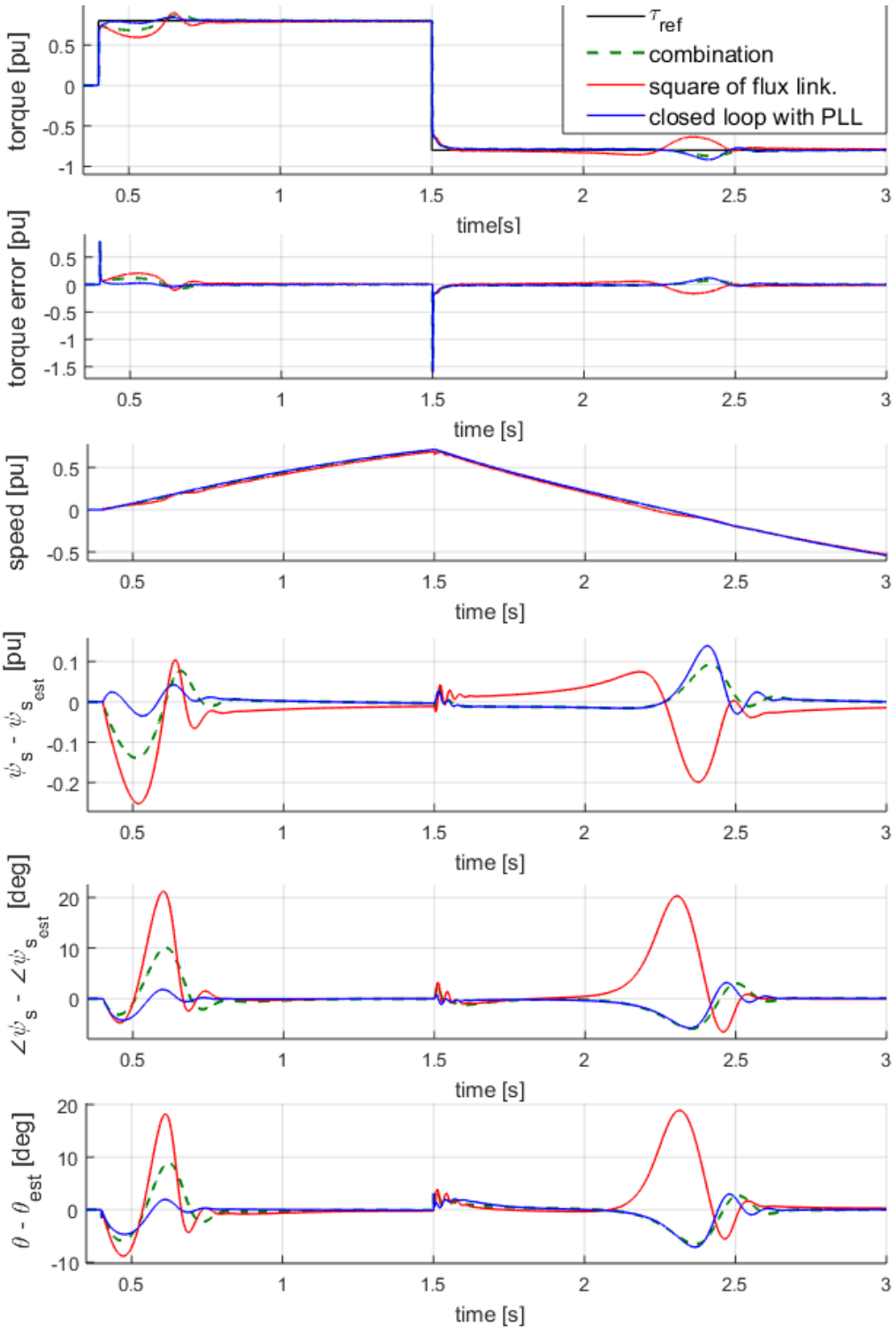

Figure 7.7: Comparing the correction method based on the square of the stator flux linkage amplitude with the closed loop observer with PLL

In figure 7.7, the stator flux linkage estimates and the sensorless operation with the closed loop observer, with PLL and a feedback gain of 0.1, is compared with the correction method based on

the square of the flux linkage amplitude. The damper winding resistances and the stator resistance are underestimated by 20 %, while the inductances are assumed correctly estimated. In the figure, a combination of the two models is also presented. It is illustrated that the closed loop observer with PLL provides significantly better flux linkage estimates than the correction method based on the square of the stator flux linkage amplitude during the whole simulation. When the machine drives through zero speed, the flux estimates and the performance of the sensorless operation is slightly improved by combining the models. At start up, after the initialisation of the machine, the closed loop observer with PLL alone provides the best estimates, as the correction method based on the square of the stator flux linkage amplitude was found to perform bad during step in torque from standstill.

The closed loop observer, with feedback gain of 0.1, with and without a PLL is now compared with the correction method based on the square of the stator flux linkage amplitude when all parameters in the machine is estimated correctly. This is the ideal scenario if the parameters are updated correctly during operation, either based on measured temperatures and operating characteristics, or by on-line parameter identification. When the PLL is used, $\zeta = 0.8$ and $\omega_0 = 50$. A combination of the closed loop observer with PLL and the correction method based on the square of the flux linkage amplitude is also included. The result, presented in figure 7.8, reveals that the correction method based on the square of the flux linkage amplitude performs way better than the closed loop observer with PLL when the parameters are correctly estimated. Especially while driving through zero speed the closed loop observer with PLL performs bad. The best performance is obtained by the closed loop observer without PLL, which estimates the flux linkage more or less perfectly throughout the whole simulation. Especially during the first step in torque reference, this observer has an advantage compared to the correction method based on the square of the flux linkage amplitude, as the latter method gives an undesired contribution with the current tuning, as discussed previously in this thesis. This indicates that a closed loop observer, with the difference between the flux linkage estimate from the current model and the estimate from the voltage model multiplied by 0.1 as feedback, is preferable for sensorless control of this machine when all parameters are known with high accuracy. The peak errors for the different methods while driving through zero speed, with accurately estimated parameters, are summarised in table 3.

Table 3: Peak values while driving through zero speed in figure 7.8

Correction	$\Delta\hat{\psi}_s$	$\Delta\angle\hat{\psi}_s$	$\Delta\hat{\theta}$
square of flux link.	0	-0.013	0
closed loop w PLL	0.51	-18.6	-25
closed loop wo PLL	0	-0.02	0
combination	0.36	-19.3	-23

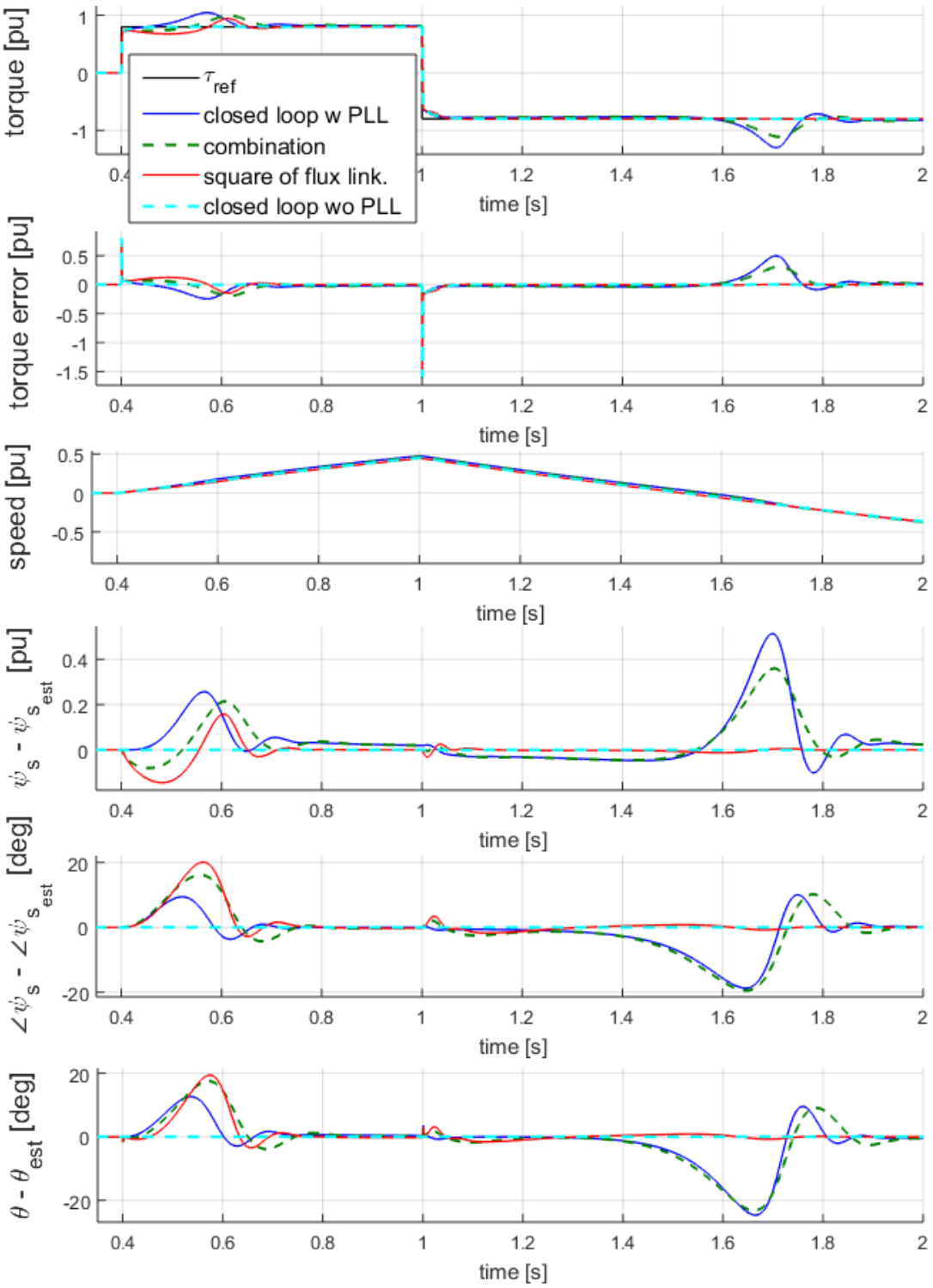

Figure 7.8: Comparing the correction methods when all parameters are estimated correctly

From the results, it is obvious that the behaviour of the closed loop observer depends on the estimated parameters is the model. The closed loop observer without PLL, with a gain of 0.1 in the feedback, and without any external drift correction yielded the best results when all parameters are accurately estimated. A final simulation was run with this model, where all the parameters in the model are estimated 20 % too low and too high, to see if the performance is significantly reduced when also the inductances are erroneously estimated. The torque reference is also slightly reduced compared to figure 7.8. The results are presented in figure 7.9. As expected, the erroneously estimated inductances degrade the performance of the closed loop observer, as the accuracy of the current model is reduced. This must be taken into consideration in future search of an optimal estimator. Despite this, the generated torque still follows its reference quite good, especially when the rotational speed is high, and the sensorless control is not lost after driving through zero speed.

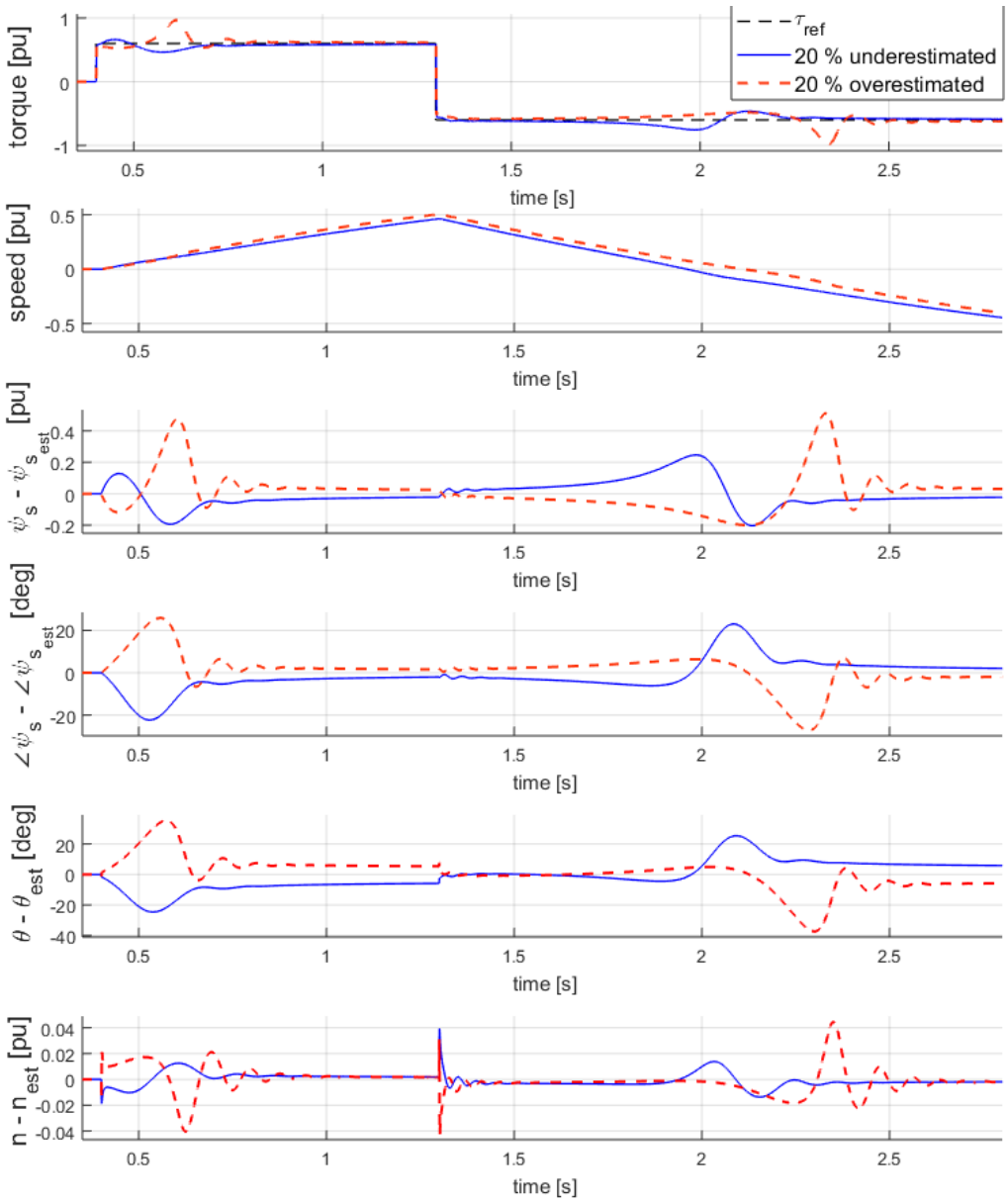

Figure 7.9: Closed loop observer without PLL, all parameters overestimated and underestimated by 20 %

7.3 Suggested Compensation Methods

In this subsections, some more ideas for how the current model and voltage model can be combined are presented. The suggested methods have not been analysed in detail, but they may be investigated and used in further work to obtain a flux model even less sensitive to the estimated parameters.

7.3.1 Measuring the Speed or Position

If the gain at the feedback signal is high enough, the feedback will make the current model and the voltage model follow each other completely. If an accurate position sensor is used at the current model, and the inductances and the rotor resistances are estimated accurately, the current model estimates the flux linkage perfectly. The feedback to the voltage model then corrects also the voltage model to estimate the flux linkage accurately. This was tested by simulations with success. This can be useful for updating the voltage model, but if these assumptions are made, one could just as well use the flux estimate from the current model directly as input to the control system.

7.3.2 Compensation Proportional to the Magnitude Difference

This method is inspired by the correction method based on the square of the stator flux linkage amplitude. In figure 7.2 it was illustrated that the estimated flux linkage amplitude from the current model is better than the estimated amplitude from the voltage model, assuming accurately estimated inductances. Thus, the stator flux linkage estimated by the voltage model can be multiplied by the difference between the flux linkage amplitude estimated by the current model, and the amplitude estimated by the voltage model, and added to the voltage integral in equation 3.1 as a compensation term. As long as the angle of the stator flux linkage estimated by the voltage model and current model are quite similar, this method gives the same compensation as by using the difference between the flux linkages directly as in figure 7.1. Drifting is compensated for by correcting the stator flux linkage amplitude. By simulations in Simulink, the same observations were made for this method as for the method described in section 7.1; the method corrects the flux linkage at higher speeds, but it is challenged while crossing zero speed. Also for this method, the flux linkage estimate while driving through zero speed is improved by reducing the feedback gain.

7.3.3 Compensation by Comparing the Rotor Flux Linkage Estimates

A third method suggested is to compare the rotor flux linkages ψ_{Rd} and ψ_{Rq} obtained from the two models. The motivation behind this is that these quantities will change more slowly than the stator flux linkages, as they are filtered by the rotor time constants and change during dynamic operation only. First, ψ_{Rd} and ψ_{Rq} are estimated from equation 2.38 and 2.39. Then the stator flux linkage amplitude from the voltage model, and the corresponding estimated rotor position are used to find the d and q component of the stator flux linkage from the voltage model. The rotor flux linkages from the voltage model is then found by solving equation 2.40 and 2.41 with respect to ψ_{Rd} and ψ_{Rq}. Correction by this method was however not successfully achieved.

7.3.4 On-Line Parameter Estimation

Another way of improving the voltage model during operation is by updating the estimated parameters regularly. It was found in this thesis that updating the stator resistance do not compensate for drifting occurred, and hence it is not a compensation method, but it can be combined with a drift compensation method such as the correction method based on the square of the stator flux linkage amplitude, to remove the steady state error in the estimated stator flux linkage amplitude. If the flux linkage estimate obtained from the current model is better than the one from the voltage

model, the stator resistance can be estimated during operation by comparing the stator flux linkage estimate from the two models. If a speed measuring sensor is available, and the inductances are known, this is typically the case. In the doctoral thesis of Tom Nestli, it is stated that if the voltage measurement is assumed to be accurate, any deviation between the current model and the voltage model at low speed operation will be mainly due to the stator resistance. It is suggested to compare either the amplitudes or the angles of the estimated stator flux linkages from the two models, filter the difference through a PI-filter, with the updated stator resistance as the output [19]. By using this estimated resistance as input to the voltage model, a closed loop is obtained. The estimated resistance will then be updated until the flux estimates from the two models are equal, and the error is zero. Similarly the rotor resistances and the inductances can be estimated in the upper speed region, where the voltage model is known to be more reliable than the current model.

8 Discussion

In this master's thesis, the parameter sensitivity of flux models and the sensorless operation of a separately magnetised synchronous machine have been analysed. The sensorless operation with the flux models and the control structure that was developed and implemented in Simulink during the specialisation project, the fall semester 2017, has been investigated [4]. As the sensorless operation uses the estimated flux as input to the control system, results from the sensitivity analysis must be used to analyse and evaluate the sensorless control. The voltage model was found to be very sensitive to the estimated stator resistance at low speeds, and the dependency increased with the torque reference. Even a small deviation between the actual and the estimated stator resistance such as 20 % of 0.048 pu, which is only 0.0096 pu, may cause a significant error of several pu in the estimated flux linkage amplitude if the speed is low enough and the current is high enough. It should be emphasised that this is not only due to drifting, but it happens during steady state as well.

In the steady state analysis it was concluded that the inductance with the highest value, which for this machine is the d axis inductance, is the most important inductance to estimate accurately for the purpose of obtaining an accurate stator flux linkage estimate. The inductances along the q axis are however included in the expression used for estimating the rotor position, equation 3.2. How sensitive this expression is to the estimation of x_q and x_Q, and how theses parameters influence the sensorless control has not been analysed in this thesis. Hence, it will not be concluded which of the inductances that influence the sensorless operation most. The steady state analysis of the current model assumed measured rotor position. In the dynamic analysis performed later, the current model sometimes uses the estimated rotor position from the voltage model as input. This estimate is often inaccurate, and hence it would have been interesting to perform a thorough analysis of how sensitive the current model is to the rotor position input.

A deviation of 20 % between the actual stator resistance and the estimated one caused drifting during dynamics, and the sensorless control without correction was not satisfying. The drifting flux linkage is actually an offset in the integral in the voltage model, and hence the estimated flux linkage vector moves along a displaced trajectory when a new steady state is obtained. In the literature it is often stated that the voltage model is more reliable at higher speeds, which the results in this work confirm, but it is important to be aware of that once the flux linkage has drifted, the offset in the flux linkage estimate is not removed by increasing the speed or by updating the erroneous parameters in the voltage model to correct values. These actions will only correct the estimated magnitude of the flux linkage vector, but the flux linkage vector is still displaced. This results in an oscillating error in both the estimated flux linkage amplitude, and in the estimated flux linkage angle. This thesis has made a major point out of this. A similar situation is encountered when the voltage model is erroneously initialised; an offset occurs in the voltage integral. It was reasoned that a long magnetisation and initialisation period will reduce the likelihood of wrong initialisation of the voltage model, as the current model depends on the damper winding resistances during transients only. Hence, if the magnetisation and initialisation period is long enough, the initial value of the voltage model is unaffected by the damper winding resistances.

Further actions must be taken to remove the offset if drifting occurs. The correction method

based on the square of the stator flux linkage amplitude, and a closed loop observer with the difference between the stator flux linkage estimate from the current model and the flux linkage estimate the from voltage model as a compensating feedback to the voltage model, are two methods for this purpose that have been investigated in this work. During most of the work, the correction method based on the square of the stator flux linkage amplitude was utilised. It was observed that this method had some problems during step in the torque reference from stand still. The method used to initialise the rotor position, by supplying a constant voltage vector along the stator phase a axis turned out to challenge the method even more, as the d axis current then changes from a positive value to a negative value, as seen for instance in figure 6.11, instead of from zero to a negative value which is the case without initialisation of the rotor position. This causes the flux to vary even more during the step in torque, resulting in an undesired contribution from the correction algorithm. The advantage of this initialisation method is that it is easy, and it requires no extra installed equipment, but it requires that the sensorless operation starts from standstill, which is not always desired. It is realised in retrospect that it would have been wiser to initialise the rotor in the opposite direction, by supplying a constant negative d axis current instead of a positive one, as the d axis current is negative for all operations after initialisation to obtain unity power factor. It is concluded that the initialisation method used, and the correction method based on the square of the flux linkage amplitude is a bad combination.

When using the correction algorithm based on the square of the stator flux linkage amplitude, the drifting is compensated for. The offset in the integration is removed, yielding zero error in the estimated flux linkage angle. The error in estimated flux linkage amplitude stops oscillating, as the trajectory of the estimated flux linkage vector is now origin centred. However, if the stator resistance is still estimated incorrectly, a steady state error in the estimated flux linkage amplitude will occur. Hence, to obtain a perfect flux linkage estimate, the stator resistance must be updated to the correct value. This can either be done by using temperature sensors and a characteristic of how the resistance change with temperature, or by utilising a combination of the flux linkage models to estimate the parameters on-line. Increasing the speed while using drift correction should also reduce this steady state offset, according to the steady state results obtained.

The torque control at very low speed was not very accurate, but the drive remained stable due to the low generated torque. Successful sensorless operation through zero speed was also achieved, but the accuracy was significantly reduced when the drive used a long time crossing zero speed, and when the generated torque was large at low speeds. The synchronous machine investigated, with the implemented sensorless control, is hence suitable for operating as motor in applications where the load is low for low speeds, such as pumps, or applications where it is not necessary to operate at zero speed, but rather just drive through zero speed, such as ship propulsion. It can not be used in applications that require a high torque at standstill operation, such as lifts. This requires other techniques, such as high frequency signal injection [10]. The control seems to be well suited for use in adjustable speed hydro, where holding a load at standstill is not required.

A closed loop observer was implemented by combining the voltage model and the current model. The rotor position, estimated by the stator flux linkage estimate from the voltage model, was used as input to the current model. As the current model was observed to estimate the flux linkage amplitude significantly more accurately than the voltage model without any correction, when the

stator resistance and the damper winding resistances were all underestimated by 20 % and the inductances were correctly estimated, the current model was used as a reference for the voltage model. The difference between the current model and the voltage model was used as a compensating feedback to the voltage model, and the estimate from the compensated voltage model was used as input to the control system. This yielded better sensorless control compared to the correction method based on the square of the stator flux linkage amplitude when all parameters were correctly estimated. With correctly estimated parameters, no correction is needed, and the undesired correction during the first step in torque reference, as discussed in section 6.2.1, was avoided when using the closed loop observer. The stator flux linkage estimate while driving through zero speed was more or less perfect for both of the correction methods, when all parameters were estimated accurately. From this it is concluded that the closed loop observer is preferable when all parameters are known with high accuracy, such as if high quality temperature sensors, and voltage and current measurement devices are used. When the resistances in the stator and in the damper windings were all underestimated by 20 %, assuming correctly estimated inductances, the two correction methods investigated resulted in equally good sensorless control. By filtering the estimated rotor position by a PLL before using it as input in the current model, better control while driving through zero speed was obtained by using the closed loop observer. However, this estimator yielded a bad stator flux linkage estimate when all parameters were correctly estimated. The PLL was tuned from an assumption of that the stator resistance and the damper winding resistances were underestimated by 20 %, that the feedback gain was 0.1, and that all inductances were estimated correctly, which is a quite specific scenario. From these results it is evident that no correction method that is optimal for all scenarios was obtained. It is known that the current model depends heavily on the estimated inductances. If the inductances are inaccurately estimated, it may be that the current model no longer estimates the flux linkage amplitude better than the voltage model, and using the current model as a reference for the voltage model will then no longer improve the voltage model. More thorough analysis of how the inductances influence the current model during dynamics, and how this influence the closed loop observer is suggested as further work. It should also be mentioned that the comparisons conducted between the closed loop observer and the correction method based on the square of the stator flux linkage amplitude depend on the tuning of both methods. It was stated in section 6.2.1 that the tuning of the correction method based on the square of the stator flux linkage amplitude has room for improvements, and hence a better tuning of the parameters in this algorithm may change the conclusions. Other operations of the machine, obtained by changing the torque reference, will also have an impact on the performance of the estimators considered. This thesis do not claim to have found an optimal closed loop observer, but it has rather illustrated that it is possible to improve the flux linkage estimation at low speeds by combining the models in some way or another, by tuning the feedback gain, and by using a PLL. It is also stated that external drift correction algorithms can be omitted by using compensating feedback to the voltage model, as the closed loop observer investigated, when all inductances are known with high accuracy. The simulation time limited the number of scenarios investigated. Experiments in a real lab setup, based on the results in this work, would give a more complete analysis of the sensorless operation, and of how the closed loop observer can be improved.

In most of the simulation results presented, the error in the estimated speed is not included. This is because the speed in general was found to be estimated with higher accuracy than the estimated rotor position. This is because the speed is estimated by using the definition of the

derivative on the estimated rotor position. Hence, a steady state error in the estimated rotor position has no impact on the estimated speed, and as long as the error in estimated rotor position changes slowly, the estimated speed is not influenced very much. When a closed loop observer with a too high gain was used, as in figure 7.3, the error in estimated angle increased rapidly. The speed was then estimated to decrease, while the actual speed increased significantly for a short time interval. This erroneously estimated speed may cause major consequences if the machine is speed controlled, or if the machine operates close to the field weakening region. If the speed exceeds 1 pu, the control system may not have knowledge about this, and hence field weakening is not applied. The back emf may then exceed the voltage rating of the motor, and overmodulation occurs [18].

A final point to discuss is that the controllers were tuned based on the machine parameters in the specialisation project. When the parameters in the machine are erroneously estimated, this will affect the gains and time constants in the PI controllers. These effects have been neglected in the analysis conducted in this thesis, and they are hence a possible source of error. In the specialisation project it was found that especially the flux controller is sensitive to the gain, where a too high gain resulted in a high frequent oscillating stator flux linkage. This may explain the high frequent oscillating current in the dynamic analysis of an erroneously estimated d axis inductance, performed in section 6.3.1.

9 Conclusion

In this master's thesis, flux models and sensorless control of a separately magnetised synchronous machine has been analysed in detail. The machine is able to drive slowly through zero speed, but with a less accurate flux estimate in the low speed region, affecting the control of the machine. A new method for estimating the rotor position based on the estimated stator flux linkage was successfully implemented in Simulink, yielding accurate estimates of the rotor position for accurate flux estimates. The estimated stator flux linkage from the voltage model is sensitive to the estimated stator resistance, and an erroneously estimated stator resistance causes an erroneously estimated stator flux linkage magnitude, even during steady state operation. The combination of whether the stator resistance is underestimated or overestimated, and whether the machine operates as a motor or as a generator determines whether the stator flux linkage magnitude becomes overestimated or underestimated. The voltage model is more sensitive to both the estimated stator resistance, and to the estimated voltage supplied at lower speeds. The sensitivity to the estimated stator resistance increases significantly with the torque reference, especially at low speeds.

During steady state, the flux estimate from the current model depends on the accuracy of the estimated inductances and on the measured currents only. The sensitivity of the current model to the d axis inductance decrease with the torque, and it is also drastically reduced in the field weakening region. The opposite observations were made for the analysis of an inaccurately estimated q axis inductance. It is concluded that the current model is independent of the speed in the normal operating region only, below ± 1 pu, as field weakening affects the model.

From the dynamic analysis, it is concluded that an erroneously estimated stator resistance makes the estimated stator flux linkage drift during dynamics. This causes an oscillating error in both the estimated amplitude and in the estimated angle of the stator flux linkage. The error in estimated angle was not revealed by the steady state analysis, as drifting due to an erroneously estimated stator resistance occurs during dynamics only. During sensorless control, the actual stator flux linkage is also exposed to drifting, as the control system uses the estimated flux linkage as input. The drifting due to an incorrect estimate of the stator resistance was proven to have a linear dependence on the speed at the instant the drifting occurs, but once the flux linkage estimate has drifted, the offset is not removed by increasing the speed, nor by updating the stator resistance to it correct value. It is concluded that the estimated flux linkage by the voltage model depends on the current state of the machine, but also the past, due to the integration. Offsets in the voltage measurement cause drifting also during steady state operation. Sensorless operation without drift correction is not satisfying with an erroneously estimated stator resistance, or when the voltage model is incorrectly initialised.

To correct for the drifting, the correction method based on the square of the stator flux linkage amplitude was initially used with success. The method removes the offset in the estimated flux linkage estimate, resulting in zero error in the estimated flux linkage angle, and in a constant amplitude error if the stator resistance is erroneously estimated. With the implemented control system, and with this correction method, satisfying sensorless control is obtained. The sensorless performance is reduced for lower speeds, and it is also heavily dependent on how fast the machine drives through zero speed, and on the generated torque while driving through zero speed. The

machine drives successfully through zero speed while generating a torque of 0.4 pu and with a load of 0.6 pu, but as the generated torque is increased to 0.6 pu, and the load is increased to 0.8 pu, the control is lost. Standstill sensorless operation while generating a torque is not possible with the control structure investigated.

When the inductances of the machine are known with high accuracy, it is possible to replace the correction method based on the square of the stator flux linkage amplitude by a closed loop observer. The closed loop observer uses the difference between the stator flux linkage estimated by the current model and the stator flux linkage estimated by the voltage model as a compensating feedback to the voltage model. The correction method based on the square of the stator flux linkage amplitude and the closed loop observer yield equally good results when the stator and damper winding resistances are underestimated by 20 %, while the closed loop observer yields better results than the correction method based on the square of the stator flux linkage amplitude when all parameters are correctly estimated. Filtering the estimated rotor position input to the current model by a PLL improves the closed loop observer when the stator and damper winding resistances are all underestimated by 20 %. With correctly estimated parameters the PLL will degrade the performance of the closed loop observer. A gain reducing the compensating feedback is necessary to maintain stability while driving through zero speed. A closed loop observer with improved flux estimation for all operations and scenarios was not obtained.

9.1 Recommendation for Further Work

From the sensitivity analysis performed in this text it is evident that the flux models are sensitive to the estimated parameters. In the dynamic analysis of the sensorless operation there was a focus on the sensitivity to the stator resistance. In further work, it is recommended to analyse how sensitive the estimated rotor position is to estimated parameters such as the inductance along the q axis, the resistance in the q axis damper winding, or leakage coefficients along the q axis. It is also recommended to perform dynamic analysis in the field weakening region, as the steady state analysis in this text revealed that the current model is sensitive to field weakening. The sensitivity of the current model to the estimated rotor position should also be analysed, both during steady state and during dynamics. The drift correction method based on the square of the stator flux linkage amplitude works for the separately excited synchronous machine investigated, but especially during the first step in torque reference, from zero speed, the model has room for improvement. Further tuning of the gains k_{T_0} and k_2, the filter time constant T_{filter} or the low pass filter which the torque generating current is filtered through may improve the performance.

The combination of the current model and the voltage model was found to correct for the drifting. For some investigated scenarios the sensorless control performed better with the closed loop flux observer than with the voltage model only, corrected by the correction method based on the square of the stator flux linkage amplitude. From this it is evident that it is possible to replace the correction method initially used, and to improve the sensorless operation. Further analysis should be conducted to optimise the closed loop observer, for instance by using a PI controller in the compensating feedback, or by compensating the voltage model in another way. The PLL was found to improve the closed loop observer when only the stator and damper winding resistances are erroneously estimated, an observation that can be investigated more thoroughly. It should also

be investigated how the closed loop observer performs when when the inductances are incorrectly estimated, as this reduces the accuracy of the flux linkage estimate from the current model. Experiments in a lab setup, based on the findings in this thesis, is recommended for investigating a broader range of scenarios and operations.

10 References

[1] M. Alakula. On the control of saturated synchronous machines. In *1994 Fifth International Conference on Power Electronics and Variable-Speed Drives*, pages 386–389, Oct 1994.

[2] Jens G. Balchen, Trond Andresen, and Bjarne A. Foss. *Reguleringsteknikk*. Institutt for teknisk kybernetikk, 5 edition, 2003.

[3] Felix Blaschke and Walter Dreiseitl. Method and apparatus for determining the initial rotor angle in a rotating field machine, September 30 1975. US Patent 3,909,688.

[4] Magnus Bolstad. Control of synchronous machines used in ASH, Project thesis. *NTNU*, 2017.

[5] Hansruedi Bühler. *Einführung in die Theorie Geregelter Drehstromantriebe: Band 1: Grundlagen*. Birkhäauser Verlag, Basel, 1977.

[6] Alfio Consoli, Giuseppe Scarcella, and Antonio Testa. Sensorless control of ac motors at zero speed. In *Industrial Electronics, 1999. ISIE'99. Proceedings of the IEEE International Symposium on*, volume 1, pages 373–379. IEEE, 1999.

[7] Bendik Fossen. Modelling and identification of multi-phase machines. Specialisation project, NTNU, December 2016.

[8] Oddmund Grøvan. Identifikasjon og regulering av en synkronmotordrift. Master's thesis, NTNU, June 2004.

[9] Joachim Holtz and Juntao Quan. Drift-and parameter-compensated flux estimator for persistent zero-stator-frequency operation of sensorless-controlled induction motors. *IEEE Transactions on Industry Applications*, 39(4):1052–1060, 2003.

[10] Ji-Hoon Jang, Seung-Ki Sul, Jung-Ik Ha, K. Ide, and M. Sawamura. Sensorless drive of surface-mounted permanent-magnet motor by high-frequency signal injection based on magnetic saliency. *IEEE Transactions on Industry Applications*, 39(4):1031–1039, July 2003.

[11] P. L. Jansen and R. D. Lorenz. Accuracy limitations of velocity and flux estimation in direct field oriented induction machines. In *1993 Fifth European Conference on Power Electronics and Applications*, pages 312–318 vol.4, Sept 1993.

[12] P. L. Jansen and R. D. Lorenz. A physically insightful approach to the design and accuracy assessment of flux observers for field oriented induction machine drives. *IEEE Transactions on Industry Applications*, 30(1):101–110, Jan 1994.

[13] Jukka Kaukonen et al. Salient pole synchronous machine modelling in an industrial direct torque controlled drive application. *Acta Universitatis Lappeenrantaensis*, 1999.

[14] Cristian Lascu, Ion Boldea, and Frede Blaabjerg. A modified direct torque control for induction motor sensorless drive. *IEEE Transactions on industry applications*, 36(1):122–130, 2000.

[15] Julius Luukko. *Direct torque control of permanent magnet synchronous machines-analysis and implementation*. PhD thesis, Acta Universitatis Lappeenrantaensis, 2000.

[16] Julius Luukko, Markku Niemela, and Juha Pyrhonen. Estimation of the flux linkage in a direct-torque-controlled drive. *IEEE Transactions on Industrial Electronics*, 50(2):283–287, 2003.

[17] Jan Machowski, Janusz W. Bialek, and james R. Bumby. *Power System Dynamics stability and control*. John Wiley & Sons, Ltd, second edition edition, 2008.

[18] Ned Mohan. *Advanced Electric Drives, Analysis, Control and Modeling Using MATLAB/Simulink*. John Wiley & Sons, Ltd, 2014.

[19] Tom Fagernes Nestli. *Modelling and Identification of Induction Machines*. PhD thesis, NTH, 1995.

[20] M Niemelä, J Luukko, J Pyrhönen, O Pyrhönen, and J Kaukonen. Position-sensorless direct-torque-controlled synchronous motor drive for ship propulsion. *International Transactions on Electrical Energy Systems*, 10(6):353–360, 2000.

[21] Markku Niemelä et al. Position sensorless electrically excited synchronous motor drive for industrial use based on direct flux linkage and torque control. *Tieteellisiä julkaisuja-Research reports*, 1999.

[22] Roy Nilsen. *Electric Drives*. Department of Electric Power Engineering, spring 2016.

[23] Roy Nilsen. *Electric Drives*. Department of Electric Power Engineering, spring 2018.

[24] Arne Nysveen. *TET 4200 Maritime and Offshore Power Systems*. Department of Electric Power Engineering, spring 2016.

[25] M. C. Paicu, I. Boldea, G. D. Andreescu, and F. Blaabjerg. Very low speed performance of active flux based sensorless control: interior permanent magnet synchronous motor vector control versus direct torque and flux control. *IET Electric Power Applications*, 3(6):551–561, November 2009.

[26] R. Sporild, J. O. Gjerde, and T. Gjengedal. Economic and technical aspects of adjustable speed hydro (ash) machines applied for improved stability in power networks. In *2000 Power Engineering Society Summer Meeting (Cat. No.00CH37134)*, volume 4, pages 2469–2474 vol. 4, 2000.

[27] Peter Vas. *Sensorless Vector and Direct Torque Control*. Oxford University Press, 3 edition, 1998.

[28] WÄRTSILÄ. Technical note from supervisor , Power Drive Motor Software spesifikasjon.

[29] A. Yoo and S. K. Sul. Design of flux observer robust to parameter variation of interior permanent magnet synchronous motor. In *2008 IEEE Industry Applications Society Annual Meeting*, pages 1–7, Oct 2008.

A Machine Parameters

Table 4: Machine parameters

Parameter	Symbol	Value [pu]
stator resistance	r_s	0.048
damper winding D resistance	r_D	0.02
damper winding Q resistance	r_Q	0.03
field winding resistance	r_f	0.02
d-axis reactance	x_d	1.17
q-axis reactance	x_q	0.57
field winding reactance	x_f	1.32
damper winding D reactance	x_D	1.12
damper winding Q reactance	x_Q	0.59
stator leakage reactance	x_{s_σ}	0.12
Moment of inertia	J	0.58
Torque constant	k	0.003

Table 5: Other parameters in the model

Parameter	Symbol	Value
Triangular signal period	T_{tri}	$\frac{1}{3000}$ s
Sample time	T_{samp}	$\frac{T_{tri}}{2}$
frequency	f	50 Hz
Field circuit converter supply	u_{dc_f}	500 V
Stator circuit inverter supply	u_{dc_s}	1050 V

B Controller Parameters

In table 6, the controller parameters obtained in the specialisation project, which are also used in this master thesis are presented [4].

Table 6: Controller parameters

Parameter	Symbol	Value
Field current controller gain	K_{p_f}	1.98
Field current controller integration time	T_{i_f}	0.03
Stator d-axis current controller gain	K_{p_d}	0.54
Stator d-axis current controller integration time	T_{i_d}	0.01
Stator q-axis current controller gain	K_{p_q}	0.72
Stator q-axis current controller integration time	T_{i_q}	0.01
Flux controller gain	K_{ψ}	4
Flux controller integration time	$T_{i_{\psi}}$	0.18
Speed controller gain	K_{ω}	247.26
Speed controller integration time	$T_{i_{\omega}}$	0.004

C Derivation of the Alternative pu Model

I this section, the full derivation of the alternative pu voltage equations and flux equations from the specialisation project of Magnus Bolstad is repeated [4]. There is no new information in this appendix that can not be found in the project thesis. The starting point are the equations derived in the master thesis of Oddmund Grøvan [8]:

$$u_d = r_d^{'} i_d + \frac{x_d \sigma_{dD}}{\omega_n}\frac{di_d}{dt} - \frac{\psi_D}{(1+\sigma_D)\omega_n T_D} + \frac{r_D}{(1+\sigma_D)^2}(i_f + \sigma_D T_D \frac{di_f}{dt}) - n\psi_q \tag{C.1}$$

$$u_q = r_q^{'} i_q + \frac{x_q \sigma_{qQ}}{\omega_n}\frac{di_q}{dt} - \frac{\psi_Q}{(1+\sigma_Q)\omega_n T_Q} + n\psi_d \tag{C.2}$$

$$u_f = r_f^{'} i_f + \frac{x_f \sigma_{Df}}{\omega_n}\frac{di_f}{dt} - \frac{\psi_D}{(1+\sigma_D)\omega_n T_D} + \frac{r_D}{(1+\sigma_D)^2}(i_d + \sigma_D T_D \frac{di_d}{dt}) \tag{C.3}$$

$$\frac{d\psi_D}{dt} = -\frac{\psi_D}{T_D} + \frac{x_{md}}{T_D}(i_d + i_f) \tag{C.4}$$

$$\frac{d\psi_Q}{dt} = -\frac{\psi_Q}{T_Q} + \frac{x_{mq}}{T_Q} i_q \tag{C.5}$$

$$\psi_d = x_d \sigma_{dD} i_d + \frac{\psi_D}{1+\sigma_D} + \frac{x_{md}\sigma_D}{1+\sigma_D} i_f \tag{C.6}$$

$$\psi_q = \sigma_{qQ} x_q i_q + \frac{\psi_Q}{1+\sigma_Q} \tag{C.7}$$

$$\psi_f = \sigma_{Df} x_f i_f + \frac{\psi_D}{1+\sigma_D} + \frac{x_{md}\sigma_D}{1+\sigma_D} i_d \tag{C.8}$$

where

$$\sigma_{dD} = 1 - \frac{1}{(1+\sigma_d)(1+\sigma_D)}$$
$$\sigma_{Df} = 1 - \frac{1}{(1+\sigma_f)(1+\sigma_D)}$$
$$\sigma_{qQ} = 1 - \frac{1}{(1+\sigma_q)(1+\sigma_Q)}$$
$$r_d^{'} = r_s + \frac{r_D}{(1+\sigma_D)^2}$$
$$r_q^{'} = r_s + \frac{r_Q}{(1+\sigma_Q)^2}$$
$$r_f^{'} = r_f + \frac{r_D}{(1+\sigma_D)^2}$$

Eq. C.1 and C.3 contains derivatives of both the field current and the d- axis stator current. Inserting the one equation into the other, the derivative of i_f and the derivative of i_d are eliminated in eq. C.1 and C.3 respectively. Rearranging the terms on the right hand side gives the following expressions:

$$u_d = r_d^{'} i_d + \left[\frac{x_d \sigma_{dD}}{\omega_n} - \frac{r_D}{(1+\sigma_D)^2}\sigma_D T_D \frac{\omega_n}{\sigma_{Df} x_f}\frac{r_D}{(1+\sigma_D)^2} T_D \sigma_D\right]\frac{di_d}{dt} - \frac{\psi_D}{(1+\sigma_D)\omega_n T_D} + \frac{r_D}{(1+\sigma_D)^2}\left[1 - \sigma_D T_D \frac{\omega_n}{\sigma_{Df} x_f} r_f^{'}\right] i_f + \frac{r_D}{(1+\sigma_D)^2}\sigma_D T_D \frac{\omega_n}{\sigma_{Df} x_f}\left[u_f + \frac{\psi_D}{(1+\sigma_D)\omega_n T_D} - \frac{r_D}{(1+\sigma_D)^2} i_d\right] - n\psi_q \tag{C.9}$$

$$u_f = r_f^{'} i_f + \left[\frac{\sigma_{Df}}{\omega_n} x_f - \frac{r_D}{(1+\sigma_D)^2} T_D \sigma_D \frac{\omega_n}{x_d \sigma_{dD}}\frac{r_D}{(1+\sigma_D)^2}\sigma_D T_D\right]\frac{di_f}{dt} - \frac{\psi_D}{(1+\sigma_D)\omega_n T_D} + \frac{r_D}{(1+\sigma_D)^2}\left[1 - T_D \sigma_D \frac{\omega_n}{(x_d \sigma_{dD})} r_d^{'}\right] i_d + \frac{r_D}{(1+\sigma_D)^2} T_D \sigma_D \frac{\omega_n}{x_d \sigma_{dD}}\left[u_d + \frac{\psi_D}{(1+\sigma_D)\omega_n T_D} - \frac{r_D}{(1+\sigma_D)^2} i_f + n\psi_q\right] \tag{C.10}$$

Further manipulation:

$$u_d = \left[r_d^{'} - \frac{r_D}{(1+\sigma_D)^2}\sigma_D T_D \frac{\omega_n}{\sigma_{Df} x_f}\frac{r_D}{(1+\sigma_D)^2}\right] i_d + \left[\frac{x_d \sigma_{dD}}{\omega_n} - \frac{r_D}{(1+\sigma_D)^2}\sigma_D T_D \frac{\omega_n}{\sigma_{Df} x_f}\frac{r_D}{(1+\sigma_D)^2} T_D \sigma_D\right]\frac{di_d}{dt} - \frac{\psi_D}{(1+\sigma_D)\omega_n T_D} + \frac{r_D}{(1+\sigma_D)^2}\left[1 - \sigma_D T_D \frac{\omega_n}{\sigma_{Df} x_f} r_f^{'}\right] i_f + \frac{r_D}{(1+\sigma_D)^2}\sigma_D T_D \frac{\omega_n}{\sigma_{Df} x_f}\left[u_f + \frac{\psi_D}{(1+\sigma_D)\omega_n T_D}\right] - n\psi_q \tag{C.11}$$

$$u_f = \left[r_f^{'} - \frac{r_D}{(1+\sigma_D)^2} T_D \sigma_D \frac{\omega_n}{x_d \sigma_{dD}}\frac{r_D}{(1+\sigma_D)^2}\right] i_f + \left[\frac{\sigma_{Df} x_f}{\omega_n} - \frac{r_D}{(1+\sigma_D)^2} T_D \sigma_D \frac{\omega_n}{x_d \sigma_{dD}}\frac{r_D}{(1+\sigma_D)^2}\sigma_D T_D\right]\frac{di_f}{dt} - \frac{\psi_D}{(1+\sigma_D)\omega_n T_D} + \frac{r_D}{(1+\sigma_D)^2}\left[1 - T_D \sigma_D \frac{\omega_n}{(x_d \sigma_{dD})} r_d^{'}\right] i_d + \frac{r_D}{(1+\sigma_D)^2} T_D \sigma_D \frac{\omega_n}{x_d \sigma_{dD}}\left[u_d + \frac{\psi_D}{(1+\sigma_D)\omega_n T_D} + n\psi_q\right] \tag{C.12}$$

When reactance divided by nominal frequency times the resistance is inserted for the time constants, several resistances and frequencies in C.11 and C.12 is eliminated. The equations can then be written in a more compact form as follows:

$$u_d = r_d^{\text{“}} i_d + \frac{\sigma_d^{\text{“}} x_d}{\omega_n}\frac{di_d}{dt} - (1-k_{fD})\frac{\psi_D}{(1+\sigma_D)\omega_n T_D} + \frac{r_D}{(1+\sigma_D)^2} i_f + k_{fD}(u_f - r_f^{\text{‘}} i_f) - n\psi_q \tag{C.13}$$

$$u_f = r_f^{\text{“}} i_f + \frac{\sigma_f^{\text{“}} x_f}{\omega_n}\frac{di_f}{dt} - (1-k_{dD})\frac{\psi_D}{(1+\sigma_D)\omega_n T_D} + \frac{r_D}{(1+\sigma_D)^2} i_d + k_{dD}(u_d - r_d^{\text{‘}} i_d + n\psi_q) \tag{C.14}$$

Where the following constants are introduced:

$$\begin{aligned}
r_d^{\text{“}} &= r_s + (1-k_{fD})\frac{r_D}{(1+\sigma_D)^2} \\
r_f^{\text{“}} &= r_f + (1-k_{dD})\frac{r_D}{(1+\sigma_D)^2} \\
k_{fD} &= \frac{\sigma_D}{\sigma_f\left(1+\sigma_D+\frac{\sigma_D}{\sigma_f}\right)} \\
k_{dD} &= \frac{\sigma_D}{\sigma_d\left(1+\sigma_D+\frac{\sigma_D}{\sigma_d}\right)} \\
\sigma_d^{\text{“}} &= \sigma_{dD} - k_{fD}\frac{\sigma_D}{(1+\sigma_d)(1+\sigma_D)} \\
\sigma_f^{\text{“}} &= \sigma_{Df} - k_{dD}\frac{\sigma_D}{(1+\sigma_D)(1+\sigma_f)}
\end{aligned}$$

If the definitions of $r_f^{\text{‘}}$ and $r_d^{\text{‘}}$ are now inserted into eq. C.13 and eq. C.14, the following expressions are obtained:

$$u_d = r_d^{\text{“}} i_d + \frac{\sigma_d^{\text{“}} x_d}{\omega_n}\frac{di_d}{dt} - (1-k_{fD})\frac{\psi_D}{(1+\sigma_D)\omega_n T_D} + (1-k_{fD})\frac{r_D}{(1+\sigma_D)^2} i_f + k_{fD}(u_f - r_f i_f) - n\psi_q \tag{C.15}$$

$$u_q = r_q^{\text{‘}} i_q + \frac{\sigma_{qQ} x_q}{\omega_n}\frac{di_q}{dt} - \frac{\psi_Q}{\omega_n(1+\sigma_Q)T_Q} + n\psi_d \tag{C.16}$$

$$u_f = r_f^{\text{“}} i_f + \frac{\sigma_f^{\text{“}} x_f}{\omega_n}\frac{di_f}{dt} - (1-k_{dD})\frac{\psi_D}{(1+\sigma_D)\omega_n T_D} + (1-k_{dD})\frac{r_D}{(1+\sigma_D)^2} i_d + k_{dD}(u_d - r_s i_d + n\psi_q) \tag{C.17}$$

Finally, the expressions are simplified by introducing:

$$\psi_{Rd} = \frac{\psi_D}{1+\sigma_D} \tag{C.18}$$

$$\psi_{Rq} = \frac{\psi_Q}{1+\sigma_Q} \tag{C.19}$$

$$r_{Rd} = \frac{r_D}{(1+\sigma_D)^2} \tag{C.20}$$

$$r_{Rq} = \frac{r_Q}{(1+\sigma_Q)^2} \tag{C.21}$$

This gives decoupled first order differential equations for tuning the controllers, with additional feed forward terms for the output of the controllers.

$$u_d = r_d'' i_d + \frac{\sigma_d'' x_d}{\omega_n}\frac{di_d}{dt} - (1-k_{fD})\frac{\psi_{Rd}}{\omega_n T_D} + (1-k_{fD}) r_{Rd} i_f + k_{fD}(u_f - r_f i_f) - n\psi_q \tag{C.22}$$

$$u_q = r_q' i_q + \frac{\sigma_{qQ} x_q}{\omega_n}\frac{di_q}{dt} - \frac{\psi_{Rq}}{\omega_n T_Q} + n\psi_d \tag{C.23}$$

$$u_f = r_f'' i_f + \frac{\sigma_f'' x_f}{\omega_n}\frac{di_f}{dt} - (1-k_{dD})\frac{\psi_{Rd}}{\omega_n T_D} + (1-k_{dD}) r_{Rd} i_d + k_{dD}(u_d - r_s i_d + n\psi_q) \tag{C.24}$$

C.0.1 Simplifying the Notation

The expressions are simplified further by introducing

$$x_{Md} = \frac{x_{md}}{1+\sigma_D} \tag{C.25}$$

$$x_{Mq} = \frac{x_{mq}}{1+\sigma_Q} \tag{C.26}$$

By combining equation C.20 and C.21 with equation C.25 and C.26, it is evident that the time constants T_D and T_Q can be written as:

$$T_D = \frac{x_{Md}}{\omega_n r_{Rd}} \tag{C.27}$$

$$T_Q = \frac{x_{Mq}}{\omega_n r_{Rq}} \tag{C.28}$$

The voltage equations, C.22-C.24, are then simplified further, and the final expressions are obtained:

$$u_d = r_d^{\text{“}} i_d + \frac{\sigma_d^{\text{“}} x_d}{\omega_n}\frac{di_d}{dt} - (1-k_{fD})\frac{r_{Rd}}{x_{Md}}\psi_{Rd} + (1-k_{fD})r_{Rd}i_f + k_{fD}(u_f - r_f i_f) - n\psi_q \tag{C.29}$$

$$u_q = r_q^{\text{‘}} i_q + \frac{\sigma_{qQ} x_q}{\omega_n}\frac{di_q}{dt} - \frac{r_{Rq}}{x_{Mq}}\psi_{Rq} + n\psi_d \tag{C.30}$$

$$u_f = r_f^{\text{“}} i_f + \frac{\sigma_f^{\text{“}} x_f}{\omega_n}\frac{di_f}{dt} - (1-k_{dD})\frac{r_{Rd}}{x_{Md}}\psi_{Rd} + (1-k_{dD})r_{Rd}i_d + k_{dD}(u_d - r_s i_d + n\psi_q) \tag{C.31}$$

$$\frac{d\psi_{Rd}}{dt} = -\frac{\psi_{Rd}}{T_D} + \frac{x_{Md}}{T_D}(i_d + i_f) \tag{C.32}$$

$$\frac{d\psi_{Rq}}{dt} = \frac{-\psi_{Rq}}{T_Q} + \frac{x_{Mq}}{T_Q} i_q \tag{C.33}$$

$$\psi_d = x_d \sigma_{dD} i_d + \psi_{Rd} + x_{Md}\sigma_D i_f \tag{C.34}$$

$$\psi_q = \sigma_{qQ} x_q i_q + \psi_{Rq} \tag{C.35}$$

$$\psi_f = \sigma_{Df} x_f i_f + \psi_{Rd} + x_{Md}\sigma_D i_d \tag{C.36}$$

D Expression for the Pole Wheel Angle δ

In this section, the deviation of the pole wheel angle from [5, p 17-18] is repeated, including some steps that were left out by Bühler. In steady state, the stator voltage is expressed by equation D.1 and equation D.2.

$$u_d = r_s i_d - n\psi_q \tag{D.1}$$
$$u_q = r_s i_q + n\psi_d \tag{D.2}$$

From figure 2.2a in section 2.4, it is seen that the pole wheel angle, which is defined as positive for motor operation, is expressed by equation D.4. When the resistances are neglected, which can be done since they are usually small compared to the machine rating, equation D.5 is obtained.

$$tan(\delta) = -\frac{u_d}{u_q} \tag{D.3}$$
$$= \frac{n\psi_q - r_s i_d}{n\psi_d + r_s i_q} \tag{D.4}$$
$$\approx \frac{\psi_q}{\psi_d} \tag{D.5}$$

From the phasor diagram in figure 2.2a, the following relations are obvious:

$$i_d = -i_s sin(\delta) \tag{D.6}$$
$$i_q = i_s cos(\delta) \tag{D.7}$$

Combining equation D.6 and equation D.7 with the expressions for flux linkages, and then inserting it into equation D.5, expression D.8 and D.9 are obtained:

$$tan(\delta) = \frac{x_q i_q}{x_d i_d + x_{md} i_f} \tag{D.8}$$
$$= \frac{x_q i_s cos(\delta)}{x_{md} i_f - i_s x_d sin(\delta)} \tag{D.9}$$

By solving equation D.9 for $x_{md} i_f$, equation D.10 is obtained:

$$x_{md} i_f = \frac{x_q i_s cos^2(\delta)}{sin(\delta)} + x_d i_s sin(\delta) \tag{D.10}$$

The stator flux linkage is expressed by equation D.12:

$$\psi_s^2 = \psi_d^2 + \psi_q^2 \tag{D.11}$$
$$= (x_{md} i_f - i_s x_d sin(\delta))^2 + (x_q i_s cos(\delta))^2 \tag{D.12}$$

Inserting equation D.10 into D.12 yields equation D.13.

$$\psi_s^2 = x_q^2 i_s^2 cos^2(\delta)\left[1 + \frac{1}{tan^2(\delta)}\right] \tag{D.13}$$

Finally, the trigonometric relation D.14 is inserted into D.13, yielding the final expressions D.15 and D.16:

$$cos(\delta) = \frac{1}{\sqrt{1 + tan^2(\delta)}} \tag{D.14}$$

$$tan(\delta) = \frac{x_q \dot{i}_s}{\psi_s} \tag{D.15}$$

$$= \frac{\tau_e x_q}{\psi_s^2} \tag{D.16}$$

E Tuning Of the Controllers

In this appendix, the expressions obtained for tuning of the control structure from the specialisation project of Magnus Bolstad is presented [4]. In is emphasised that there is no information in this section that can not be found in the project thesis.

E.1 Field Current Control

The field current controller is tuned based on eq. C.31. Decoupling yields a first order transfer function describing the relationship between the field voltage and the field current:

$$u_f = \ddot{r_f} i_f + \frac{\ddot{\sigma_f} \ddot{x_f}}{\omega_n} \frac{di_f}{dt} \tag{E.1}$$

Including the PI controller, the open loop transfer function from field voltage to field current is expressed as:

$$h_0 = \frac{i_f}{i_{f_{ref}}} = h_r \frac{i_f}{u_f} = K_{p_f} \frac{1 + T_{i_f} s}{T_{i_f} s} \frac{1}{\ddot{r_f}\left[1 + \frac{\ddot{\sigma_f}\ddot{x_f}}{\omega_n \ddot{r_f}} s\right]} \frac{1}{1 + T_{sum} s} \tag{E.2}$$

By applying the technique of modulus optimum, taking intro account that the controllers are discrete, the following parameters are obtained:

$$\begin{aligned} T_{i_f} &= T_1 - \frac{T_{samp}}{2} \\ &= \frac{\ddot{\sigma_f} \ddot{x_f}}{\omega_n \ddot{r_f}} - \frac{T_{samp}}{2} \\ K_{p_f} &= \frac{T_1 - \frac{T_{samp}}{2}}{\frac{1}{\ddot{r_f}}(2T_{sum} + T_{samp})} \end{aligned}$$

The decoupling terms:

$$\begin{aligned} u_{f_{II}} &= -(1 - k_{dD}) \frac{\psi_D}{(1 + \sigma_D)\omega_n T_D} + (1 - k_{dD}) \frac{r_D}{(1 + \sigma_D)^2} i_d \\ &\quad + k_{dD}(u_d - r_s i_d + n\psi_q) \qquad \text{(E.3)} \\ &= -(1 - k_{dD}) \frac{r_{Rd}}{x_{Md}} \psi_{Rd} + (1 - k_{dD}) r_{Rd} i_d \\ &\quad + k_{dD}(u_d - r_s i_d + n\psi_q) \qquad \text{(E.4)} \end{aligned}$$

are used as a feed forward compensation to the output of the controller. The expressions are based on equation C.29 and C.30

E.2 Stator Current Controllers

Also the current controllers were tuned based on the method of modulus optimum.

E.2.1 d axis Current Controller

$$h_{0_d} = \frac{i_d}{i_{d_{ref}}} = h_r \frac{i_d}{u_d} = k_{p_d} \frac{1 + T_{i_d} s}{T_{i_d} s} \frac{1}{r_d^{\text{“}} \left[1 + \frac{\sigma_d^{\text{“}} x_d}{\omega_n r_d^{\text{“}}} s \right]} \frac{1}{1 + T_{sum} s} \tag{E.5}$$

which gives the following controller parameters:

$$T_{i_d} = \frac{\sigma_d^{\text{“}} x_d}{\omega_n r_d^{\text{“}}} - \frac{T_{samp}}{2} \tag{E.6}$$

$$K_{p_d} = \frac{\frac{\sigma_d^{\text{“}} x_d}{\omega_n r_d^{\text{“}}} - \frac{T_{samp}}{2}}{\frac{1}{r_d^{\text{“}}} (2T_{sum} + T_{samp})} \tag{E.7}$$

and the decoupling term used as a feed forward to the controller is:

$$\begin{aligned} u_{d_{II}} = &-(1 - k_{fD}) \frac{r_{Rd}}{x_{Md}} \psi_{Rd} \\ &+ (1 - k_{fD}) r_{Rd} i_f + k_{fD} (u_f - r_f i_f) - n \psi_q \end{aligned} \tag{E.8}$$

E.2.2 q axis Current Controller

$$h_{0_q} = \frac{i_q}{i_{q_{ref}}} = h_r \frac{i_q}{u_q} = k_{p_q} \frac{1 + T_{i_q} s}{T_{i_q} s} \frac{1}{r_q^{\text{‘}} \left[1 + \frac{\sigma_{qQ} x_q}{\omega_n r_q^{\text{‘}}} s \right]} \frac{1}{1 + T_{sum} s} \tag{E.9}$$

which gives the following controller parameters:

$$T_{i_q} = \frac{\sigma_{qQ} x_q}{\omega_n r_q^{\text{‘}}} - \frac{T_{samp}}{2} \tag{E.10}$$

$$K_{p_q} = \frac{\frac{\sigma_{qQ} x_q}{\omega_n r_q^{\text{‘}}} - \frac{T_{samp}}{2}}{\frac{1}{r_q^{\text{‘}}} (2T_{sum} + T_{samp})} \tag{E.11}$$

The decoupling term is:

$$u_{q_{II}} = -\frac{r_{Rq}}{x_{Mq}} \psi_{Rq} + n \psi_d \tag{E.12}$$

E.3 Flux Controller

The flux controller gives the reference to the field current controller. As the field current magnetises the machine along the d-axis only, the controller is tuned based on equation E.13 and E.14.

$$\frac{d\psi_{Rd}}{dt} = -\frac{\psi_{Rd}}{T_D} + \frac{x_{Md}}{T_D}(i_d + i_f) \tag{E.13}$$

$$\psi_d = x_d\sigma_{dD}i_d + \psi_{Rd} + x_{Md}\sigma_D i_f \tag{E.14}$$

All the terms except ψ_{Rd} in equation E.14 contains leakage coefficients, which are small in value, and hence the following approximation is justified:

$$\psi_d \approx \psi_{Rd} \tag{E.15}$$

Applying the Laplace transform, equation E.17 is obtained:

$$\frac{\psi_{Rd}}{i_f} = \frac{x_{Md}}{T_D(s + \frac{1}{T_D})} \tag{E.16}$$

$$= \frac{x_{Md}}{1 + T_D s} \tag{E.17}$$

The inner field current control loop by a first order model, where the equaivalent time constant is chosen as two times T_{sum}. This assures that the differnces between references and actual values of the field current becomes similar for the real model and for the simplified first order model [22, p 114]. When the actual flux used as feedback is filtered through a first order filter, the open loop transfer function in equation E.19 is obtained for the flux controller:

$$\frac{\psi_s}{\psi_{s_{ref}}} = \frac{x_{Md}}{1 + T_D s}\frac{1}{1 + T_{eq}s}K_{p_{\psi_s}}\frac{1 + T_{i_{\psi_s}}}{T_{i_{\psi_s}}}\frac{1}{1 + T_f s} \tag{E.18}$$

$$\approx \frac{x_{Md}}{1 + T_D s}\frac{1}{1 + (T_{eq} + T_f)s}K_{p_{\psi_s}}\frac{1 + T_{i_{\psi_s}}}{T_{i_{\psi_s}}} \tag{E.19}$$

Using the method of modulus optimum, the controller parameters in E.20 and E.21 are obtained:

$$T_{i_{\psi_s}} = T_D - \frac{T_{samp}}{2} \tag{E.20}$$

$$K_{p_{\psi_s}} = \frac{T_D - \frac{T_{samp}}{2}}{x_{Md}(2(T_{eq} + T_f) + T_{samp})} \tag{E.21}$$

The time constant from E.20 was used, while the gain had to be reduced to obtain a bandwidth at least one decade lower than the bandwidth of the inner field current control loop. The tuning of the gain was performed by trial and error. It was observed that is the gain was set too high, the field current reference started to oscillate, and hence the field current, the flux and the stator currents started oscillating. A low gain was finally chosen, and the first order filter at the feedback to the flux controller was not used, as it turned out to be redundant.

E.4 Speed Controller

In the project thesis, a speed controller was implemented and tuned. This was realised by a PI controller with a speed reference as input and the torque reference as output. The tuning was performed by the technique of symmetrical optimum, by making the inner speed control loop half a decade slower than the outer armature current control loop, and by obtaining a satisfying phase margin of 38.4 °. Bode plots were used for this purpose. However, as all simulations performed in this master thesis is performed with a torque reference as input, more details of this tuning is not presented in this appendix.

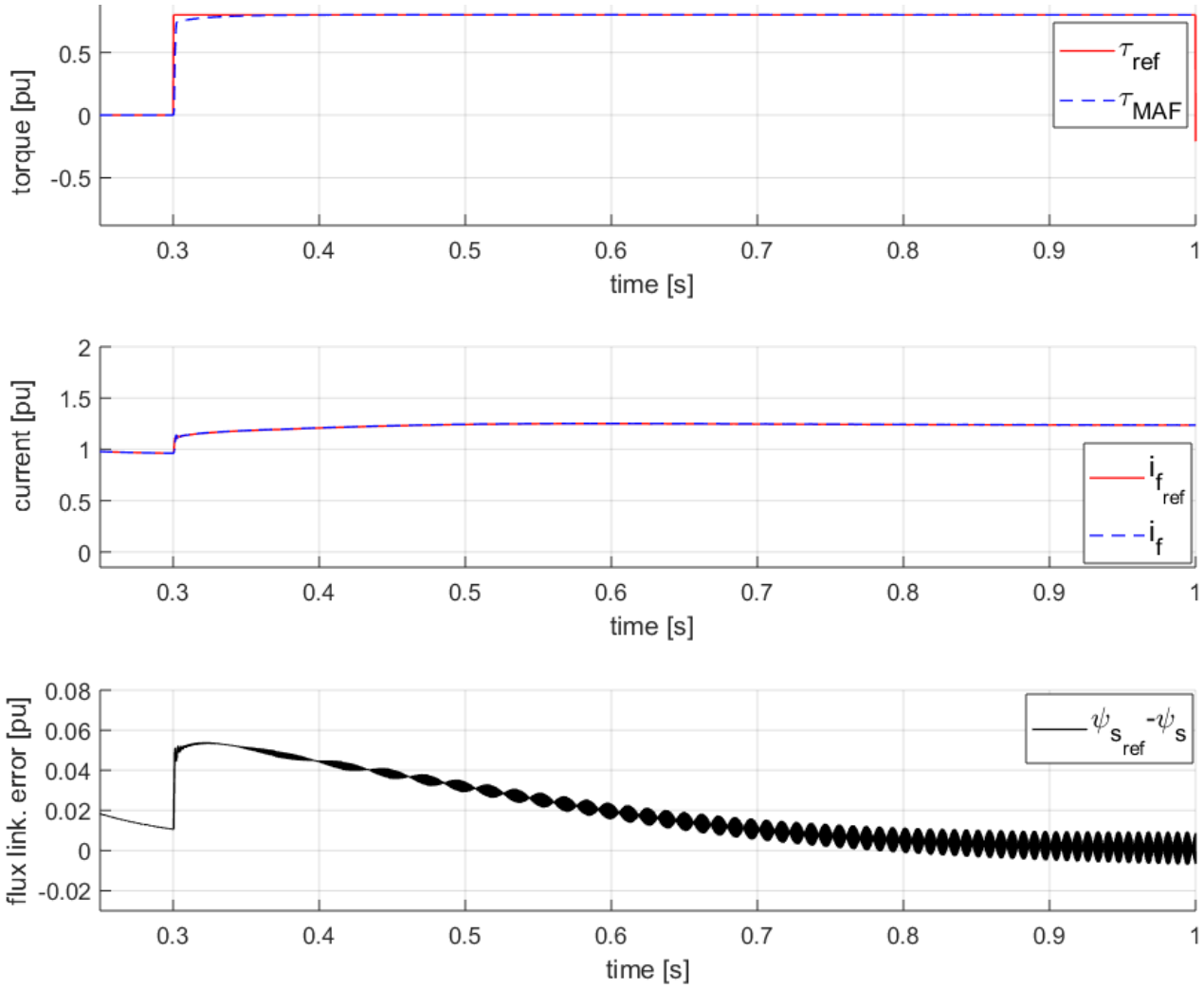

Figure E.1: Illustration of how the stator flux linkage uses some time to reach its reference entirely

F Temperature Dependence of Resistance

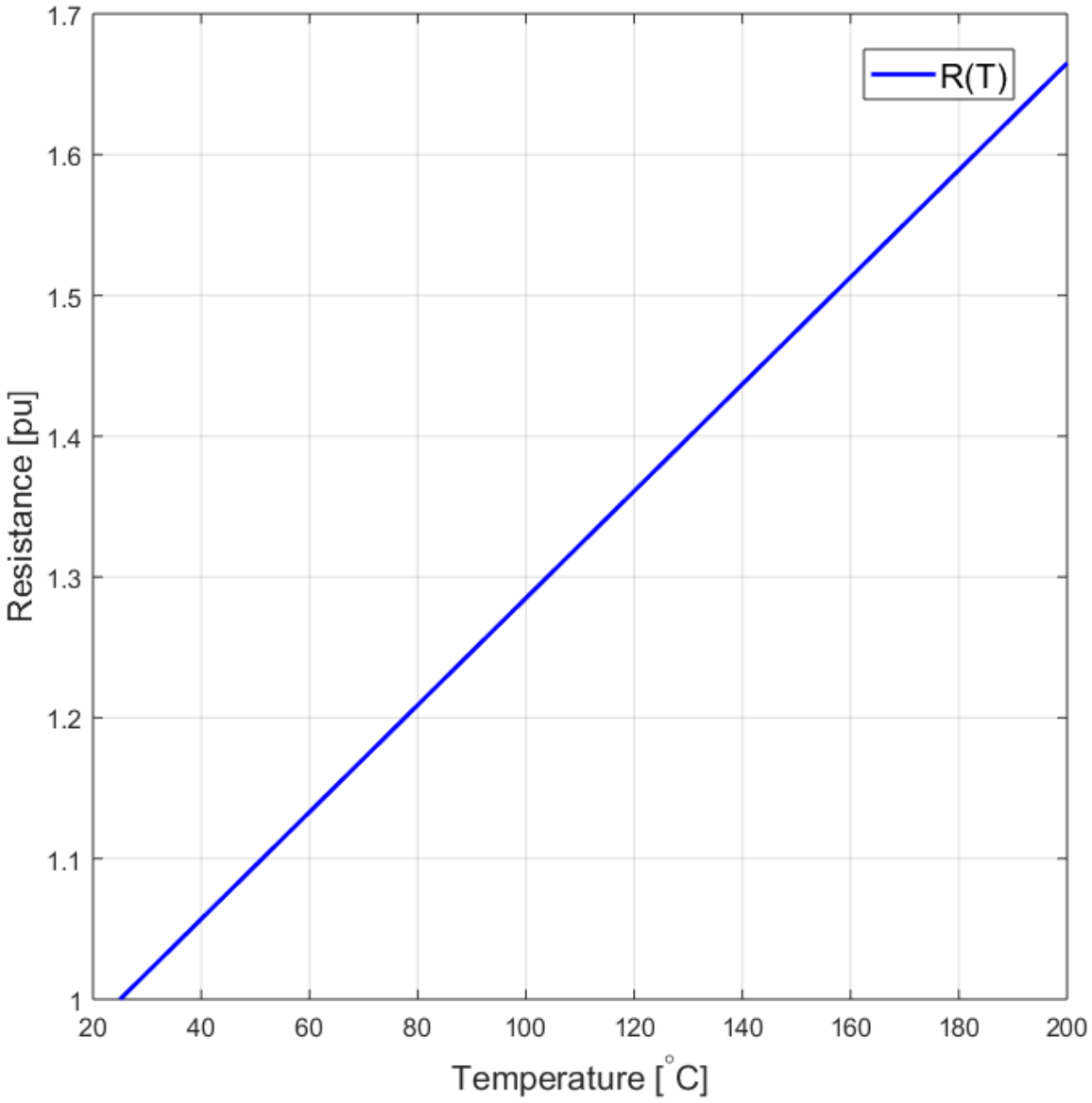

Figure F.1: The copper resistance for different temperatures

G Expression for Estimated Position, $\hat{\theta}$

In this section, the derivation of expression 3.2, obtained in the specialisation project of Magnus Bolstad is presented [4]. It is also discussed why equation 3.3 is not valid during dynamics.

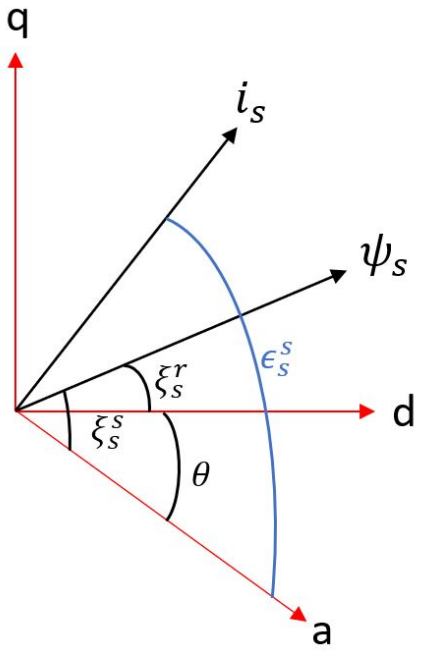

Figure G.1: Stator current and stator flux linkage related to the different coordinate systems

G.1 Equation 3.3 Derived

From figure 3.2, which is repeated in figure G.1 for convenience, it is found that:

$$i_q = i_s cos(90° - \epsilon_s^s + \theta) = i_s sin(\epsilon_s^s - \theta) \tag{G.1}$$

$$sin(\xi_s^r) = \frac{\psi_q}{\psi_s} = \frac{\sigma_{qQ} x_q i_q + \psi_{Rq}}{\psi_s} \tag{G.2}$$

Utilising equation 2.39, equation G.2 can be expressed as:

$$sin(\xi_s^r) = \frac{\sigma_{qQ} x_q i_q + \frac{x_{Mq}}{1+T_{Q}s} i_q}{\psi_s} \tag{G.3}$$

Inserting G.1 into G.3, the following expression is obtained:

$$sin(\xi_s^r) = \frac{\left[\sigma_{qQ} x_q + \frac{x_{Mq}}{1+T_{Q}s}\right]}{\psi_s} i_s sin(\epsilon_s^s - \theta) \tag{G.4}$$

From figure G.1:

$$\xi_s^r = \xi_s^s - \theta \tag{G.5}$$

This gives:

$$sin(\xi_s^s - \theta) = \frac{\left[\sigma_{qQ} x_q + \frac{x_{Mq}}{1+T_Q s}\right]}{\psi_s} i_s sin(\epsilon_s^s - \theta) \tag{G.6}$$

The transfer function is discretised by the Tustin's method, as in equation G.7.

$$\begin{aligned} \frac{x_{Mq}}{1+T_Q s} &\approx \frac{x_{Mq}}{1+T_Q\left[\frac{2}{T_{samp}}\frac{z-1}{z+1}\right]} \\ &= \frac{(z+1)x_{Mq}}{(1+\frac{2T_Q}{T_{samp}})z + (1-\frac{2T_Q}{T_{samp}})} \end{aligned} \tag{G.7}$$

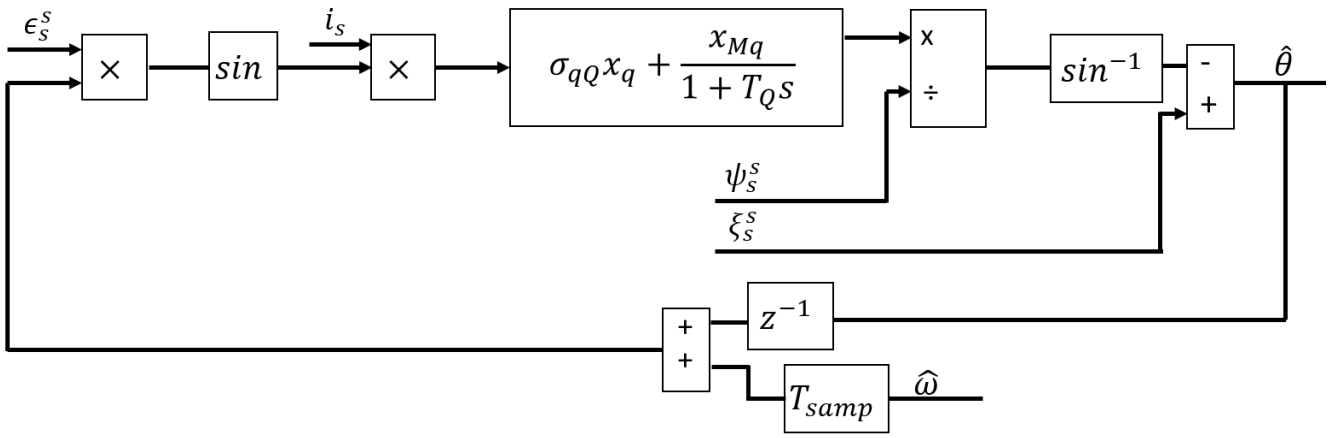

Figure G.2: Block diagram illustrating the algorithm for estimating the rotor position by equation G.6

G.2 Manipulating to Explicit Expression

In the project thesis [4], equation G.6 was manipulated further to an explicit equation by using the trigonometric identity:

$$sin(a-b) = sin(a)cos(b) - cos(a)sin(b) \tag{G.8}$$

The following expression is obtained:

$$
\begin{aligned}
&sin(\xi_s^s)cos(\theta) - cos(\xi_s^s)sin(\theta) \\
&= \frac{\left[\sigma_{qQ}x_q + \frac{x_{Mq}}{1+T_Q s}\right]}{\psi_s} i_s \Big[sin(\epsilon_s^s)cos(\theta) - cos(\epsilon_s^s)sin(\theta)\Big]
\end{aligned} \tag{G.9}
$$

taking common terms of $sin(\theta)$ and $cos(\theta)$ outside the parenthesis gives:

$$
\begin{aligned}
&cos(\theta)\Big[sin(\xi_s^s) - \frac{\left[\sigma_{qQ}x_q + \frac{x_{Mq}}{1+T_Q s}\right]}{\psi_s} i_s sin(\epsilon_s^s)\Big] \\
&= sin(\theta)\Big[cos(\xi_s^s) - \frac{\left[\sigma_{qQ}x_q + \frac{x_{Mq}}{1+T_Q s}\right]}{\psi_s} i_s cos(\epsilon_s^s)\Big]
\end{aligned} \tag{G.10}
$$

Finally equation 3.3 is obtained:

$$
\begin{aligned}
tan(\theta) &= \frac{sin(\theta)}{cos(\theta)} \\
&= \frac{sin(\xi_s^s) - \frac{\left[\sigma_{qQ}x_q + \frac{x_{Mq}}{1+T_Q s}\right]}{\psi_s} i_s sin(\epsilon_s^s)}{cos(\xi_s^s) - \frac{\left[\sigma_{qQ}x_q + \frac{x_{Mq}}{1+T_Q s}\right]}{\psi_s} i_s cos(\epsilon_s^s)}
\end{aligned} \tag{G.11}
$$

Equation G.11 yielded accurate results during steady state, but not during dynamics. The reason for this is that equation G.6 contains a transfer function that $i_s sin(\epsilon_s^s - \theta)$, which estimates i_q, is filtered through to obtain an estimate for ψ_{Rq}. When the common terms are extracted outside the parenthesis and transformed to a tangent expression, a new expression that is not equal to i_q is filtered through the transfer function. Hence another and incorrect dynamic behaviours is described. The math would be valid if the transfer function in equation G.6 was a scalar, where to order of the products is insignificant. During steady state, the transfer function $\frac{x_{Mq}}{1+T_Q s}$ reduces to the scalar x_{Mq}. Thus equation G.11 is valid during steady state operation, and during steady state analysis. The simulations with the two expressions are compared in figure G.3, where it is evident that expression G.11 results in errors in the range of 20 ° in the estimated position, and 0.3 pu in the estimated speed. Such errors for such a long time interval is not satisfying.

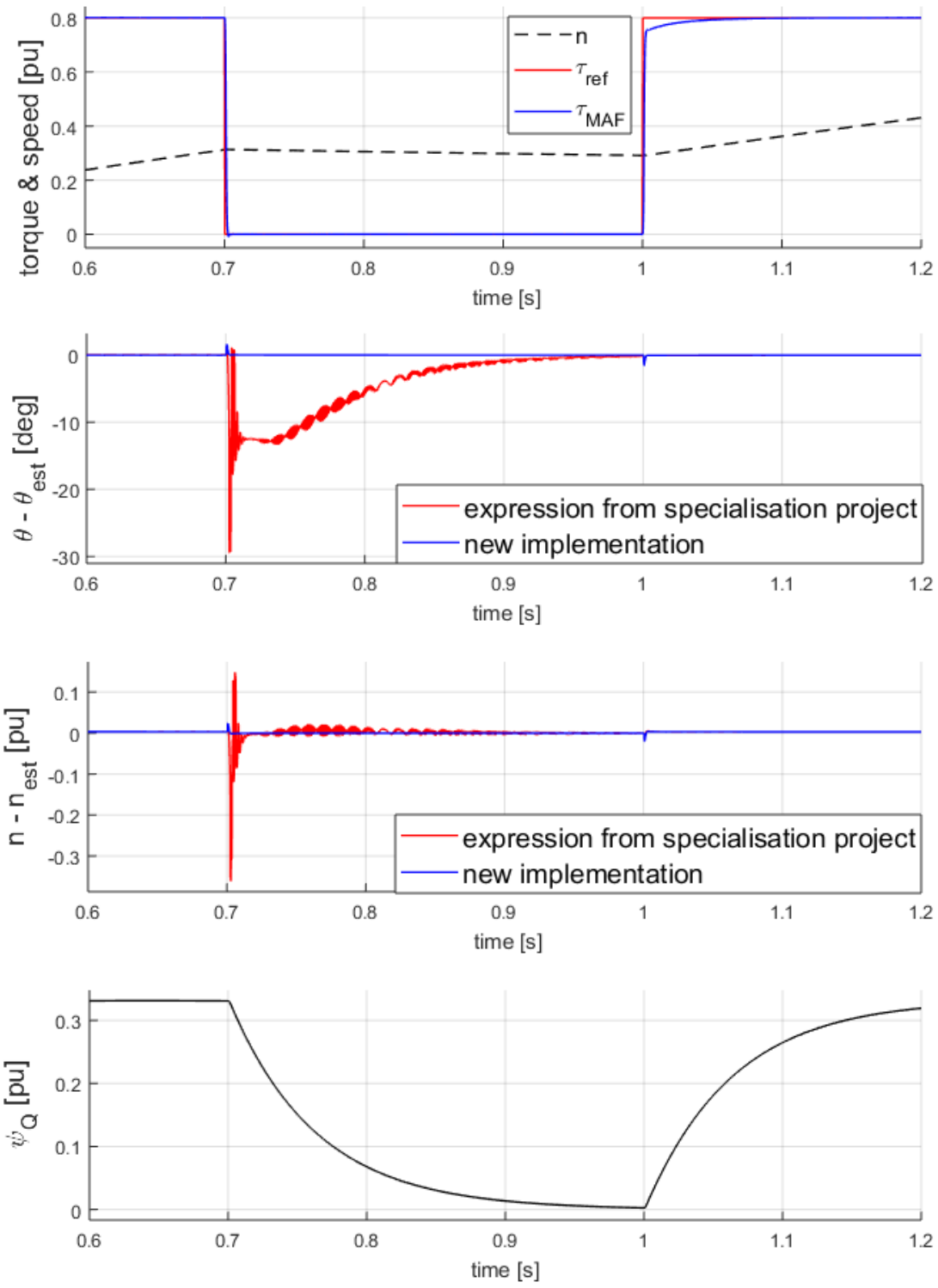

Figure G.3: Comparing the implementation of G.6 (blue) and G.11 (red)

H Steady State Sensitivity Analysis Plot

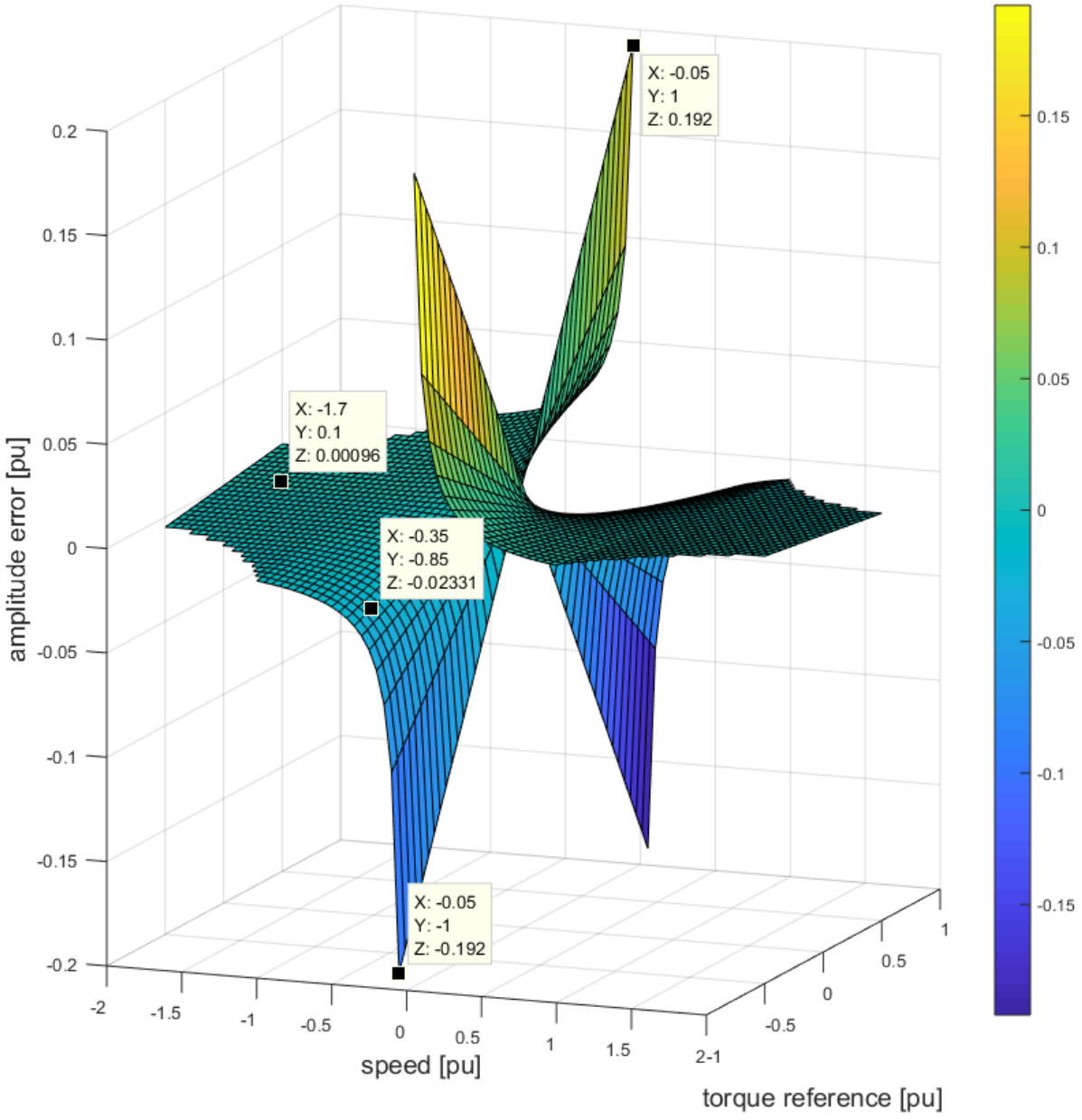

Figure H.1: $\hat{r}_s = 0.8 r_s$

I Drifting for Different Stator Resistances

In figure I.1 it is illustrated how the stator flux linkage estimated by the voltage model drifts for different estimates of the stator resistance. The actual stator flux linkage and the measured angle is used as input to the control system. The estimated stator resistance is constant throughout the whole simulation, and the same torque reference is applied in all the scenarios. The impact of the erroneously estimated stator resistance on the PI controllers is neglected, and hence the speed is the same at the instant of drifting for all the scenarios. In all the scenarios the actual flux linkage is given by the origin centred, dashed red circle, corresponding to the flux linkage estimate when $\hat{r}_s = r_s$.

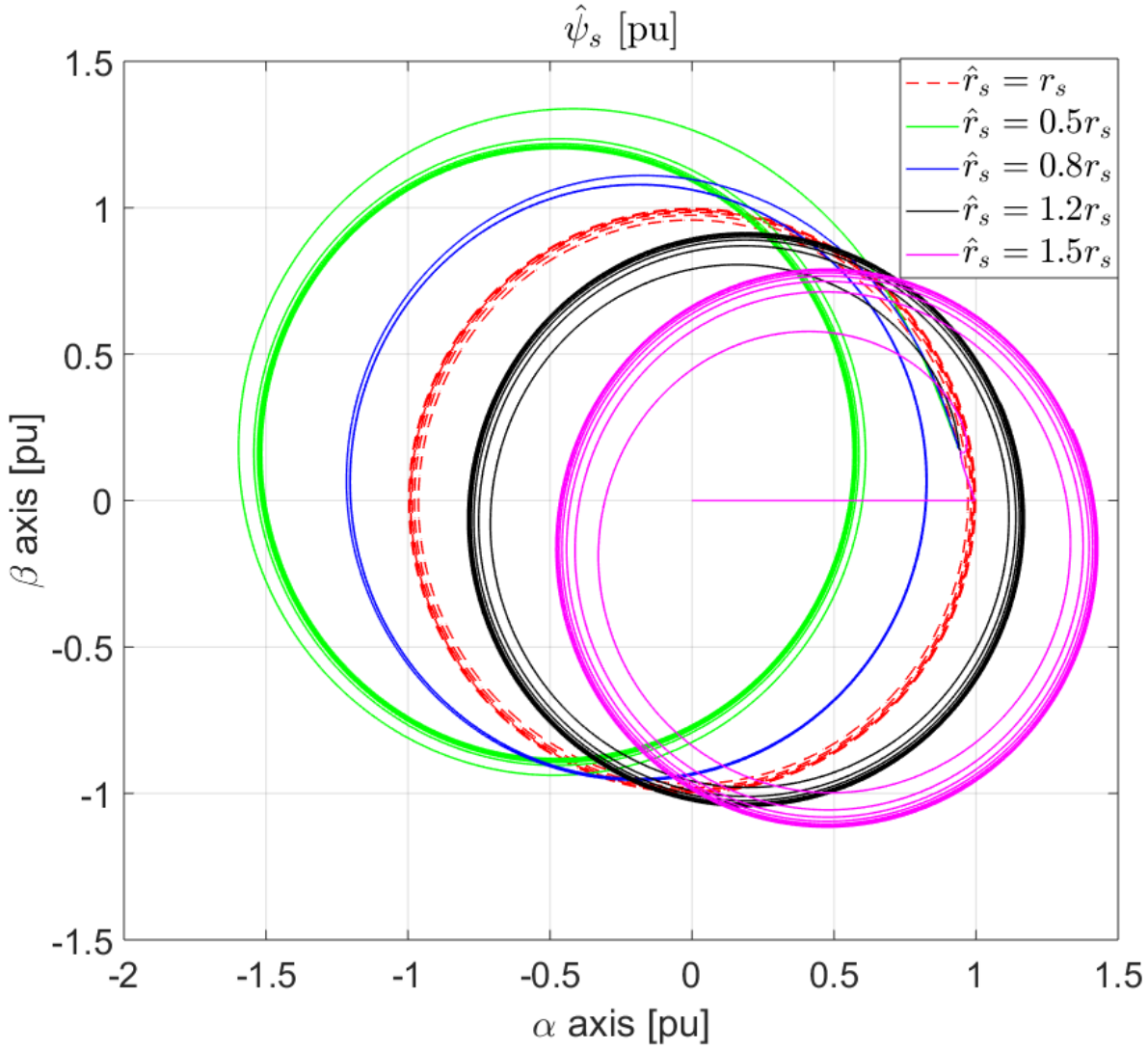

Figure I.1: Drifting when the stator resistance is overestimated and underestimated by 20 % and 50 % during step in the torque reference

J Sensorless Operation Without Correction

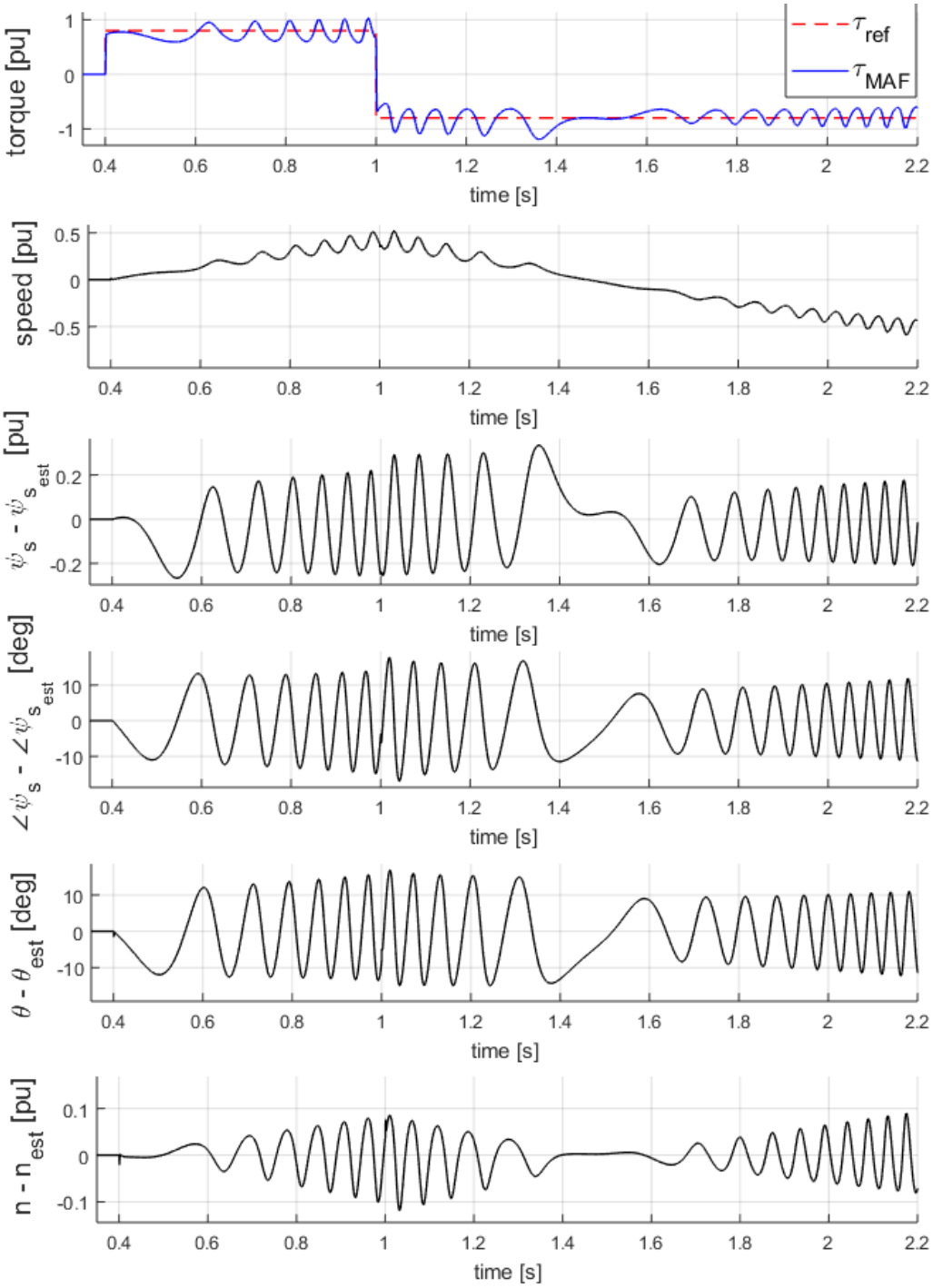

Figure J.1: Sensorless operation without correction, $\hat{r}_s = 0.8 r_s$

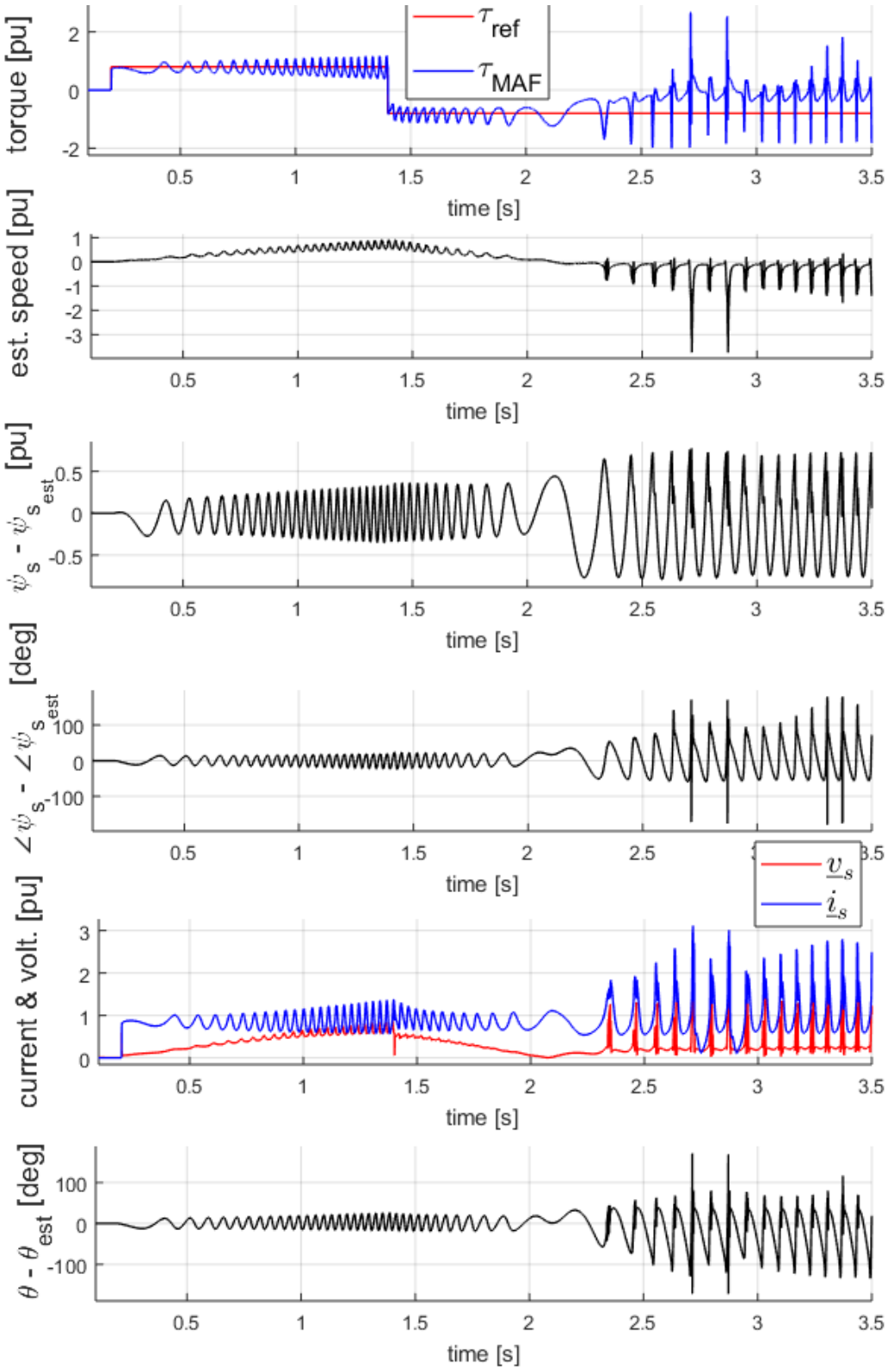

Figure J.2: Figure 6.1a in larger scale, $\hat{r}_s = 0.8r_s$

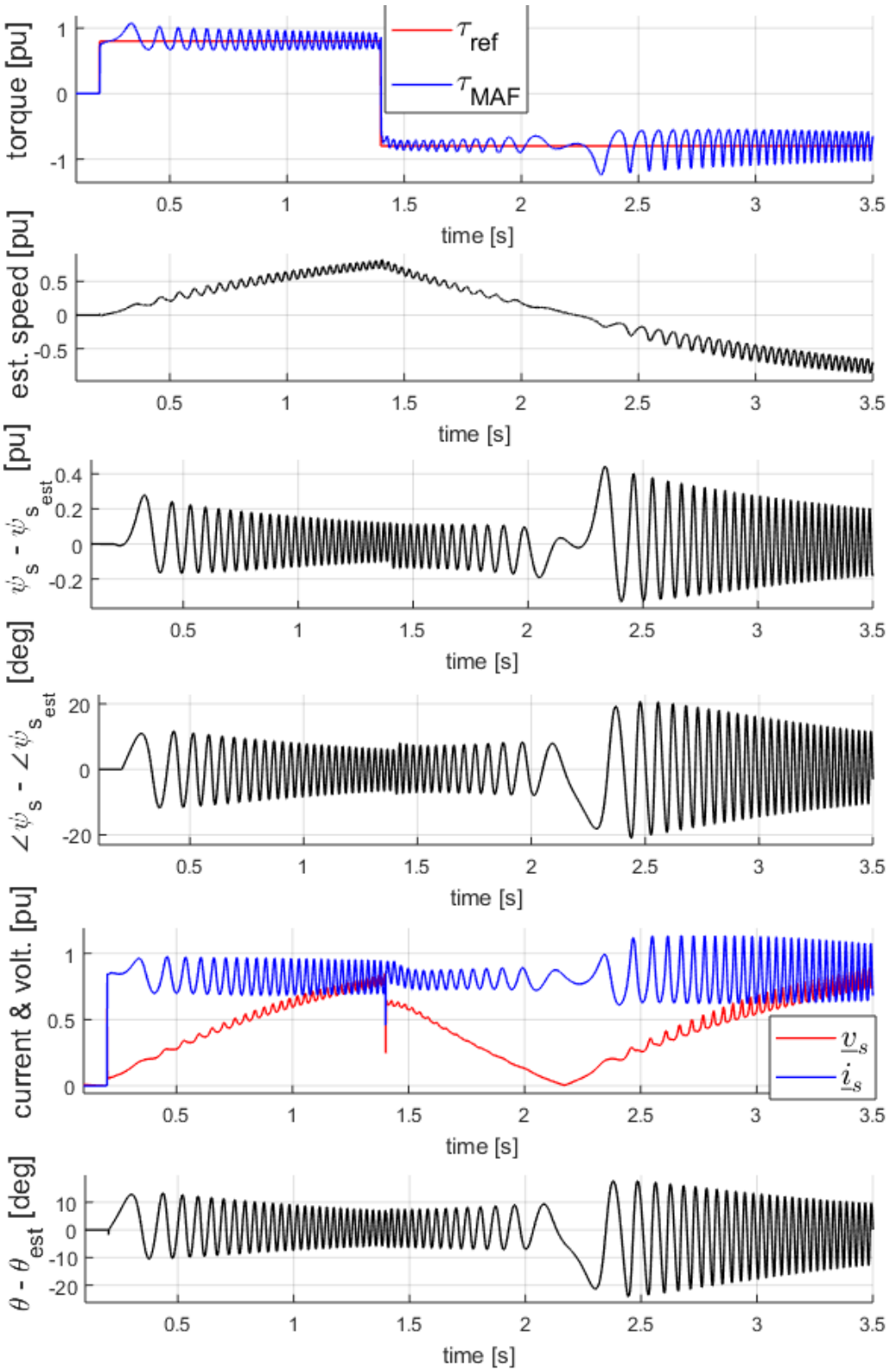

Figure J.3: Figure 6.1b in larger scale, $\hat{r}_s = 1.2r_s$

K Changing k_2

The same sensitivity analysis of k_2, as was performed for k_{T_0} in section 6.2.2.

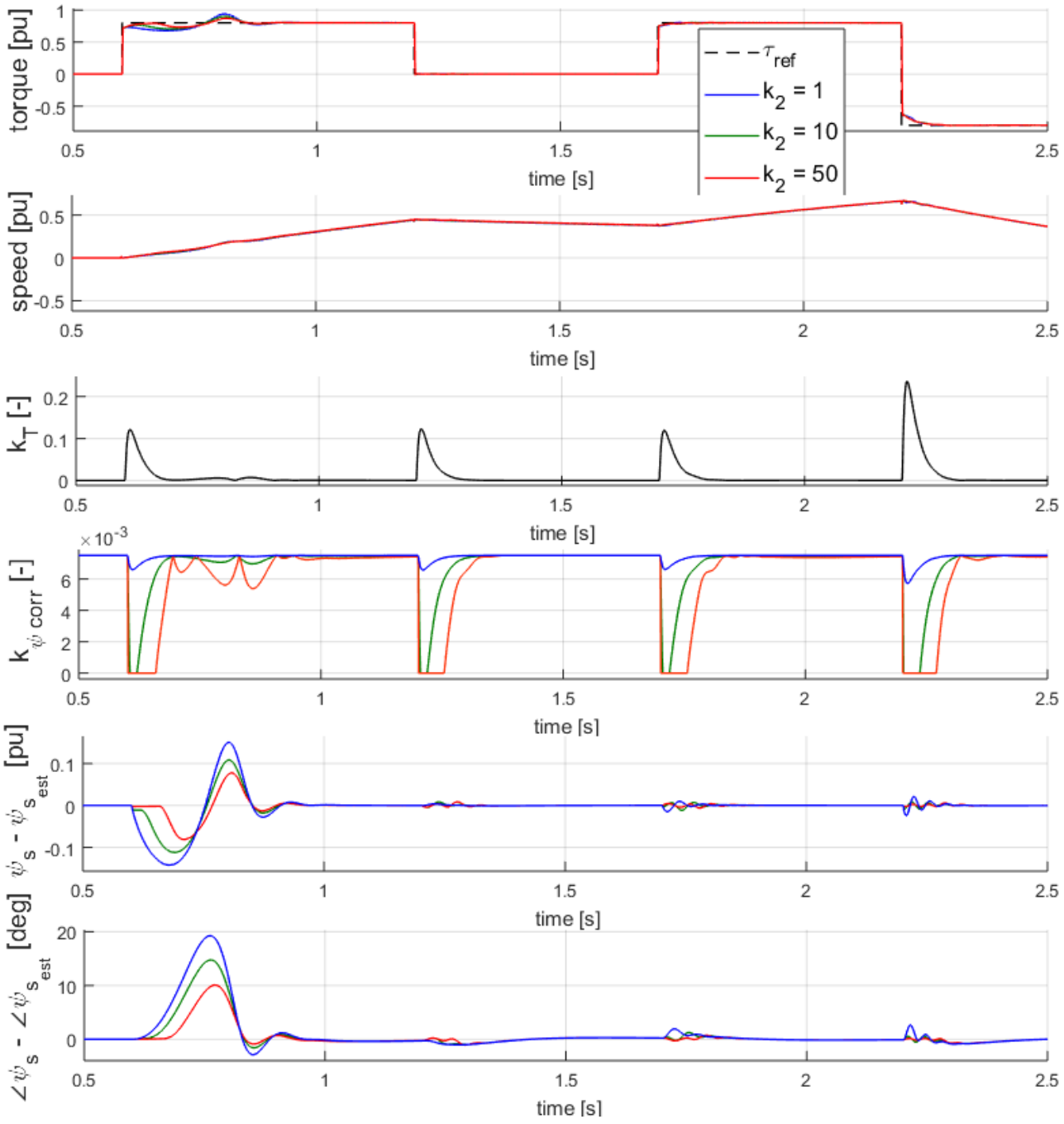

Figure K.1: Changing the constant k_2, perfectly estimated parameters

L Too High Torque Through Zero Speed

Driving through zero speed with a torque reference of 0.6 pu, and a constant load of 0.8 pu. It is evident how the dq currents supplied are displaced as the estimated rotor position exceeds 180 °. This is due to erroneous estimated stator resistance, as the voltage model is very sensitive to this parameter at low speeds and high torques. The generated torque exceeds 4 pu, which is unphysical.

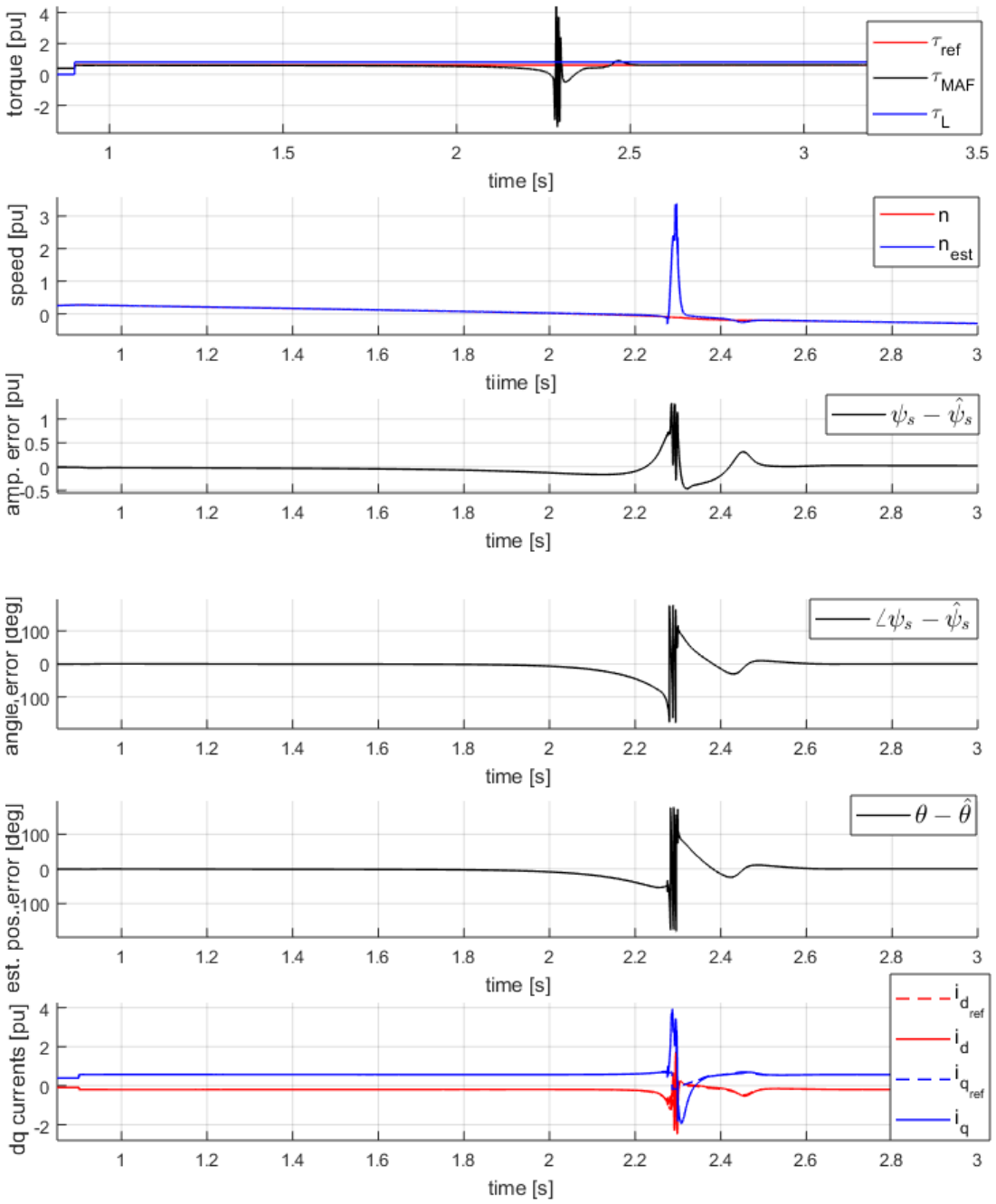

Figure L.1: $\tau_{ref} = 0.6$ pu while driving through zero speed, $\hat{r}_s = 0.8 r_s$

M Erroneously Estimated d axis Inductance

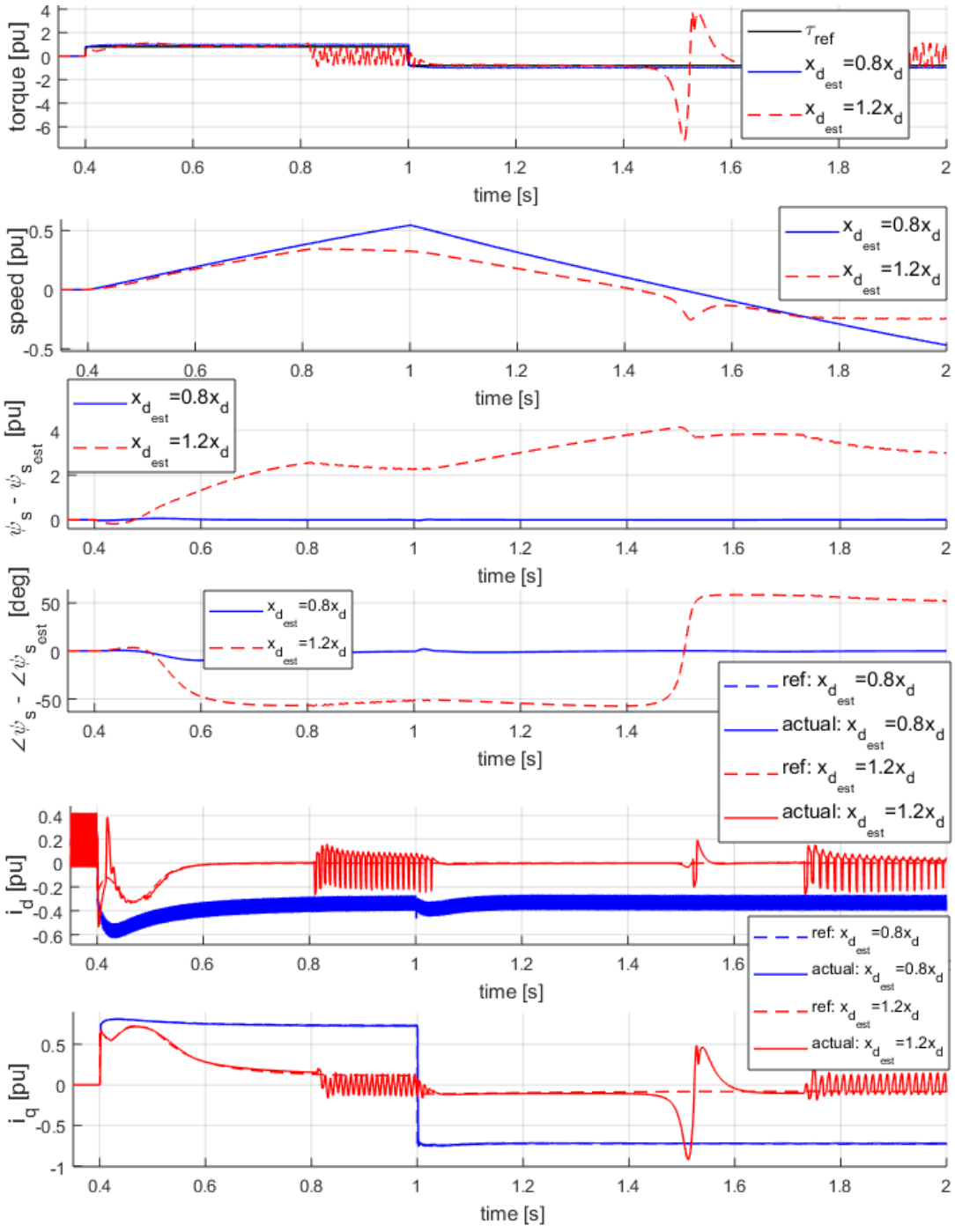

Figure M.1: Sensorless operation when the d axis inductance is overestimated and underestimated by 20 %

N Combining the Voltage Model and the Current Model

Sensorless operation with the difference between the current model and the voltage model as a compensating feedback with unity gain to the voltage model. The stator resistance is underestimated by 20 %, all other parameters are correctly estimated.

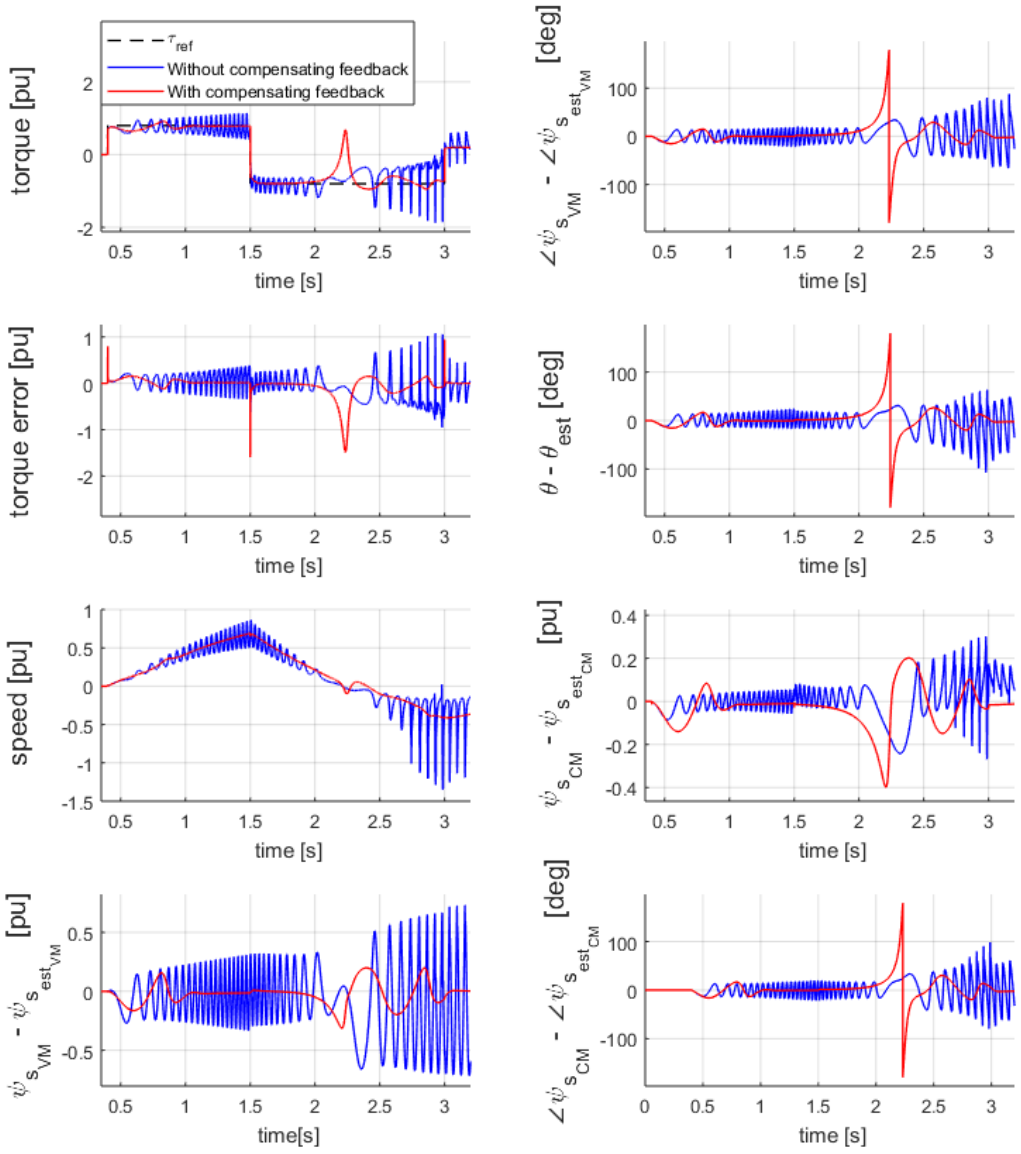

Figure N.1: Combining the voltage model and the current model

O Tuning of PLL

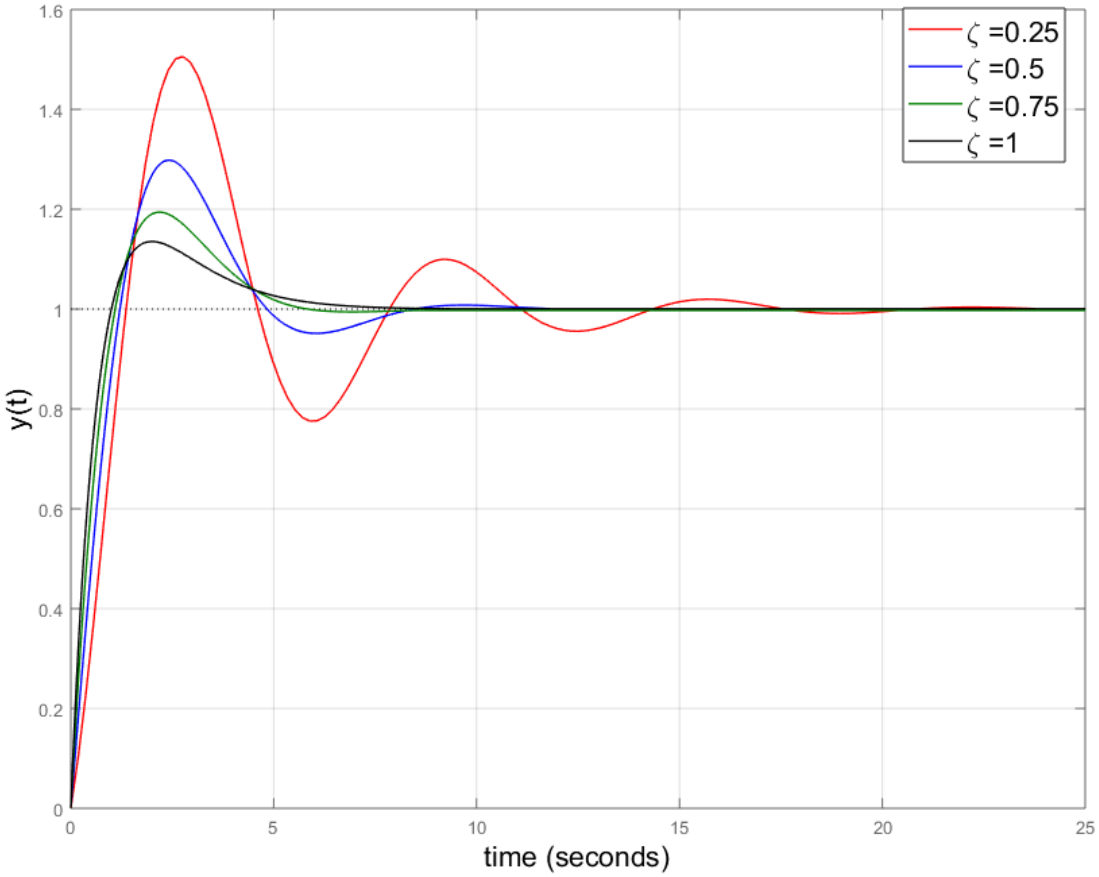

Figure O.1: Scaled step response of the PLL loop for different relative damping ratios, ζ

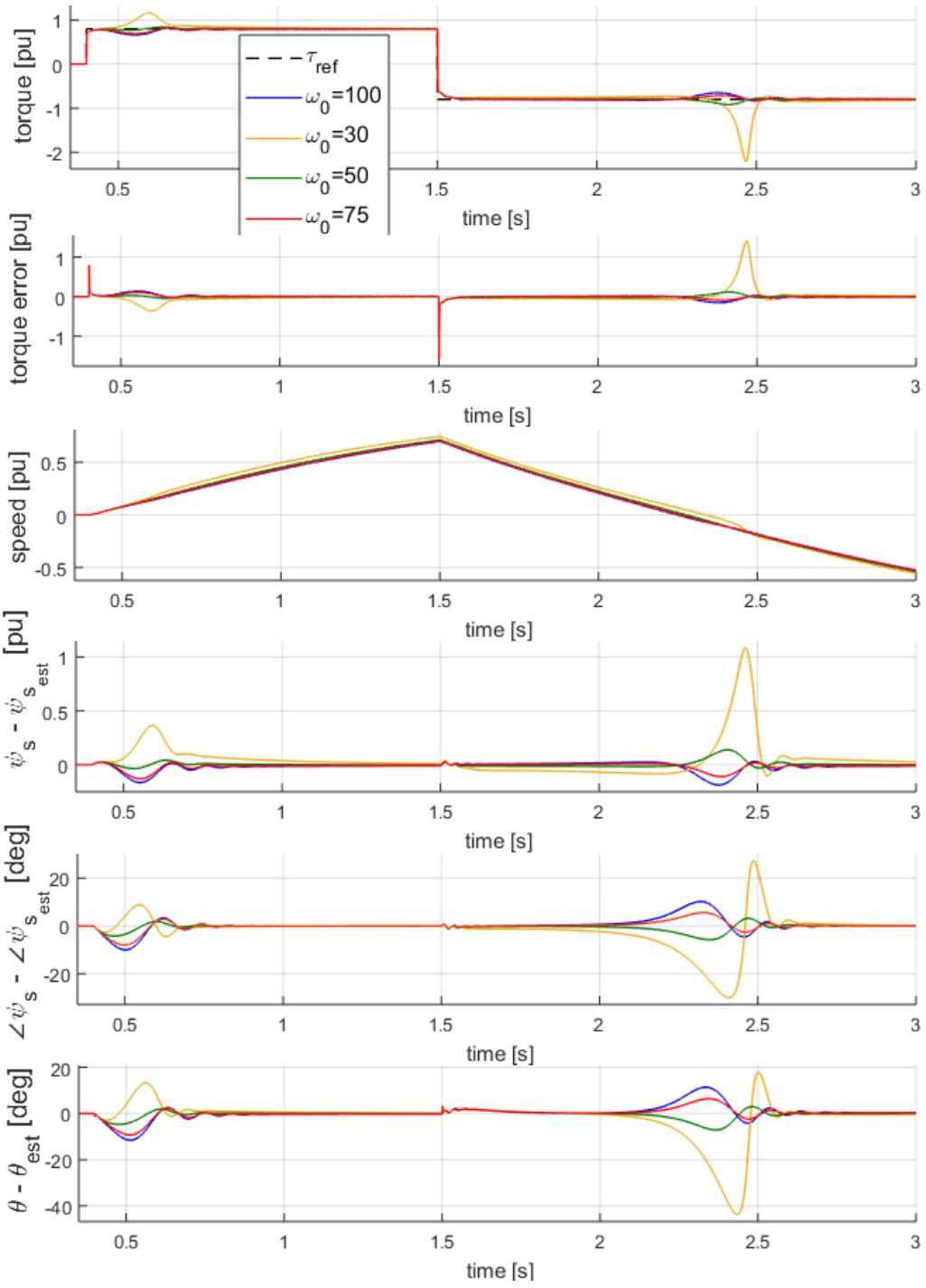

Figure O.2: Changing the undamped resonance frequency with a relative damping of 0.8

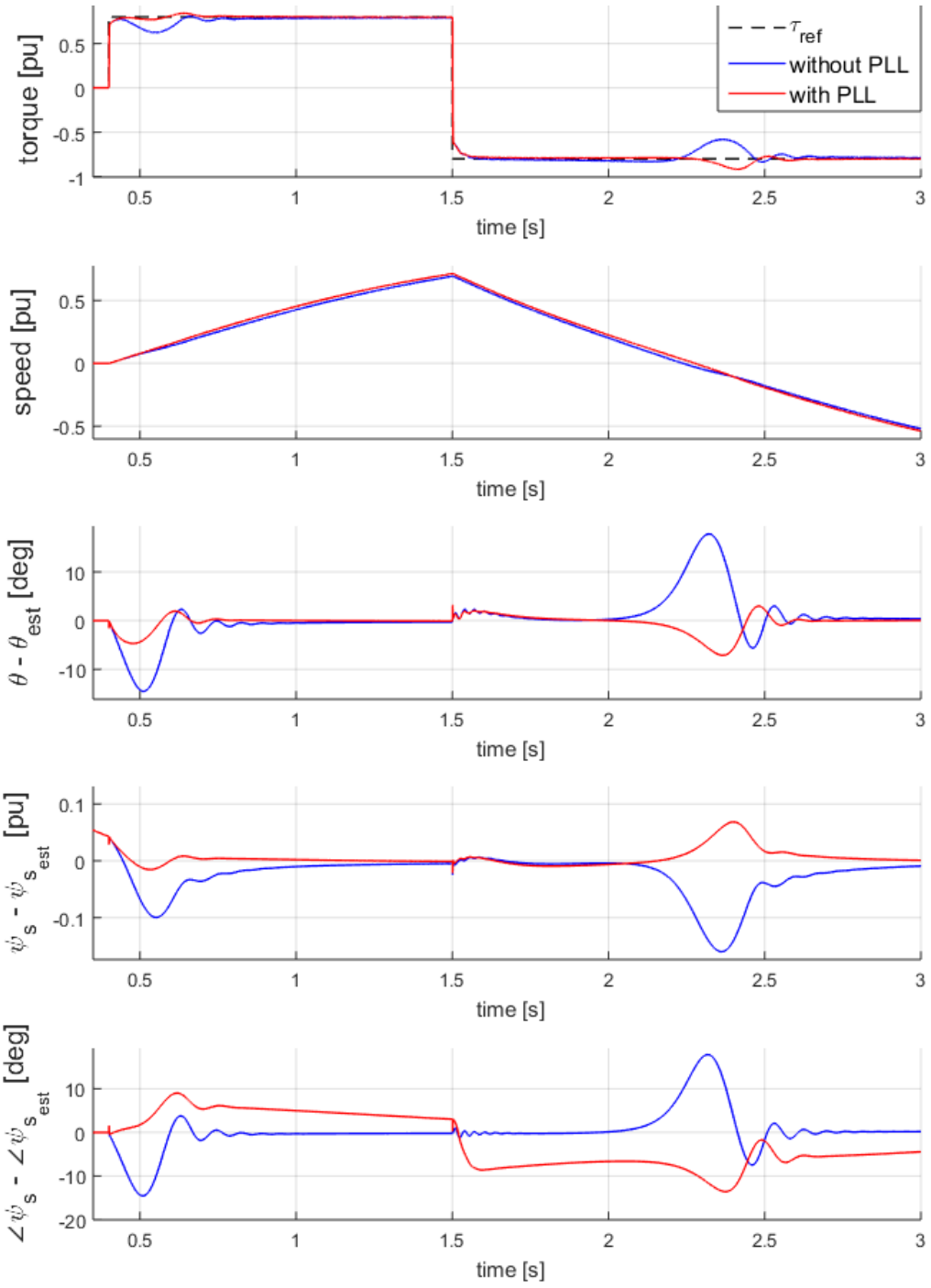

Figure O.3: Stator flux linkage estimated by the current model with and without PLL

P Steady State Analysis Matlab Code

P.1 Voltage Model

```
clc
clear all
%Defining parameters:
sigma_qQ = 0.3979;
x_q = 0.57;
xMq = 0.3432;
x_d = 1.17;
x_ad = 1.05;
r_s=0.048;

%Performing calculations for torque references between -1 pu and 1 pu,
%and for speeds between -2 pu and 2 pu:
t=[-1:0.05:1];
n_vec=[-2:0.05:2];
[N,T]=meshgrid(n_vec,t);
for k=1:length(t)
    for l=1:length(n_vec)
tau_e =t(k);
n = n_vec(l);

%Field weakening for speeds above 1 pu:
if (abs(n_vec(l))<1) || (abs(n_vec(l))==1)
        psi_s_amp = 1;
else
        psi_s_amp =1/abs(n);
end

%Assumimng that unity power factor control is obtained:
i_s_amp =abs(tau_e)/psi_s_amp;
i_s = i_s_amp*exp(j*(pi/2)*sign(tau_e));
psi_s = psi_s_amp*exp(j*0);

%Determine estiamted stator resistance:
r_s_est=1.2*r_s;

%Placing the stator voltage 90 degree ahead of the stator flux linkage
    :
v_s = r_s*i_s + j*n*psi_s;
psi_s_est = (v_s- r_s_est*i_s)/(n*j);
psi_s_est_amp = abs(psi_s_est);

```

```
41 %Looking at the instant where the stator flux linkage is aligned with
       the
42 %stator phase a-axis. The stator flux linkage is assumed 90 degrees
       ahead
43 %of the curent:
44 xi_s_s =0;
45 epsilon_s_s=(pi/2)*sign(tau_e);
46
47 %Alternative way of calculating the angle theta, which is not used:
48 %angleExpression =@(theta) sin(xi_s_s-theta)-((sigma_qQ*x_q+xMq)/
       psi_s_amp)*i_s_amp*sin(epsilon_s_s-theta);
49 %theAngleAlt = fzero(angleExpression,0.0001);
50
51 %The calculting theta:
52 theta_real = atan2((sin(xi_s_s)-((sigma_qQ*x_q+xMq)/psi_s_amp)*i_s_amp
       *sin(epsilon_s_s)),((cos(xi_s_s)-((sigma_qQ*x_q+xMq)/psi_s_amp)*
       i_s_amp*cos(epsilon_s_s))));
53 theta_est = atan2((sin(xi_s_s)-((sigma_qQ*x_q+xMq)/psi_s_est_amp)*
       i_s_amp*sin(epsilon_s_s)),((cos(xi_s_s)-((sigma_qQ*x_q+xMq)/
       psi_s_est_amp)*i_s_amp*cos(epsilon_s_s))));
54
55 %Transforming stator current and stator flux linkages to dq system
56 i_sd = real(i_s)*cos(theta_real)+imag(i_s)*sin(theta_real);
57 i_sq = -real(i_s)*sin(theta_real)+imag(i_s)*cos(theta_real);
58
59 i_sd_est = real(i_s)*cos(theta_est)+imag(i_s)*sin(theta_est);
60 i_sq_est = -real(i_s)*sin(theta_est)+imag(i_s)*cos(theta_est);
61
62 psi_d = real(psi_s)*cos(theta_real)+imag(psi_s)*sin(theta_real);
63 psi_q = -real(psi_s)*sin(theta_real)+imag(psi_s)*cos(theta_real);
64
65 psi_d_est = real(psi_s_est)*cos(theta_est)+imag(psi_s_est)*sin(
       theta_est);
66 psi_q_est = -real(psi_s_est)*sin(theta_est)+imag(psi_s_est)*cos(
       theta_est);
67
68 %Findig the error in the estimated stator flux linkage amplitude,
69 %in the estimated torque, and in the estimated
70 %rotor position:
71 psi_s_amplitude_error = real(psi_s-psi_s_est);
72 theta_error = (theta_real-theta_est)*180/pi;
73
74 %Error in Torque = Torque_{ref}-Torque_{WithEstimatedValues}
75 torque_error = (psi_d*i_sq-psi_q*i_sd)-(psi_d_est*i_sq_est-psi_q_est*
       i_sd_est);
```

```
76
77 %Avoiding plotting the error in estimated rotor
78 %position at n=0. Comment out this if statement to include the error
      in
79 %estimated rotor position:
80 if n==0;
81     theta_error=0/0;
82 end
83
84 TorqueError(k,l) = torque_error;
85 AmplitudeError(k,l) = psi_s_amplitude_error;
86 ThetaError(k,l) = theta_error;
87
88 %Removing the points from the graph where operation is not possible
      due to
89 %stator current limitation of 1 pu:
90 if ((abs(tau_e)>1/abs(n)) && abs(n)>1)
91     TorqueError(k,l)=0/0;
92     AmplitudeError(k,l) =0/0;
93     ThetaError(k,l) = 0/0;
94 end
95
96     end
97 end
98
99 figure(1)
100 surf(N,T,TorqueError)
101 xlabel('speed [pu]')
102 ylabel('torque reference [pu]')
103 zlabel('torque error [pu]')
104
105 figure(2)
106 surf(N,T,AmplitudeError)
107 xlabel('speed [pu]')
108 ylabel('torque reference [pu]')
109 zlabel('amplitude error [pu]')
110
111 figure(3)
112 surf(N,T,ThetaError)
113 xlabel('speed [pu]')
114 ylabel('torque reference [pu]')
115 zlabel('\theta error [deg]')
```

P.2 Current Model

```
clc
clear all
%Defining the actual motor parameters
x_d = 1.17;
x_q = 0.57;
xs_sigma = 0.12;
x_md = x_d-xs_sigma;
x_mq = x_q -xs_sigma;

%Defining the estimated motor parameters
x_d_est = 0.8*x_d;
x_q_est = 0.8*x_q;
xs_sigma_est = xs_sigma;
x_md_est = x_d_est-xs_sigma_est;
x_mq_est = x_q_est -xs_sigma_est;

%Performing calculations for torque references between -1 pu and 1 pu,
%and for speeds between -2 pu and 2 pu:
t=[-1:0.05:1];
n_vec=[-2:0.05:2];
[N,T]=meshgrid(n_vec,t);

for k=1:length(t);
    for l=1:length(n_vec);
tau_e =t(k);
n = n_vec(l);

%Implementing field weakening:
if (abs(n_vec(l))<1) || (abs(n_vec(l))==1)
        psi_s_amp = 1;
else
        psi_s_amp =1/abs(n);
end

i_s_amp =abs(tau_e)/psi_s_amp;
delta = atan((tau_e)*x_q_est/(psi_s_amp^2));

psi_d_est = psi_s_amp*cos(delta);
psi_q_est = psi_s_amp*sin(delta);

i_f = ((psi_s_amp^2)+x_d_est*x_q_est*i_s_amp^2)/(x_md_est*sqrt(
   psi_s_amp^2+(x_q_est^2)*i_s_amp^2));

```

```
43 i_d = (psi_d_est-x_md_est*i_f)/x_d_est;
44 i_q = psi_q_est/x_q_est;
45 psi_d_actual = x_d*i_d+x_md*i_f;
46 psi_q_actual = x_q*i_q;
47
48 %Finding the error in estimated stator flux linkage amplitude and in
49 %estimated torque generated.
50 AmplitudeError(k,l) = sqrt(psi_d_actual^2+psi_q_actual^2)-sqrt(
       psi_d_est^2+psi_q_est^2);
51 TorqueError(k,l) =(psi_d_actual-psi_d_est)*i_q - (psi_q_actual-
       psi_q_est)*i_d;
52 i_d_plot(k,l)= i_d;
53 i_q_plot(k,l)=i_q;
54 i_f_plot(k,l) = i_f;
55 psi_d_plot(k,l) =(psi_d_actual-psi_d_est);
56
57 %Removing the areas where the machine is unable to operate
58 %due to the field weakening, and due to limitation of maximum
59 %1 pu stator current:
60 if ((abs(tau_e)>1/abs(n)) && abs(n)>1)
61     TorqueError(k,l)=0/0;
62     AmplitudeError(k,l) =0/0;
63     i_d_plot(k,l)=0/0;
64     i_q_plot(k,l)=0/0;
65     i_f_plot(k,l)=0/0;
66     psi_d_plot(k,l) =0/0;
67 end
68
69
70     end
71 end
72
73
74 figure(4)
75 surf(N,T,AmplitudeError)
76 xlabel('Actual Speed [pu]')
77 ylabel('Torque Ref. [pu]')
78 zlabel('Amplitude Error [pu]')
79
80 figure(5)
81 surf(N,T,TorqueError)
82 xlabel('Actual Speed [pu]')
83 ylabel('Torque Ref. [pu]')
84 zlabel('Torque Error [pu]')
85
```

```
86
87  figure(6)
88  surf(N,T,i_d_plot)
89  xlabel('Actual Speed [pu]')
90  ylabel('Torque Ref. [pu]')
91  zlabel('i_d [pu]')
92
93  figure(7)
94  surf(N,T,i_q_plot)
95  xlabel('Actual Speed [pu]')
96  ylabel('Torque Ref. [pu]')
97  zlabel('i_q [pu]')
98
99  figure(8)
100 surf(N,T,i_f_plot)
101 xlabel('Actual Speed [pu]')
102 ylabel('Torque Ref. [pu]')
103 zlabel('i_f [pu]')
104
105 figure(9)
106 surf(N,T,psi_d_plot)
107 xlabel('Actual Speed [pu]')
108 ylabel('Torque Ref. [pu]')
109 zlabel('\Delta \psi_d [pu]')
```

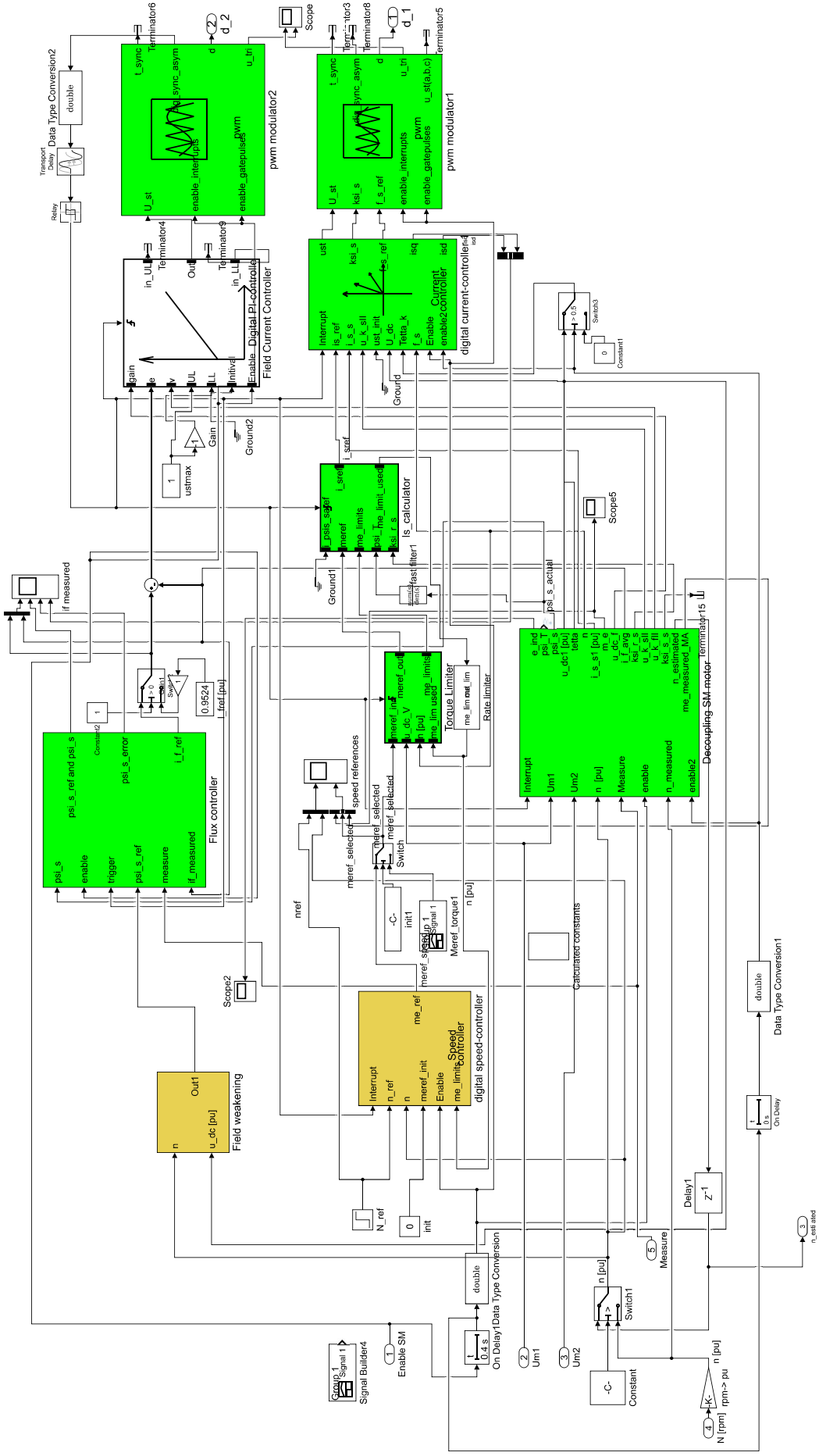

Figure P.1: The outer layer of the control system block in Simulink